Supramolecular Assemblies of Cyclotricatechylene

Jessica Louise Holmes

ORCID: 0000-0002-9807-6112

Submitted in total fulfilment of the requirements

of the degree of Doctor of Philosophy

School of Chemistry

University of Melbourne

November 2019

Abstract

This thesis presents the results of synthetic and structural investigations of novel cyclotricatechylene-based supramolecular assemblies. Cyclotricatechylene is a bowl-shaped *tris*-catechol that has been shown to associate with other chemical species through hydrogen bonding and metal coordination.

The research focuses on the synthesis and characterisation of novel crystalline supramolecular assemblies of cyclotricatechylene. The compounds described in the four experimental chapters include assemblies of cyclotricatechylene and its related anions with *s*, *p*, *d* and *f*-block elements of the periodic table. The compounds have been characterised X-ray crystallography.

Synthetic and structural investigations of compounds formed from the combination of cyclotricatechylene with *s*-block metal cations reveal a diverse array of network materials, with cyclotricatechylene in various protonation states. The *s*-block cations are commonly found to associate with the oxygen atoms of the ligand, however Rb^+ and Cs^+ also exhibit an affinity for the inner and outer aromatic surfaces of the ligand. Two compounds containing cyclotricatechylene 'clams', $H[Cs(ctcH_5)(ctcH_5)]$ and $[Cs(ctcH_6)_2]^+$ are reported, in which cyclotricatechylene is found in different protonation states. In these compounds, the large group 1 metal cation Cs^+ associates with the electron-rich aromatic surfaces of the cyclotricatechylene bowls, an interaction present in many structures described in this thesis.

Metal-cyclotricatechylene polymeric structures are reported, in which *s*-block metal cations are chelated by catechol(ate) oxygen atoms. These structures include 2D sheets containing

Ca^{2+}, Sr^{2+} and Ba^{2+} cations, $[Cs_2Li_4(ctcH_3)_4]^{6-}$ metallocycles that hydrogen bond to each other to form a 3D network that has the topology of diamond, undulating 'honeycomb' networks with Cs^+ or Rb^+, and a 3D network with the topology of the (10,3)-*a* net, containing Cs^+ in cyclotricatechylene bowls and Sr^{2+} chelated by catecholate units.

Four high-symmetry cubic structures formed from the specific combination of cyclotricatechylene with Cs^+ or Rb^+, K^+, acetone, water and an oxyanion contain metallocubes of formula $[K_4(ctcH_6)_4(H_2O)_8]^{4+}$. The assemblies are arranged in a symmetrical manner, which reflects high level of complementarity in these crystalline supramolecular assemblies.

The combination of cyclotricatechylene with vanadyl or uranyl units leads to the formation several large, anionic coordination 'cage' assemblies with fully deprotonated cyclotricatechylene. An aesthetically pleasing example is an assembly with trigonal prismatic geometry, of formula $[(VO)_9Cs_6(ctc)_6]^{18-}$, in which vanadyl oxo groups are directed both into and out of the cage. Systems containing the uranyl cation (UO_2^{2+}) were found to exhibit considerable structural diversity that can be attributed to the formation small clusters of uranyl cations with oxo, hydroxo, peroxo and aqua ligands. The co-precipitation of uranyl-based side products provides significant challenges with respect to the characteristion of these materials.

A robust tetrahedral assembly of cyclotricatechylene with silicon, $[(PhSi)_6(ctc)_4]^{6-}$, was found to be identical in topology to, but much easier to characterise than, its *d*-block metal analogues. Unlike geometrically similar metal-based cages, all bonds within the anionic assembly are covalent. The cage has been shown to persist in the gas phase and also when

crystals of the compound are boiled in water. The crystalline material can also uptake Cs^+ cation guests, which occupy the bowls of the tetrahedra.

Declaration

This is to declare that:

i. This thesis comprises my original work towards the PhD except where indicated in the preface.

ii. Any material in the text that does not comprise the author's own work has been appropriately attributed.

iii. The thesis is less than 100,000 words in length.

Jessica Louise Holmes

Preface

Initial work on supramolecular assemblies of cyclotricatechylene were performed as part of the candidate's Master of Science (chemistry) degree, with A. Prof. Brendan Abrahams and Prof. Richard Robson at the University of Melbourne.

Concerning the work reported in chapter 2: X-ray crystal data of compound 2A was originally collected during the candidate's MSc, however the preliminary structure determination was of poor quality and it was necessary to resynthesise and re-determine the crystal structure. Simulated neutron powder diffraction patterns were calculated by Dr. Helen Maynard-Casely from ANSTO. All additional analyses, including alternative crystal structure solutions, were performed during the candidate's PhD. The candidate assisted a collaborator, Dr. Nicole Rijs (Karlsruhe Institue of Technology, Germany) with her gas phase nanoESI mass spectrometry experiments of 'clam' compounds by synthesising cyclotricatechylene and various clams for these experiments, and by providing a literature review of the behaviour of the compounds. The relevant preliminary results of this collaboration are outlined in chapter 2 for additional context.

Concerning the work reported in chapter 3: Syntheses and preliminary structure determinations of compounds 3A – 3D were performed by Steven Russell who was a past PhD candidate in the Robson-Abrahams group. In order to provide a satisfactory characterisation of the compounds, as well as addressing ambiguities associated with the crystallography, new syntheses were developed by the candidate yielding crystals that were suitable for elemental analysis and X-ray crystallography.

Concerning the work reported in chapter 4: A uranyl-based $M_{12}(ctc)_8$ metallocages cage containing cyclotricatechylene and sodium counterions was originally synthesised by Dr. Nicholas FitzGerald. The crystalline material was difficult to characterise using X-ray crystallography and elemental analysis. Further study of the uranyl-based $[UO_2(ctc)_8]^{24-}$ metallocage was therefore performed during the candidate's MSc, yielding a structure solution in a different space group, however additional elemental characterisation and synthetic optimisation was still required, which was subsequently performed during the candidate's PhD. The crystal structure of one compound that was synthesised during the candidate's MSc was unable to be solved and refined successfully during the candidate's MSc and was therefore not reported at that time. The structure was solved and refined during the candidate's PhD candidature (compound 4B). Another experiment performed during the candidate's MSc did not yield crystals until after the commencement of the PhD and therefore the X-ray data and analysis was performed during the PhD (compound 4C).

Concerning the work reported in chapter 5: High resolution mass spectrometry experiments were performed with the assistance of Dr. Berin Boughton and the resultant mass spectrometry data was analysed with the assistance of Dr. Dinaiz Thinagaran. The bulk of this work, however, was performed by the candidate. Subsequent to the candidate's work, PhD Candidate Anna Ahveninen replicated the experiments that yielded compound 5A and confirmed that 5A could also be generated without microwave irradiation.

Assistance with the candidate's X-ray crystallography was provided by post-doctoral research fellows Dr. Timothy Hudson and Dr. Keith White, and Assoc. Prof. Brendan Abrahams.

Elemental analyses were performed at the Campbell Microanalytical Laboratory, University of Otago, Dunedin, New Zealand and at the Microanalytical Unit at ANU Research School of Chemistry, Canberra, Australia

Concerning the additional data in the appendices: XPS experiments were performed by the RMIT Microscopy and Microanalysis Facility. Solid state NMR experiments were performed by Dr. Aditya Rawal at the Mark Wainwright Analytical Centre, Nuclear Magnetic Resonance Facility at UNSW.

The work reported herein was supported by the University of Melbourne through an Australian Postgraduate Award Scholarship. Additional support was provided by the Australian Research Council (ARC), the Australian Synchrotron and The Australian Nuclear and Scientific Research Organisation (ANSTO).

Publications resulting from work reported in this thesis

Self-assembly of a Si-based cage by the formation of 24 equivalent covalent bonds.

Holmes, Jessica L., Abrahams, Brendan F., Ahveninen, Anna, Boughton, Berin A., Hudson, Timothy A., Robson, Richard, Thinagaran, Dinaiz.

Chem. Commun., 2018, **54**, 11877

DOI: 10.1039/c8cc06405a

Acknowledgements

I would like to thank the following people for their support throughout my candidature:

Associate Professor Brendan F. Abrahams for teaching me so much about supramolecular chemistry, crystallography and how to conduct oneself as a professional. He is the most supportive and thoughtful supervisor I could have hoped for. I will be forever grateful for the way he instructed and guided me in my studies – always respectfully, patiently, kindly and with an appropriate level of humour. You're a superstar!

Professor Richard Robson for being a font of knowledge, exceptionally encouraging and very inspirational. Richard - for such an incredible and successful scientist you are so down-to-Earth and you are a true role model to me. I have been extremely fortunate to learn from you, and it makes me happy that we share the same birthday!

Dr Keith White. You have been my fiercest supporter, both as a post-doc and as a partner. Words can't do you justice, so I will be quiet now.

Dr Timothy Hudson, because he is the crystallography master, and for being my Lab 'Assistant' number 2.

Dr Emma Read, for going through this process with me, for driving me to achieve my goals and believe in myself (ever since undergrad!) and for understanding me and my process like no one else does, or ever could.

Dr Robert Elliott for being there for me late at night, and for anytime I needed a lab safety partner. You're like a brother to me, only better.

Thank-you to Paul Donnelly, Jonathan White and Spas Kolev for being on my panel, and happily chatting to me if ever I needed it.

Thanks to all of the teaching staff that both taught me, and later worked with me as a colleague. In particular, thank you to Penny Commons and Mick Moylan for mentoring me and believing in me – you really helped launch my career.

I would also like to thank all of my friends, family, co-workers, collaborators and School of Chemistry staff who have supported me throughout my PhD, and who have tolerated both my presence and my absence over the years. No woman is an island!

Abbreviations

$ctcH_6$	=	cyclotricatechylene (neutral)
ctc	=	cyclotricatechylene (neutral or anionic)
ctv	=	cyclotriveratrylene
DMF	=	*N*,*N*-dimethyl formamide
DMSO	=	dimethyl sulfoxide
OAc	=	acetate
1D	=	one-dimensional
2D	=	two-dimensional
3D	=	three-dimensional
MeOH	=	methanol
EtOH	=	ethanol
MeCN	=	acetonitrile
Me	=	methyl
Et	=	ethyl
Pent	=	pentyl
Ph	=	phenyl
Bz	=	benzyl
$MePPh_3^+$	=	methyltriphenylphosphonium
NMe_4^+	=	Tetramethylammonium
NEt_4^+	=	Tetraethylammonium
DABCO	=	1,4-diazabicyclo[2.2.2]octane
NMR	=	nuclear magnetic resonance (spectrometry)
MS	=	mass spectrometry

ESI	=	electrospray ionisation
MALDI	=	matrix assisted laser desorption ionisation
IR	=	infrared (spectroscopy)
ICP-OES	=	inductively coupled plasma optical emission spectroscopy
XPS	=	X-ray photoelectron spectroscopy

Table of contents

List of figures

Chapter 1

Chapter 2

Chapter 3

Chapter 4

Chapter 5

Chapter 1 Introduction

Contents

The purpose of the work reported in this thesis was to explore the structural diversity and host-guest chemistry of supramolecular assemblies containing the bowl-shaped molecule *tris*-catechol cyclotricatechylene, ctcH_6.

This thesis describes several novel assemblies of cyclotricatechylene that were generated using the principles of coordination chemistry and supramolecular chemistry. The assemblies have been primarily characterised using X-ray crystallography. The assemblies of the most interest were further investigated to explore their host-guest behaviour, formation conditions and relative stability.

This chapter will provide a brief introduction to supramolecular chemistry with a particular emphasis on metal-based assemblies. It will also provide an overview of the chemistry of cyclotricatechylene and related compounds. The rationale for the exploration of supramolecular assemblies of cyclotricatechylene will also be presented.

1.1 Supramolecular chemistry

1.1.1 Context

A new paradigm in chemical synthesis, processing and analysis has emerged over the past half century, arguably as a result of increasing appreciation of the weak chemical interactions that govern natural systems. Studies in the fields of biology and biochemistry have shown that, beyond the covalent bond, many of the physiological functions and biochemical processes that are essential to life are possible due to non-covalent interactions and the reversible formation of non-covalent bonds. These non-covalent bonds include hydrogen bonds, coordinate bonds, π-attractions, hydrophilic and hydrophobic interactions. The typical

strength of these non-covalent forces ranges from approximately 5 kJ mol^{-1} to 400 kJ mol^{-1} for strong coordinate bonds - on par with many covalent single bonds.[1]

An important representative example illustrating the importance of these non-covalent interactions in nature relates to enzyme activity. Enzymes are catalytic receptor molecules that display specificity for substrate (guest) molecules, which means an individual enzyme will only bind *complementary* substrates, i.e. those with appropriate size, shape and electronic properties. Although the concept of enzyme specificity was previously known, Emil Fischer is credited with first detailing the mechanism by which it could occur in seminal 1890 and 1894 papers that describe the non-covalent and reversible binding of substrates via a 'lock and key' mechanism.[2–4] The theory of enzyme action was later elaborated by Koshlan, who proposed the 'induced fit' mechanism in 1954.[5] As a direct result of the binding of a substrate - generally a 'signaling' molecule, macromolecule or a monomer at the receptor site of the enzyme - a cascade of electronic and steric changes take place in the enzyme, substrate or both. This in turn leads to a specific biochemical reaction that produces the appropriate chemical products at the rate required by the organism.

In the years following these initial studies on enzyme activity it was recognized that the same non-covalent interactions that so effectively allow enzyme-substrate binding and enzymatic activity could also be deliberately employed in chemical synthesis, analysis, processing, material design, host-guest chemistry and catalysis. This is the supramolecular approach to chemistry.

Cram, Lehn and Pederson are recognised as pioneers in supramolecular chemistry. In 1987 they were awarded the Nobel prize in chemistry for their contributions to the field of

supramolecular chemistry. Conferred for their research into the supramolecular binding of alkali metal cations by rationally selected macrocycles, the prize highlighted the emergence of a new approach to chemistry. Their visionary work demonstrated that so-called weak, non-covalent interactions could be used to form host-guest complexes in which alkali cation guest molecules were selectively bound, and for which the formation constants were very high.[6–11]

Lehn articulated the definition of modern supramolecular chemistry as the chemistry of "molecular assemblies and of the intermolecular bond"[12] and more succinctly as "chemistry beyond the molecule"[13,14] As Lehn noted, "Supramolecular chemistry is a highly interdisciplinary field of science at the intersection of chemistry, biology and physics".[15] This field has grown so large as to include more than a dozen sub-areas including but not limited to: hydrogen-bonded systems, coordination chemistry, molecular cage chemistry, host-guest chemistry, molecular recognition and sensing, catalysis, chromatography (separation and purification), dynamic materials, adaptive materials, liquid crystals and gels, combinatorial synthesis, chemomechanical materials, molecular devices and machines, organic electronics; data storage and processing; gas sorption, storage and conversion; photodynamic therapy, solar energy conversion, self-healing materials, soft nanotechnology, drug delivery and medicine, food and textile science.[16,17] Supramolecular interactions are also recognized to play important roles in various other systems such as micelles and clays for example, and have been identified as central the development of molecular computation, nanoscience, photonics and electronics technologies. The field of supramolecular chemistry is too large to review in detail, however key principles and developments in supramolecular chemistry that are relevant to this thesis are outlined hereafter.

The emergence of interest in supramolecular systems within the discipline of chemistry is understandable when the beauty, utility and intricacy of biological systems on the micro- and nanoscopic levels is appreciated.

There are multitudinous desirable features in biological systems that chemists have begun to, and continue to emulate;[18] for example, a key feature of many biological supramolecular systems is their dynamic nature on a useful timescale. Biological supramolecular systems, far from being static and isolated, can be viewed as a conglomeration of intricate and interconnected nanoscale mechanical systems with moving parts, specific functions, and chemical and energetic inputs and outputs. Artificial supramolecular systems may also be dynamic, which is important for several reasons; in supramolecular synthesis, bonds, once formed, can be easily broken by deliberate application of external stimuli, or they can easily break because of low activation energy barriers. The low energy processes associated with bond formation and disruption allow for the correction of 'errors' during reactions and self-assembly processes, as well as permitting post-synthetic modifications.[19–21] This dynamism also allows for the synthesis of 'molecular machines' i.e. assemblies with moving parts. Chemists have also endeavoured to engender the dynamism observed in biology into synthetic supramolecular architectures as it may give rise to a variety of additional useful properties; a prime example of which is the reversible opening and closing of molecular cages allowing the ingress and trapping of guest molecules as well as controlled egress of guests (see 1.1.4.2 coordination cages).[22–25]

In order to achieve the same desirable features displayed by biological systems in artificial assemblies, Cram and co-workers deliberately employed models based upon biological systems to design their host-guest assemblies, such as a large family of spherands and their

spheraplexes with cations.[26,27] Their complexes "were designed through extensive use of Corey-Pauling-Koltun (CPK) molecular models. These models were developed under the auspices of the U.S.: National Institutes of Health, Education and Welfare, the National Science Foundation, and the American Society of Biological Chemists"[26] and "…are based on crystal structures of biologically important compounds"[26]. In reference to his 1986 paper Cram identified that, in fact, "Most of the complementary relationships between hosts and guests of our design could not have been anticipated without use of CPK models."[26]

Soon after Cram, Lehn and Pedersen were awarded their Nobel prize, the United States Government Defense Advanced Research Projects Agency (DARPA) also acknowledged the self-assembly of biological supramolecular systems as the basis for the design of useful new nanoscale architectures; in 1991 they commissioned a report about chemical strategies for synthesis of nanostructures via molecular self-assembly pathways. The report (produced at Harvard University and published in the journal *Science*) articulated that

"Molecular self-assembly is ubiquitous in biological systems, and underlies the formation of a wide variety of complex biological structures. Understanding self-assembly and the associated non-covalent interactions that connect complementary interacting molecular surfaces in biological aggregates is a central concern in structural biochemistry. Self-assembly is also emerging as a new strategy in chemical synthesis, with the potential of generating non-biological structures having dimensions of 1-10^2 nanometers (with molecular weights of 10^4-10^{10} Daltons). Structures in the upper part of this range of sizes are presently inaccessible through chemical synthesis, and the ability to prepare them would open a route to structures comparable in size (and perhaps complementary in function) to

those that can be prepared by microlithography and other techniques of microfabrication".[28,29]

The *Science* paper aimed to outline the biological precedent for modular, noncovalent molecular self-assembly and to elucidate those features of self-assembly processes that would also make it suitable for the preparation of nanostructures. It was concluded that self-assembly offered a novel and unique pathway to otherwise inaccessible chemical structures. The hypothesis offered, that "New ways of assembling molecules should lead to new ideas for their uses"[29], has proven true.

Since this time, supramolecular biological systems have been emulated in laboratories in various ways, from attempts to replicate biological processes such as photosynthesis to efforts directed towards water splitting for the production of hydrogen gas.[30–34] Biological molecules have even themselves become the basis for many synthetic supramolecular systems; notably, due to its programmable properties and non-toxic nature, deoxyribonucleic acid (DNA) has been extensively employed as a supramolecular building block in order to produce sophisticated nanostructures with targeted geometries and patterns, molecular scaffolds, and systems with desirable *in vivo* properties.[35,36,45,37–44] Supramolecular chemistry has matured to the point that it "…has come full circle, studying the biology and its molecules which initially inspired its conception".[46] In essence, knowledge of existing biological systems and the supramolecular interactions that govern their assembly and function can guide the design of novel functional nano- or macro-scale architectures, which can be synthesised using a 'bottom-up'[47,48] approach and subsequently be employed for purpose.

Outstanding pioneers in the field of supramolecular chemistry such as Atwood, Constable, Etter, Feringa, Fujita, Raymond, Sauvage, Stang, Steele and Stoddart – were trail blazers in an ever-growing community of scientists who continue to use the supramolecular approach to chemistry to design, synthesise and analyse elegant functional architectures, and use them to perform frontier chemistries.

In 2016, 29 years after Cram, Lehn and Pedersen received it, the Nobel Prize in Chemistry was awarded jointly to Sir Fraser Stoddart, Jean-Pierre Sauvage and Bernard Feringa "for the design and synthesis of molecular machines".[49] This body of work, spanning almost 40 years, has (so far) culminated in the synthesis of the first dynamic nanometer scale machines that have the ability to mechanically control their surroundings and that may be deliberately controlled by the application of external stimuli. These molecular assemblies would appear to have the potential to revolutionise technology.

The work described above has its roots in the chemistry of Cram and Pedersen's macrocycles, many of which were synthesised using supramolecular templation based on metal or organic ions. Formative research in this area of 'molecular machines' was performed by Sauvage, who was a protégé of Jean-Marie Lehn's. Sauvage *et al*. used supramolecular (coordination) interactions with Cu(I) ions to hold two proto-macrocycles together such that, when each macrocycle was completed through covalent bonding, the two macrocycles were interlinked.[50] From that starting point, a great deal more strategic chemistry has been performed by the Feringa, Stoddart and Sauvage groups, generating a wide variety of catenanes, rotaxanes, molecular knots, 'elevators', logic gates, rotors, pivoting molecules and numerous other proto-molecular machines. Many of the synthetic pathways to these molecules, as well as the *function* of these molecules, are dependent on supramolecular

interactions and crystal engineering. Several excellent summaries of the work in this area as well as its potential applications have been published.[51–53]

The award of the Nobel Prize in Chemistry for a joint endeavour that heavily draws upon supramolecular principles evidences the utility and utmost importance of the supramolecular approach to chemistry in the advancement of science.

1.1.2 Alkali metal cations in host guest chemistry

Much of the work performed by Cram, Lehn and Pederson in the arena of supramolecular and host-guest chemistry focused on the binding of alkali metal cations. The binding and separation of alkali metal cations is critical in the modern world, beyond the use of the ubiquitous lithium, sodium and potassium salts in synthesis. Cram noted that "The importance of Li^+, Na^+, and K^+ to biological processes, the susceptibility of Rb^+ and Cs^+ to neutron activation, and the possible use of Li^+ as a fusion fuel combine to generate increasing interest in hosts that differentially bind these ions".[26] Expanding on Cram's comments, it has become increasingly urgent to identify ways to sequester radiocaesium from the environment,[54] as ^{137}Cs is a major environmental contaminant resulting from nuclear events. This isotope has a half-life of approximately 30 years, which is long enough to affect multiple generations, and active enough to emit significant radiation into the environment.[55]

Ligands and host materials designed to display selectivity and high binding energies for the group 1 metal cations generally possess electron rich Lewis base groups and/or aromatic moieties and are typically macrocyclic (crown ethers,[8,56–60] calixarenes,[8,54,61–65]

spherands,[26,27,66–69] and cyclotriveratrylenes (see 1.3.1)) or macropolycyclic species (cryptands,[6,69–71] and cyclodextrins[64]), examples of which are given in the references provided.[7,60,72]

In the design of supramolecular host-guest assemblies in which multiple components self-assemble it is desirable for the building block to have groups oriented favourably for guest binding and complexation prior to the assembly process. If the host retains its conformation after assembly and binding its guest(s) it is termed *preorganized*. Cram explained that "to complex, hosts must have binding sites which can simultaneously contact and attract the binding sites of the guests without generating internal strains or strong nonbonded repulsions."[73] When the components of a host are preorganised, the resultant host assembly is more likely to be able to accommodate guest molecules as desired. Further, the complexation process will be entropically favourable as the host does not need to re-arrange to become more 'ordered' in the process of binding the guest.

Complementarity is another key concept in host-guest chemistry. The host must have binding sites which converge, and the guest must have binding sites that diverge. Complementarity refers to the binding sites of the host and guest being sterically and electronically matched with each other.[74] Complementarity allows for both strong binding and the predictable/directed assembly of the components. The concept of complementarity also extends to the assembly of other supramolecular assemblies such as molecular cages, which require components that have matched binding sites to assemble together. Complementarity is most famously observed in the cases of the adenine – thymine and cytosine – guanine base pairs in DNA, each possessing both hydrogen-bond donor and acceptor moieties that complement one another.

Alkali metal cations are versatile and can form a part of an extensive range of assemblies. Alkali metal cations are ideally placed to form interactions with a wide variety of host molecules, due in large part to the ability of the cations to adopt geometrically irregular coordination geometries. The key differentiators between hosts for group 1 cations are their cavity size and shape, as the major differences between alkali metal cations are their size and charge density. As such, size complementarity between host molecule and guest alkali metal cation can be key to alkali metal cation binding, separation and sequestration.

Lehn has written widely on the virtues of host preorganization and employing components that are complementary to one another, and Wittenberg and Isaacs have laid out the principles of these concepts as relevant to supramolecular chemistry in their review *Complementarity and Preorganization*.[75] Their reports demonstrate how incorporating these principles has become a recognised synthetic strategy for the self-assembly of host molecules and their complexes with guests.

Cram, Lehn and Pedersen each synthesised complexes of alkali metal cations in which the components were complementary and/or preorganized. Examples of this include crown ethers (Pedersen), cryptands (Lehn) and spherands (Cram).

Crown ethers are a family of cyclic molecules that contain multiple ether linkages. Cyclic polyethers with four or more ether linkages appeared in the literature as early as 1937[76] however Pederson was the first to report stable cyclic polyether–alkali metal complexes.[60] The compound formed between K^+ and dibenzo-18-crown-6 (Figure 1.1: Left) is a beautiful example of complementarity between an alkali metal cation and a ligand of the correct ring size that can replace part of the solvent shell of the cation. The crystal structure of the $[K(\text{dibenzo-18-crown-6})]^+$ complex in $[K(\text{dibenzo-18-crown-6})][Al_2(CH_3)_6O_2]$ reported by

Atwood and coworkers is shown in Figure 1.1: The image on the right indicates the binding of the metal cation by the ligand.[77]

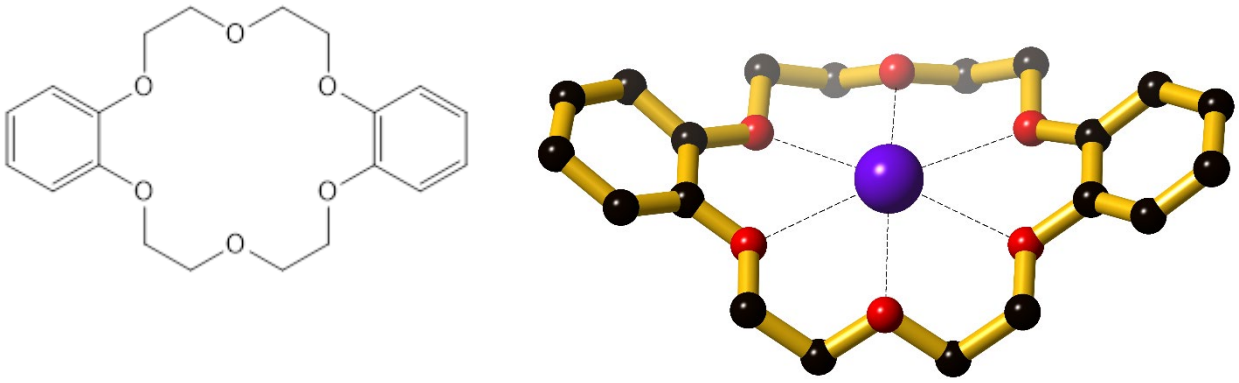

Figure 1.1 Left: A schematic representation of Pedersen's dibenzo 18-crown-6. Right: A ball and stick representation of the $[K(\text{dibenzo 18-crown-6})]^+$ complex in the crystal structure of $[K(\text{dibenzo-18-crown-6})][Al_2(CH_3)_6O_2]$ reported by Atwood and co-workers. K^+ is represented by a purple sphere. Hydrogen atoms have been omitted for clarity.

A family of molecules very similar to the crown ethers are the macrobicyclic cryptands. The first such example reported by Lehn and coworkers in 1969, [2.2.2]cryptand (Figure 1.2: Left), was shown, like dibenzo-18-crown-6, to bind K^+ in a complementary fashion.[78,79] The crystal structure of the $[K[2.2.2]\text{cryptand}]^+$ complex in $[K[2.2.2]\text{cryptand}]_2[Sb_2Se_6]$ reported by Smith and coworkers is shown in Figure 1.2: The image on the right indicates the binding of the metal cation by the ligand.[80]

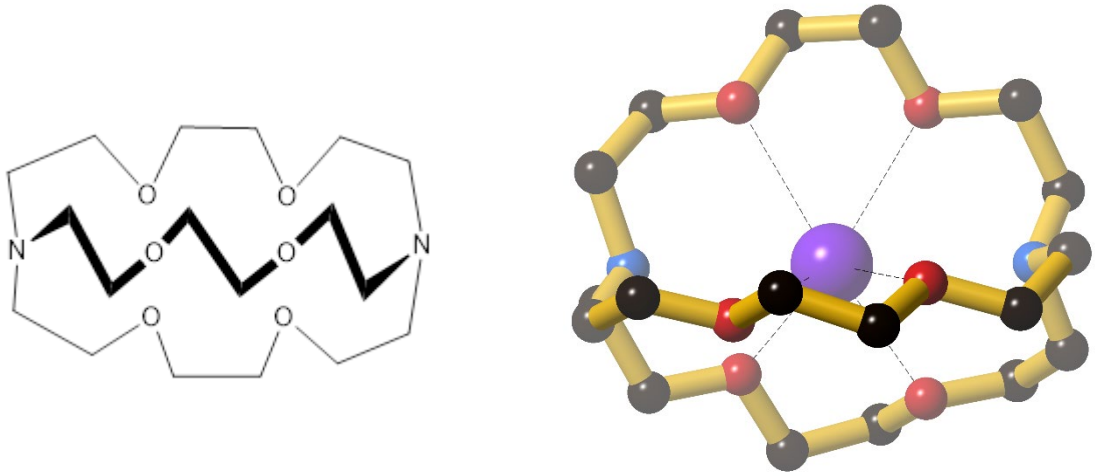

Figure 1.2 Left: A schematic representation of Lehn's [2.2.2]cryptand. Right: A ball and stick representation of the $[K[2.2.2]cryptand]^+$ complex in the crystal structure of $[K(2.2.2\text{-cryptand})]_2[Sb_2Se_6]$ reported by Smith and coworkers. K^+ is represented by a purple sphere. Hydrogen atoms have been omitted for clarity.

Spherands are macrocycles with rigid cavities and are a type of cavitand (container shaped molecule[81]). Like crown ethers and cryptands, spherands can form complexes via oxygen donor sites with various complementary guests including alkali metal cations. Due to their rigidity, spherands undergo very little conformational change on guest complexation, i.e. they are preorganized for guest binding. Interestingly, many spherands are preorganized for guest complexation during synthesis by employing their guest as a template, such as Cram's octaspherand for which the yield is maximized by using CsBr in the synthesis.[82] The prototypical spherand of formula $(CH_3C_6H_2OCH_3)_6$ (Figure 1.3: Left) reported by Cram in 1981 is selective for Li^+ and Na^+ and has high binding energies for both.[66,67] The crystal structure of the $[Li(CH_3C_6H_2OCH_3)_6]^+$ complex in $[Li(CH_3C_6H_2OCH_3)_6]Cl$ reported by Trueblood and coworkers is shown in Figure 1.3: The image of the right indicates the binding of the metal cation by the ligand.[83]

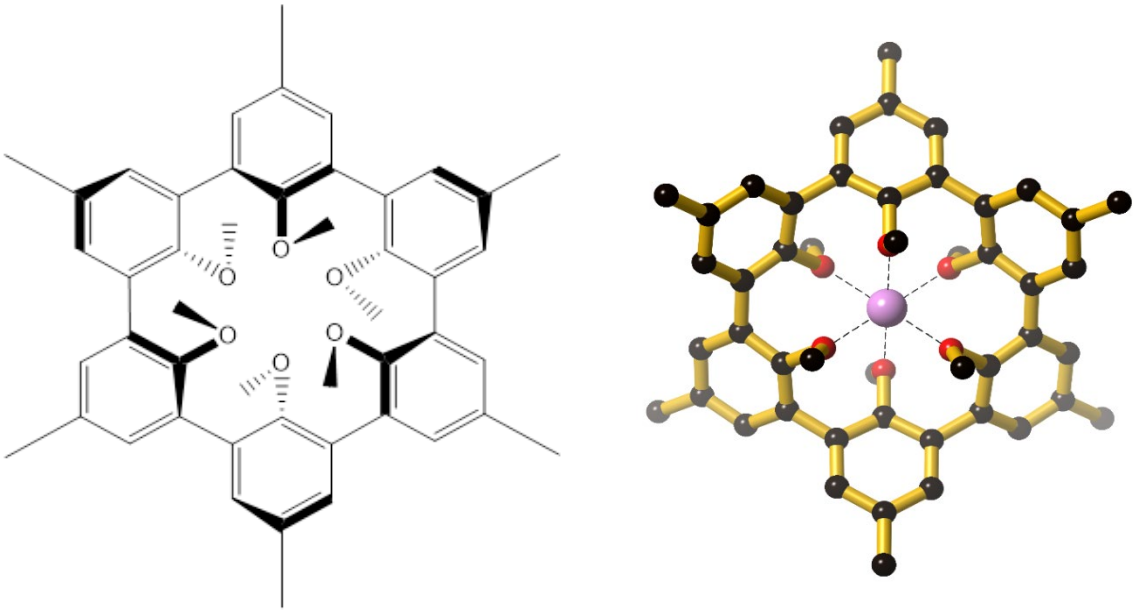

Figure 1.3 Left: A schematic representation of Cram's spherand of formula $(CH_3C_6H_2OCH_3)_6$. Right: A ball and stick representation of the $[Li(CH_3C_6H_2OCH_3)_6]^+$ complex in the crystal structure of $[Li(CH_3C_6H_2OCH_3)_6]Cl$ reported by Trueblood and coworkers. Li^+ is represented by a pink sphere. Hydrogen atoms have been omitted for clarity.

In the above host-guest complexes of alkali metal cations, the metal cations interact with electron rich oxygen atoms, however, the interaction of π-systems with cations[84,85] has also been shown to be an important feature of many self-assembled supramolecular systems.

π-cation interactions have been documented since the late 1980s when the π-cation interaction was first defined by Dougherty, who recognised its importance in protein biology.[85–88] Both organic and inorganic cations can interact with π-systems in what is mostly an electrostatic interaction. These interactions are not only important in biology but also in the synthesis of supramolecular assemblies, for guest capture, molecular recognition and catalytic purposes.[84] The π-cation interaction is of such magnitude that molecules with π-systems such as cyclophanes can extract water-soluble cations into their electron-rich hydrophobic cavity.

Alkali metal cations can also be taken up from aqueous solution when an appropriate π-donor is present. Smaller alkali metal cations are expected to have a larger electrostatic attraction to π-systems due to their higher charge density. Larger alkali metal cations, however, can also have significant interactions with π-systems of host molecules and benefit from being able to interact with multiple π-systems simultaneously due to their larger size.

Calixarenes are a family of cavitands that has been investigated with a view to probing their host-guest chemistry. Calixarenes, such as calix[4]arene, can adopt a preferred bowl-like conformation in which there are intramolecular hydrogen bonds between the hydroxyl groups. In this conformation, alkali metal cations such as Cs^+ have been incorporated into the bowl, where they participate in π-cation interactions, such as in Figure 1.4 which shows a compound reported by Thuery and coworkers.[89,90] Calixarenes are also able to bind alkali metal cations via oxygen atoms on their lower rim. In the example below, the exposed hemisphere of the Cs^+ cation interacts with solvent and the hydroxyl oxygens of an adjacent calixarene, and it is common to see the smaller, harder alkali metal cations such as Li^+ and Na^+ interact with the hydroxyl groups in preference to the aromatic surfaces.

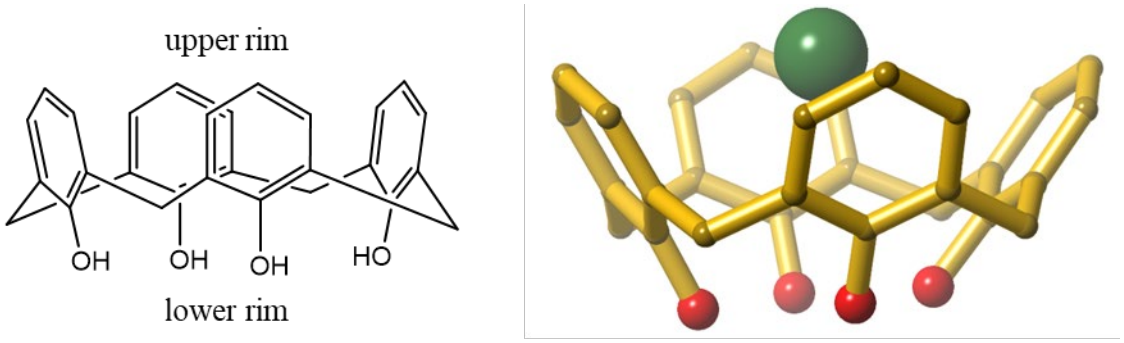

Figure 1.4 Left: A schematic representation of calix[4]arene. Right: A ball and sick representation of Cs^+ (green) in the bowl of calix[4]arene in the compound of formula [Cs(calix[4]arene)(py)]. Hydrogen atoms have been omitted for clarity.

1.1.3 Hydrogen bonding and coordinate bonding

Cavities within supramolecular assemblies can be created using components that, unlike crown ethers, cryptands and spherands, do not in isolation possess cavities for guest molecules. Two approaches generate assemblies with cavities involve using hydrogen bonding and/or coordinate bonding. Supramolecular assemblies containing hydrogen bonds and coordinate bonds rely on the assembly of components that are complementary to each other.

1.1.3.1 Hydrogen bonding

A classical description of the hydrogen bond is an electrostatic interaction between a hydrogen atom that is covalently bonded to an electronegative atom (the hydrogen bond donor), and another electron rich atom (the hydrogen bond acceptor). Both the electronegative atom from the donor and the electron rich acceptor are usually N, O or F. In general, the length and geometry of a bond between a donor and acceptor is key in establishing if a given interaction is a 'hydrogen bond'.[91]

The work of Etter provides an excellent introduction to the early investigations of hydrogen bonding and also provides a framework for defining hydrogen bonds called "Etter's rules"[92]; Hydrogen bonding criteria are further described in *Basicity. A comparison of hydrogen bonding and proton transfer to some Lewis bases,* and *Hydrogen-bond geometry in organic crystals* [93,94]; Specific information regarding hydrogen bonding in crystal engineering has been reported. [95,96]

Hydrogen bonding is emphasized in this thesis as it is a most important structure directing feature in many supramolecular architectures, self-assembled systems and crystalline materials, and contributes to the properties of the resultant molecular or crystal system. Etter *et al.* provides a detailed discussion of this in *Structure Correlation Vol 2., Ch. 11. The Role of Hydrogen Bonding in Molecular Assemblies.*[97] Many of the assemblies reported in this thesis display self-complementarity that occurs due to a molecule (i.e. cyclotricatechylene) having hydrogen bond donor and acceptor sites that can interact with each other.

1.1.3.2 Coordinate bonding

Coordination chemistry is a key tool in building molecular and framework architectures. Transition metal cations are useful building blocks in rationally designed assemblies because they display a strong preference for certain coordination geometries. Predictable architectures result from the self-assembly of transition metal cations with ligands that also display a strong preference for particular geometries. Cations of *f*-block elements show similar preferences but to a lesser extent. In addition to the strong directionality displayed by transition metal cations, they also form relatively strong bonds with a variety of ligands to form robust architectures. However, like other supramolecular interactions, coordinate bonds also have a degree of lability conducive to "error correction" in the self-assembly process. Coordination compounds may be discrete (including coordination cages and coordination complexes), or infinite (coordination polymers).

1.1.4 Cages

A cage compound is, by IUPAC definition, a "polycyclic compound with the shape of a cage"[98]. Using hydrogen bonding, coordinate bonding or a combination of both, discrete assemblies with cavities, i.e. cages, can be synthesised. Molecular cages that contain only covalent bonds are also possible. Molecular cages can be closed, with covered faces, or open, allowing for easier ingress and egress of guests without any rearrangement of the components or bond breakage. An important feature of many cage assemblies generated using hydrogen and coordinate bonding is that they are able to open and close to allow ingress and egress of guest species, which is less often possible with covalent cages.

Cage compounds have proven useful in the capture of various species (including those that are environmentally harmful), the stabilization of reactive species and in chemical separation and sensing.[99,100] They also have the potential to act as 'stealthy' or slow-release drug delivery vehicles for therapeutic cargo. Most exciting is their ability to catalyse chemical reactions within their cavities that would otherwise not be possible (e.g. stereo/regioselective reactions, photoadditions).[101–103]

Cages can be engendered with desirable properties by choosing appropriate building blocks. For example, inclusion of transition metals may give rise to magnetic behaviour[104], spin-crossover systems[104] and coloured compounds;[105] redox active ligands can react with guest molecules inside the cage and participate in charge transfer.[102,103,105] Although self-assembly provides a reliable synthetic route to form non-covalent molecular cages, these assemblies can be challenging to study in some cases. Cages that are constructed using non-covalent interactions can be unstable once removed from the environment from which they have been synthesised and are therefore often difficult to isolate.[106,107]

Molecular cages can also be produced by forming covalent bonds between building blocks. The synthetic processes to produce these can be more challenging than that for supramolecular cages and may produce by-products that need to be separated from the synthetic target. Once isolated, covalent cages are generally easier to study. Interesting and useful cage compounds can be produced by both supramolecular and covalent syntheses.

1.1.4.1 Hydrogen bonded cages

A variety of hydrogen bonded cages and 'capsules' have been reported in the literature, though there are fewer hydrogen bonded cages than coordination cages.[108] An early example of a hydrogen bonded assembly containing an internal cavity is Rebek's 'tennis ball'. This assembly is a hydrogen bonded dimer of two identical, self-complementary molecules wrapped around each other and connected by eight hydrogen bonds.[109,110] The assembly resembles a tennis ball, with the hydrogen bonds serving as the 'seam' that links the two halves. The tennis ball, as well as its larger analogues and the similar, but less spherical 'softballs' are examples of hydrogen bonded assemblies which assemble such that they have a cavity that can be exploited for guest encapsulation.[111–114]

Calixarenes, as well as forming complexes with metal cations, can also form hydrogen bonded assemblies. Calixarenes can be functionalized para to the OR_1 groups on the benzene rings, as shown in Figure 1.5. Shimizu first reported that when hydrogen bond donors and acceptors were incorporated into the molecule as the R_2 group, dimeric hydrogen bonded complexes between calixarenes would form.[115] It was later found that the cavity within calixarene dimers could host guests such as benzene. The first crystal structure of a dimeric calixarene capsule was reported by Mogck and coworkers who showed that the dimer was held together by a belt of hydrogen bonded amide moieties (Figure 1.5 Right).[116]

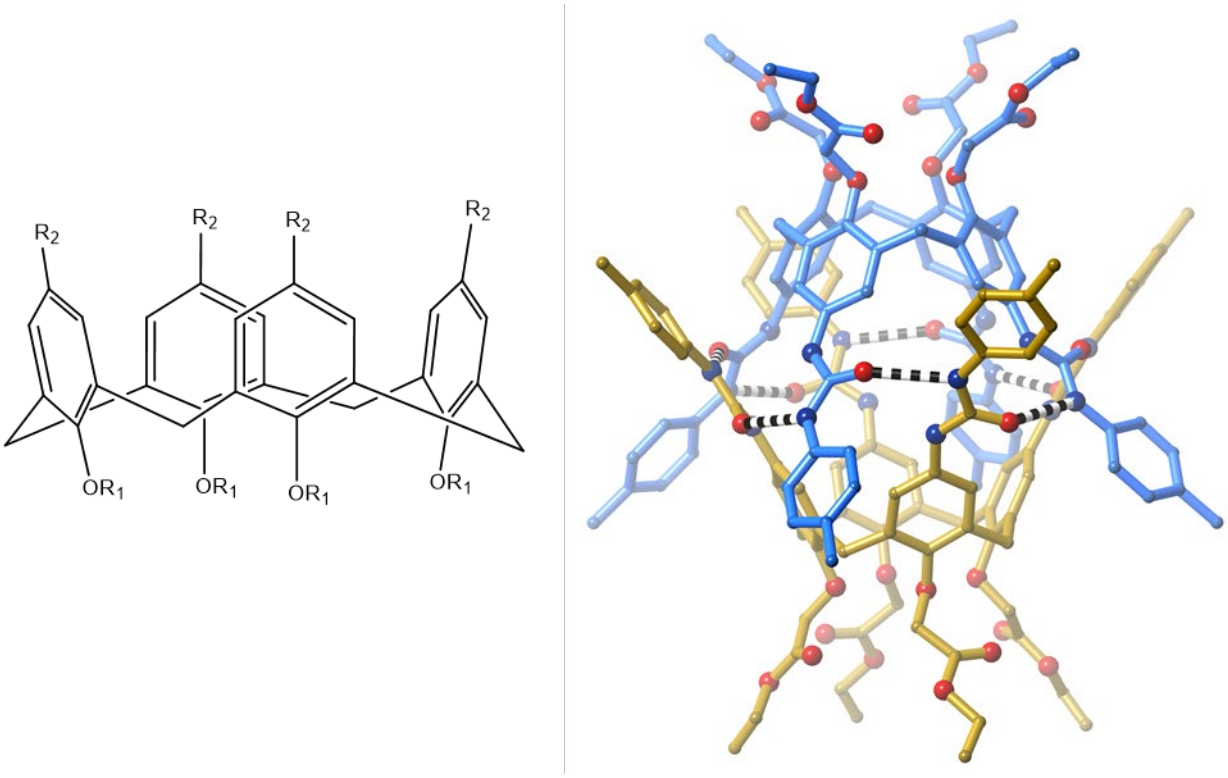

Figure 1.5 Left: Schematic of a generic calix[4]arene in its bowl conformation. Right: A ball and stick representation of the hydrogen-bonded dimer of a tetraurea calix[4]arene reported by Mocgk and coworkers. The top (blue) calixarene interdigitates with the bottom calixarene and they are held together by six hydrogen bonds. Hydrogen atoms have been omitted for clarity.

The pyrogallol[4]arenes and calix[4]resorcinarenes, which are structurally related to the calix[4]arenes above, have hydroxyl groups located on their outer rims. Atwood and coworkers showed that large hexameric molecular capsules could form when six identical pyrogallol[4]arenes or calix[4]resorcinarenes self-assemble via hydrogen bonding interactions.[117] These hexameric assemblies have large internal cavities of around 1200 $Å^3$, with one such assembly containing 60 hydrogen bonds.[118]

1.1.4.2 Coordination cages

Coordination cages or 'metallocages' comprise metal centres and ligands (which are usually organic) that are arranged such that an enclosed space is formed. Some of the most important work in cage chemistry using coordinate bonds has been performed by Fujita and Stang.

Fujita and co-workers are recognised as pioneers in this area. In their early work, they designed and prepared M_6L_4 coordination cages combining six square planar Pd^{II} centres and four three-connecting pyridyl-based bridging ligands.[119] Rather than using just preorganised building blocks, they also employed capping ligands to block coordination sites on the Pd^{II} centres such that cage formation was favoured over polymer formation – essentially organising the system *in situ.* The cage, which is constructed from the electron-deficient tripyridyltriazine ligand, TPT, was able to act as a host for the electron-rich molecule, tetrathiafulvalene, TTF, (Figure 1.6).

The Fujita group have since reported a wide variety of coordination assemblies with Pd^{II} square planar corners, including trigonal prismatic 'pillared' cage assemblies with TPT and pyrazine that can host two stacked, planar guests (Figure 1.7).[120–122]

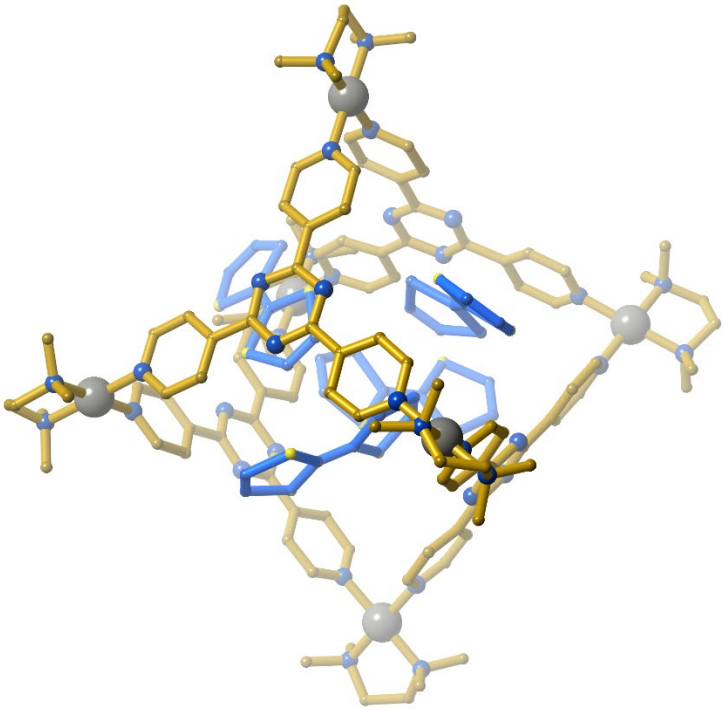

Figure 1.6 A ball and stick representation of Fujita's octahedral assembly of TPT with square planar capped Pd^{II} centres. The molecules in blue represent the TTF guests in the cage. Grey spheres represent Pd^{II} centres. Hydrogen atoms have been omitted for clarity.

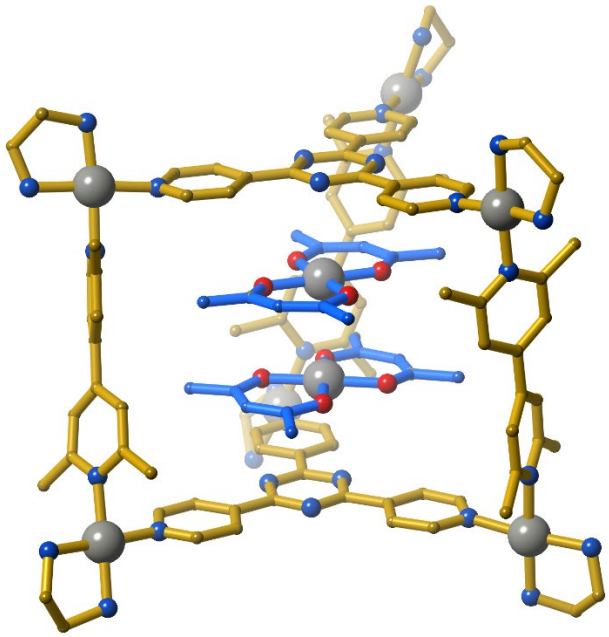

Figure 1.7 A ball and stick representation of one of Fujita's trigonal prismatic pillared assemblies. Grey spheres represent Pd^{II} centres. Hydrogen atoms have been omitted for clarity.

Stang's contributions include a trigonal prismatic pillared assembly, similar to Fujita's, above, which also contains square planar metal centres, but does not contain chelating capping ligands (Figure 1.8).[123] The reported assembly was cleverly generated using a molecular 'clip' containing two platinum centres as a preconstructed shape-defining unit. This strategy required only five components to assemble rather than the eleven (plus twelve PEt_3 ligands) that would have been needed if none of the components had been pre-assembled.

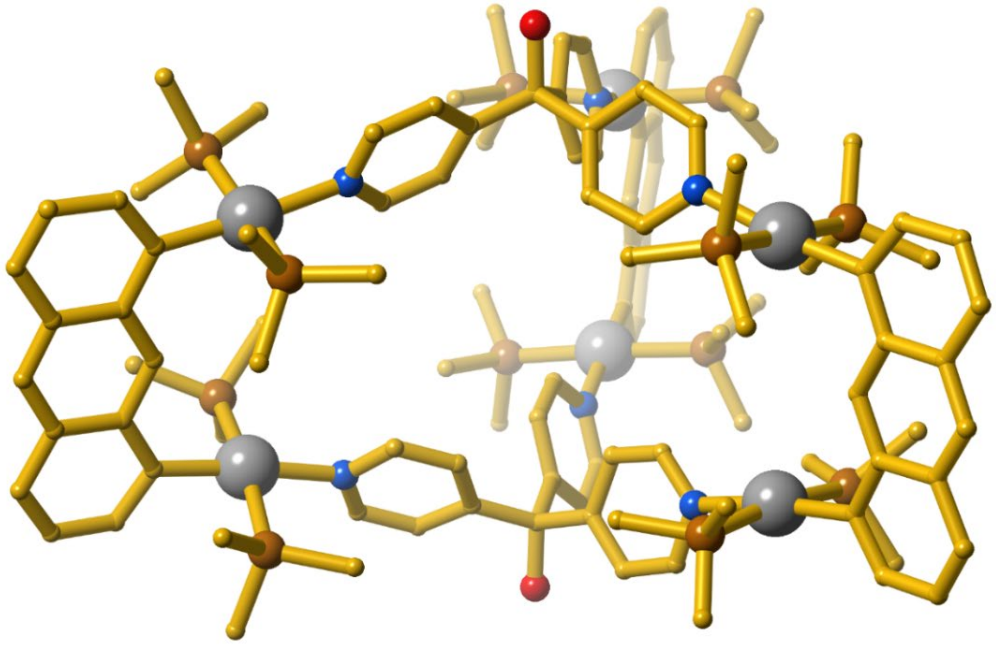

Figure 1.8 A ball and stick representation of Stang's trigonal prismatic pillared assembly in the compound of formula bicyclo[*tris*[1,8-*bis*(trans-$Pt(PEt_3)_2(NO_3)$)anthracene)]*bis*[*tris*(4-pyridyl)methanol]]. Grey spheres represent Pt^{II} centres. Hydrogen atoms and the terminal carbon atoms on the PEt_3 groups and the encapsulated nitrate anion have been omitted for clarity.

Stang and co-workers have made significant contributions to the development of symmetrical coordination cages and have written widely on strategies for coordination cage design and formation.[124–126] Ariga *et al* recently published the *Challenges and breakthroughs in recent research on self-assembly*[127] which describes the evolution of cage and capsule chemistry

as well as the synthetic challenges associated with the use of self-assembly to generate coordination cages.

1.1.5 Crystal engineering and supramolecular chemistry

The recent advances in understanding of supramolecular science allow innovators and researchers to use the supramolecular approach to chemistry to rationally design, synthesise and tune functional zero-, one-, two- and three-dimensional assemblies of interest with a reasonable idea of the properties these systems will possess. For example, the $(Cu^{I}[C(C_6H_4.CN)_4])_n^{n+}$ network described by Robson and Hoskins (discussed in Section 1.2.6) was envisaged as forming a network with the topology of diamond prior to its synthesis.[128] Using an understanding of how self-assembly occurs and the rules that govern the connectivity and arrangement of components in a crystal to deliberately design crystalline materials is known as *crystal engineering*. For decades, Desiraju has been active in the field of crystal engineering and is widely acknowledged as a world-leader in the area. According to Desiraju, "Crystal engineering has considerable overlap with supramolecular chemistry"[129] and "The aim of crystal engineering is to establish reliable connections between molecular and supramolecular structure on the basis of intermolecular interactions".[134] Desiraju's papers in this area show how the field of crystal engineering has both relied upon and informed thse area of supramolecular chemistry and has co-evolved with it.[14,96,129,131–134]

A common approach to the engineering of coordination polymers (CPs) used by crystal engineers is the 'net-based' approach to design[135] first described by Robson and Hoskins in 1989.[128] In this approach, metal ions with specific coordination geometries are combined

with, normally, rigid bridging ligands of the correct geometry and denticity to generate networks with a target topology. This strategy can give rise to structured, energetically preferred, and in some cases, low density products, which are often porous.[96,100,136] This is a desirable feature in host materials, which is one reason why self-assembled coordination polymers, which have directional bonds between metals and ligands, are often used to generate target porous materials.[137] The net-based approach to the design and description of coordination polymers is described in the following section.

1.1.6 Network structures

Coordination polymers are crystalline materials that extend infinitely in one-, two- or three-dimensions and comprise metal cations linked by bridging ligands. As 2D or 3D coordination polymers they can form networks that are commonly referred to as metal-organic frameworks (MOFs). Coordination polymers have received a great deal of attention in recent years for their potential use as materials that, amongst other applications, can sequester guest molecules such as pollutants and act as catalysts and sensors. Two notable examples of CPs that are porous in nature are 'MOF-5' and 'UiO-66'. MOF-5 (Figure 1.9) has received considerable attention due to its stability and its high porosity, with approximately 80% non-framework space in the material. It features Zn_4O units that are in a simple cubic arrangement and act as octahedral nodes that are bridged by 1,4-benzenedicarboxylate ligands. Its guest selectivity and gas sorption properties have been extensively studied.

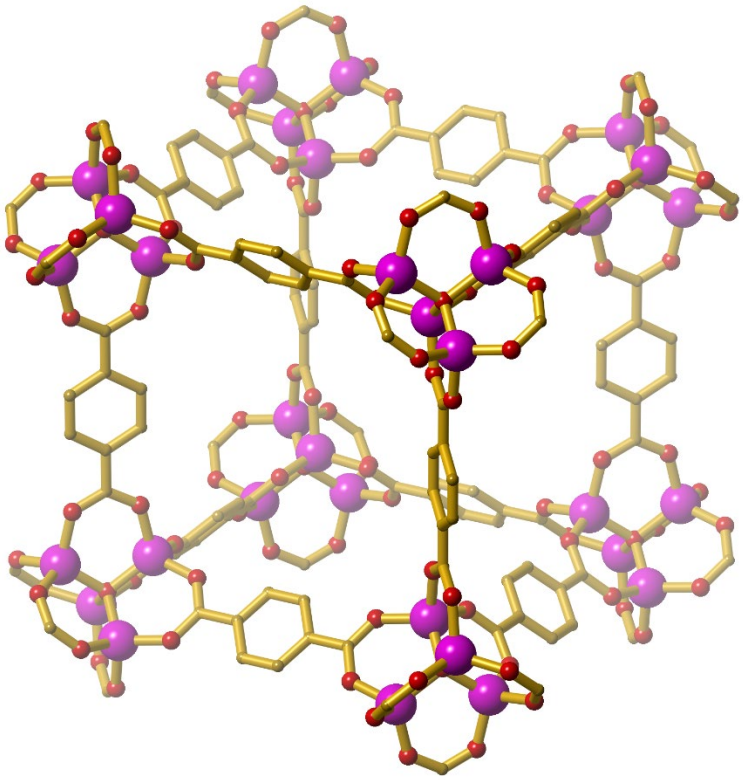

Figure 1.9 A ball and stick representation of MOF-5. Zn^{II} centres are represented by pink spheres. Hydrogen atoms have been omitted for clarity.

UiO-66 also contains metal – oxygen clusters linked by 1,4-benzenedicarboxylate bridging ligands.[138] The clusters consist of six Zr(IV) centres located at the vertices of an octahedron. Either oxide or hydroxide ions serve as μ_3 anions that occupy each triangular face of the octahedron. Carboxylate groups, coordinating in a μ_2 fashion are located along each of the twelve edges of the octahedron. Thus each $Zr_6(OH)_4O_4$ octahedron serves as a 12-connecting node in this cubic network material that has the same topology as the face-centred cubic network. UiO-66 is known for its stability towards attack by water and, as with MOF-5, its porosity has been extensively investigated.

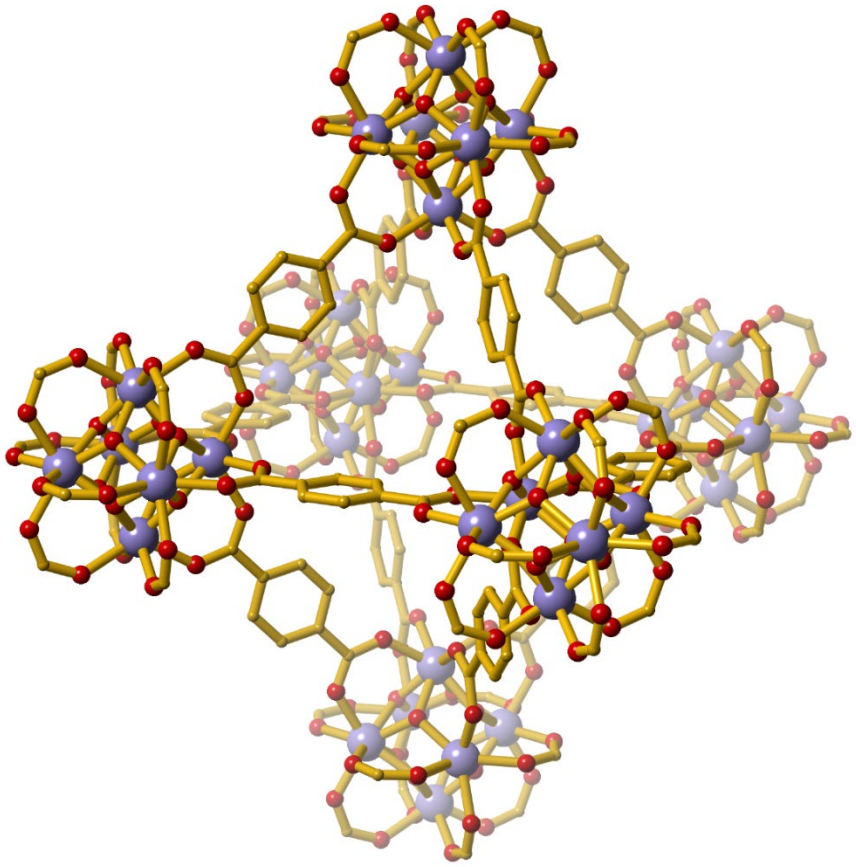

Figure 1.10 A ball and stick representation of a part of UiO-66. Purple spheres represent Zr^{IV} centres. Hydrogen atoms have been omitted for clarity.

There are several 2D and 3D network topologies that commonly occur in natural systems as well as synthetic CPs. Four noteworthy nets, which are relevant to networks reported in this thesis, are described below. In these networks the nodes can be metal cations, ligands or a combination of both. The examples indicated below commonly have centres with regular geometries, however many CPs and hydrogen bonded assemblies possess centres which have irregular geometries, depending on the choice of metal cation and ligand. It should be noted that networks that share the same topology may appear very different to each other because of geometric distortions.

(6,3) net

The (6,3) net is a 2-dimensional network in which 3-connected centres form edge-shared 6-membered circuits. A simple example of this net is the arrangement of carbon atoms in sheets of graphite. Representations of the 6,3-net are presented in Figure 1.11. In the network shown at left in Figure 1.11 all the angles between centres are 120°. A topologically identical but geometrically very different network involving T-shaped centres is represented on the right in Figure 1.11.

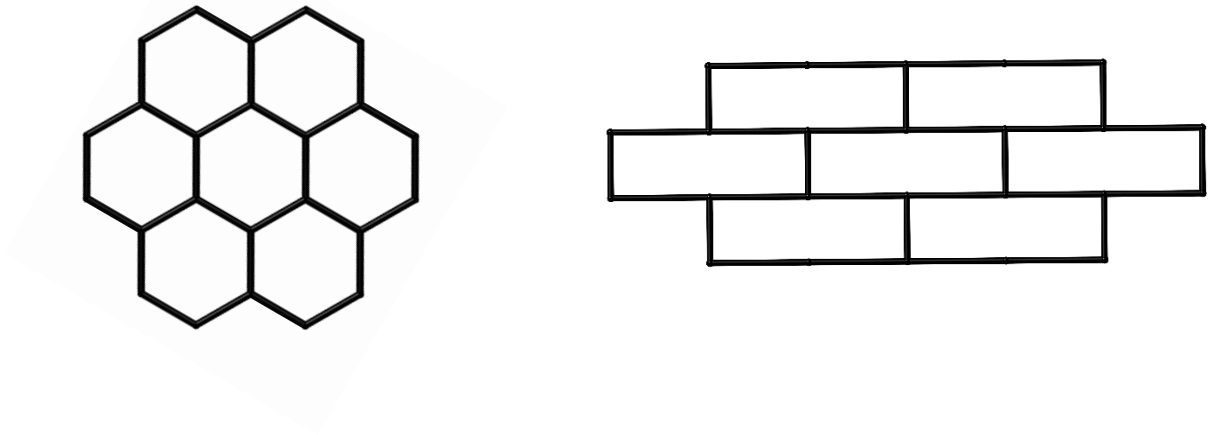

Figure 1.11 Representations of infinite 2D (6,3) nets with regular trigonal planar 3-connecting centres (left) and T-shaped connectors (right).

An example of a network with the (6,3) topology is the anionic coordination polymer, $[Zn_2(can)_3]_n^{2n-}$ in the compound $(Et_4N)_2[Zn_2(can)_3]\cdot$solvate reported by Robson and coworkers (where can = chloranilate, $C_6Cl_2O_4^{2-}$).[139] In this structure, chloranilate ligands serve as bridges between Zn^{2+} centres. Each Zn^{2+} is a 3-connecting node, and all Zn^{2+} centres lie in a plane (Figure 1.12). In the crystal structure of $(Et_4N)_2[Zn_2(can)_3]\cdot$solvate the (6,3) networks stack directly atop each other, giving rise to infinite hexagonal channels which host solvent molecules.

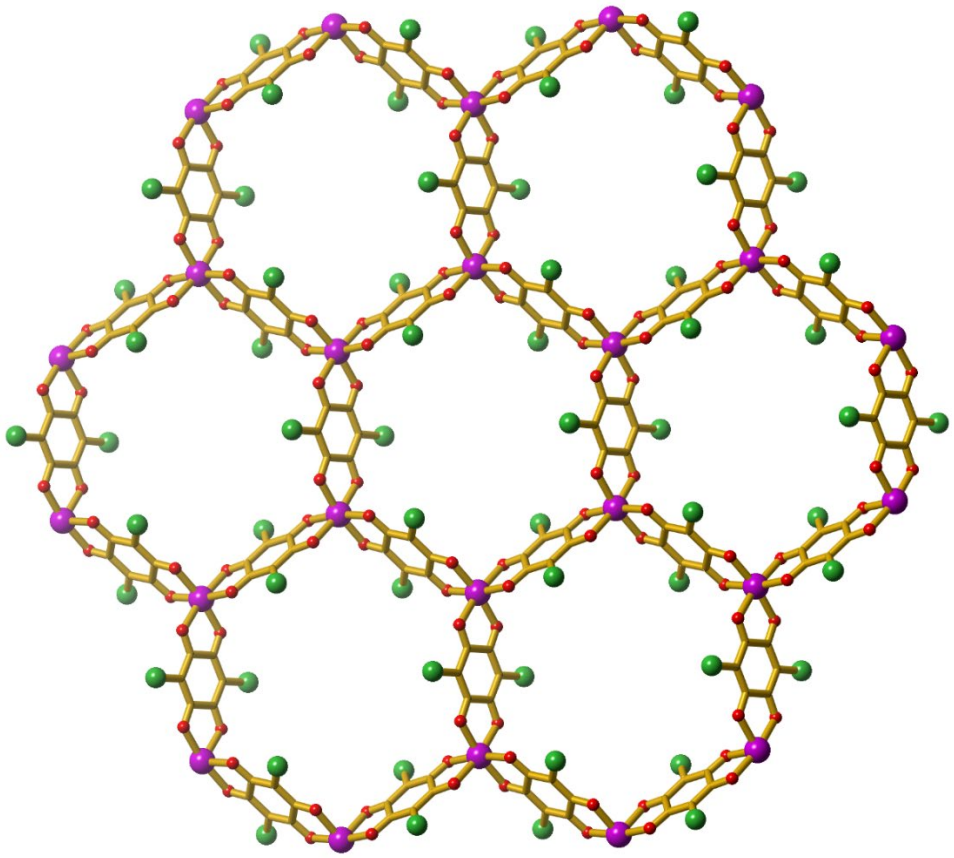

Figure 1.12 A ball and stick representation of a part of one layer of the (6,3) network in the crystal structure of $(Et_4N)_2[Zn_2(can)_3]\cdot$solvate. Pink spheres represent Zn^{2+} centres and green spheres represent chlorine atoms.

Hydrogen bonds can also lead to the formation of network materials. An archetypal example of a hydrogen-bonded (6,3) net is the 1:1 complex formed between cyanuric acid and melamine. In the crystal structure of melamine-cyanuric acid reported by Rao and coworkers, each cyanuric acid is a 3-connecting node and each melamine is a 3-connecting node (Figure 1.13).[130] Both molecules have 3-fold rotational symmetry. The cyanuric acid units form nine hydrogen bonds to three neighbouring melamine units. In six of its nine hydrogen bonds the cyanuric acid is the hydrogen bond acceptor and in three it is the donor. The melamine-cyanuric acid network represents a particularly elegant example of complementarity.

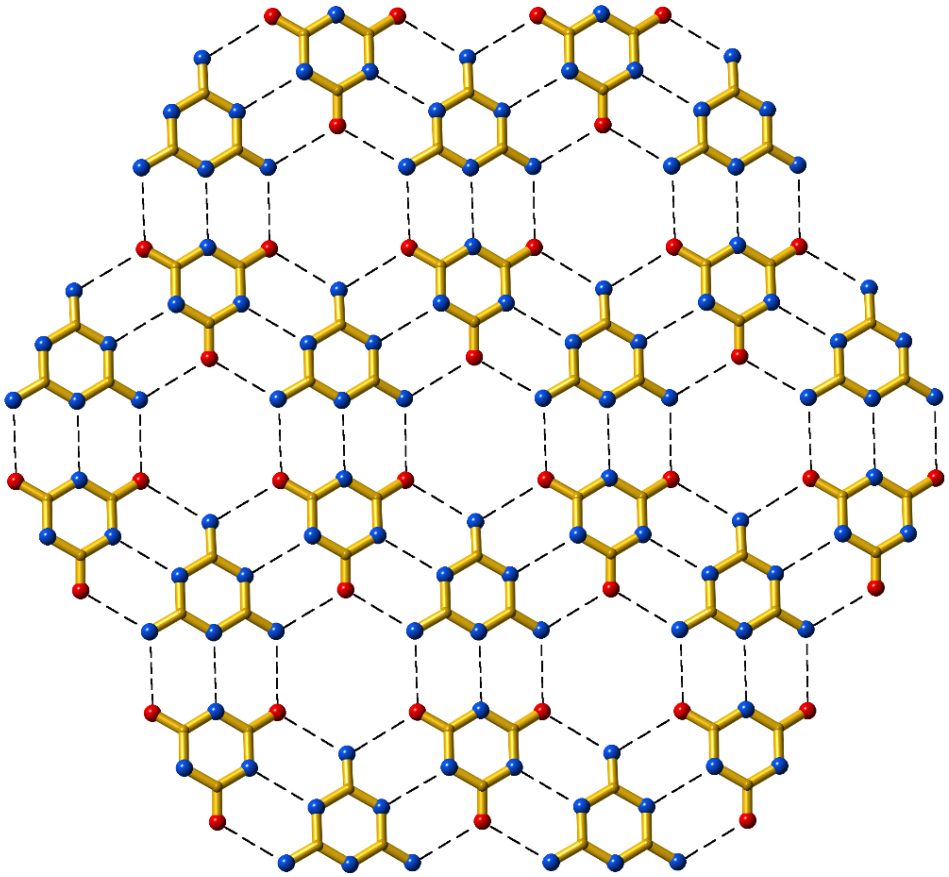

Figure 1.13 A ball and stick representation of the hydrogen bonded (6,3) net formed with a 1:1 ratio of cyanuric acid and melamine. Dashed lines indicate hydrogen bonds. Hydrogen atoms have been omitted for clarity.

Other relevant examples of hydrogen bonded (6,3) nets include Ward's guanidinium sulfonates, which can host guests between the layers of the networks,[140] and the (6,3) net composed only of trimesic acid, which takes the form of undulating sheets, by forming pairs of self-complementary hydrogen bonds via carboxylic acid groups.[141]

(10,3)-a net

The (10,3)-*a* net, first described in the 1950s by Wells[142], is a 3D network that has cubic symmetry and is inherently chiral.[143] An example of this net in its most symmetrical form

is found in the arrangement of the silicon centres in the crystal structure of $SrSi_2$. This net is characterised by several features: it contains 3-connecting nodes, the shortest circuit has ten nodes, and fourfold helices run parallel to each of the three crystallographic axes (Figure 1.14). All fourfold helices have the same handedness.

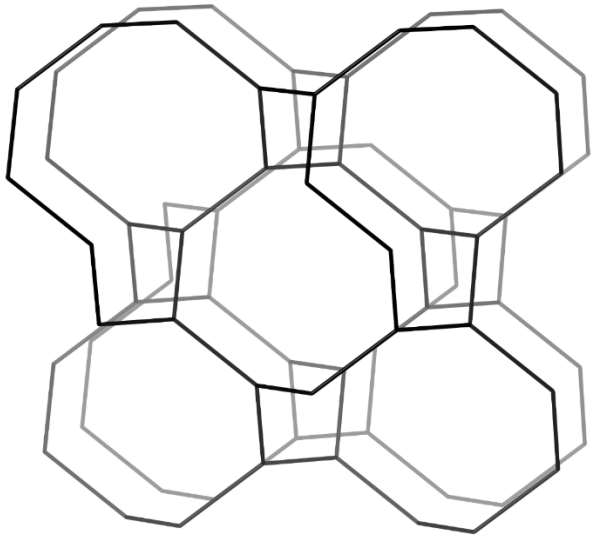

Figure 1.14 Part of a (10,3)-*a* net.

Robson, Abrahams and coworkers showed that (10,3)-*a* nets can be generated using chloranilate by selecting appropriate divalent metal cations and counter cations.[144] For example, the (10,3)-*a* network in the compound of formula $(NBu_4)_2[Zn_2(can)_3]\cdot 3MeOH$ consists of a $[Zn_2(can)_3]^{2-}$ anionic network (Figure 1.15) with NBu_4^+ serving as the countercation, whereas combining an octahedral metal centre with chloranilate in the presence of the Et_4N^+ cation results in the formation of the (6,3) net described earlier. In both cases the ligands act as bridges between three-connecting divalent metal cations. In the case of the (10,3)-*a* network however, the metal centres all have the same absolute configuration (either all Λ or all Δ, except in special cases where all ligands around the metal centre lie in

a plane) whereas in the 6,3 network the configuration of the metal centres alternates, with metal centres existing in both Λ and Δ configurations within the 2D network. In the crystal structure of $(NBu_4)_2[Zn_2(can)_3]\cdot 3MeOH$, two interpenetrated $[Zn_2(can)_3]_n^{2n-}$ networks are present. A single $[Zn_2(can)_3]_n^{2n-}$ network is depicted in Figure 1.15.

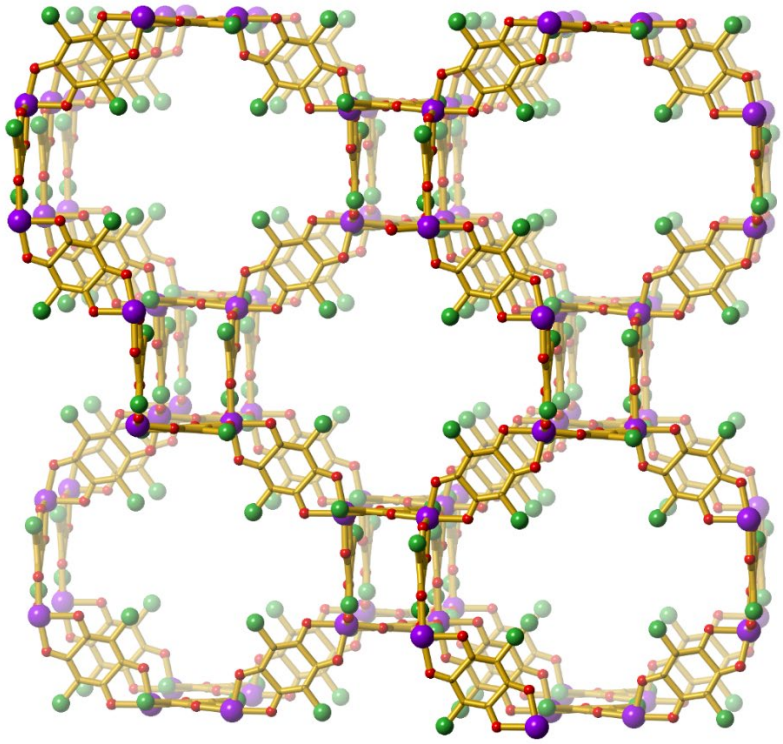

Figure 1.15 A ball and stick representation of one of the two interpenetrated (10,3)-*a* nets of formula $[Zn_2(can)_3]_n^{2n-}$ in the compound $(NBu_4)_2[Zn_2(can)_3]\cdot 3MeOH$. Purple spheres represent Zn^{2+} centres and green spheres represent chlorine atoms. Hydrogen atoms have been omitted for clarity.

Diamond

In diamond, tetrahedral carbon centres are linked in a 3D network with each C-C bond being perfectly staggered. The unit cell is face-centred cubic and consists of eight carbon atoms, with carbon atoms at each of the unit cell vertices and at the centre of each face; in addition half of the tetrahedral holes are occupied by carbon atoms. The connectivity of diamond is

represented in Figure 1.16. A key substructure within the diamond network is the adamantane unit, which consists of four fused six-membered rings in the cyclohexane chair conformation.

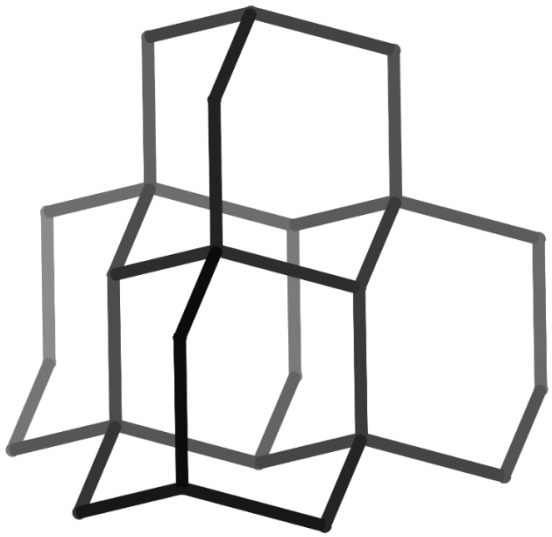

Figure 1.16 Part of the structure of diamond showing four adamantane-type units.

An example of a network possessing the diamond topology is the rationally designed $(Cu^{I}[C(C_6H_4.CN)_4])_n^{n+}$ coordination polymer reported by Robson and Hoskins in which tetrahedral Cu^{I} centres assemble with tetrahedral 4,4',4",4'"-tetracyanotetraphenylmethane (tccp) ligands (Figure 1.17).[128] Both metal cation and the ligand were chosen on the basis of their geometry, with the tccp ligand having arms extending in a tetrahedral arrangement and the Cu^{+} centre having a preference for tetrahedral geometry. The combination of the tetracyano ligand and Cu^{I} centre generates a diamond-type network in which $NC\text{-}C_6H_4$ "rods" link a tetrahedral C atom and Cu^{I} centre. Replacement of the C-C covalent bonds in the dense structure of diamond with relatively long $Cu\text{-}NC\text{-}C_6H_4\text{-}C$ connections results in extensive intraframework spaces in the crystal structure that are occupied by solvent and counteranions.

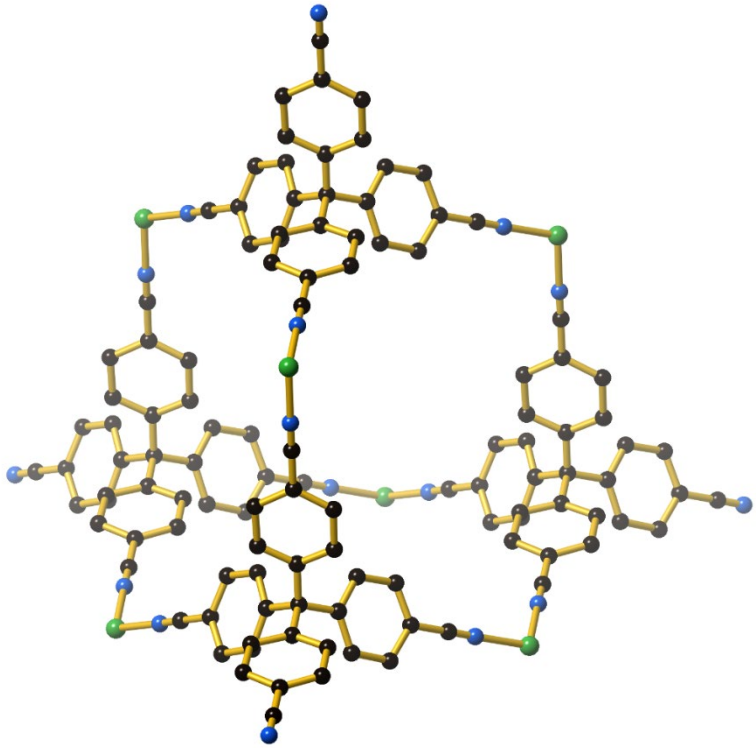

Figure 1.17 A ball and stick representation of an adamantane-type unit in the diamond framework of $(Cu^{I}[C(C_6H_4.CN)_4])_n^{n+}$ reported by Robson and Hoskins. Green spheres represent Cu^{+} centres. Hydrogen atoms have been omitted for clarity.

Platinum Sulfide

In the crystal structure of $Pt^{II}S$, there are two types of nodes. The Pt^{2+} centres serve as square planar nodes while the S^{2-} centres are tetrahedral nodes. In this 3D network, square planar nodes are only linked to tetrahedral nodes and vice versa. In coordination polymers the role of the tetrahedral and planar 4-connecting centres may be played by metal ions and/or ligands.

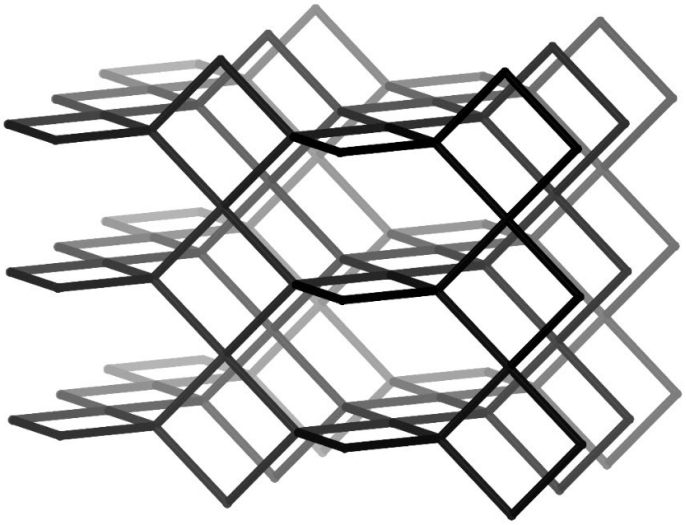

Figure 1.18 Part of the 3D network with the topology of PtS.

An example of a CP that was deliberately designed to have the topology of PtS is the $[[Cu(II)(tpp)Cu(I)]_n]^{n+}$ (tpp = 5,10,15,20-tetra(4-pyridyl)-21*H*,23*H*-porphine, shown in Figure 1.19) network in the compound $[Cu(II)(tpp)Cu(I)]BF_4 \cdot$solvate, reported by Robson and coworkers (Figure 1.20).[145] [Cu(II)(tpp)] was chosen as the square planar node, due to its four pyridyl donor groups which allow the [Cu(II)(tpp)] to serve as a planar 4-connecting centre. Cu(I) was again selected as the tetrahedral node due to its tendency to adopt a tetrahedral coordination geometry when combined with N-donor ligands such as pyridyl.

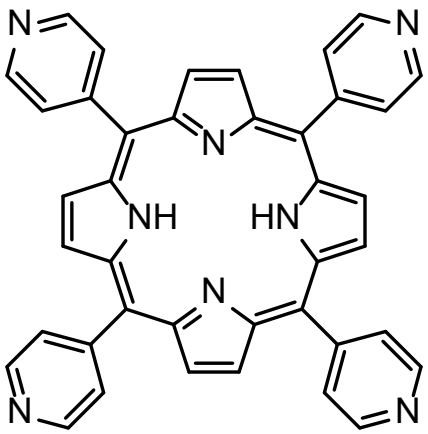

Figure 1.19 A schematic representation of the 5,10,15,20-tetra(4-pyridyl)-21*H*,23*H*-porphine ligand that can act as a square planar node.

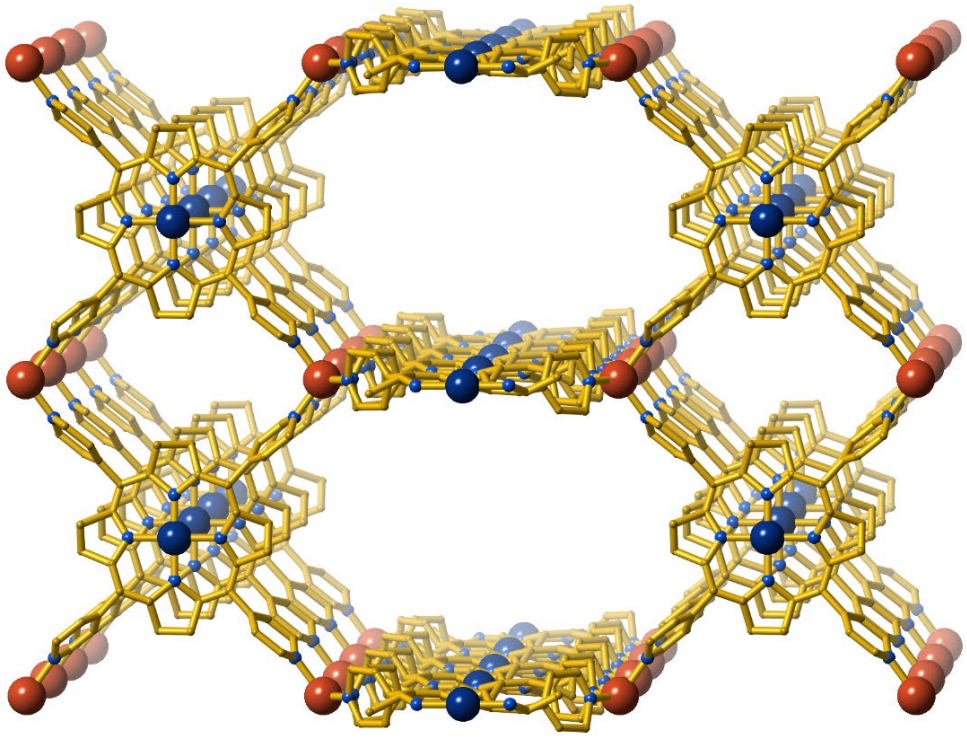

Figure 1.20 A ball and stick representation of the $[[Cu(II)(tpp)Cu(I)]_n]^{n+}$ net of PtS topology in the compound of formula $[Cu(II)(tpp)Cu(I)]BF_4$.solvate. Red spheres represent Cu(II) centres and blue spheres represent Cu(I) centres. Hydrogen atoms have been omitted for clarity.

1.2 Catechol-related Supramolecular Systems

The focus in this thesis is on the *tris*(catechol) ligand, cyclotricatechylene which forms a variety of supramolecular assemblies. The following discussion provides background related to supramolecular assemblies described in the following chapters .

1.2.1 Cyclotriveratrylene

Cyclotricatechylene (ctc, $C_{21}H_{18}O_6$, Figure 1.21 Right) is closely related to cyclotriveratrylene (ctv, $C_{27}H_{30}O_6$, Figure 1.21 Left). Molecules in the cyclotriveratrylene family are rigid cavitands that are preorganised to bind guest molecules in their bowl-shaped cavities in a similar fashion to calixarenes. Cyclotriveratrylene and its derivatives have been extensively studied with respect to their host-guest and coordination chemistry. Ctv and ctc can adopt a chair (or 'saddle') conformation, however studies of supramolecular assemblies of these compounds reveal that they almost exclusively adopt a crown or bowl-shaped conformation in the solid state.[146,147]

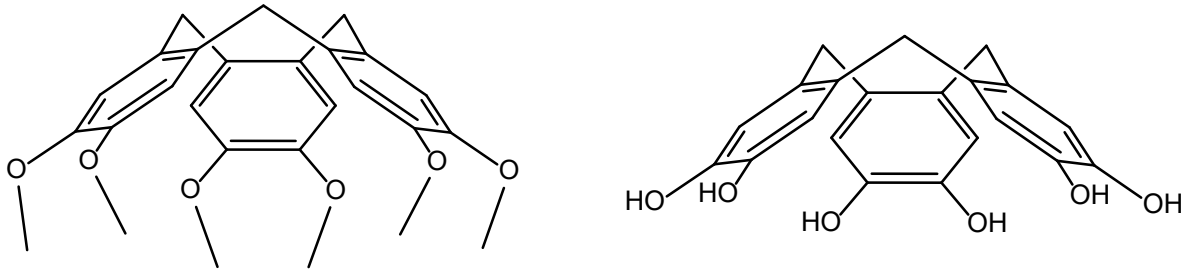

Figure 1.21 Left: A schematic representation of cyclotriveratrylene (ctv) in its crown conformation. Right: A schematic representation of cyclotricatechylene (ctc) in its crown conformation

The compound ctv was first reported in 1915 by Gertrude Maud Robinson,[147] and its inclusion properties were first described by Bhagwat in 1931.[146] As a bowl-shaped molecule, ctv has been shown to host various small molecules, including methylene chloride,

DMSO, ethanol and xenon. Notable examples of the host-guest chemistry of ctv are its 'ball and socket' inclusion compounds with fullerenes first reported by Atwood and coworkers, in which a molecule of C_{60} sits within the bowl of a single ctv molecule.[148]

Hardie and coworkers have been major contributors to the area of the supramolecular chemistry of ctv.[149,150,159–166,151–158] As well as investigating the host-guest properties of ctv and its derivatives, such as the inclusion of C_{70},[162] they have also shown that ctv has interesting supramolecular chemistry beyond inclusion compounds. For example, ctv forms 1D polymers when combined with alkali metal cations (Cs^+, Rb^+ and K^+) in the presence of icosahedral $[CB_{11}H_{12}]^-$ and DMF, such as in the compound $[Cs(ctv)_2(H_2O)_3(DMF)_2](CB_{11}H_{12})$, one unit of which is shown in Figure 1.22.[149] In this compound, the methoxy oxygen atoms from two of the ctv arms chelate disordered Cs^+ cations. Each unit is bridged by two water molecules (shown in the figure) to an adjacent unit. Each ctv contains a DMF guest and $[CB_{11}H_{12}]^-$ counterions are located between the chains.

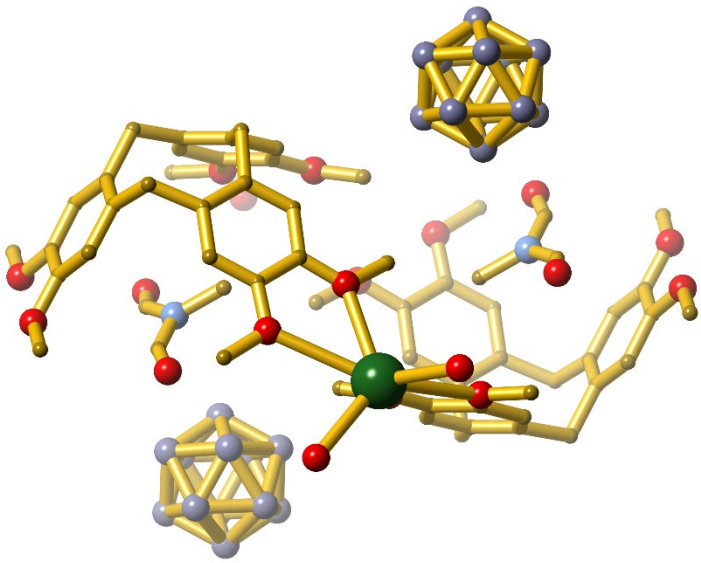

Figure 1.22 A ball and stick representation of one unit of Hardie's $[Cs(ctv)_2(H_2O)_3(DMF)_2](CB_{11}H_{12})$. Disorder associated with the Cs^+ cations, DMF and $[CB_{11}H_{12}]^-$ is not indicated. Hydrogen atoms have been omitted for clarity.

Hardie and coworkers have also reported the synthesis of large molecular cage compounds of ctv derivatives with coordinate bonds to transition metal centres. One of these contains two *hexakis*(isonicotinoyl)cyclotricatechylene units fused together by six Co^{II} cations (Figure 1.23), which resembles the calixarene dimers described earlier.[150] The solvent-accessible void space in the compound is significant, accounting for approximately 60% of the unit cell volume. The cages in the compound of formula $[Co_3(H_2O)_6$(hexakis(isonicotinoyl)cyclotricatechylene$)_2](NO_3)_6 \cdot$n(DMF) are connected to each other, forming a 2D coordination polymer.

Several larger cages with ctv derivatives have been reported which contain an even greater void volume. In one example of a large cage assembly, six ctv-derived ligands form part of a spherical M_6L_8 assembly comprising *tris*(isonicotinoyl)cyclotriguaiacylene and Pd^{II}

(Figure 1.24).[164] Because this assembly contains large solvent filled voids, unsurprisingly, crystals of the compound rapidly deteriorate when removed from their mother liquor.

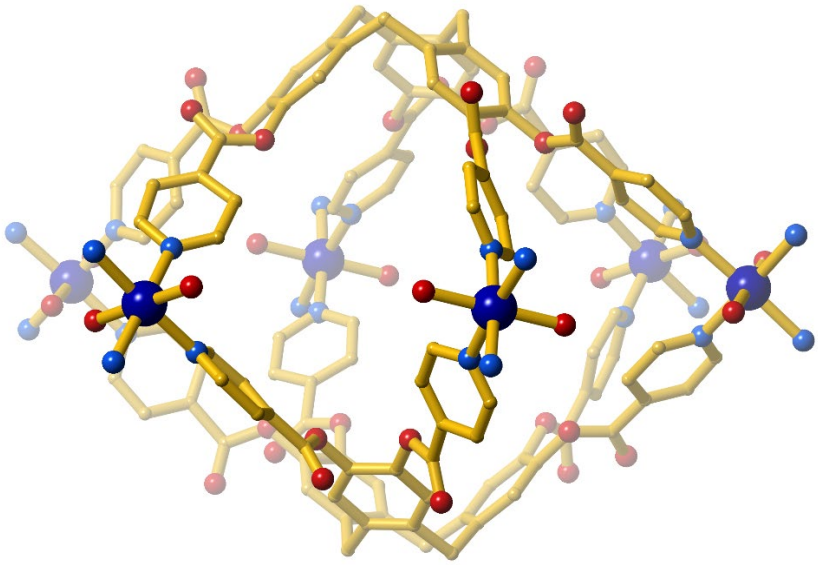

Figure 1.23 A ball and stick representation of the M_6L_2 assembly in the crystal structure of $[Co_3(H_2O)_6$(*hexakis*(isonicotinoyl)cyclotricatechylene$)_2]\cdot(NO_3)_6\cdot$n(DMF). Co^{II} centres are shown as dark blue spheres. Hydrogen atoms have been omitted for clarity.

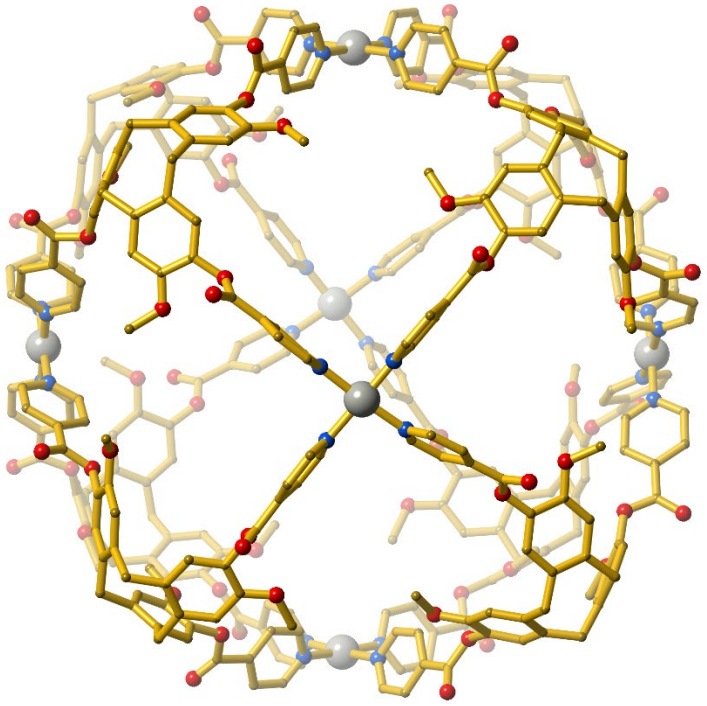

Figure 1.24 A ball and stick representation of the M_6L_8 assembly in the crystal structure of $[Pd_6(tris(isonicotinoyl)\text{-}cyclotriguaiacylene)_8](NO_3)_{12}\cdot n(DMSO)\cdot m(H_2O)$. Pd^{II} centres are shown as grey spheres. Hydrogen atoms have been omitted for clarity.

Other important derivatives of ctv in the literature are the cryptophanes, which are molecules containing two ctv moieties that have been covalently bonded together to form a capsule type molecule. Cryptophanes, such as the one shown in Figure 1.25, reported by Brotin and coworkers, have been shown to host environmentally and medically significant guests such as Cs^+ and Xe, respectively.[167–173]

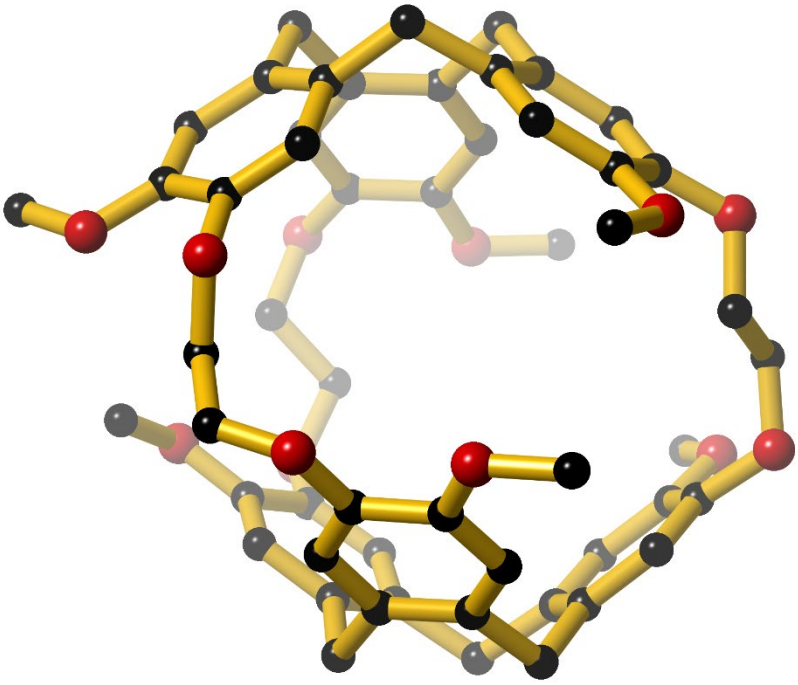

Figure 1.25 A ball and stick representation of a cryptophane reported by Brotin and coworkers. Hydrogen atoms have been omitted for clarity.

With a variety of coordination compounds of ctv and its substituted derivatives having been reported, it is anticipated that ctc should also exhibit a rich coordination chemistry associated with its three catechol groups being potentially able to bind metal centres.

1.2.2 Catechol-containing compounds in supramolecular chemistry

Catechol (cat, 1,2-dihydroxybenzene) is an important moiety in biology, and the catechol moiety is present in many biological molecules such as hormones and antioxidants. It has also become very important in supramolecular chemistry, with protonated catechol-containing compounds able to form hydrogen bonded supramolecular assemblies, such as the architectures formed through the solid state self-assembly of triptycene-based catechol

derivatives.[174] The catechol unit can also act as a Lewis base that strongly and predictably coordinates Lewis acidic centres, frequently metal cations, usually in a bidentate chelating mode.[175] This is possible when catechol is protonated, but most commonly occurs when catechol has been deprotonated and is present as the catecholate dianion (cat^{2-}). Both the entropy driven chelate effect and the electrostatic attraction between the cat^{2-} and the cationic metal centre contributes to the stability of the resultant coordinate bond. The ability of catechol to bind strongly and predictably to a wide range of metal centres makes it a desirable moiety to include in a supramolecular building block. Additionally, catechols can form covalent bonds to *p*-block elements such as silicon and boron using synthetic techniques similar to those used to generate coordination architectures.

Catechol is a redox-active species whose dianion can undergo a one electron oxidation to a semiquinone form or a two-electron oxidation to 1,2-benzoquinone (Figure 1.26). Catechol-containing compounds are therefore useful building blocks in redox-active materials.[175,176] Furthermore, the incorporation of catechol-containing ligands in multi-metal systems may give rise to interesting (tunable) magnetic properties due to the different spin states of the various oxidation states.[177]

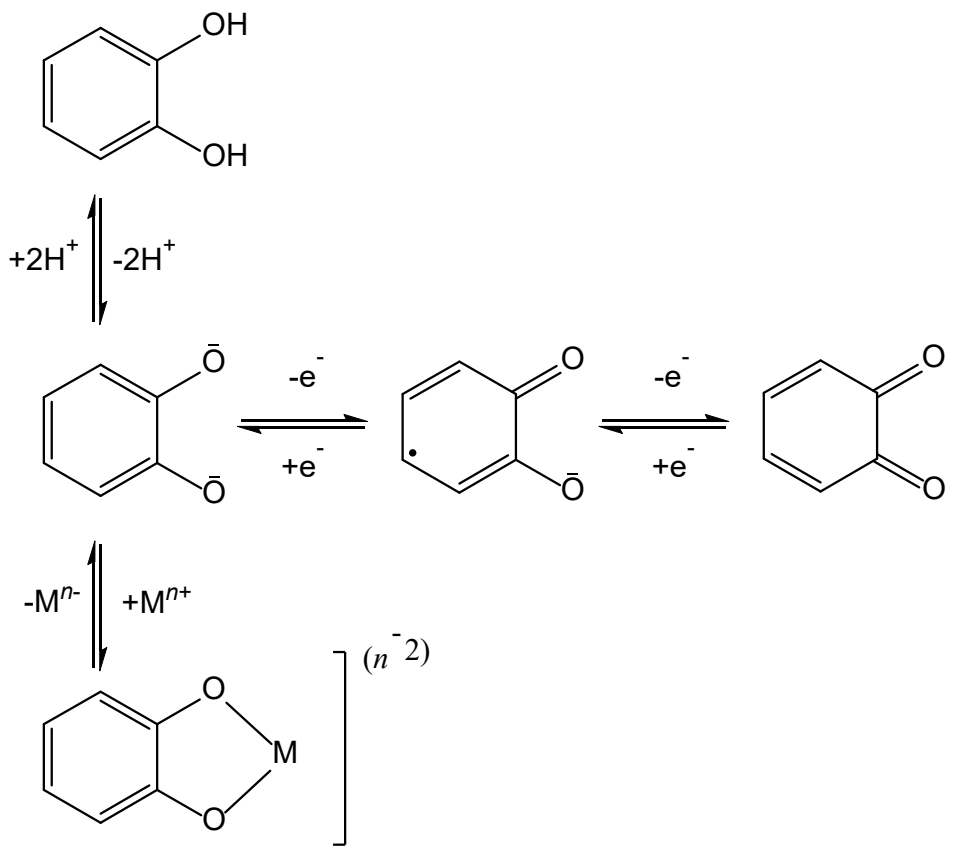

Figure 1.26 Top: A schematic representation of catechol. Middle: common oxidation states arising from the catecholate anion. The radical semiquinone (centre) is only shown here in one of its possible resonance forms. Bottom: schematic of a metal-catecholate chelate with a stable 5 membered chelate ring (M= metal cation of charge n^+).

Nature employs various polydentate ligands as metal scavengers. These ligands possess an appropriate size, shape and electronic properties to bind a given metal ion with high affinity, specificity and produce a complex with high thermodynamic stability. An important metal ion scavenger is the *tris*-catechol enterobactin (ent, Figure 1.27) which scavenges Fe^{III} and has an extremely large formal stability constant of 10^{49} for aqueous Fe^{III} when deprotonated (pFe^{III} = 35.5).[178–180] This chelating agent is not only predisposed to bind Fe^{III} in a highly stable octahedral *tris*-bidentate manner (shown in Figure 1.27 right, as determined by Nolan and coworkers) but also adopts a configuration that allows it to "prospect" for iron and rapidly bind it following a change in orientation of its catecholamide groups. Enterobactin

has inspired the investigation of many catechol-based chelating agents as metal scavengers and, as discussed later in this thesis, as building blocks for the generation of zero, one, two and three-dimensional coordination and covalent assemblies.

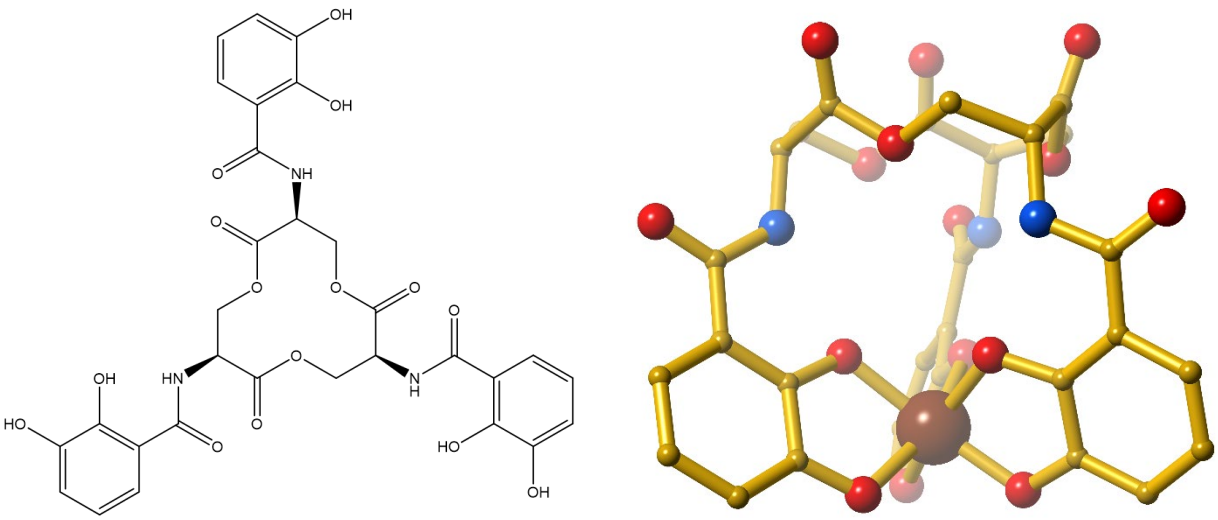

Figure 1.27 Left: A structural representation of the biological *tris*-catechol enterobactin. Right: A ball and stick representation of $[Fe(ent)]^{3-}$. Fe^{III} centres are represented by brown spheres. Hydrogen atoms have been omitted for clarity.

Various *bis*- and *tris*- catechols have been investigated for their ability to form supramolecular assemblies. Raymond, in particular, has been prolific in his investigations of supramolecular assemblies of catechol-containing ligands, including metal complexes of enterobactin.[178,179,189–196,181–188] A relevant example of his work is a rationally designed tetrahedral L_4M_4 assembly containing four Ti^{IV} centres, each having a coordination geometry between trigonal-prismatic and octahedral, and four *tris*-catechol ligands.[184] The single bonds between the catechol groups and the central aromatic ring allow the catechol groups in the ligand to rotate such that they are orientated in a position that allows them to chelate to Ti^{IV} centres.

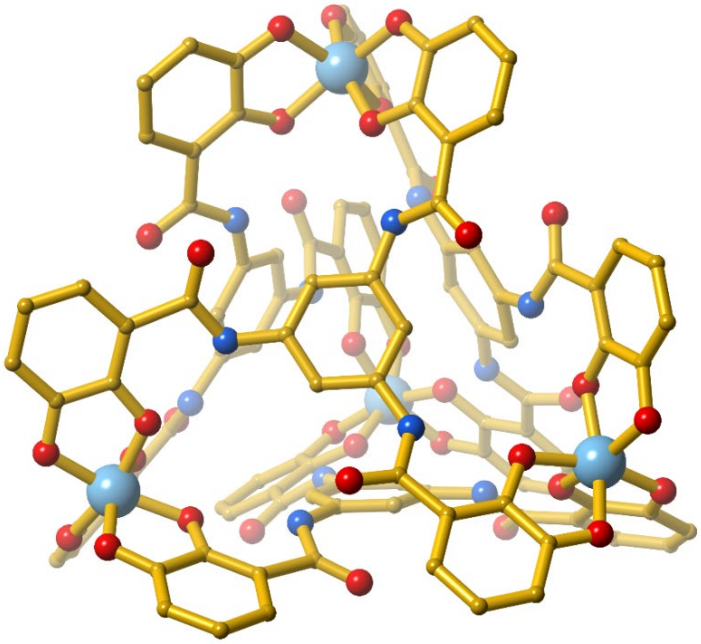

Figure 1.28 A ball and stick representation of Raymond's tetrahedral supramolecular Ti_4L_4 cluster. Ti^{IV} centres are represented by light blue spheres. Hydrogen atoms have been omitted for clarity.

Albrecht, similarly, has provided plentiful examples of supramolecular metal-ligand assemblies based on *bis*- and *tris*-catechol ligands, including $[M_4L_4]$ tetrahedral assemblies similar to the above example from Raymond, but based on triangular acylhydrazone catechol ligands.[197,198]

Notably, Albrecht and co-workers have reported numerous $[M_2L_3]$ 'helicate' assemblies in which L is a *bis*-catechol ligand with terminal catechol moieties, as indicated in Figure 1.29.[70,199,200] A variety of assemblies were obtained, their features depending on 1) the metal cation, M in the assembly (usually a hard octahedral metal centre such as Ti^{IV} or Ga^{III}); 2) the geometric arrangement of the catecholate groups about the metal centre (Δ or Λ); 3) the identity of the organic linker bridging between the two catecholate groups (indicated by a wavy bond in Figure 1.29, often a diimine or aliphatic linker). In several examples, alkali metal cation guests such as Li^+ and Na^+ were present within the helicate cage.[70]

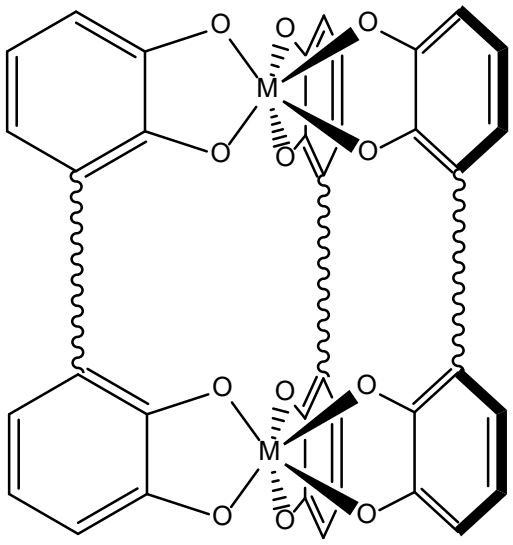

Figure 1.29 A schematic representation of the generic form of a [M_2L_3] helicate assembly. Wavy connections indicate a variety of organic links between the catecholate moieties.

Work within our group at the University of Melbourne has also focused on the generation of metallocages, macrocycles, metallocycles and coordination polymers using *bis*-catechol ligands including the spiro ligand (spiroH_4 - 3,3,3',3'-tetramethyl-1,1'-spirobisindane-5,5',6,6'-tetrol), the fluorone ligand (fluorH_4 - 9-phenyl-2,3,7-trihydroxy-6-fluorone) and a rigid angular ligand (rigidH_4 - tetrahydroxy-9,10-dimethyl-9,10-dihydro-9,10-ethanoanthracene) shown in Figure 1.30. These assemblies display structural diversity and interesting packing motifs.

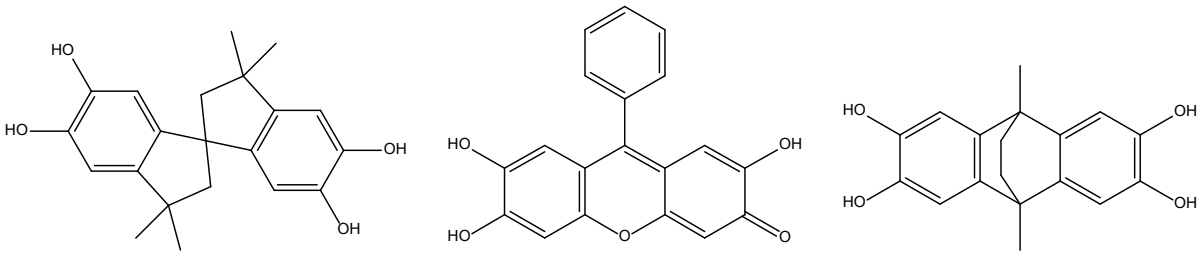

Figure 1.30 Left to right: Schematic representations of the spiro ligand, the fluorone ligand and the rigid angular ligand.

The spiro ligand (left in Figure 1.30) is a readily available, chiral *bis*-catechol ligand that can be used as a bent linker in covalent and metal-ligand assemblies. In early work with spiroH_4, Duhme and co-workers reported the formation of approximately square shaped [2+2] metallocycles comprising two MoO_2^{2+} units each chelated by two spiro^{4-} ligands.[201] Crystals of the compound of formula $Na_4[(MoO_2(spiro))_2]$ contain two types of metallocycles – Λ,Λ-$[(MoO_2(spiro))_2]^{4-}$ and Δ,Δ-$[(MoO_2(spiro))_2]^{4-}$ – which are enantiomers of each other.

Shea and coworkers also reported the formation of a square macrocycle containing spiro moieties. In this case, the [4+4] macrocycle was generated by combining phenyltriethoxysilane with spiroH_4. Whereas only two of the four corners in Duhme's metallocycle were formed by the spiro^{4-} ligands, all four corners of Shea's square macrocycle are formed by the ligands. The four silicon centres are each chelated by two spiro moieties and lie along the four edges of the square. Each macrocycle contain two of each of the spiro enantiomers, making the macrocycle itself achiral. The Robson-Abrahams group has reported that when spiroH_4 is combined with boron centres under solvothermal conditions, both [3+3] triangles[201] and [4+4] macrocycles[202] form (left and right, respectively in Figure 1.31). In a compound of formula $(Et_3NH)_4[B_4(spiro)_4]\cdot$solvate, each square macrocycle contains only spiro moieties of the same handedness that form the four corners, with boron centres located on the four edges. The single crystal structure determinations revealed a racemic mixture of macrocycles and infinite columns of macrocycle are present with each containing only one of the two enantiomers. The packing appears to be influenced by the counterions present, which lie in the plane of the columns, directly above and below each boron centre. A variety of ammonium-based cations have been reported to produce crystals of the macrocycle with similar packing arrangements.

Triangular macrocycles of formula $(Et_3NH)_3[B_3(spiro)_3]$·solvate are generated in a similar fashion to $(Et_3NH)_4[B_4(spiro)_4]$·solvate, but form after two to three weeks at room temperature from a methanolic solution. The triangular macrocycles also form infinite columns in the solid state, with columns containing macrocycles of one handedness interdigitating with columns of macrocycles of the other handedness. Like the square macrocycles, the triangular macrocycles can be generated with various protonated nitrogen-based cations.

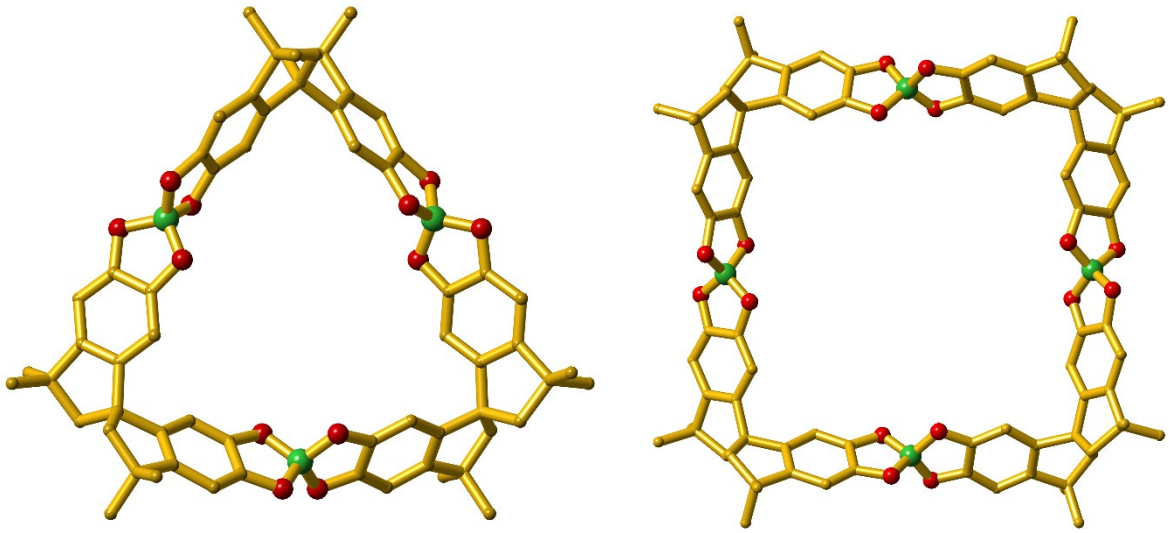

Figure 1.31 Left: A ball and stick representation of the triangular macrocycle of formula $[B_3(spiro)_3]^{3-}$ reported by Abrahams, Robson and co-workers. Right: A ball and stick representation of the square macrocycle of formula $[B_4(spiro)_4]^{4-}$ reported by Abrahams, Robson and co-workers. Green sphered represent B^{3+} centres. Hydrogen atoms have been omitted for clarity.

The fluorH_3 ligand (centre in figure 1.30), though not strictly a *bis*(catechol), has been shown to coordinate in a similar way to catechol. It is of interest because of its redox properties, as it able to be oxidised to a radical dianion, and for its potential to be used in spectrophotometric determination of metals. In combination with *cis*-$M^{VI}O_2^{2+}$ where M = W or Mo, square metallocycles of formula $[(MO_2)_4(fluor)_4]^{4-}$ form.[203] The four metal centres are located at the corners of the metallocycle and have a slightly distorted octahedral coordination

environment. The metal centres are chiral and alternate in absolute configuration – Λ, Δ, Λ, Δ – around the metallocycle. The four ligands in the metallocycle are all orientated such that the phenyl groups point away from the centre of the metallocycle at about a 45° angle to the plane of the four metal centres. In the solid state, the arrangement of metallocycles is determined by the countercations in the system.

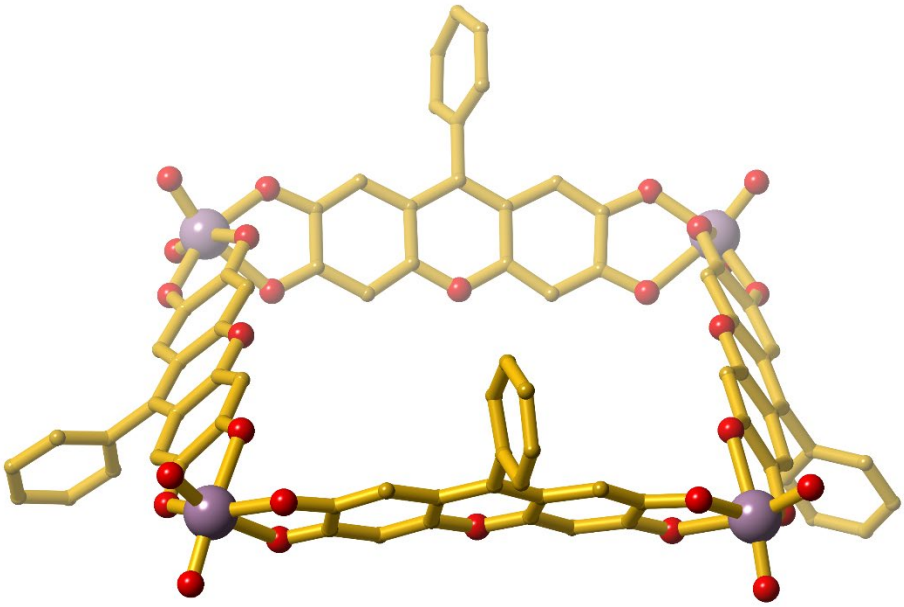

Figure 1.32 A ball and stick representation of the $[(MoO_2)_4(fluor)_4]^{4-}$ anion. The grey spheres represent Mo^{VI} centres. Hydrogen atoms have been omitted for clarity.

Few examples of metal complexes of the rigid *bis*-catechol, $rigidH_4$ (Figure 1.30 right), have been reported in the literature to date. Remarkably, prior to work commencing in our group, the only example was an 'octa-uranate' cage in a compound of formula $[HNEt_3]_8[(UO_2)_8(rigidH_2)_4(O_2)_8]\cdot 22H_2O$ reported by Thúery and Masci.[204] In this high symmetry assembly, four partially deprotonated rigid ligands act as bridges between two $[(UO_2)(O_2)]_4$ squares (Figure 1.33). In the crystal structures, the cages, which possess an

approximately spherical shape, pack in a body centred cubic arrangement with solvent and counterions between them.

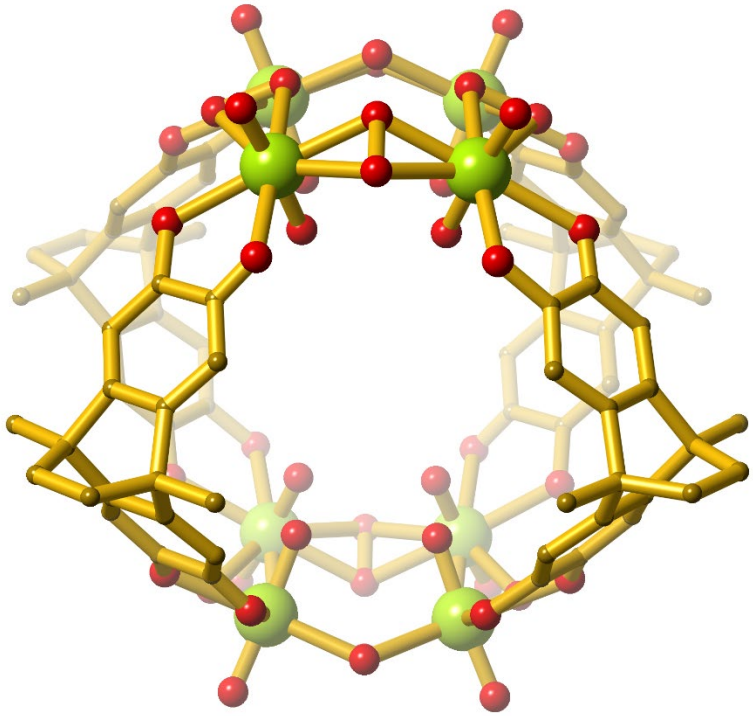

Figure 1.33 A ball and stick representation of the $[(UO_2)_8(rigidH_2)_4(O_2)_8]^{8-}$ octa-uranate cage reported by Thúery and Masci. Green spheres represent U^{VI} centres. Hydrogen atoms have been omitted for clarity.

Metallocycles can be generated with the rigid *bis*-catechol ligand, $rigidH_4$, including [4+4] metallocycles with W^{IV} and V^{IV}. While *bis*-catecholates have a propensity to form essentially planar macrocycles, the rigid ligand can combine with Nb^{V} centres to form a trigonal prismatic cage of formula $[(NbO)_{12}(OH)_6(rigid)_{12}]^{18-}$ and with Mn^{III} to form a bulky, hexagonal 'doughnut' assembly of formula $[Mn_{12}(H_2O)_{12}(rigid)_{12}]^{12-}$ (Figure 1.34).

The doughnut is a fascinating assembly that comprises two parts (shown in blue and yellow), each being composed of what resembles a [6+6] metallocycle in which each rigid ligand chelates two Mn^{III} centres and each Mn^{III} is chelated by two rigid ligands. An unusual feature of this assembly is that each rigid ligand not only chelates two Mn^{III} centres from one

hemisphere, it also binds in a *bis*-monodentate fashion to two Mn^{III} centres from the partner macrocycle, which 'fuses' the two pseudo-[6+6] metallocycles together.

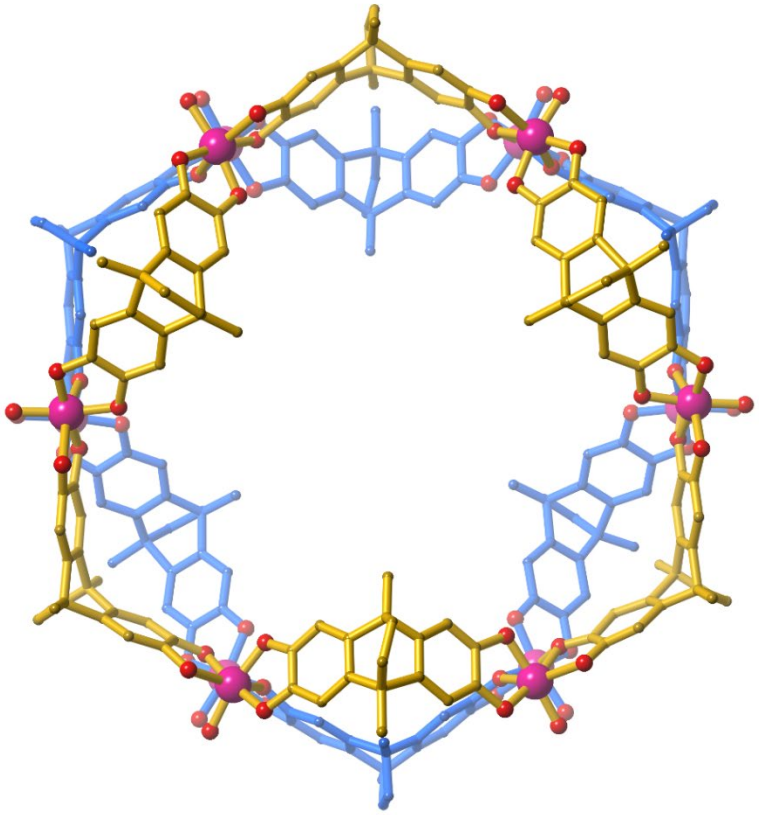

Figure 1.34 A ball and stick representation of the doughnut assembly of formula $[Mn_{12}(H_2O)_{12}(rigid)_{12}]^{12-}$. Each hemisphere is represented by a different colour. Pink spheres represent Mn^{III} centres. Hydrogen atoms have been omitted for clarity.

Halcrow and co-workers also synthesised and investigated three discrete assemblies of the rigid ligand, each chelated to two capped Pt^{II} centres, and found that all three complexes gave radical derivatives in electrochemical studies.[205]

The Robson-Abrahams group's success in generating fascinating assemblies with catecholate ligands combined with the rich supramolecular chemistry associated with ctv prompted our investigations into supramolecular assemblies of cyclotricatechylene.

1.2.3 Cyclotricatechylene

Cyclotricatechylene (10,15-Dihydro-5H-tribenzo[A,D,G]cyclononene-2,3,7,8,12,13-hexol) is a pyramidal, cyclic *tris*-catechol that is related to the more heavily studied ctv. $CtcH_6$ can be easily deprotonated and can carry a minus six charge when all six of its phenolic protons have been removed i.e. ctc^{6-}. Hereafter, $ctcH_6$ and its related anions will be referred to collectively as ctc.

$CtcH_6$ was first reported in 1965 by Lindsey when it was deliberately isolated during the study of cyclotriveratrylene and its derivatives. [206] The compound $ctcH_6$ can be synthesised in good yield from relatively inexpensive materials, and only the demethylation step of the synthesis requires special precautions. Crude $ctcH_6$ is a light grey powder that can be recrystallised from dioxane to form a colourless crystalline solvate. This solvate can be desolvated under inert atmosphere at temperatures above 100°C to afford pure $ctcH_6$. Though it is a redox-active molecule $ctcH_6$ is relatively stable towards aerial oxidation in the solid state. Its dioxane solvate obtained from recrystallization, however, discolours more quickly than the crude product obtained from Lindsey's synthesis.

$CtcH_6$ has many desirable features as a supramolecular building block. Its three catechol groups are divergent, which makes it an ideal candidate as a bridging ligand upon deprotonation. Some other *tris*-catechol complexes, such as enterobactin, are quite flexible and can orientate their catecholate groups in such a way that they chelate convergently to a single metal centre *or* divergently to multiple metal centres. Ctc is more rigid in nature and does not have as many available binding modes. As such, anions derived from $ctcH_6$ can chelate to multiple metal cations to generate extended coordination networks of zero, one,

two and three-dimensionality, but will not form a discrete complex with a single metal cation chelated by multiple catecholate groups from the same ctc ligand.

The additional negative charge donated into the ring by the phenolate moieties upon deprotonation of $ctcH_6$ makes the 'bowl' of the molecule the appropriate residence for cations of a certain size.

Some difficulties arise when working with cyclotricatechylene. It is hard to control the protonation state of the ligand without buffering the solution. Buffering is usually not an option as any additional chemical species present in a reaction matrix can influence both the assembly that is formed and the crystal packing. Although one can estimate how much strong base is necessary to deprotonate the average $ctcH_6$ molecule to a given anion, there is likely to be a distribution of anions in various protonation states. In the case where a very large excess of strong base is added, full deprotonation of the catechol oxygen atoms can be assumed but under such circumstances the ctc^{6-} anion is particularly susceptible to oxidation. The protonation level may also depend on what Lewis acid groups are present as these may increase the acidity of the six phenolic protons.

The susceptibility of ctc to oxidation, can lead to challenges in solution state reactions. Silver and copper 'mirrors' and may form when cyclotricatechylene is combined with these metal cations at elevated pH values. This does not prevent some ctc from forming supramolecular assemblies with the metals noted, however a mixture of solid products may form from experiments and the yield of the desired supramolecular assembly may be lowered due to the redox processes consuming both ctc and metal cations.

Notably, the redox chemistry of ctc has been investigated electrochemically by many groups and cyclotricatechylene has become important in electrochemical studies in which it is used in the selective electrochemical detection of cysteine. [207]

1.2.4 Supramolecular assemblies of cyclotricatechylene

Hyatt and coworkers were the first to report inclusion compounds of $ctcH_6$.[208] In 1980 they reported that a variety of small guest molecules could be hosted in the cavity of cyclotricatechylene and Hardie, Atwood and coworkers have subsequently reported several other solid-state inclusion compounds of ctc with small guests. These guests are predominantly solvent molecules including acetone, DMSO, HPMA, *N,N*-dimethylformamide, *N,N*-dimethylacetamide, *N*-pyrrolidone, propanol and water.[209–211] In all the inclusion compounds above, hydrogen bonding is observed between $ctcH_6$ units and in many cases is observed between solvent molecules and ctc.

Prior to our group commencing work with ctc, very few examples of assemblies of ctc with metal cations had been reported. In 1998, Bohle and Stasko reported an extended-rim assembly of ctc with capped Pt^{II} centres (Figure 1.35). [212] In this assembly, of formula $(ctc)[Pt(dppb)]_3$ (dppb = 1,2-*bis*(diphenylphosphino)benzene), each catechol is fully deprotonated and chelates to a Pt^{II} ion. The square planar platinum centres are capped by chelating dppb ligands. Cyclic voltammetry indicates that this compound can undergo three reversible one electron oxidations. This behavior is also reported for the analogous $(ctc)[Pt(dppfc)]_3$ compound (dppfc = diphenylphosphinoferrocene).

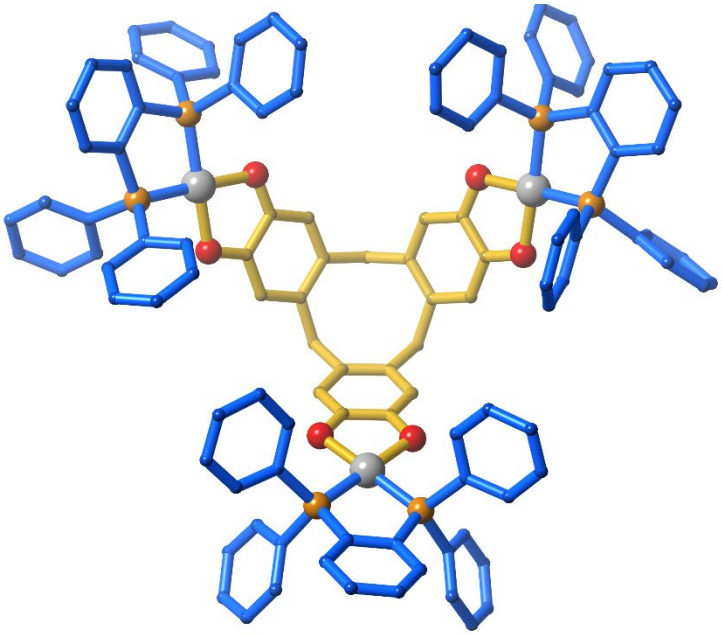

Figure 1.35 A ball and stick representation of a redox active, extended rim compound of formula (ctc)[Pt(dppb)]$_3$ reported by Bohle and Stasko. Diphenylphosphinobenzene ligands are shown in blue; Pt^{II} centres are represented by grey spheres; phosphorus atoms by orange spheres. Hydrogen atoms have been omitted for clarity.

Three extended rim Pt^{II} complexes of ctc were also investigated by Halcrow and co-workers in 2015.[205] The complexes contained the dppb, dppe (1,2-*bis*(diphenylphosphino)ethane and *t*Bu$_2$bipy (4,40-*bis*(*tert*-butyl)-2,20-bipyridyl) ligands respectively, and were shown to undergo stepwise oxidation of the ctc^{6-} catecholate moieties to the semiquinonate level.

Recent work performed by Purohit and co-workers reveals that attractive 'propeller' shaped supramolecular capsules form through hydrogen bonding and π-π interactions when ctcH$_6$ is combined with 4,4'-bipyridine, 2,2'-bipyridine or phenanthroline.[213] The capsule formed with phenanthroline is capable of enclosing a naphthalene or pyrene guest. Purohit has subsequently reported new assemblies of ctc with 9,10-phenanthraquinone and phenanthrene.[214]

Boronate esters of ctc are of interest for their properties such as stimuli responsiveness, gas uptake and host-guest chemistry. In 2007, Kubo and co-workers reported the formation of a heterodimeric capsule of ctc with a boronic acid-appended hexahomotrioxacalix[3]arene that was investigated using NMR. The capsule can incorporate NEt_4OAc as a guest.[215] In 2008 Kubo and coworkers also reported the formation of an organogel composed of ctc bound to 4-(4-octyloxybenzeneoxymethyl)phenylborane in toluene, which can undergo reversible gel-to-sol transitions when $HNEt_2$ is added and removed.[216] This compound is posited to have a 2D sheet structure that can be disrupted by chemical stimuli. Notably, in 2012 a highly porous boronate ester of ctc, 'CTC-COF' (Figure 1.36) was reported by Zheng and coworkers.[217]

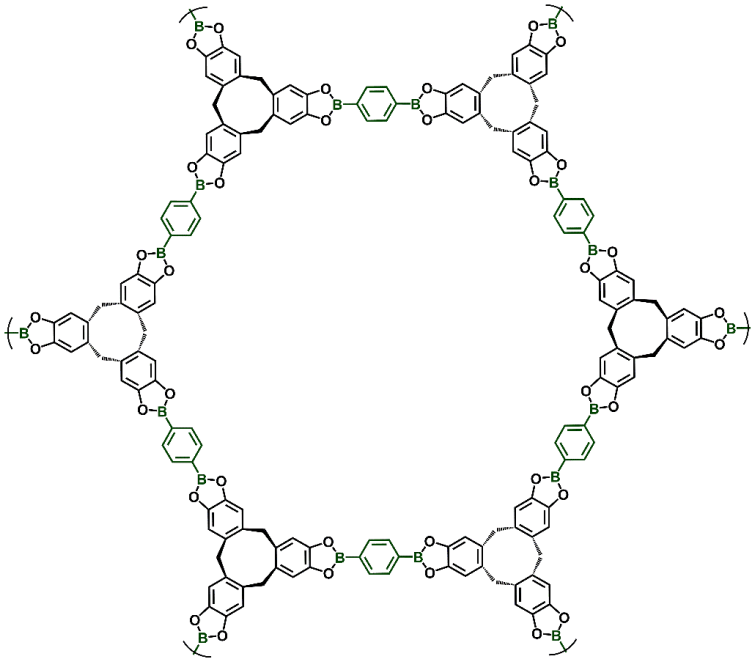

Figure 1.36 A schematic representation of the undulating hexagonal framework of CTC-COF.

This covalent organic framework was synthesised by the reaction of $ctcH_6$ with 1,4-benzenediboronic acid. The material contains stacked, undulating 2D sheets with hexagonal

pores of 2.26 nm cross-section (Figure 1.36). The material is reported to have a high surface area, comparable to COF-10[205], and a H_2 uptake/wt% of 1.2%. Other CTC-COF materials have since been reported.[218]

Work within the Robson-Abrahams group with the $ctcH_6$ ligand has yielded several host-guest assemblies and coordination cage compounds, which have been characterised by X-ray crystallography. The group has reported several inclusion compounds in which anions of cyclotricatechylene are combined with alkali metal cations. Most commonly these assemblies are clam-like dimers of partially deprotonated cyclotricatechylene units, which participate in six complementary hydrogen bonds that fuse the two $ctcH_n^{(6-n)-}$ units together.[219] An example of a clam-type dimer with an encapsulated Cs^+ is shown at the top-left of Figure 1.37. The closed-up ctc clams are host to unsolvated alkali metal cations, either Cs^+ or Rb^+ (but never smaller alkali metal cations), which associate with the electron-rich aromatic surfaces of both ctc bowls rather than the hydroxyl groups. Under the same conditions that yielded Cs^+ and Rb^+ clams, a different crystalline material of composition $K(ctcH_5)\cdot C_2H_5OH$ is formed when K^+ is used in place of the heavier alkali metal ions. K^+ associates with the bowl of one $ctcH_5^-$ anion but is not located equidistant from the three catechol(ate) π systems of the ctc. This suggests that potassium is too small to interact with all three aromatic rings from a single ctc unit at once. While approximately half of the space around the K^+ is occupied by a $ctcH_5^-$ bowl, the other hemisphere is bound to three oxygens from two adjacent $ctcH_5^-$ units and by an ethanol molecule, an arrangement resulting in bilayered chains as shown at the bottom in Figure 1.37. When larger cations such as tetramethylammonium are used, open clam-type structures are formed (top right in Figure 1.37)

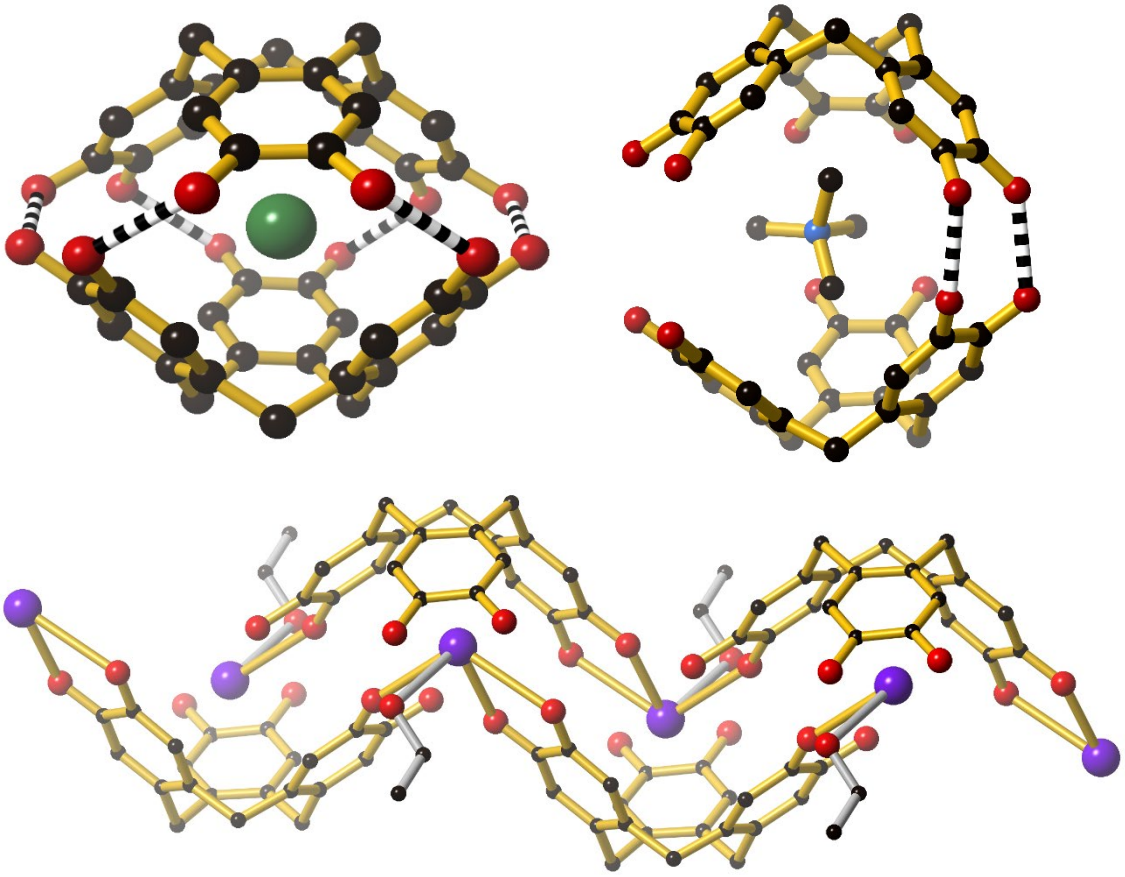

Figure 1.37 Ball and stick representations of three ctc–alkali metal cation assemblies reported by the Robson-Abrahams group. Hydrogen atoms have been omitted for clarity. Hydrogen bonds are indicated by black and white striped connections. At top left is a 'clam' assembly enclosing a Cs^+ cation. At top right is shown a partially open clam with a tetramethylammonium guest. At bottom is shown a portion of the bilayered chain of formula $K(ctcH_5)\cdot C_2H_5OH$. Ethanol molecules are indicated in grey; Cs^+ in green; K^+ in purple.

Under basic conditions cyclotricatechylene can be combined with Co^{II}, Cu^{II}, Mn^{II}, Mn^{III} or VO^{2+} in the presence of appropriate cations to form anionic tetrahedral cages.[220–222] In these tetrahedra, pairs of catecholate units chelate the transition metal cation in a square O_4 environment.

When metal ions with a preference for square pyramidal or octahedral coordination geometry are used to generate coordination cages, additional coordination sites are available when only two catecholate units chelate the centre. These sites can be occupied by a variety of different co-ligands, which can give rise to 3D architectures if the co-ligands bridge to other cages. An example of this is the Mn^{III}-derived tetrahedron in which dioxane and water coordinate to the metal centre and form bridges between tetrahedra to create a cubic network.[220]

The tetrahedral cages have large solvent filled interiors and, in some cases, can host guests such as alkali metal cations and, in the case of a Cu^{II} derived tetrahedron, the organic cation methyltripentylammonium.[221]

The literature on charged, oligomeric metal-ligand assemblies indicates that the packing arrangement of the oligomers is influenced by the counterions and solvent present in crystals of the compound. Additionally, the geometry and topology of the oligomer can be influenced by the counterions and solvents present. Our group has found that a large, trigonal prismatic M_9L_6 vanadyl-based cage can be deliberately synthesised, in preference to a tetrahedral cage, by employing methyltriphenylphosphonium as a counterion.[222]

Some of the largest and most interesting cages generated by the Robson-Abrahams group to date contain the uranyl cation. It has been found that when ctc is combined with UO_2^{2+} under basic conditions an M_8L_8 cube can be generated with a variety of cations including Na^+,[222] and Cs^+ and Li^+ together.[223] During the candidate's MSc, several novel cage architectures of ctc and UO_2^{2+} were generated including: a $[(UO_2(H_2O))_6(ctc)_6]^{7-}$ hexagonal prismatic assembly with Cs^+ counterions; a cage with tetrahedral geometry of formula $[(UO_2(H_2O))_6(O)(ctc)_3]^{7-}$ that contains a trimer of uranyl centres and has Li^+ and tetraphenylphosphonium cations; a 'heart' shaped cage of formula

$[((UO_2)_3(OH)_3(O))_4(ctc)_4]^{20-}$ containing four uranyl trimers and having both Cs^+ and Na^+ counterions; an 'hourglass' shaped cage of formula $[(UO_2)_{16}(O_2)_{12}(ctc)_8]^{40-}$ containing four peroxo-bridged uranyl dimers and two peroxo-bridged uranyl tetramers with Li^+ counterions; and, most massive of all, a highly symmetrical 'nanosphere' of formula $[((UO_2)_4(O_2)_4)_6(ctc)_8]^{40-}$, which has only Na^+ countercations and packs in a body centred cubic arrangement in the solid state.[223] As with the tetrahedral cages above, the vanadyl and uranyl containing cages with ctc all contain large voids filled with difficult-to-model solvent molecules, and in some cases, counterions. A detailed discussion of metallocages containing ctc is presented in chapter 4 of this thesis.

The impressive diversity in the type of supramolecular assemblies obtained by our group prompted us to continue research with ctc. The research aims of this body of work were to:

- explore the structural diversity of supramolecular assemblies of ctc in combination with different chemical elements
- investigate the host-guest and coordination chemistry of $ctcH_6$ in its protonated form
- further characterise selected ctc-derived nanocages that presented difficulties previously
- generate robust, novel cages with ctc

1.2.5 Work reported in this thesis

This thesis presents several novel crystalline supramolecular assemblies of cyclotricatechylene that have been characterised using X-ray crystallography.

Chapter 2 presents ten new assemblies of ctc with alkali metal cations. Many of these assemblies have commonly encountered network topologies. The work in this chapter shows that the Cs^+ cation, in particular, has an affinity for the ctc bowl, both when ctc is in its neutral and anionic forms.

Chapter 3 describes four cubic assemblies of ctc of formula $[M_4ctc_4]^{4+}$ ($M = K^+$ or Rb^+). The assemblies pack in a highly regular fashion that is uniquely possible due the arrangement of the counterions (the oxyanion sulfate or phosphate and the octahedral $[M(acetone)_6]^+$ complex in which $M = Cs^+$ or Rb^+) in the crystal structure.

Chapter 4 presents coordination assemblies of deprotonated ctc with vandyl and zinc cations. The structural diversity of systems containing the uranyl cation is also explored and the challenges associated with constructing large assemblies containing the uranyl cation are discussed.

Chapter 5 describes the synthesis and analysis of a novel and robust tetrahedral assembly of ctc with silicon. The host-guest and gas phase chemistry of this assembly is discussed.

1.3 References

[1] J. W. Steed, J. L. Atwood, *Supramolecular Chemistry*, Wiley, **2013**.
[2] E. Fischer, *Berichte der Dtsch. Chem. Gesellschaft* **1890**, *23*, 2611–2624.
[3] E. Fischer, *Berichte der Dtsch. Chem. Gesellschaft* **1894**, *27*, 2985–2993.
[4] D. E. Koshland, *Angew. Chemie Int. Ed. English* **1995**, *33*, 2375–2378.
[5] D. E. Koshland, *Proc. Natl. Acad. Sci. U. S. A.* **1958**, *44*, 98–104.
[6] J. M. Lehn, *Acc. Chem. Res.* **1978**, *11*, 49–57.
[7] J. Lehn, J. Sauvage, *Helv. Chim. Acta* **1976**, *59*, 1099–1111.
[8] R. M. Izatt, K. Pawlak, J. S. Bradshaw, R. L. Bruening, *Chem. Rev.* **1991**, *91*, 1721–2085.
[9] J. J. Christensen, D. J. Eatough, R. M. Izatt, *Chem. Rev.* **1974**, *74*, 351–383.
[10] R. M. Izatt, K. Pawlak, J. S. Bradshaw, R. L. Bruening, *Chem. Rev.* **1995**, *95*, 2529–2586.
[11] R. M. Izatt, J. S. Bradshaw, S. A. Nielsen, J. D. Lamb, J. J. Christensen, D. Sen, *Chem. Rev.* **1985**, *85*, 271–339.
[12] J. Lehn, *Angew. Chemie Int. Ed. English* **1988**, *27*, 89–112.
[13] J. Lehn, *J. Incl. Phenom.* **1988**, *6*, 351–396.
[14] G. R. Desiraju, *Nature* **2001**, *412*, 397–400.
[15] J. Lehn, *Resonance* **1996**, *1*, 39–53.
[16] H. J. Schneider, *Applications of Supramolecular Chemistry*, CRC Press, **2012**.
[17] J. Hardy, F. Schacher, Eds., *Functional Metallosupramolecular Materials*, Royal Society Of Chemistry, Cambridge, **2015**.
[18] D. N. Reinhoudt, **2011**, *2403*, 2403–2408.
[19] J. Liu, D. P. Wernette, Y. Lu, *Angew. Chemie - Int. Ed.* **2005**, *44*, 7290–7293.
[20] Y. Lu, J. Liu, *Acc. Chem. Res.* **2007**, *40*, 315–323.
[21] J. Lehn, *Angew. Chemie - Int. Ed.* **2015**, *54*, 3276–3289.
[22] K. Hermann, Y. Ruan, A. M. Hardin, C. M. Hadad, J. D. Badjić, *Chem. Soc. Rev.* **2015**, *43*, 500–514.
[23] S. Rieth, K. Hermann, B.-Y. Wang, J. D. Badjić, *Chem. Soc. Rev.* **2011**, *40*, 1609–1622.
[24] X. Zhang, C. Wang, in *Mol. Self Assem. Adv. Appl.*, Standford Publishing, **2013**, pp. 207–222.
[25] E. Aznar, M. Oroval, L. Pascual, J. R. Murguía, R. Martínez-Máñez, F. Sancenón, *Chem. Rev.* **2016**, *116*, 561–718.
[26] D. J. Cram, *Angew. Chemie Int. Ed. English* **1986**, *25*, 1039–1057.
[27] D. J. Cram, J. M. Cram, in *Contain. Mol. Their Guests* (Eds.: D.J. Cram, J.M. Cram), Royal Society Of Chemistry, Cambridge, **1997**, pp. 20–48.
[28] G. M. Whitesides, J. P. Mathias, T. Seto, Christoph, *Molecular Self-Assembly and Nanochemistry: A Chemical Strategy for the Synthesis of Nanostructures (Technical Rept. No. 45)*, **1991**.
[29] G. M. Whitesides, J. P. Mathias, C. T. Seto, *Science* **1991**, *254*, 1312–1319.
[30] D. Dini, M. T. Pryce, M. Schulz, J. G. Vos, in *Funct. Met. Mater.* (Eds.: J. Hardy, F. Schacher), Royal Society Of Chemistry, Cambridge, **2015**.
[31] M. D. Kärkäs, O. Verho, E. V Johnston, B. Åkermark, *Chem. Rev.* **2014**, *114*, 11863–12001.
[32] T. Zhang, W. Lin, *Chem. Soc. Rev.* **2014**, *43*, 5982–5993.
[33] D. Gust, *Faraday Discuss.* **2015**, *185*, 9–35.
[34] S. R. Peurifoy, C. X. Guzman, A. B. Braunschweig, *Polym. Chem.* **2015**, *6*, 5529–5539.
[35] S. H. Park, C. Pistol, S. J. Ahn, J. H. Reif, A. R. Lebeck, C. Dwyer, T. H. LaBean,

Angew. Chemie Int. Ed. **2006**, *45*, 735–739.
[36] H. Yan, *Science* **2003**, *301*, 1882–1884.
[37] P. W. K. Rothemund, *Nature* **2006**, *440*, 297–302.
[38] G. Vindigni, S. Raniolo, A. Ottaviani, M. Falconi, O. Franch, B. R. Knudsen, A. Desideri, S. Biocca, *ACS Nano* **2016**, *10*, 5971–5979.
[39] C. M. Erben, R. P. Goodman, A. J. Turberfield, *J. Am. Chem. Soc.* **2007**, *129*, 6992–6993.
[40] N. C. Seeman, *Nature* **2003**, *421*, 427–431.
[41] M. A. Batalia, E. Protozanova, R. B. Macgregor, D. A. Erie, *Nano Lett.* **2002**, *2*, 269–274.
[42] C. K. McLaughlin, G. D. Hamblin, H. F. Sleiman, *Chem. Soc. Rev.* **2011**, *40*, 5647–56.
[43] T. J. Bandy, A. Brewer, J. R. Burns, G. Marth, T. Nguyen, E. Stulz, *Chem. Soc. Rev.* **2011**, *40*, 138–148.
[44] Y. He, T. Ye, M. Su, C. Zhang, A. E. Ribbe, W. Jiang, C. Mao, *Nature* **2008**, *452*, 198–201.
[45] K. Kim, *Chem. Soc. Rev.* **2002**, *31*, 96–107.
[46] D. A. Uhlenheuer, K. Petkau, L. Brunsveld, *Chem. Soc. Rev.* **2010**, *39*, 2817–2826.
[47] E. K. Drexler, *Engines of Creation: The Coming Era of Nanotechnology*, Anchor Books, New York, **1986**.
[48] V. Balzani, A. Credi, M. Venturi, *Chem. Eur. J.* **2002**, *8*, 5524–5532.
[49] Nobel Media AB, "The Nobel Prize in Chemistry 2016," can be found under https://www.nobelprize.org/nobel_prizes/chemistry/laureates/2016/**.**
[50] C. O. Dietrich-Buchecker, J. P. Sauvage, J. P. Kintzinger, *Tetrahedron Lett.* **1983**, *24*, 5095–5098.
[51] W. R. Browne, B. L. Feringa, *Nat. Nanotechnol.* **2006**, *1*, 25–35.
[52] K. Kinbara, T. Aida, *Chem. Rev.* **2005**, *105*, 1377–1400.
[53] "Scientific Background on the Nobel Prize in Chemistry 2016 Molecular machines", compiled by the Class for Chemistry of the Royal Swedish Academy of Sciences, can be found under https://www.nobelprize.org/prizes/chemistry/2016/press-release/**.**
[54] F. Pichierri, *J. Radioanal. Nucl. Chem.* **2017**, *311*, 1251–1263.
[55] M. P. Unterweger, D. D. Hoppes, F. J. Schima, J. S. Coursey, "Radionuclide Half-Life Measurements Data," can be found under https://www.nist.gov/pml/radionuclide-half-life-measurements-data.
[56] G. G. Talanova, N. S. A. Elkarim, R. E. Hanes, H. S. Hwang, R. D. Rogers, R. A. Bartsch, *Anal. Chem.* **1999**, *71*, 672–677.
[57] J. W. Steed, *Coord. Chem. Rev.* **2001**, *215*, 171–221.
[58] M. Yoshio, H. Noguchi, *Anal. Lett.* **2006**, *15*, 1197–1276.
[59] M. B. More, D. Ray, P. B. Armentrout, *J. Am. Chem. Soc.* **1999**, *121*, 417–423.
[60] C. J. Pedersen, *J. Am. Chem. Soc.* **1967**, *89*, 7017–7036.
[61] R. Assmus, V. Bohmer, J. M. Harrowfield, M. Ogden, W. R. Richmond, B. W. Skelton, A. H. White, *J. Chem. Soc. Dalton Trans*. **1993**, 2427–2433.
[62] W. Sliwa, T. Girek, *J. Incl. Phenom. Macro*, **2010**, 15-41.
[63] D. Diamond, M. A. McKervey, *Chem. Soc. Rev*, **1990**, 15–24.
[64] A. F. Danil De Namor, R. M. Cleverley, M. L. Zapata-Ormachea, *Chem. Rev.* **1998**, *98*, 2495–2526.
[65] V. Böhmer, *Angew. Chemie Int. Ed. English* **1995**, *34*, 713–745.
[66] D. J. Cram, G. M. Lein, T. Kaneda, R. C. Helgeson, C. B. Knobler, E. Maverick, K. N. Trueblood, *J. Am. Chem. Soc.* **1981**, *103*, 6228–6232.
[67] D. J. Cram, I. B. Dicker, *J. Chem. Soc. Chem. Commun.* **1982**, 1219–1221.

[68] D. J. Cram, R. A. Carmack, M. P. Degrandare, G. M. Lein, I. Goldberg, C. B. Knobler, E. F. Maverick, K. N. Trueblood, *J. Am. Chem. Soc.* **1987**, *109*, 7068–7073.
[69] L. F. Lindoy, K.-M. Park, S. Sung Lee, in *Supramol. Chem.*, John Wiley & Sons, Ltd, Chichester, UK, **2012**.
[70] M. Albrecht, H. Röttele, P. Burger, *Chem. - A Eur. J.* **1996**, *2*, 1264–1268.
[71] B. G. Cox, J. Stroka, H. Schneider, *J. Am. Chem. Soc.* **1978**, *4146*, 4146–4149.
[72] J. H. Jordan, B. C. Gibb, *Chem. Soc. Rev.* **2015**, *44*, 547–585.
[73] D. J. Cram, J. M. Cram, *Container Molecules and Their Guests*, Royal Society Of Chemistry, Cambridge, **1997**.
[74] D. J. Cram, J. M. Cram, *Acc. Chem. Res.* **1978**, *11*, 8–14.
[75] J. B. Wittenberg, L. Isaacs, *Supramol. Chem. From Mol. to Nanomater. Online* **2012**, 1–19.
[76] A. Lüttringhaus, K. Ziegler, *Justus Liebig's Ann. der Chemie* **1937**, *528*, 155–161.
[77] D. C. Hrncir, R. D. Rogers, J. L. Atwood, *J. Am. Chem. Soc.* **1981**, *103*, 4277–4278.
[78] B. Dietrich, J. M. Lehn, J. P. Sauvage, *Tetrahedron Lett.* **1969**, *10*, 2889–2892.
[79] J. M. Lehn, J. P. Sauvage, *J. Am. Chem. Soc.* **1975**, *97*, 6700–6707.
[80] D. M. Smith, C.-W. Park, J. A. Ibers, *Inorg. Chem.* **1997**, *36*, 3798–3800.
[81] J. R. Moran, S. Karbach, D. J. Cram, *J. Am. Chem. Soc.* **1982**, *104*, 5826–5828.
[82] D. J. Cram, R. A. Carmack, M. P. DeGrandpre, G. M. Lein, I. Goldberg, C. B. Knobler, E. F. Maverick, K. N. Trueblood, *J. Am. Chem. Soc.* **1987**, *109*, 7068–7073.
[83] K. N. Trueblood, E. F. Maverick, C. B. Knobler, *Acta Crystallogr. Sect. B Struct. Sci.* **1991**, *47*, 389–398.
[84] A. S. Mahadevi, G. N. Sastry, *Chem. Rev.* **2013**, *113*, 2100–2138.
[85] D. A. Dougherty, *Acc. Chem. Res.* **2013**, *46*, 885–893.
[86] T. J. Shepodd, M. A. Petti, D. A. Dougherty, *J. Am. Chem. Soc.* **1986**, *108*, 6085–6087.
[87] D. A. Stauffer, R. E. Barrans, D. A. Dougherty, *Angew. Chemie Int. Ed. English* **1990**, *29*, 915–918.
[88] D. Stauffer, R. E. J. Barrans, D. A. Dougherty, *J. Org. Chem.* **1990**, *55*, 2762–2767.
[89] P. Thuéry, Z. Asfari, J. Vicens, V. Lamare, J. F. Dozol, *Polyhedron* **2002**, *21*, 2497–2503.
[90] T. A. Hanna, L. Liu, A. M. Angeles-Boza, X. Kou, C. D. Gutsche, K. Ejsmont, W. H. Watson, L. N. Zakharov, C. D. Incarvito, A. L. Rheingold, *J. Am. Chem. Soc.* **2003**, *125*, 6228–6238.
[91] E. Arunan, G. R. Desiraju, R. a. Klein, J. Sadlej, S. Scheiner, I. Alkorta, D. C. Clary, R. H. Crabtree, J. J. Dannenberg, P. Hobza, et al., *Pure Appl. Chem.* **2011**, *83*, 1637–1641.
[92] Anon., *Chem. Mater.* **1994**, *6*, 1090–1092.
[93] E. M. Arnett, E. J. Mitchell, T. S. S. R. Murty, *J. Am. Chem. Soc.* **1974**, *96*, 3875–3891.
[94] R. Taylor, O. Kennard, *Acc. Chem. Res.* **1984**, *17*, 320–326.
[95] V. A. Russell, M. D. Ward, *Chem. Mater.* **1996**, *8*, 1654–1666.
[96] G. R. Desiraju, *Cryst. Growth Des.* **2011**, *11*, 896–898.
[97] J. Bernstein, M. C. Etter, L. Leiserowitz, in *Struct. Correl.*, Wiley-VCH Verlag GmbH, Weinheim, Germany, **1994**, pp. 431–507.
[98] P. Muller, *Pure Appl. Chem.* **1994**, *66*, 1077–1184.
[99] A. Galan, P. Ballester, *Chem. Soc. Rev.* **2016**, *45*, 1720–1737.
[100] T. Hasell, A. I. Cooper, *Nat. Rev. Mater.* **2016**, *1*, 16053.
[101] Y. Fang, J. A. Powell, E. Li, Q. Wang, Z. Perry, A. Kirchon, X. Yang, Z. Xiao, C. Zhu, L. Zhang, et al., *Chem. Soc. Rev.* **2019**, *48*, 4707–4730.
[102] Y. Inokuma, M. Kawano, M. Fujita, *Nat. Chem.* **2011**, *3*, 349–58.
[103] M. Yoshizawa, J. K. Klosterman, M. Fujita, *Angew. Chemie Int. Ed.* **2009**, *48*, 3418–

3438.
[104] S. Wang, J.-L. Zuo, H.-C. Zhou, H. J. Choi, Y. Ke, J. R. Long, X.-Z. You, *Angew. Chemie Int. Ed.* **2004**, *43*, 5940–5943.
[105] C. H. M. Amijs, G. P. M. van Klink, G. van Koten, *Dalt. Trans.* **2006**, *60*, 308–327.
[106] L. R. Nassimbeni, *Acc. Chem. Res.* **2003**, *36*, 631–637.
[107] L. J. Barbour, *Chem. Commun.* **2006**, 1163–1168.
[108] L. Adriaenssens, P. Ballester, *Chem. Soc. Rev.* **2013**, *42*, 3261–3277.
[109] R. Wyler, J. de Mendoza, J. Rebek, *Angew. Chemie Int. Ed. English* **1993**, *32*, 1699–1701.
[110] J. Rebek, *Acc. Chem. Res.* **1999**, *32*, 278–286.
[111] J. Rebek, *Angew. Chemie - Int. Ed.* **2005**, *44*, 2068–2078.
[112] J. M. Rivera, *Science,*. **1998**, *279*, 1021–1023.
[113] R. S. Meissner, J. Rebek, J. de Mendoza, *Science* **1995**, *270*, 1485–1488.
[114] J. Rebek Jr., *Chem. Commun.* **2000**, 637–643.
[115] D. Ken, Shimizu, J. Rebek, *Proc. Natl. Acad. Sci.* **1995**, *92*, 12403–12407.
[116] O. Mogck, E. F. Paulus, V. Böhmer, I. Thondorf, W. Vogt, *Chem. Commun.* **1996**, 2533–2534.
[117] J. L. Atwood, L. J. Barbour, A. Jerga, *Proc. Natl. Acad. Sci. U. S. A.* **2002**, *99*, 4837–4841.
[118] J. L. Atwood, L. R. MacGillivray, *Nature* **1997**, *389*, 469–472.
[119] Y. Inokuma, T. Arai, M. Fujita, *Nat. Chem.* **2010**, *2*, 780–783.
[120] M. Yoshizawa, J. Nakagawa, K. Kumazawa, M. Nagao, M. Kawano, T. Ozeki, M. Fujita, *Angew. Chemie - Int. Ed.* **2005**, *44*, 1810–1813.
[121] K. Ono, M. Yoshizawa, T. Kato, K. Watanabe, M. Fujita, *Angew. Chemie - Int. Ed.* **2007**, *46*, 1803–1806.
[122] K. Kumazawa, K. Biradha, T. Kusukawa, T. Okano, M. Fujita, *Angew. Chemie - Int. Ed.* **2003**, *42*, 3909–3913.
[123] C. J. Kuehl, Y. K. Kryschenko, U. Radhakrishnan, S. Russell Seidel, S. D. Huang, P. J. Stang, *Proc. Natl. Acad. Sci. U. S. A.* **2002**, *99*, 4932–4936.
[124] B. H. Northrop, Y. Zheng, K. Chi, P. J. Stang, *Acc. Chem. Res.* **2009**, *42*, 1554–1563.
[125] P. J. Stang, B. Olenyuk, *Acc. Chem. Res.* **1997**, *30*, 502–518.
[126] S. R. Seidel, P. J. Stang, *Acc. Chem. Res.* **2002**, *35*, 972–983.
[127] K. Ariga, J. P. Hill, M. V Lee, A. Vinu, R. Charvet, S. Acharya, *Sci. Technol. Adv. Mater.* **2008**, *9*, 1–96.
[128] B. Hoskins, R. Robson, *J. Am. Chem. Soc.* **1989**, *111*, 5962–5964.
[129] G. R. Desiraju, *Angew. Chemie - Int. Ed.* **2007**, *46*, 8342–8356.
[130] A. Ranganathan, V. R. Pedireddi, C. N. R. Rao, *J. Am. Chem. Soc.* **1999**, *121*, 1752–1753.
[131] D. Braga, F. Grepioni, G. R. Desiraju, *Chem. Rev.* **1998**, *98*, 1375–1405.
[132] G. R. Desiraju, *Curr. Opin. Solid State Mater. Sci.* **1997**, *2*, 451–454.
[133] G. R. Desiraju, *J. Am. Chem. Soc.* **2013**, *135*, 9952–9967.
[134] G. R. Desiraju, *Angew. Chemie Int. Ed. English* **1995**, *34*, 2311–2327.
[135] R. Robson, *J. Chem. Soc., Dalton Trans*. **2000**, 3735–3744.
[136] P. F. Damasceno, M. Engel, S. C. Glotzer, *ACS Nano* **2012**, *6*, 609–614.
[137] S. Kitagawa, R. Kitaura, S. Noro, *Angew. Chemie - Int. Ed.* **2004**, *43*, 2334–2375.
[138] G. Kickelbick, U. Schubert, *Chem. Ber.* **1997**, *130*, 473–478.
[139] C. J. Kingsbury, B. F. Abrahams, D. M. D'Alessandro, T. A. Hudson, R. Murase, R. Robson, K. F. White, *Cryst. Growth Des.* **2017**, *17*, 1465–1470.
[140] T. Adachi, M. D. Ward, *Acc. Chem. Res.* **2016**, *49*, 2669–2679.

[141] D. J. Duchamp, R. E. Marsh, *Acta Crystallogr. Sect. B Struct. Crystallogr. Cryst. Chem.* **1969**, *25*, 5–19.
[142] A. F. Wells, *Three-Dimensional Nets and Polyhedra*, John Wiley & Sons, Ltd, New York, **1977**.
[143] S. R. Batten, S. M. Neville, D. R. Turner, *Coordination Polymers*, The Royal Society Of Chemistry, **2009**.
[144] B. F. Abrahams, T. A. Hudson, L. J. McCormick, R. Robson, *Cryst. Growth Des.* **2011**, *11*, 2717–2720.
[145] B. F. Abrahams, B. F. Hoskins, D. M. Michail, R. Robson, *Nature* **1994**, *369*, 727–729.
[146] V. K. Bhagwat, D. K. Moore, F. L. Pyman, S. Kao, C. H.; Ma, J. L. Simonsen, J. Hewitt, T., W. J. Lewcock, *J. Chem. Soc.* **1931**, 443.
[147] A. Collet, J.-P. Dutasta, B. Lozach, J. Canceill, in *Supramol. Chem. I - Dir. Synth. Mol. Recognit.*, Springer Berlin Heidelberg, Berlin, Heidelberg, **1993**, pp. 103–129.
[148] J. W. Steed, P. C. Junk, J. L. Atwood, M. J. Barnes, C. L. Raston, R. S. Burkhalter, *J. Am. Chem. Soc.* **1994**, *116*, 10346–10347.
[149] M. J. Hardie, C. L. Raston, *Cryst. Growth Des.* **2001**, *1*, 53–58.
[150] F. L. Thorp-Greenwood, G. T. Berry, S. S. Boyadjieva, S. Oldknow, M. J. Hardie, *CrystEngComm* **2018**, *20*, 3960–3970.
[151] F. L. Thorp-Greenwood, A. N. Kulak, M. J. Hardie, *Nat. Chem.* **2015**, *7*, 526–531.
[152] T. K. Ronson, H. Nowell, A. Westcott, M. J. Hardie, *Chem. Commun. (Camb).* **2011**, *47*, 176–8.
[153] M. J. Hardie, R. M. Mills, C. J. Sumby, *Org. Biomol. Chem.* **2004**, *2*, 2958–2964.
[154] R. Ahmad, M. J. Hardie, *Crystengcomm* **2002**, 4(42), 227–231.
[155] J. J. Henkelis, M. J. Hardie, *Chem. Commun. (Camb).* **2015**, *51*, 11929–43.
[156] M. A. Little, J. J. Loughrey, A. Santoro, M. A. Halcrow, M. J. Hardie, *Tetrahedron Lett.* **2014**, *55*, 2530–2533.
[157] R. Ahmad, I. Dix, M. J. Hardie, *Inorg. Chem.* **2003**, *42*, 2182–2184.
[158] M. J. Hardie, R. Ahmad, C. J. Sumby, *New J. Chem.* **2005**, *29*, 1231–1240.
[159] M. J. Hardie, *Chem. Soc. Rev.* **2010**, *39*, 516–527.
[160] M. J. Hardie, *Chem. Lett.* **2016**, *45*, 1336–1346.
[161] M. J. Hardie, *Isr. J. Chem.* **2011**, *51*, 807–816.
[162] M. J. Hardie, P. D. Godfrey, C. L. Raston, *Chem. - A Eur. J.* **1999**, *5*, 1828–1833.
[163] J. J. Henkelis, J. Fisher, S. L. Warriner, M. J. Hardie, *Chemistry* **2014**, *20*, 4117–25.
[164] T. K. Ronson, J. Fisher, L. P. Harding, M. J. Hardie, *Angew. Chemie - Int. Ed.* **2007**, *46*, 9086–9088.
[165] C. J. Sumby, K. C. Gordon, T. J. Walsh, M. J. Hardie, *Chemistry* **2008**, *14*, 4415–4425.
[166] C. J. Sumby, J. Fisher, T. J. Prior, M. J. Hardie, *Chem. - A Eur. J.* **2006**, *12*, 2945–2959.
[167] D. Cavagnat, T. Brotin, J. L. Bruneel, J. P. Dutasta, A. Thozet, M. Perrin, F. Guillaume, *J. Phys. Chem. B* **2004**, *108*, 5572–5581.
[168] H. A. Fogarty, P. Berthault, T. Brotin, G. Huber, H. Desvaux, J. P. Dutasta, *J. Am. Chem. Soc.* **2007**, *129*, 10332–10333.
[169] T. Brotin, J.-P. Dutasta, *Chem. Rev.* **2009**, *109*, 88–130.
[170] A. Bouchet, T. Brotin, M. Linares, H. Ågren, D. Cavagnat, T. Buffeteau, *J. Org. Chem.* **2011**, *76*, 1372–1383.
[171] T. Brotin, J. P. Dutasta, *Chem. Rev.* **2009**, *109*, 88–130.
[172] T. Brotin, V. Roy, J.-P. Dutasta, *J. Org. Chem.* **2005**, *70*, 6187–6195.
[173] T. Brotin, R. Montserret, A. Bouchet, D. Cavagnat, M. Linares, T. Buffeteau, *J. Org. Chem.* **2012**, *77*, 1198–1201.
[174] Y. Han, Y. Jiang, C. F. Chen, *Chinese Chem. Lett.* **2013**, *24*, 475–478.

[175] C. G. Pierpont, R. M. Buchanan, *Coord. Chem. Rev.* **1981**, *38*, 45–87.
[176] C. G. Pierpont, C. W. Lange, *The Chemistry of Transition Metal Complexes Containing Catechol and Semiquinone Ligands*, Wiley, **2007**, pp. 331–442.
[177] E. Evangelio, D. Ruiz-Molina, *Eur. J. Inorg. Chem.* **2005**, 2957–2971.
[178] L. D. Loomis, K. N. Raymond, *Inorg. Chem.* **1991**, *30*, 906–911.
[179] K. N. Raymond, E. A. Dertz, S. S. Kim, *Proc. Natl. Acad. Sci. U. S. A.* **2003**, *100*, 3584–3588.
[180] R. C. Hider, X. Kong, *Nat. Prod. Rep.* **2010**, *27*, 637–657.
[181] W. R. Harris, C. J. Carrano, S. R. Cooper, S. R. Sofen, A. E. Avdeef, J. V Mcardle, K. N. Raymond, *J. Am. Chem. Soc.* **1979**, *101*, 6097–6104.
[182] C. J. Carrano, K. N. Raymond, *J. Am. Chem. Soc.* **1979**, *101*, 5401–5404.
[183] S. König, C. Brückner, K. N. Raymond, J. A. Leary, *J. Am. Soc. Mass Spectrom.* **1998**, *9*, 1099–1103.
[184] C. Brückner, R. E. Powers, K. N. Raymond, *Angew. Chemie Int. Ed.* **1998**, *37*, 1837–1839.
[185] D. L. Caulder, R. E. Powers, T. N. Parac, K. N. Raymond, *Angew. Chemie Int. Ed.* **1998**, *37*, 1840–1843.
[186] D. L. Caulder, K. N. Raymond, *Acc. Chem. Res.* **1999**, *32*, 975–982.
[187] D. Fiedler, D. H. Leung, R. G. Bergman, K. N. Raymond, *Acc. Chem. Res.* **2005**, *38*, 349–358.
[188] U. N. Andersen, G. Seeber, D. Fiedler, K. N. Raymond, D. Lin, D. Harris, *J. Am. Soc. Mass Spectrom.* **2006**, *17*, 292–296.
[189] A. V. Davis, D. Fiedler, G. Seeber, A. Zahl, R. Van Eldik, K. N. Raymond, *J. Am. Chem. Soc.* **2006**, *128*, 1324–1333.
[190] D. Fiedler, R. G. Bergman, K. N. Raymond, *Angew. Chem. Int. Ed. Engl.* **2006**, *45*, 745–748.
[191] C. J. Brown, R. G. Bergman, K. N. Raymond, *J. Am. Chem. Soc.* **2009**, *131*, 17530–17531.
[192] C. J. Hastings, M. D. Pluth, R. G. Bergman, K. N. Raymond, *J. Am. Chem. Soc.* **2010**, *132*, 6938–6940.
[193] C. Zhao, Q. F. Sun, W. M. Hart-Cooper, A. G. Dipasquale, F. D. Toste, R. G. Bergman, K. N. Raymond, *J. Am. Chem. Soc.* **2013**, *135*, 18802–18805.
[194] K. N. Raymond, B. E. Allred, A. K. Sia, *Acc. Chem. Res.* **2015**, *48*, 2496–2505.
[195] C. J. Brown, F. D. Toste, R. G. Bergman, K. N. Raymond, *Chem. Rev.* **2015**, *115*, 3012–3035.
[196] W. M. Hart-Cooper, C. Zhao, R. M. Triano, P. Yaghoubi, H. L. Ozores, K. N. Burford, F. D. Toste, R. G. Bergman, K. N. Raymond, *Chem. Sci.* **2015**, *6*, 1383–1393.
[197] M. Albrecht, Y. Shang, T. Rhyssen, J. Stubenrauch, H. D. F. Winkler, C. A. Schalley, *European J. Org. Chem.* **2012**, *6*, 2422–2427.
[198] M. Albrecht, I. Janser, R. Fröhlich, *Chem. Commun.* **2005**, 157–165.
[199] M. Albrecht, M. Schneider, H. Röttele, *Angew. Chemie - Int. Ed.* **1999**, *38*, 557–559.
[200] M. Albrecht, *Chem. Soc. Rev.* **1998**, *27*, 281–287.
[201] A.-K. Duhme, S. C. Davies, D. L. Hughes, *Inorg. Chem.* **1998**, *37*, 5380–5382.
[202] B. F. Abrahams, D. J. Price, R. Robson, *Angew. Chem. Int. Ed. Engl.* **2006**, *45*, 806–10.
[203] L. J. McCormick, B. F. Abrahams, B. A. Boughton, M. J. Grannas, T. A. Hudson, R. Robson, *Inorg. Chem.* **2014**, *53*, 1721–1728.
[204] P. Thuéry, B. Masci, *Supramol. Chem.* **2003**, *15*, 95–99.
[205] A. P. Côté, H. M. El-Kaderi, H. Furukawa, J. R. Hunt, O. M. Yaghi, *J. Am. Chem. Soc.* **2007**, *129*, 12914–12915.

[206] A. S. Lindsey, *J. Chem. Soc.* **1965**, 1685–1692.
[207] P. T. Lee, J. E. Thomson, A. Karina, C. Salter, C. Johnston, S. G. Davies, R. G. Compton, *Analyst* **2015**, *140*, 236–242.
[208] J. A. Hyatt, E. N. Duesler, D. Y. Curtin, I. C. Paul, *J. Org. Chem.* **1980**, *45*, 5074–5079.
[209] J. J. Loughrey, C. A. Kilner, M. J. Hardie, M. A. Halcrow, *Supramol. Chem.* **2012**, *24*, 2–13.
[210] J. W. Steed, H. Zhang, J. L. Atwood, *Supramol. Chem.* **1996**, *7*, 37–45.
[211] C. J. Sumby, M. J. Hardie, *Acta Crystallogr. Sect. E Struct. Reports Online* **2007**, *63*, 1537–1539.
[212] D. Scott Bohle, D. Stasko, *Chem. Commun.* **1998**, 567–569.
[213] P. Satha, G. Illa, C. S. Purohit, *Cryst. Growth Des.* **2013**, *13*, 2636–2641.
[214] P. Satha, C. S. Purohit, *Proc. Natl. Acad. Sci. India Sect. A Phys. Sci.* **2014**, *84*, 221–225.
[215] K. Kataoka, T. D. James, Y. Kubo, *J. Am. Chem. Soc.* **2007**, *129*, 15126–15127.
[216] Y. Kubo, W. Yoshizumi, T. Minami, *Chem. Lett.* **2008**, *37*, 1238–1239.
[217] J. T. Yu, Z. Chen, J. Sun, Z. T. Huang, Q. Y. Zheng, *J. Mater. Chem.* **2012**, *22*, 5369–5373.
[218] J. Zhen, S. Ding, W. Wang, J. Liu, J. Sun, Z. Huang, Q. Zheng, *Chinese J. Chem.* **2016**, *34*, 783–787.
[219] B. F. Abrahams, N. J. Fitzgerald, T. A. Hudson, R. Robson, T. Waters, *Angew. Chem. Int. Ed. Engl.* **2009**, *48*, 3129–32.
[220] B. F. Abrahams, N. J. FitzGerald, R. Robson, *Angew. Chemie - Int. Ed.* **2010**, *49*, 2896–2899.
[221] B. F. Abrahams, B. A. Boughton, N. J. FitzGerald, J. L. Holmes, R. Robson, *Chem. Commun.* **2011**, *47*, 7404–7406.
[222] N. J. FitzGerald, Supramolecular Assemblies from Catechol-Based Ligands, PhD Thesis, The University of Melbourne, **2010**.
[223] J. L. Holmes, Supramolecular Structures of Cyclotricatechylene, MSc Thesis, The University of Melbourne, **2011**.

Chapter 2 Structural diversity of supramolecular cyclotricatechylene compounds with group 1 and 2 metal cations

Contents

2.1 Introduction

The binding of Group 1 metal cations by macrocycles has been the focus of considerable attention since Pederson's serendipitous discovery of crown ethers in 1967.[1,2] The importance of systems that exhibit a high degree of specificity in binding to alkali metal ions was recognised with the award of the 1987 Nobel Prize in chemistry to Cram, Lehn and Pedersen "for their development and use of molecules with structure-specific interactions of high selectivity".[3] Much of the work in this area of supramolecular chemistry has focused on the deliberate design of ligands and host materials with high binding energies and/or good selectivities for the group 1 and 2 cations. Typically, such compounds are macrocycles (crown ethers, cryptands, spherands); and cyclic aromatic systems (cyclophanes and calixarenes).[4–7] The importance of the recovery and separation of group 1 and 2 metals is widely acknowledged, given their prominence in industry and technological applications. Their host-guest chemistry is also notable in developing technologies such as molecular switches and machines. A notable example of this is the use of Li^+ as a templating guest in the synthesis of a switchable bistable rotaxane, reported by Stoddart *et al*, prior to the award of the 2017 Nobel Prize in chemistry to Feringa, Sauvage and Stoddart for their work in this area.[8] More recently, a structurally diverse range of organic-, inorganic- and bio-adsorbent materials for alkali and alkaline earth metals, and in particular, radiocaesium (^{137}Cs and ^{134}Cs) and radiostrontium (^{90}Sr), have been investigated.[9–11]

As described in chapter 1, the tripodal tris-catechol cyclotricatechylene and its family of related rigid, bowl-shaped aromatic molecules from the cyclotriveratrylene family have been shown to act as the host molecule for cationic and neutral guests in supramolecular inclusion compounds.[12–27] $CtcH_6$ and its related anions have been shown to be excellent hosts for the

larger alkali metal cations Cs^+, Rb^+ and in some cases K^+. The Robson-Abrahams group have described the formation of anionic 'clam' type species, crystallised from aqueous solution, in which bare Cs^+ or Rb^+ cations are encapsulated within a 'shell' composed of two ctc units that are hydrogen bonded together (Figure 2.1).[28] A summary of the clam-type compounds and assemblies of alkali metals with ctc that have been generated within our group prior to this work is presented in Table 2.1.

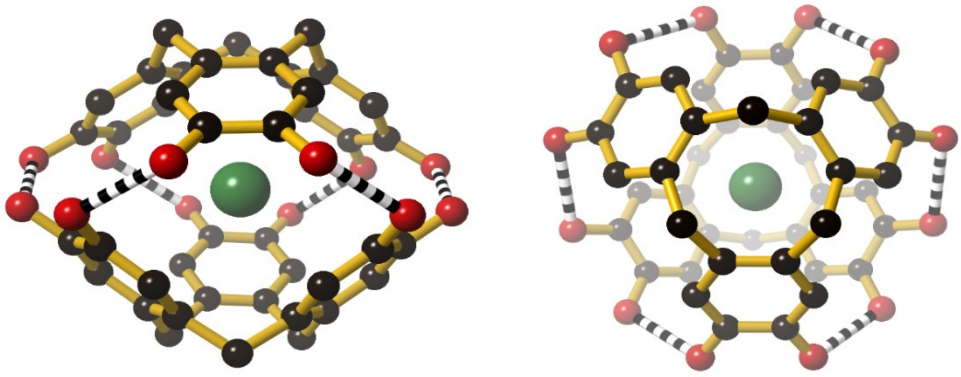

Figure 2.1 Left: 'side' view of the anionic clam compound of formula $[Cs(ctcH_5)(ctcH_4)]^{2-}$ in the compound $[C(NH_2)_3]_2[Cs(ctcH_5)(ctcH_4)]$ reported by Abrahams *et al.*[28] The two ctc units are 'fused' together by six complementary hydrogen bonds, represented by black and white banded connections. The Cs^+ cation, represented by a green sphere, within the 'shell' lies equidistant to the six electron-rich aromatic rings in an approximately octahedral environment. Right: top view of the clam.

Table 2.1 A summary of the clam and alkali metal cation assemblies with ctc previously generated within the Abrahams-Robson group. Charges have been omitted in the assembly descriptions.

Composition	Crystal system	Space group	Description of assembly
$(C(NH_2)_3)_2[Rb(ctcH_5)(ctcH_4)].4H_2O$[28]	Tetragonal	*I*-42*d*	**M₁ctc₂** closed clam*
$Rb_2[Rb(ctcH_5)(ctcH_4)].solv$[28]	Trigonal	*R*-3*c*	**M₁ctc₂** closed clam
$(C(NH_2)_3)_2[Cs(ctcH_5)(ctcH_4)].solv$[28]	Monoclinic	$P2_1/c$	**M₁ctc₂** closed clam
$Cs[Cs(ctcH_5)_2].solv$[28]	Monoclinic	$P2_1/c$	**M₁ctc₂** closed clam
$K(ctcH_5).EtOH$[28]	Monoclinic	$P2_1/c$	**$M_n$ctc$_n$** zig-zag polymer
$(NH_4)[NMe_4(ctcH_5)_2].solv$[28]	Monoclinic	$P2/c$	**cation₁ctc₂** partially open clam**
$(NEt_4)[NMe_4(ctcH_5)_2].solv$[28]	Monoclinic	$P2_1/m$	**cation₁ctc₂** open clam
$[DABCO)(ctcH_6)_2].solv$[46]	Triclinic	*P*-1	**cation₁ctc₂** fully open clam***
$Li_6[Li(ctcH_2)((CH_3)_2DABCO)_2]_6$ $[(ctcH_6)_2((CH_3)_2DABCO)].solv$[46]	Trigonal	*R*-3	**$M_n$ctc$_n$** helical 1D polymer

* 'closed clam' refers to a clam with six complementary hydrogen bonds between ctc units. ** 'partially open clam' refers to a dimer of ctc units that host a guest between them and are connected by two hydrogen bonds. *** 'fully open clam' refers to a dimer of ctc units that host a guest between them and are not connected hydrogen bonds.

The ctc unit can also chelate *d*-block metal cations thereby allowing the assembly of anionic molecular 'cage' architectures, which can host group 1 cations.[29,30] Interest has also been directed towards covalently bonded compounds of ctc with *p*-block elements. A porous 2D framework containing ctc bonded to boron centres has been reported,[31] as has a tetrahedral cage assembly with silicon centres, which can uptake Cs^+ from aqueous solution post-synthetically.[25,32] The silicon-based assembly is reported in chapter 5 of this thesis.

As such, ctc is a suitable building block in zero, 1, 2 or 3-dimensional architectures designed to bind, separate or detect large group 1 cations.

The nature of the interaction between ctc and group 2 metal cations, however, remains underexplored, as does the aqueous chemistry of ctc with group 1 and 2 cation mixtures. The interaction of ctc with ubiquitous group 2 dications is worthy of investigation, as they may compete with alkali metal cations, given their higher charge. Their combination with ctc is also expected to yield structurally diverse systems.

In systems containing dioxolene moieties, the pH of the reaction mixture can impact upon the formation of the assembly, given that the H^+ concentration will influence the protonation state. This, in turn, affects not only hydrogen bonding, but also the number of counterions required for charge balance. The aforementioned assemblies of ctc with group 1 cation guests are anionic and were often formed from basic media. It is not clear if the interaction between fully protonated ctc and Cs^+ is strong enough to allow for the formation of a $ctcH_6$–Cs^+ species. Additionally, exploration of ctc–Cs^+ complex formation under acidic conditions is of great interest as it can be compared to the behavior of the hexamethyl analogue of ctc, ctv, which does not form an anion under basic conditions. Ctv has been shown to interact with

caesium preferentially through the methoxy oxygen atoms rather than the electron-rich bowl, in this way forming 1D chains and 2D networks.[33]

Herein are reported 10 supramolecular assemblies generated from the combination of $ctcH_6$ with group 1 and 2 metal cations, under a range of conditions.

When ctc is combined with Cs^+ or Rb^+ in acidic conditions, 6,3-networks can be simply generated. This differs from previous experiments performed under basic conditions in which 'clam' formation was preferred, regardless of the ctc to cation ratio. Stoichiometry was found to have an effect on major reaction products of the experiments performed in acidic conditions, indicating that clam formation occurs in acidic conditions when the ctc to Cs^+ ratio in the reaction mixture is 4:1.

Group 2 metals – which are commonly present in mixtures with the group 1 metals – were also combined with $ctcH_6$ under identical conditions to those yielding Cs^+ clams, in order to investigate possible differences in assemblies of ctc with the group 1 and 2 metal ions. Three unique products were obtained from these experiments, with no clam formation apparent. Competition experiments were also performed, in which both Cs^+ and a group 1 or group 2 metal cation were present. These experiments yielded a notable 3-dimensional assembly, the first reported with ctc, a (10,3)-a network that forms in the reaction with strontium, and a [4+4] metallocycle, whose extended structure displays diamond topology, in the reaction involving lithium.

Notable in this chapter is the structure directing influence of Cs^+ and, to a lesser extent, Rb^+ cations. The Cs^+ and Rb^+ 'clam' and 'half-clam' motifs are recurring in this body of work,

confirming the preference of the large alkali metal cations for the electron-rich ctc bowl, even when the cyclotricatechylene is fully protonated.

2.2 Results and discussion

Work within our research group has produced a number of closed and open clam-like assemblies (see Figure 2.1 for example) in which a ctc dimer hosts a cation.[28] The dimer-guest complexes reported to date have been exclusively anionic in nature, as the number of phenolic protons removed exceeds the charge of the guest monocations. External counterions are therefore present in all previous systems. The motivation for additional study of the alkali metal clams was threefold:

1) to determine if precipitation of the clams from aqueous solutions can be achieved with less base;
2) to identify if altering the pH results in new types of assemblies; and
3) to investigate whether highly charged anionic clams could be synthesised for the purposes of using them as a starting material to generate large coordination cages.

2.2.1.1 Compound 2A – $H_z[Cs(ctcH_x)(ctcH_y)]$ clam

A solution of $ctcH_6$ and CsCl in aqueous methanol, when exposed to ammonia vapour (or layered over aqueous ammonia) yields deep yellow crystals of composition $H_z[Cs(ctcH_x)(ctcH_y)]$ (x = 5 or 6, y = 5 or 6, and $x + y + z = 11$), in which caesium 'clams' are present (Scheme 2.1). A preliminary investigation of this compound was first reported in the candidate's Master of Science thesis, but was re-synthesised in order to obtain better

quality crystals for structure determination. Part of the motivation for continuing this work was to determine the location of one particular phenolic proton, which was of interest due to its potentially important role in hydrogen bonding within the 3D-network.

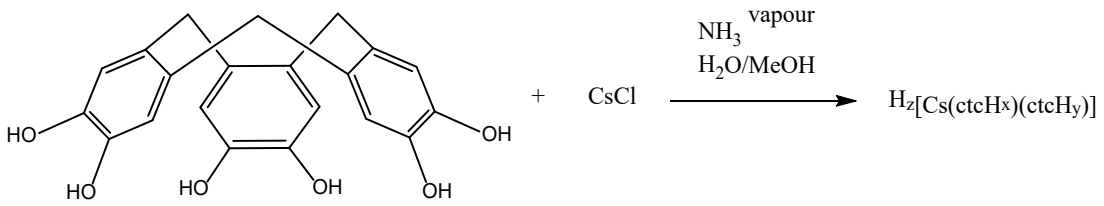

Scheme 2.1 Reaction of $ctcH_6$ with CsCl in an aqueous methanolic solution with ammonia vapour to yield caesium 'clams'.

The crystal structure was solved in the space group $P4_2/ncm$. In the compound, hydrogen bonded clam-like dimers of ctc enclose a Cs^+ cation (Figure 2.2), which is located on a centre of inversion. The two ctc units are rotated 60° relative to one another, adopting a staggered conformation and the catechol oxygen atoms of one ctc are directed toward the space between two catechol units of the other ctc. This staggered arrangement allows phenolic oxygen atoms to make close contact and form six complementary hydrogen-bonds that 'fuse' the two ctc units together (O–H···O separations of 2.63 – 2.68 Å).

Enclosed in each anionic clam shell is an unsolvated Cs^+ that interacts with the aromatic surfaces of the catechol moieties. The centres of each aromatic ring lie at the vertices of an octahedron about the Cs^+; the closest contact between the cation and the clam-shell occurs with the twelve aromatic carbons adjacent to the methylene groups (shortest Cs^+–C distance = 3.449(4) Å).

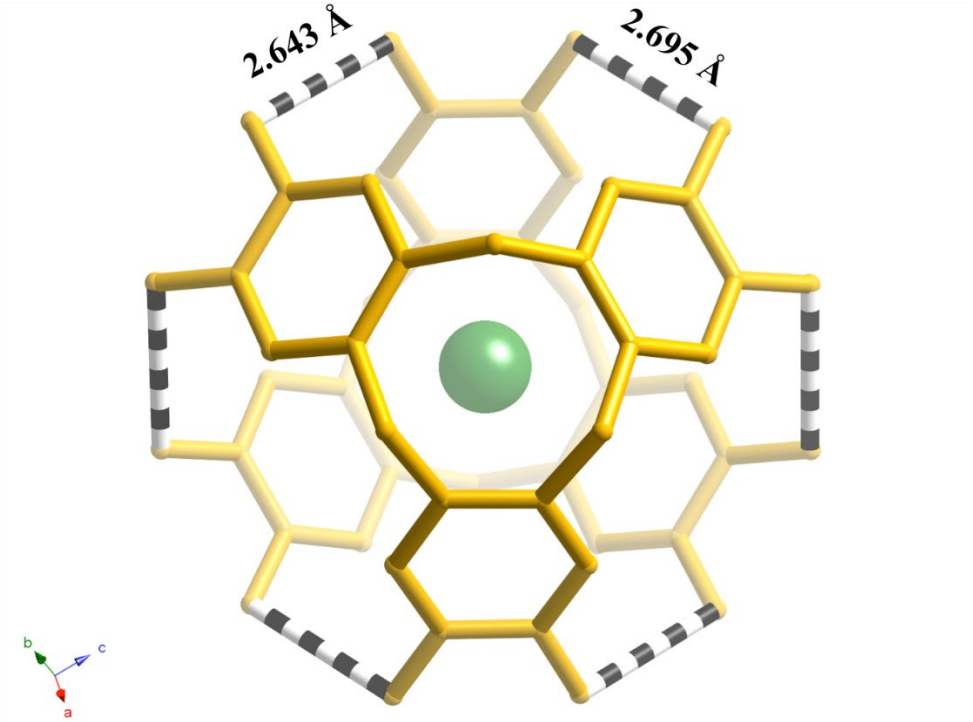

Figure 2.2 A stick figure representation of the 'clam' in compound 2A. The black and white banded connections represent the six complementary hydrogen bonds that 'fuse' the ctc units together. The green sphere at the centre of the clam represents a Cs^+ cation.

An interesting feature of this system is the intermolecular hydrogen bonding interactions that occur in the solid state. Unlike previously reported examples, in which the anionic clams are charge-balanced by external alkali metal or small organic cations, there are no solvent molecules (as indicated by TGA- see appendix) metal ions or organic cations external to the clam. Charge balance is achieved by having eleven hydrogen atoms associated with the catechol oxygen atoms. While ten of these have been crystallographically accounted for, due to the challenges in assigning protons using X-ray crystallography and the high crystallographic symmetry of this system, the position of the 'final' hydrogen atom was unable to be unambiguously identified. Three plausible crystallographic solutions were modelled, but the solutions could not distinguish the location of the hydrogen atom based on either the thermal parameters of the hydrogen atoms in the structure solutions, nor the

difference in their crystallographic *R*-values, which are only slight (Table 2.2). The CIFs of all three solutions have been included in the appendix.

Table 2.2 Details of the three crystallographic structure refinements for compound 2A.

Crystallographic solution name	**Crystallographic structure solution details**	**Crystallographic *R*1 value**
No hydrogen	The final hydrogen atom was assumed to be highly disordered and therefore excluded from the structure solution.	0.0598
Quarter hydrogen	The final hydrogen atom was modelled at a geometrically estimated position on one phenolic oxygen, that by crystallographic symmetry represents four phenolic oxygens in the clam. As such, the hydrogen was assigned one-quarter site occupancy. The relevant oxygen was chosen based on residual electron density and due to the solution being chemically sensible, as the oxygen was bonded to one other phenolic hydrogen, which was only at one-half site occupancy.	0.0592
Special position hydrogen	The final hydrogen atom was positioned on a site which is in a distorted tetrahedral environment, at the location of highest residual electron density according to a difference map (Figure 2.4). This location is equidistant between oxygens of four adjacent clams at 2.026 Å.	0.0589

Solid state ^{1}H and ^{13}C NMR spectra were recorded in order to provide an indication of this hydrogen, but these experiments failed to provide clear information regarding the hydrogen atom's location (see appendix). Single crystal neutron diffraction was not possible due to the small size of the crystals. Simulated powder neutron diffraction patterns corresponding to each of the three plausible crystallographic solutions showed that powder neutron diffraction

analysis would likely fail to discriminate between the three possibilities. The simulated patterns were generated for both hydrogenous and deuterated samples (Figure 2.3). The simulated data were produced by Dr Helen Maynard-Casely (ANSTO) using the GSAS II program[34], and employing the parameters from the high-resolution ECHIDNA instrument at ANSTO using a wavelength of 2.41 Å. It was concluded that the small intensity differences would only make a small difference to the *R*-value obtained for the structure solution.

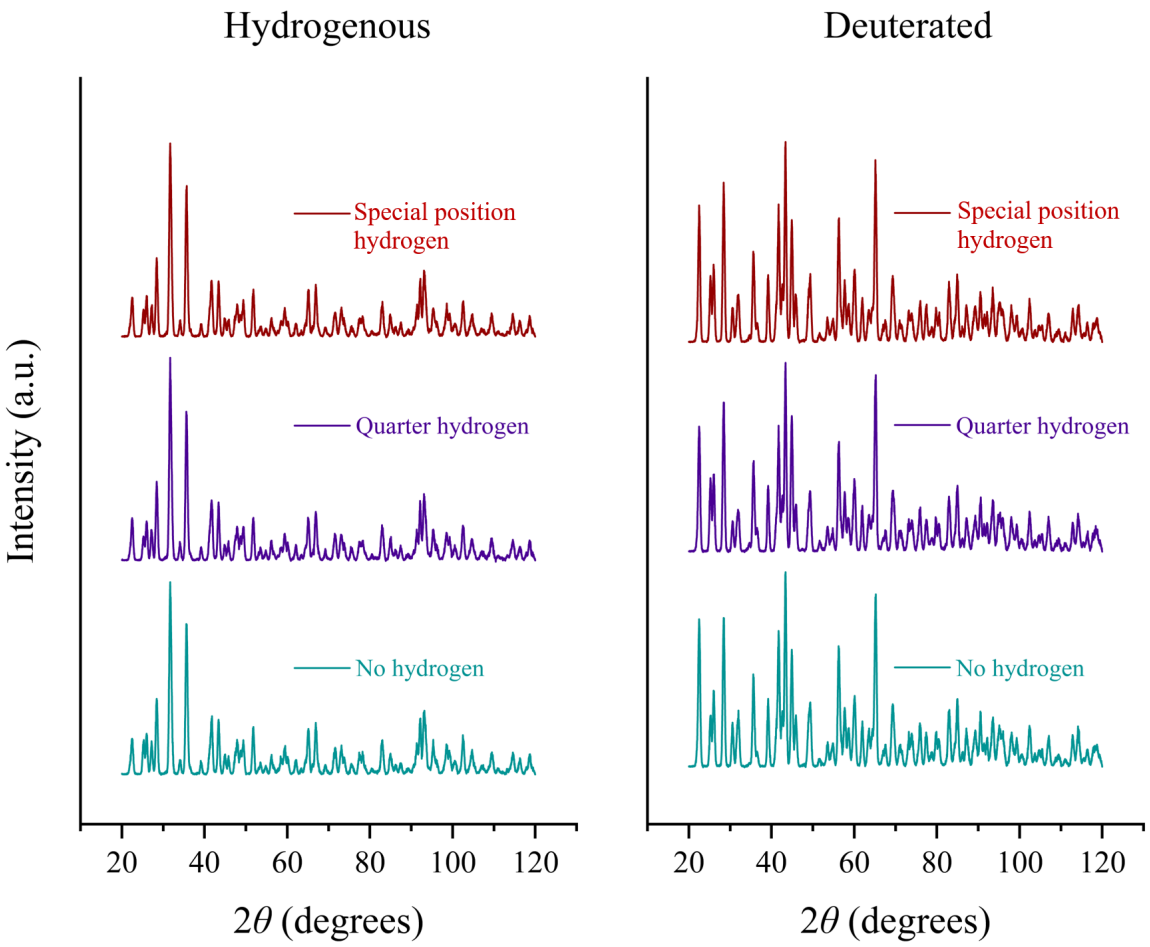

Figure 2.3 Simulated hydrogenous (left) and deuterated (right) neutron powder diffraction patterns for the three X-ray crystallographic solutions for compound 2A. Peaks from all three models are of similar intensities for both the deuterated and hydrogenous compounds.

The structure of 2A described herein was assigned the formula H[Cs(ctcH$_5$)(ctcH$_5$)] and is the result of modelling the data as per the 'special position hydrogen' details in Table 2.1. Inspection of the difference electron density map generated by the WinGX program (Figure 2.4) is also consistent with this assignment. This approach was chosen because it yielded the best crystallographic agreement value, but the result should be treated with caution given the similarity of the *R*-values for all models.

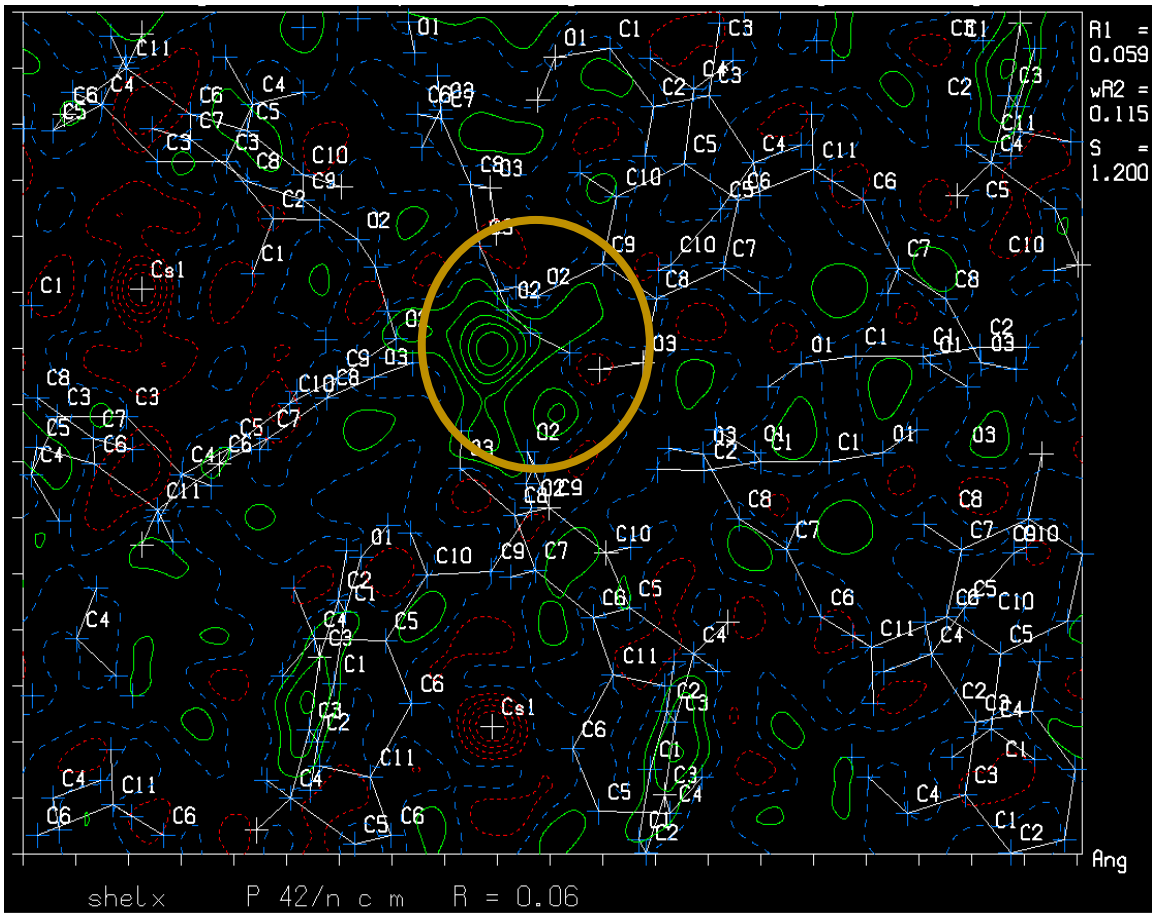

Figure 2.4 Difference map generated from the WinGX program for compound 2A before the final hydrogen required was assigned. The region of highest electron density is indicated by close, concentric green loops (shown within the gold circle).

The network that is formed through intermolecular hydrogen bonding interactions possesses the platinum sulfide (PtS) topology. The aforementioned hydrogen atom acts as a four-connecting distorted 'tetrahedral' node (Figure 2.5), while each clam acts as a four-connecting 'planar' node. The overall network, indicating the underlying PtS topology, is presented in Figure 2.6. There are additional hydrogen bonds with an O−H···O distance of 2.798 Å that exist between adjacent clams which also fuse the network together. These form around the special position at which the proton was modelled.

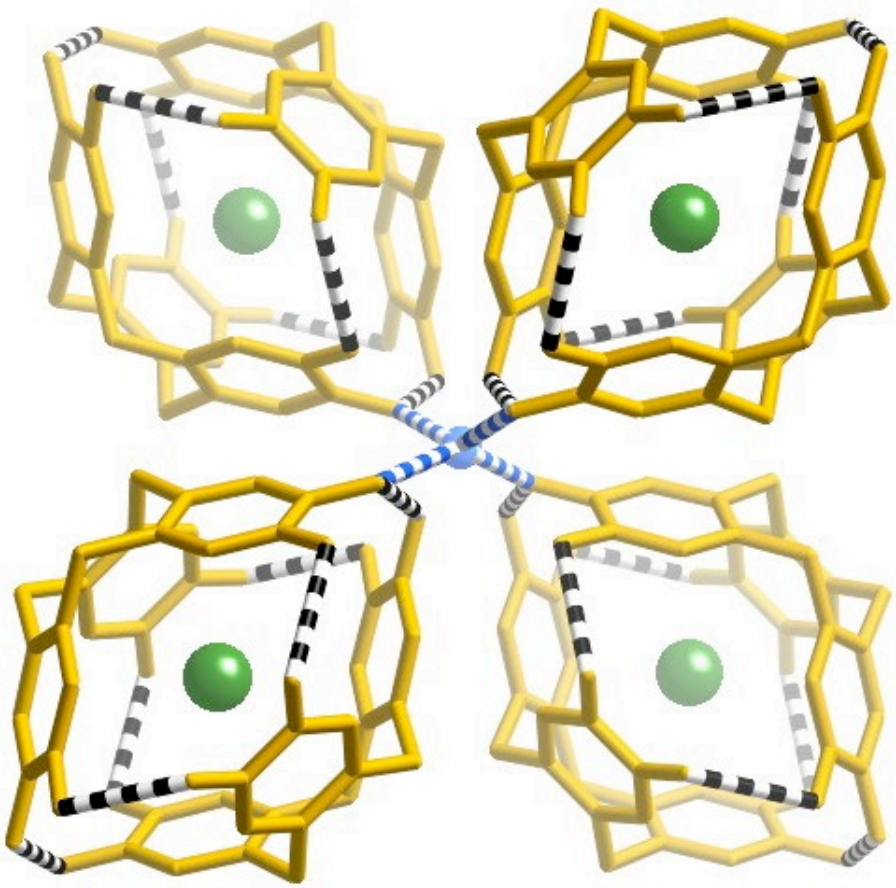

Figure 2.5 A stick figure representation of four adjacent caesium clams in 2A in a distorted tetrahedral arrangement around a proton (blue). Additional hydrogen bonds between clams have been omitted for clarity.

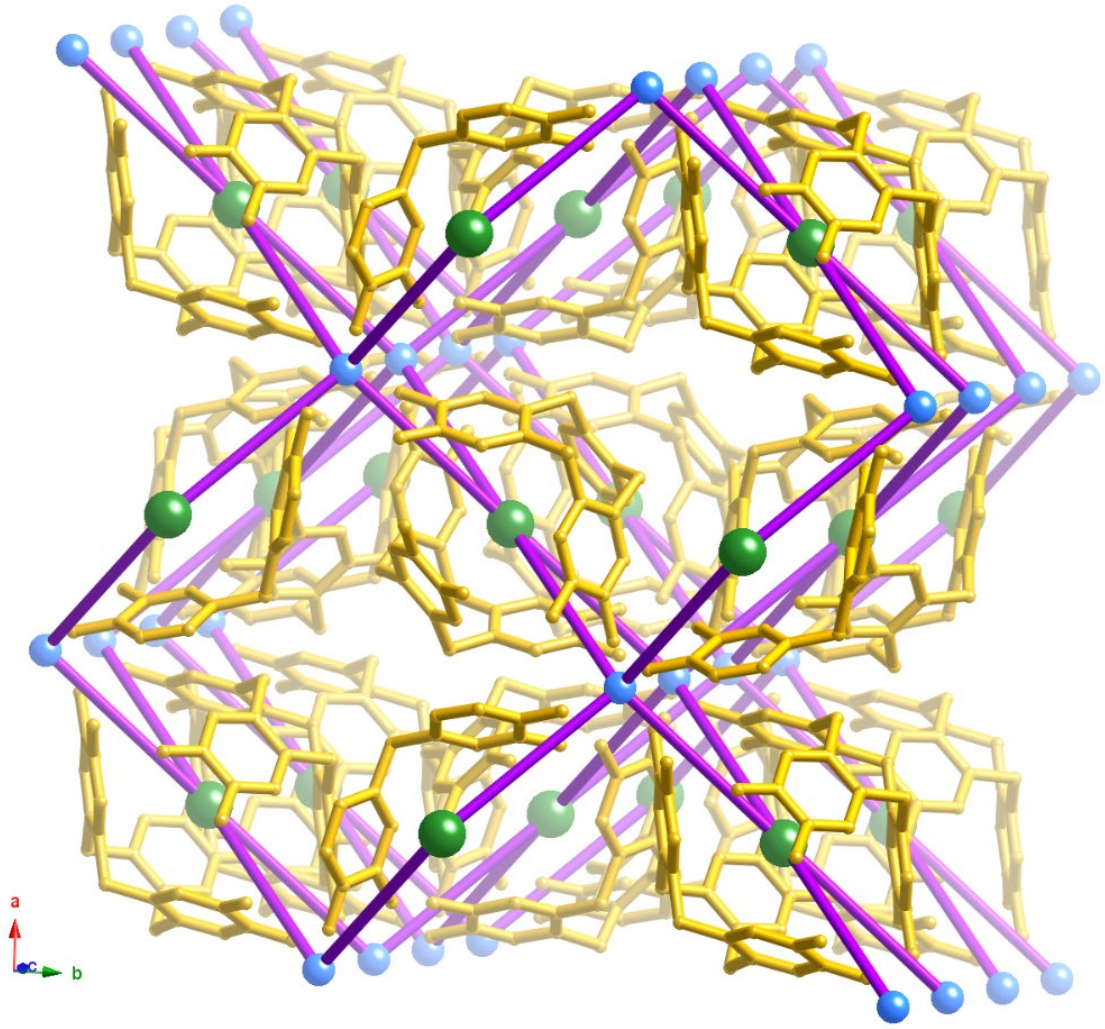

Figure 2.6 A view of the extended network in 2A. The purple connections indicate the PtS topology of the network. The distorted square planar nodes are located at the centre of each clam and are therefore at the position of the Cs^+ (green sphere). The distorted tetrahedral nodes are the protons (blue sphere), which interact with four adjacent clams.

In this configuration of molecules arranged equidistantly around a single H^+ cation, the four oxygen atoms may all be considered donor atoms. In this example, the H^+ cation is equally shared between the donor oxygen atoms by virtue of strong hydrogen bonds. This differs from the classical hydrogen bond in which one atom (the donor) is covalently bonded to a hydrogen atom, and another electronegative atom (the acceptor) interacts less strongly with the hydrogen atom, via predominantly electrostatic interactions.

Symmetrical hydrogen bonds between degenerate donor atoms, such as those in 2A, usually fall into a class of bonds referred to as single well hydrogen bonds.[35] In the literature, a similar example of four donor atoms arranged about a central proton is a cage adamanzane of formula [H[3^6]adamanzane]Br] in which four nitrogen atoms surround a central proton.[35] Although in the solid state the proton is located at one of the four identical nitrogen atoms, the solution state ^{1}H and ^{13}C NMR data indicate that the complex has tetrahedral symmetry and therefore that the proton interacts equally with all for nitrogen donor atoms when in solution.

The generation of 2A is achieved by slow liquid/vapour or liquid/liquid diffusion of ammonia into the ctc/Cs^+ solution, allowing for a single deprotonation per pair of ctc molecules. The formation of multiple hydrogen bonds between clams appears to drive crystallisation and may explain the insolubility of the resultant product in most common non-hydroxylic laboratory solvents, both polar and non-polar.

Mass spectrometry experiments were performed on the clam complex to probe its gas phase chemistry with a view to discovering if ctc dimers bonded to Cs^+ from compound 2A persist in the gas phase, as they were observed to do when ctc, a caesium salt and ammonia were combined in methanol (ESI-MS *m/z* observed = 863.1082 for the 1− species[28]). For a clam species from 2A to be observed, one or more protons must be lost from or gained by H[Cs($ctcH_5$)($ctcH_5$)], unlike the anionic clam, which did not require ionization in the spectrometer. Due to the insolubility of 2A in common laboratory solvents, Matrix Assisted Laser Desorption Ionisation (MALDI) experiments were undertaken. A small amount of dilute acetic acid was used to assist the experiment. Interestingly, very little signal was observed in negative ion mode above *m/z* = 500, suggesting that the 1− species was not

present. In positive ion mode a protonated cationic clam adduct ($Cs(ctcH_6)_2$) was observed at *m/z* = 865.124951 (calculated *m/z* = 865.125575, error = 0.722 ppm), shown in Figure 2.7.

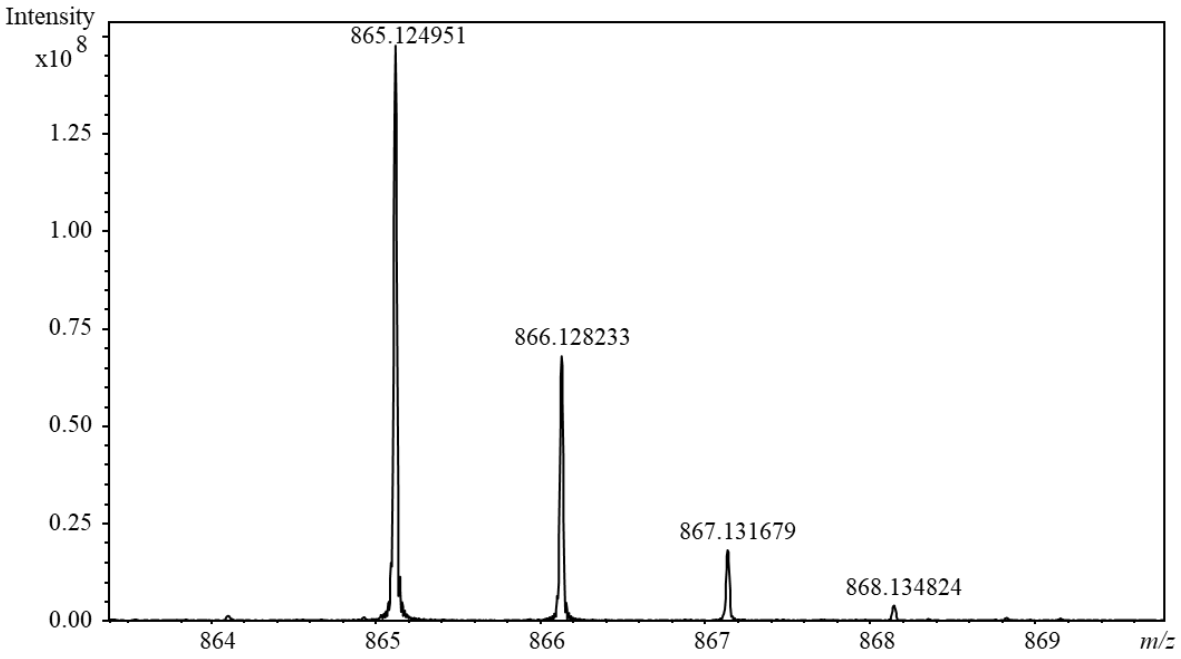

Figure 2.7 Positive ion mode MALDI spectrum of 2A from *m/*z = 863 to *m/z* = 870, showing a series of isotopologues resulting from a positively charged clam species of composition $Cs(ctcH_6)_2$.

A wide variety of clam decomposition products were observed in the negative ion mode (detailed in Figure 2.8 and Table 2.3). This is consistent with the known rich redox chemistry of ctc, which is often exploited in electrochemical studies.[36] The most abundant of these species is found at *m/z* = 497.000727 (error = –0.088) corresponding to a species of composition $[Cs(C_{21}H_{16}O_6)]^-$, which is a ctc adduct with caesium that has lost both two protons and two electrons. In addition, adducts of ctc with ubiquitous alkali metal cations (Na^+, K^+) are observed in the gas phase, with expectedly lower abundance, as are free ctc and many of its decomposition products (see appendix).

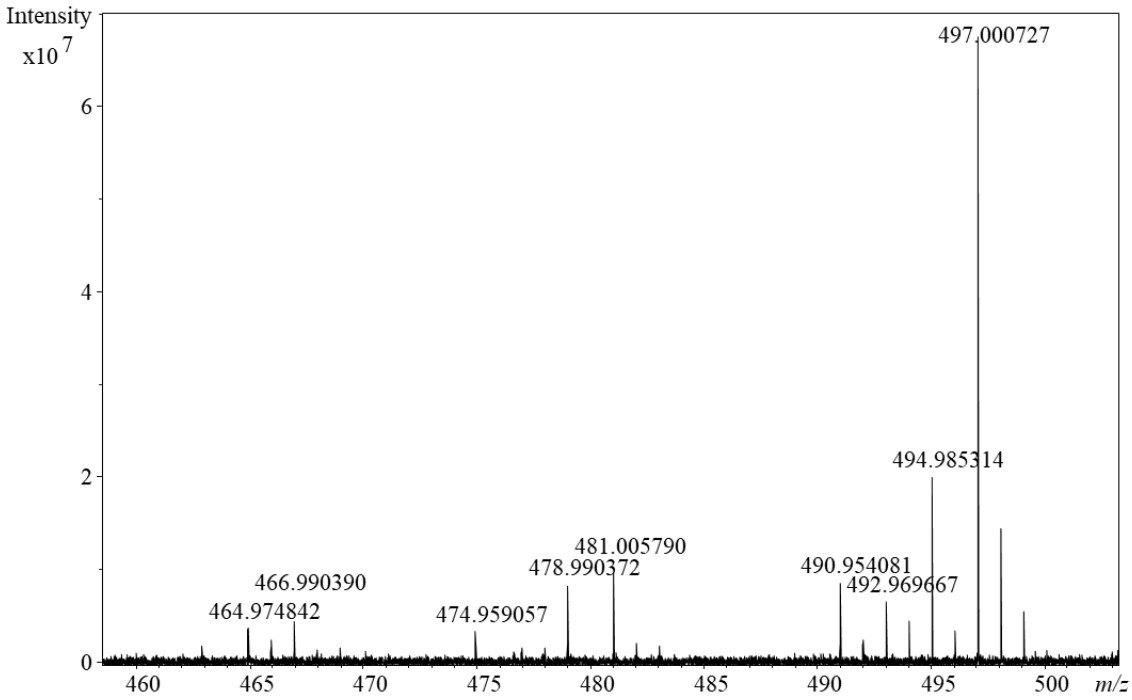

Figure 2.8 Negative ion mode MALDI spectrum of 2A from *m/z* = 460 to *m/z* = 500, showing various decomposition products of 2A, which are all monoanions.

Table 2.3 Negative mode MALDI data for 2A from *m/z* = 460 to *m/z* = 500, showing various decomposition products of 2A, which are all monoanions.

Measured *m/z*	**Formula**	**Calculated *m/z***	**Error [ppm]**
464.974842	$Cs(C_{20}H_{12}O_5)$	464.974469	0.803
466.99039	$Cs(C_{20}H_{14}O_5)$	466.990119	-0.581
474.959057	$Cs(C_{21}H_{10}O_5)$	474.958819	-0.502
478.990372	$Cs(C_{21}H_{14}O_5)$	478.990119	-0.529
481.00579	$Cs(C_{21}H_{16}O_5)$	481.005769	-0.043
492.969667	$Cs(C_{21}H_{12}O_6)$	492.969384	-0.575
494.985314	$Cs(C_{21}H_{14}O_6)$	494.985034	-0.566
497.000727	$Cs(C_{21}H_{16}O_6)$	497.000684	-0.088

The species (from top to bottom of Table 2.3) correspond to:

Cs^+ with ctc (− O, − C, − $6H^+$); Cs^+ with ctc (− O, − C, − $4H^+$);

Cs^+ with ctc (− O, − $8H^+$); Cs^+ with ctc (− O, − $4H^+$); Cs^+ with ctc (− O, − $2H^+$);

Cs^+ with ctc (− $6H^+$) that has undergone a $4e^-$ oxidation; Cs^+ with ctc (− $4H^+$) that has undergone a $2e^-$ oxidation; Cs^+ with ctc (− $2H^+$).

The presence of the monocation at *m/z* = 865.124951 in the gas phase does not unambiguously confirm the clam-type conformation of the assembly in the gas or solution state. Samples of the clam compound and $ctcH_6$ were provided to Dr. Nicole Rijs at the Karlsruhe Institute of Technology for further investigation using nanoESI. Relevant preliminary results of this collaborative investigation are presented below.

Halide salts of the alkali metal cations were combined with $ctcH_6$ in solution and their N_2 collisional cross-sectional areas were measured using nanoESI experiments. Compounds of formula $[(ctcH_6)_2 \cdot M]^+$ were observed in the gas phase for M = Li^+, Na^+, K^+, Rb^+ and Cs^+. The $[(ctcH_6)_2 \cdot M]^+$ species in the gas phase were observed to have different collisional cross sectional areas, that depended on two factors: 1) the size of the alkali metal cation and 2) the arrangement of the three components in the complex (i.e. the isomer formed).

The smaller cations, lithium and sodium were observed to form two isomers each, whereas the larger cations – potassium, rubidium and caesium were each only observed to form one isomer.

The identity and structures of the isomers were determined by comparing the experimental collisional cross-sectional areas to collisional cross-sectional areas computationally predicted for theoretical $[(ctcH_6)_2 \cdot M]^+$ isomers (whose values were optimized at UB3LYP-

D3/def2TZVP). A match between the experimentally determined collisional cross-sectional area of an ion with that of a computationally predicted isomer provided evidence for the formation of that particular structural isomer.

Comparison of experimental and theoretical data indicate that lithium and sodium both form an isomer where the cation is located outside of a hydrogen bonded clam, and is chelated by a catechol from just one of the ctc units. The structure of the second experimentally observed $[(ctcH_6)_2 \cdot Li]^+$ isomer could not be unambiguously identified, but it was confirmed that lithium did not form any of the theoretically predicted complexes in which there were cation-π interactions, preferring to interact with catechol oxygens. This is consistent with both the literature and the condensed phase work reported in this thesis. Surprisingly, the second experimentally observed $[(ctcH_6)_2 \cdot Na]^+$ isomer was a clam. This is an interesting result that warrants further investigation as a sodium 'clam' has not been observed in the condensed phase, despite attempts to crystallise one.

The $[(ctcH_6)_2 \cdot M]^+$ (M = K^+ and Rb^+) complexes were also determined to be clams. The $[(ctcH_6)_2 \cdot Cs]^+$ cation was observed based on its mass to charge ratio, however the three dimensional arrangement of the components in the complex could not be unambiguously identified in this study. At the time of writing, the computational and experimental parameters for the study of ctc with caesium still require refinement. Details of the preliminary studies and further studies with the caesium cation will be presented in a forthcoming publication.

The nanoESI studies showed that, as per condensed phase experiments, the types of adduct formed are highly solution dependent and vary with factors such as pH, anion, concentration and solvent. Employing different nanoESI experimental conditions is also expected to affect

the results and the effect of changing the experimental conditions is currently being investigated further by our collaborators.

Regardless of experimental conditions, the general trends of adduct size of ctc–group 1 complexes from the nanoESI computational and experimental studies mirror the trends in the condensed phase (Table 2.4), i.e. the size of complexes increases as cation size increases, and compounds with smaller cations are more likely to have M^+–O interactions than those with larger cations, which preferentially have associations between the cation and the aromatic surfaces of the ctc.

Table 2.4: Atomic separations in selected ctc adducts with alkali metal cations in the condensed phase. Distances were determined using X-ray crystallography, typically performed at 130 K.

Condensed phase compound(s)*	**Identifier(s)**	**Shortest M^+– aromatic C distance(s) (Å)**	**Longest O_{ctc1}– O_{ctc2} distance(s) (Å)****	**Longest C_{ctc1}– C_{ctc2} distance(s) (Å)****	**Shortest M^+– O_{ctc} distance(s) (Å)*****
Clam: $[Cs(ctcH_5)(ctcH_4)]^{2-}$	CCDC: HOXYEZ[28]	3.47	9.96	8.36	–
Clam: $H_z[Cs(ctcH_x)(ctcH_y)]$	Compound 2A	3.45	10.01	8.14	–
Clam: $[Cs(ctcH_6)_2]^+$	Compound 2B	3.44	10.24	8.27	–
Clams: $[Rb(ctcH_5)(ctcH_4)]^{2-}$	CCDC: HOXYAV[28] HOXYOJ[28]	3.36 3.35	9.91 10.22	7.99 7.91	–
Half-clam motif in network: $([Cs(ctcH_6)]^+)_n$	Compound 2C Compound 2D	3.63 3.48	–	–	3.20 2.98
Half-clam motif in network: $([Rb(ctcH_6)]^+)_n$	Compound 2E	3.43	–	–	2.82
Half-clam motif in network: $([K(ctcH_6)EtOH]^+)_n$	CCDC: HOXXUO[28]	3.20	–	–	2.58
Clam in network: $([Cs_2[Li_4(ctcH_3)_4]]^{6-})_n$ for M = Cs^+ in clam	Compound 2J	3.47	9.59	8.24	–

Network: $([Cs_2[Li_4(ctcH_3)_4]]^{6-})_n$ for M = Li^+	Compound 2J	–	–	–	1.94
Half-clam in network: $[CsSr(ctc)]_n^{3n-}$ for M = Cs^+ in bowl	Compound 2I	3.53	–	–	–
Cage in $(Cs_n[K_4(ctcH_6)_4])^{(4+n)+}$ for M = Cs^+ in bowl	Compound 3A Compound 3C	3.52 3.55	–	–	–
Cage in $(Cs_n[K_4(ctcH_6)_4])^{(4+n)+}$ for M = K^+	Compound 3A Compound 3C	–	–	–	2.85 2.87
Cage in $(Rb_n[K_4(ctcH_6)_4])^{(4+n)+}$ for M = Rb^+	Compound 3B Compound 3D	3.39 3.47	–	–	–
Cage in $(Rb_n[K_4(ctcH_6)_4])^{(4+n)+}$ for M = K^+ in bowl	Compound 3B Compound 3D	–	–	–	2.87 2.88

. *The formula of the compound is given for the oligomer or polymer framework containing ctc; external counterions and non-coordinated solvent molecules are omitted. **The subscripts 'ctc1' and 'ctc2' indicate that the distance reported is between atoms from the two adjacent ctc units in a clam. ***The subscript 'ctc' indicates that the distance reported is to the oxygen of a ctc to which the metal is bonded, not to another ligand such as water.

The above results indicate that there is a rich chemistry associated with ctc when it is combined with the caesium cation. The species formed include a novel cationic adduct of two ctc units with caesium in the gas phase, that had not previously been observed in the solid state.

A number of additional experiments were undertaken to identify if clam-type adducts of ctc with Cs^+ could be formed where the charge on the clam was greater than 2−. The intention of these synthetic attempts was to discover if clam motifs could be incorporated into larger supramolecular structures. Having building blocks in which ctc was already deprotonated would allow for reactions in the absence of common bases such as hydroxides and amines, and would therefore eliminate potential confounding counterions in the resultant compounds.

In these experiments, $ctcH_6$ (24 mg, 0.065 mmol) was dissolved in a solvent (e.g. acetone, dioxane, ethanol, methanol or isopropanol) and layered above an aqueous solution containing either 6 or 24 molar equivalents of CsOH. These solutions turned brown at the interface and most produced flocculent white material after less than a day. Only one of many synthetic attempts produced crystals suitable for X-ray diffraction studies, however a structure solution could not be obtained. Some experiments produced microcrystalline materials that were unable to be identified at the time.

The results of this set of experiments are in line with many other experiments in which CsOH has been combined with ctc, wherein white precipitate is resultant (sometimes immediately) on combination of the reagents. In some experiments (not detailed in this thesis) this precipitate has been shown via powder diffraction to be the clam, 2A, described above. In other experiments this clam had been observed in single crystal form, despite numerous other reagents being present in the reaction mixture. In other experiments the precipitate has been amorphous.

The results detailed here, in addition to observations made during the candidate's MSc research, indicate that while clams with a higher charge (without non-caesium counterions) may be possible to obtain in the solid state under the right conditions, they are not simply formed using approaches commonly employed in this work. For example, although clams with only six of a possible twelve phenolic protons can, in theory, form the six complementary hydrogen bonds observed in the other closed clam species reported by the group, such clams, which would have an overall charge of 5–, have not been isolated in the solid state. This is despite numerous synthetic attempts involving excess base to deprotonate the ctc, as well as employing a variety of countercations to balance the charge.

To investigate the potential of a clam with a positive charge in the condensed phase, synthetic procedures employing ctc in combination with caesium under acidic conditions were undertaken.

2.2.2 Chemistry of ctc and caesium under acidic conditions

A set of experiments, which yielded products 2B – 2D, was conducted to investigate the structural diversity of assemblies of ctc with caesium cations when combined under acidic conditions. In acidic conditions ctc may be reasonably expected to remain fully protonated based on the pK_a values for catechol (pK_{a1} = 9.45; pK_{a2} = 12.8),[37] however it is important to note that the degree of protonation in solution may not necessarily be representative of the protonation state of the ctc within the crystals formed from the solution.

Fully protonated ctc has a reduced electron density on the 'bowl' compared to anions of ctc formed under basic conditions. It follows that caesium and rubidium cations may not interact as strongly with the ctc bowl and may therefore form different assemblies than previously observed. Additionally, the presence of any counter anions necessary to balance the charge of the caesium cations would be expected to influence the 3D-crystal structure.

The preparation of products under acidic conditions was achieved by combining the metal chloride with ctc in ethanol which contained concentrated hydrochloric acid. These reactions were performed in ethanol rather than using methanol because while ctcH_6 can easily be dissolved in methanol under basic conditions, rapid precipitation of the methanol solvate of ctc occurs in acidic or neutral conditions.

The combination of caesium chloride with ctc under acidic conditions yielded a clam type structure (2B) and bilayered honeycomb networks (2C and 2D). The formation of the caesium-containing compounds 2B, 2C and 2D is indicated in Scheme 2. A feature of the three honeycomb assemblies is the 'half-clam' motif in which each ctc hosts a metal cation in its bowl but the metal cation does not sit in the bowl of a second ctc.

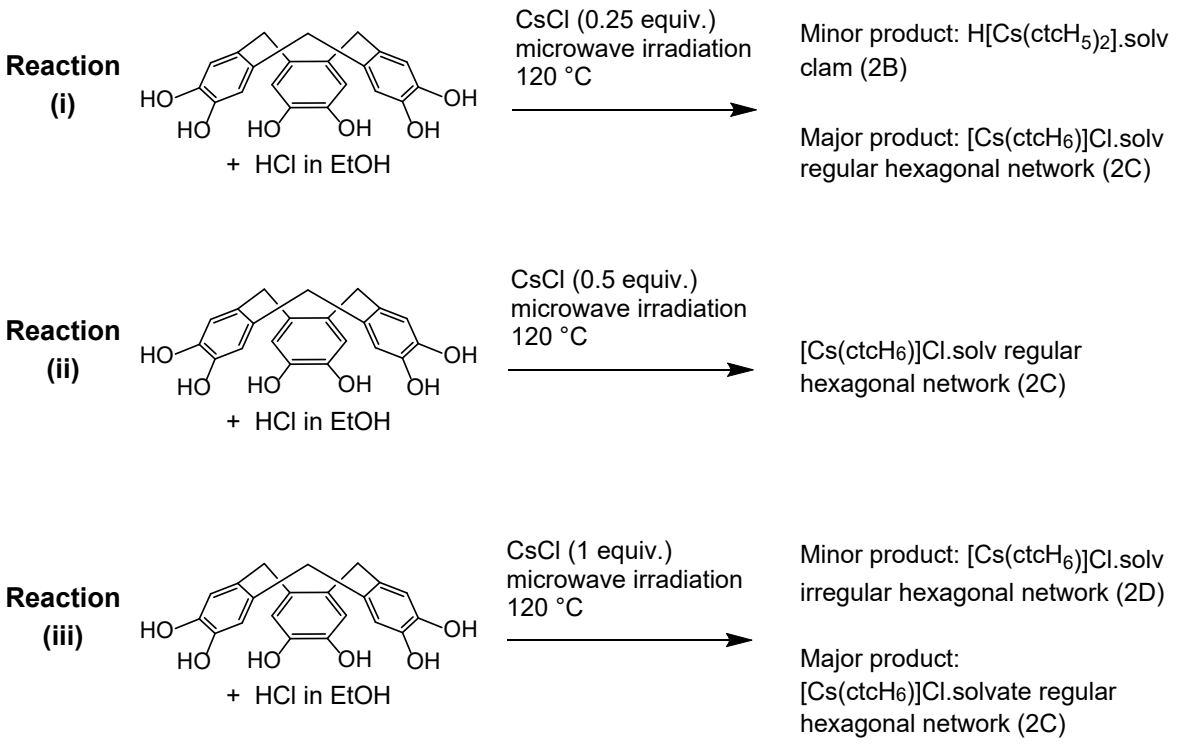

Scheme 2 The products of the reactions of $ctcH_6$ with CsCl in EtOH in the presence of HCl. In reaction (i), crystals of compound 2B suitable for X-ray crystallography were obtained, however the bulk product was found to be predominantly 2C. In reaction (ii), crystals of compound 2C suitable for X-ray crystallography were obtained. In reaction (iii) crystals of compound 2D suitable for X-ray crystallography were obtained, however the bulk product was found to be predominantly 2C.

2.2.2.1 Compound 2B – $[Cs(ctcH_6)_2]Cl{\cdot}EtOH$ cationic clam

The previously unobserved cationic clam complex crystal structure, consisting of two fully protonated cyclotricatechylene molecules encapsulating a Cs^+ centre, was predicted to form when $ctcH_6$ was combined with caesium under acidic conditions. The combination of ctc with 0.25 mole equivalents of CsCl and HCl in ethanol yielded irregular colourless crystals of composition $[Cs(ctcH_6)_2]Cl{\cdot}EtOH$ after the solution was irradiated with microwaves (Scheme 2, reaction (i)). Single crystal X-ray diffraction was performed and revealed the presence of the predicted cationic clam-type product in the crystals, which form in the triclinic crystal system. Chloride counter ions provide the necessary charge balance.

Unsurprisingly, the clams interact with each other via intermolecular hydrogen bonding interactions and are further linked through O−H···Cl interactions (six per chloride and six per clam) ranging from 2.98 to 3.43 Å. Each chloride anion is 'chelated' by catechol units from two clams and interacts with a pair of oxygen atoms from two different ctc units of a third clam (Figure 2.9). The chloride ions are crystallographically disordered over two closely separated positions. Ethanol molecules are also present, one per clam, disordered over two positions.

Hydrogen bonding and O−H···Cl interactions result in the arrangement of the clams in two dimensional sheets that stack atop of each other in an ABAB packing arrangement. This arrangement is apparent when viewed along the crystallographic *b* axis which is normal to the stacking direction (Figure 2.10).

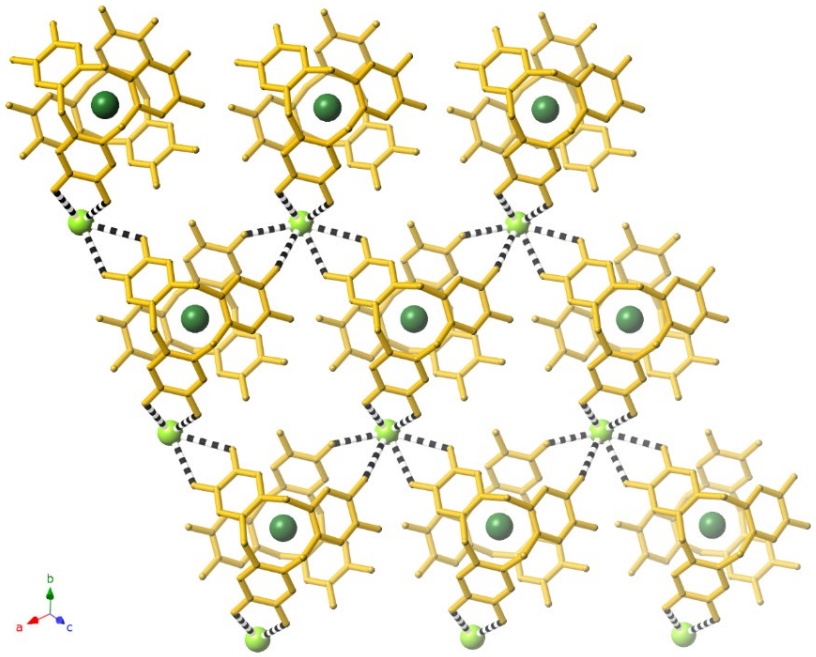

Figure 2.9 A representation of a sheet of cationic clams and chloride counter ions (fluoro green) in 2B. Black and white striped connections indicate O−H···Cl interactions. Hydrogen atoms and solvent molecules have been omitted for clarity. In this figure only one of the two crystallographic positions of the chloride ions is shown.

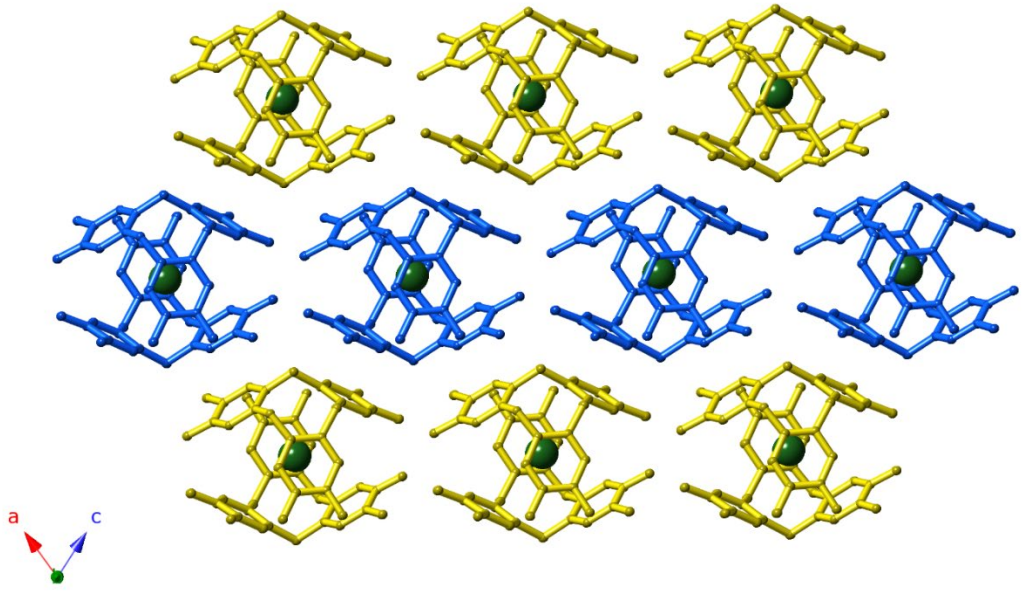

Figure 2.10 A ball and stick representation of the ABAB arrangement of the sheets of clams in compound 2B. Clams from the two sheets shown in yellow are aligned with each other, whereas clams from the sheet shown in blue are offset. Hydrogen atoms, solvent and chloride counter ions have been omitted for clarity.

The combination of ctc and CsCl under acidic conditions does not, however, exclusively form 'clams'. Synchrotron X-ray powder diffraction experiments (Figure 2.19 and Figure 2.20), which are discussed following the structure descriptions, show that the clams are a significant but minor product when ctc is in 3-fold excess over the caesium cation. The major product that results from the reaction that yielded a crystal of 2B is actually compound 2C. Compounds 2B and 2C, which are both produced via reaction (i) in Scheme 2, were not able to be separated.

2.2.2.2 Compound 2C – [Cs(ctcH$_6$)]Cl·0.5EtOH (6,3) network

When CsCl and ctc are combined in the same conditions that yielded 2B, and the ctc:CsCl ratio is ≥ 2, light-yellow block-like crystals of composition [Cs(ctcH$_6$)]Cl·0.5EtOH (2C) form (Scheme 2, reaction (ii)). Single crystal X-ray diffraction was performed, revealing a crystal structure consisting of a honeycomb-like network (known as a (6,3) net using Wellsian notation)[38] in which both Cs^+ cations and ctc act as 3-connecting nodes (Figure 2.11). This compound, 2C, was also identified as the major product in the reaction that yielded compound 2B (Scheme 2, reaction (i)) and in the reaction that yielded 2D (Scheme 2, reaction (iii)).

In compound 2C, each ctc chelates three Cs^+ cations, and each Cs^+ is chelated by three ctc molecules, therefore both ctc and Cs^+ can be considered 3-connecting nodes in the network. Only one hemisphere of each Cs^+ cation is chelated by ctc units. The other hemisphere faces into the bowl of a ctc resulting in the formation of a 'half-clam' (Figure 2.12). The host ctc is from an identical, but inverted, complementary sheet. Each ctc in a sheet also hosts a Cs^+ cation from its complementary sheet.

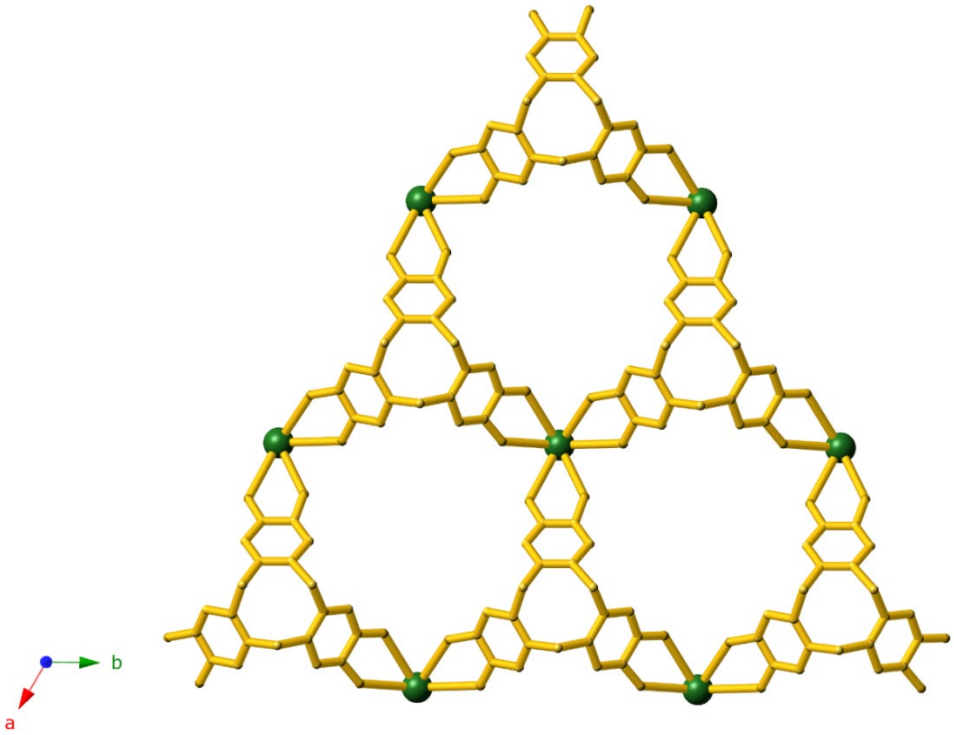

Figure 2.11 A ball-and-stick representation of a single layer of a sheet in 2C showing the (6,3) net topology wherein Cs^+ cations (green) and ctc units are both 3-connecting nodes. Hydrogen atoms have been omitted for clarity.

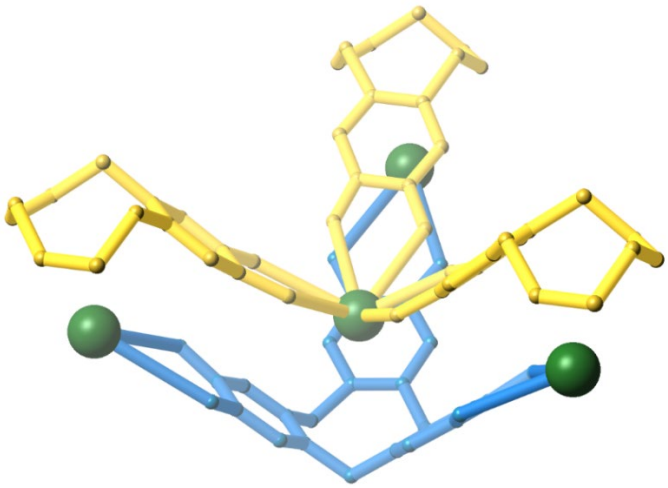

Figure 2.12 A ball-and-stick representation of the chemical environment of the caesium cation (green) in 2C. A caesium cation is shown to sit within the bowl-like cavity of a ctc, shown in blue, in a 'half-clam' motif. This ctc is bonded to three caesium cations, which each sit in bowls of ctc units (yellow) that are connected to the central caesium cation.

The result of these interactions is a puckered 'bilayered' sheet, which provides an aesthetically appealing example of self-complementarity in a supramolecular assembly (Figure 2.13). This same interaction is present in a compound of ctc with K^+, $K(ctcH_5)\cdot EtOH$, previously reported by our group (CCDC ID: HOXXUO).[28] In $K(ctcH_5)\cdot EtOH$, bilayered 1D-chains are present, and the K^+ centres of one chain lie within the bowls of ctc units from the complementary chain. Whilst in 2C the metal centres are approximately equidistant from each of the three aromatic faces of the ctc bowl, in the potassium compound the metal centres lie closer to one aromatic face of the bowl, owing to the imperfect fit of the relatively small potassium cation in the ctc bowl.

The distance between adjacent Cs^+ ions within a layer of a sheet is 12.25 Å. The closest contact between sheets in the bilayer is 2.97 Å between catechol oxygens from adjacent sheets. 3-fold rotation axes run perpendicular to the layers, through all caesium centres. A second type of 3-fold axis passes through the hexagonal windows.

The bilayered sheets stack directly atop each other (Figure 2.14) which leaves hexagonal channels running parallel to the crystallographic *c* axis. There is extensive π-π stacking *between* bilayered sheets, the shortest C−C distance being 3.521 Å. Within the hexagonal channels of the honeycomb network are disordered chloride counter ions, one per alkali metal cation (Figure 2.15). Additional electron density which could not be modelled was also present within the channels, so the structure was refined on "squeezed" data obtained using the PLATON program.[39] The calculated residual electron density was attributed to half a highly disordered ethanol molecule per ctc.

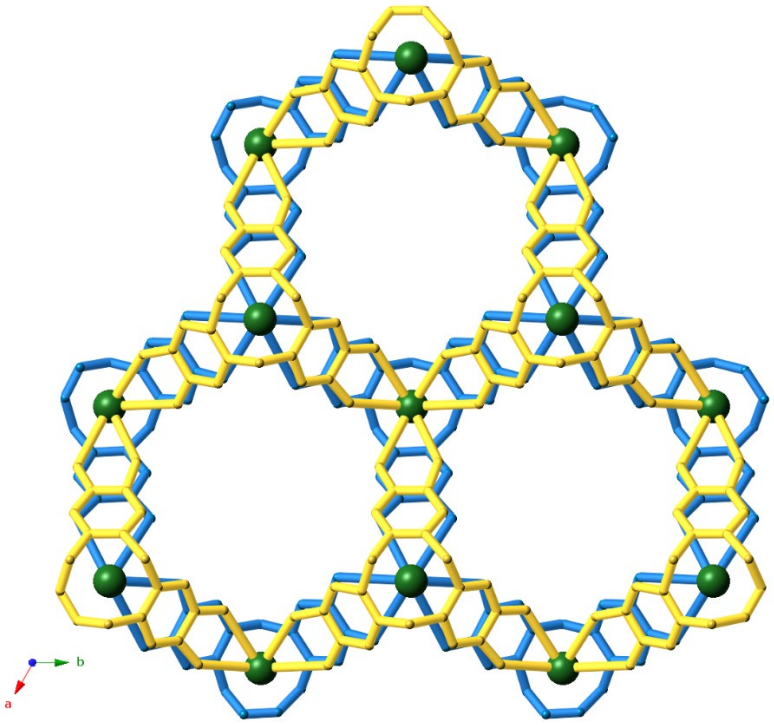

Figure 2.13 A ball-and-stick representation of the bilayered sheet in 2C. Caesium cations (green) are chelated by three ctc units from their own sheet and sit in the bowls of the complementary sheet. The sheets are shown in blue and yellow. The cation-bowl interactions give rise to the observed bilayered sheet structure.

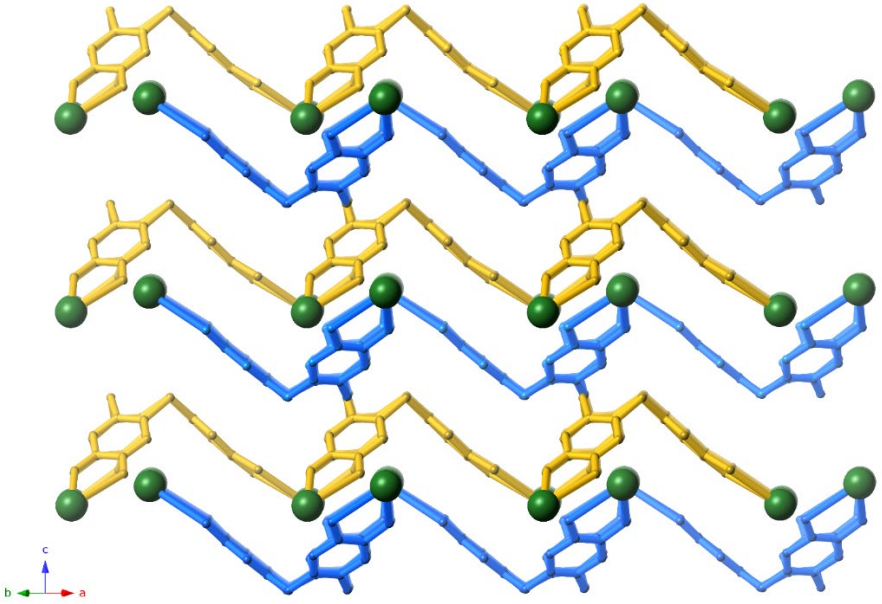

Figure 2.14 A ball and stick representation of the stacking of three bilayered sheets in 2C. Layers in yellow represent the top half of each bilayered sheet, with the blue layer beneath it representing the other half. All cations and solvent molecules have been omitted for clarity.

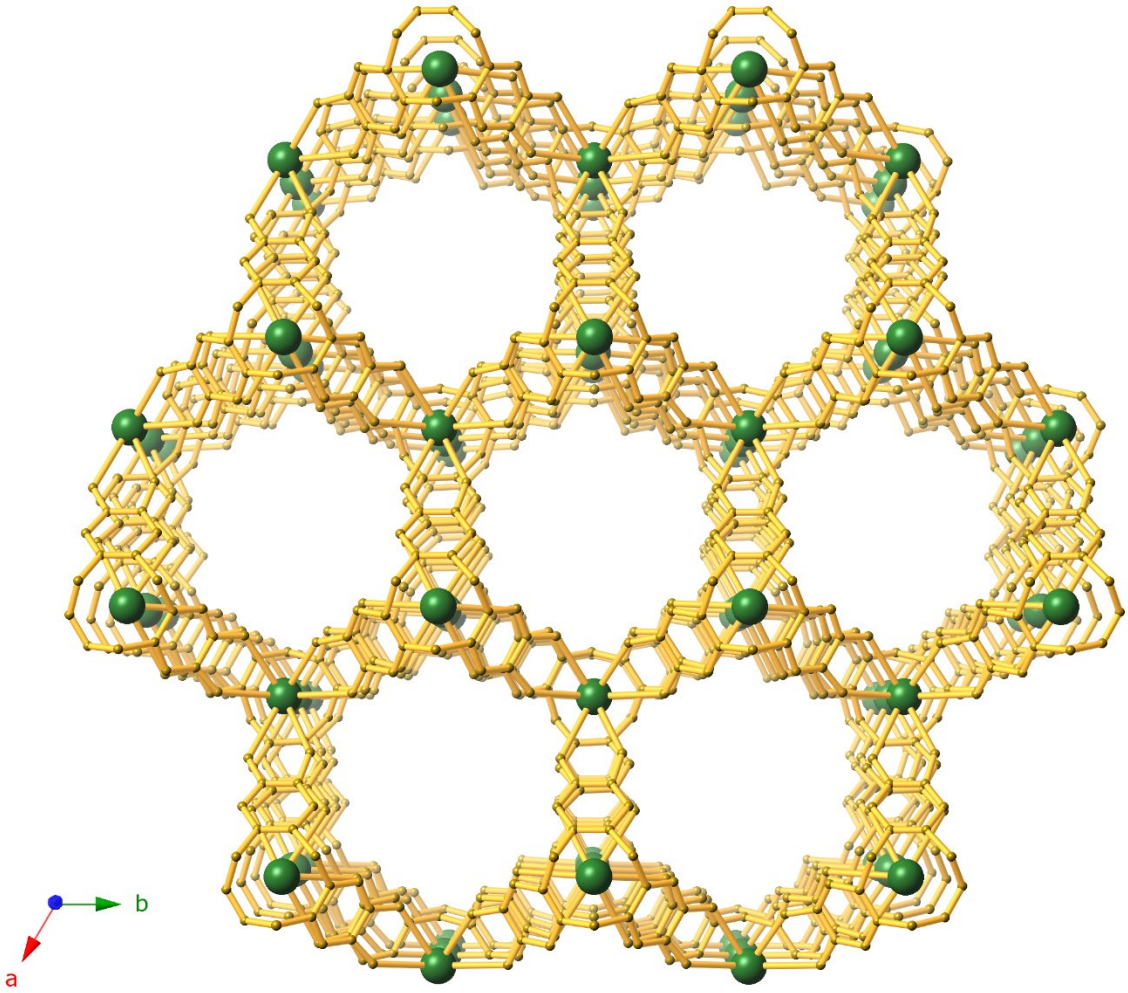

Figure 2.15 A ball-and-stick representation of the channels in 2C. Disordered chloride counterions and solvent molecules (not shown) are present in each channel. Hydrogen atoms have been omitted for clarity.

2.2.2.3 Compound 2D – [Cs(ctcH$_6$)]Cl·EtOH (6,3) network

As indicated in reaction (iii) of Scheme 2, the combination of ctc and CsCl in equimolar amounts, along with HCl and ethanol yields compounds 2C and 2D. Compound 2D is a (6,3) network that closely resembles 2C in composition and appearance. Single crystal X-ray diffraction analysis of a light-yellow rod-like crystal obtained from reaction (iii) revealed that the compound is a distorted hexagonal network of composition [Cs(ctcH$_6$)]Cl·EtOH.

The distortion of the channels from a regular hexagonal geometry arises from hydrogen bonding interactions between a catechol oxygen from one ctc and a catechol proton from an adjacent ctc (O–H···O distance 2.78 Å). The catechol group that is the hydrogen bond donor does not chelate a Cs^+ (as in 2C), rather it participates in hydrogen bonding through one of its phenol groups and binds to Cs^+ through the other. Apart from this difference the structures are very similar, with the formation of a bilayer apparent in 2D, as can be seen in Figure 2.16 and Figure 2.17.

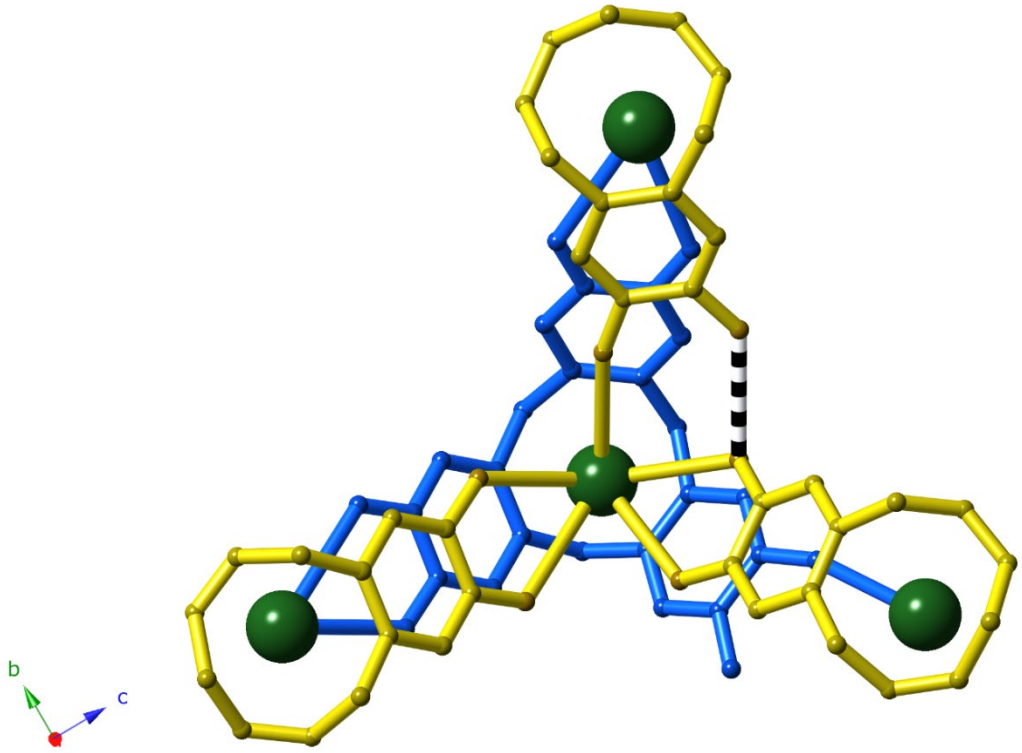

Figure 2.16 A ball-and-stick representation of a pentacoordinate caesium cation (green spheres) in the structure of 2D. The black and white striped connection represents a hydrogen bond between ctc phenol groups.

In the channels of the extended 3D network there are clearly defined ethanol molecules and Cl^- ions. There are two of each per channel per bilayered sheet, which corresponds to one chloride ion and one ethanol per caesium cation (Figure 2.17).

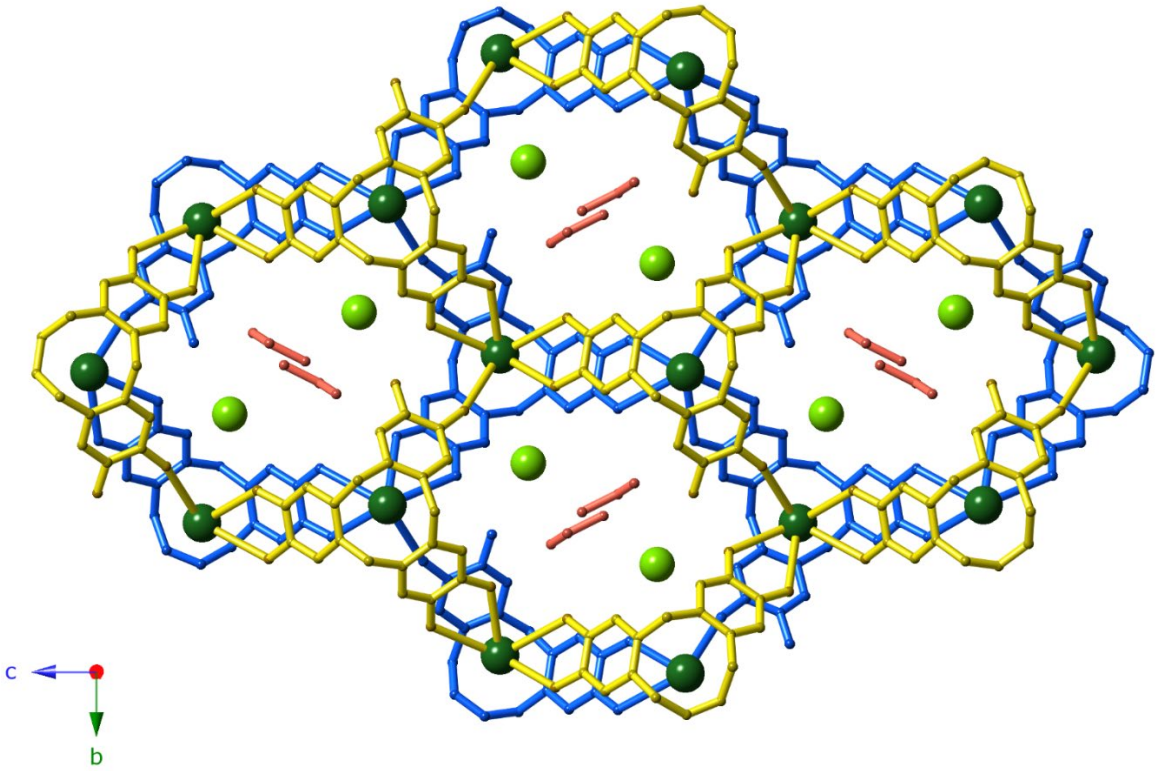

Figure 2.17 A ball-and-stick representation of one bilayered sheet in 2D. Two crystallographically ordered chloride counterions (fluoro green) and two ethanol molecules (coral) are present per channel per bilayered sheet.

Each ethanol molecule acts as a hydrogen bond acceptor in an interaction with an oxygen atom belonging to a chelating catechol group of one layer of the bilayered network (O–H···O distance 2.776 Å, Figure 2.18). In addition, the ethanol forms an O–H···O contact (2.902 Å) with a symmetry related ethanol molecule, which in turn serves as a hydrogen bond acceptor with an oxygen atom of the second layer of the bilayered network. The chloride ions each make close O–H···Cl contacts with three catechols; each chloride is close to two oxygens from one sheet (3.054 Å and 3.171 Å) and a third from the second sheet (3.082 Å).

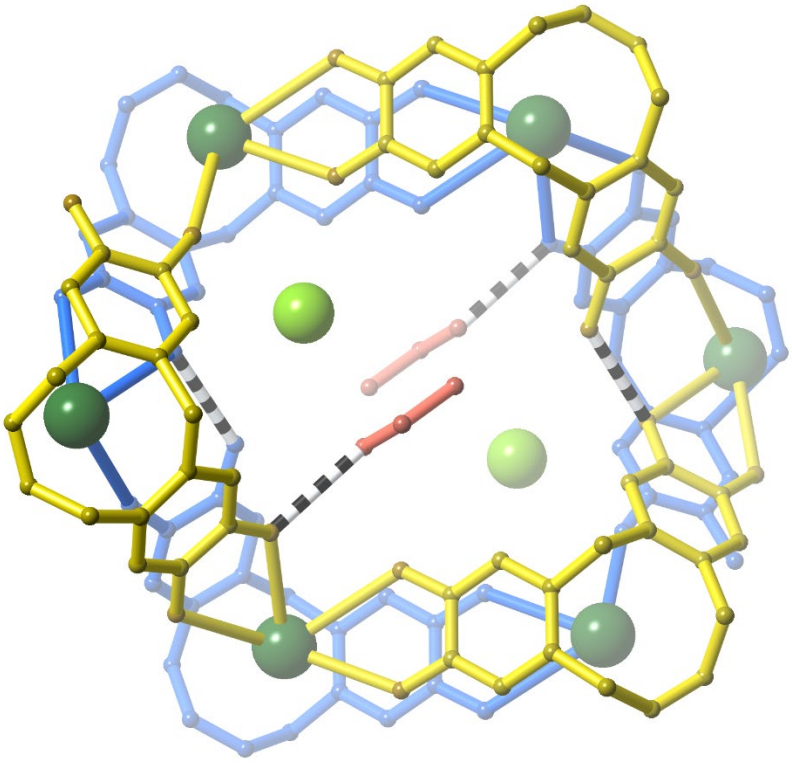

Figure 2.18 A ball-and-stick representation of one hexagonal channel of a bilayered sheet of 2D. Black and white striped connections represent hydrogen bonds between ctc phenol groups (one in each sheet of the bilayered sheet, per hexagonal channel), and between ethanol molecules (coral) and ctc phenol groups.

Given the chemical similarity of 2C and 2D it is not surprising that they are formed from the same reaction mixture. Any reaction that yields 2C might reasonably be expected to yield 2D also. Crystals of 2C and 2D are similar in appearance and have similar chemical properties, thus, the compounds could not be distinguished, with confidence, within mixtures by visual inspection. As a result, manual separation could not be achieved, and yields could not be calculated. It is also possible that some very small proportion of the product obtained from the reactions that yielded 2C and 2D could be 2B.

Powder X-ray diffraction patterns were measured at the Australian Synchrotron to further investigate the components of the solid products formed in (i), (ii) and (iii) (Scheme 2). The reactions that yielded 2B – 2D were repeated and the crystalline materials were collected and

prepared for powder X-ray diffraction studies. The crystalline materials were irradiated with X-rays of wavelength 0.7745 Å. The resulting powder patterns are presented in Figure 2.19 and 2.20 along with simulated powder patterns for pure 2B (Figure 2.20) and 2C (Figures 2.19 and 2.20) based upon single crystal investigations.

As expected, the simulated 2C pattern, based upon the single crystal structure determination, closely matches the powder pattern of the material obtained from reaction (ii). The powder diffraction analysis program Expo2014, was able to match the diffraction data obtained from sample of reaction (ii) to the following unit cell dimensions: a = 12.3645, b = 12.3645, c = 8.7121 Å and $\alpha = 90°$, $\beta = 90°$, $\gamma = 120°$, in high agreement. These unit cell parameters closely match the cell dimensions of the single crystal of 2C.

The experimental powder pattern of the material formed from reaction (iii) also closely matches the simulated 2C, indicating that 2D is only a very minor and/or metastable product of the reaction.

The crystalline material obtained from reaction (i) (top in Figure 2.19, in green) yields a diffraction pattern whose major peaks match that of 2C simulated, indicating that 2C is the major product of this reaction. There are additional peaks that are not present in the other measured patterns. When these peaks are compared to the simulated pattern for 2B (Figure 2.20) it is clear that these smaller peaks are associated with compound 2B. Thus it would appear from inspection of Figure 2.20 that reaction (i) yields compound 2C as a major product and 2B as a minor product.

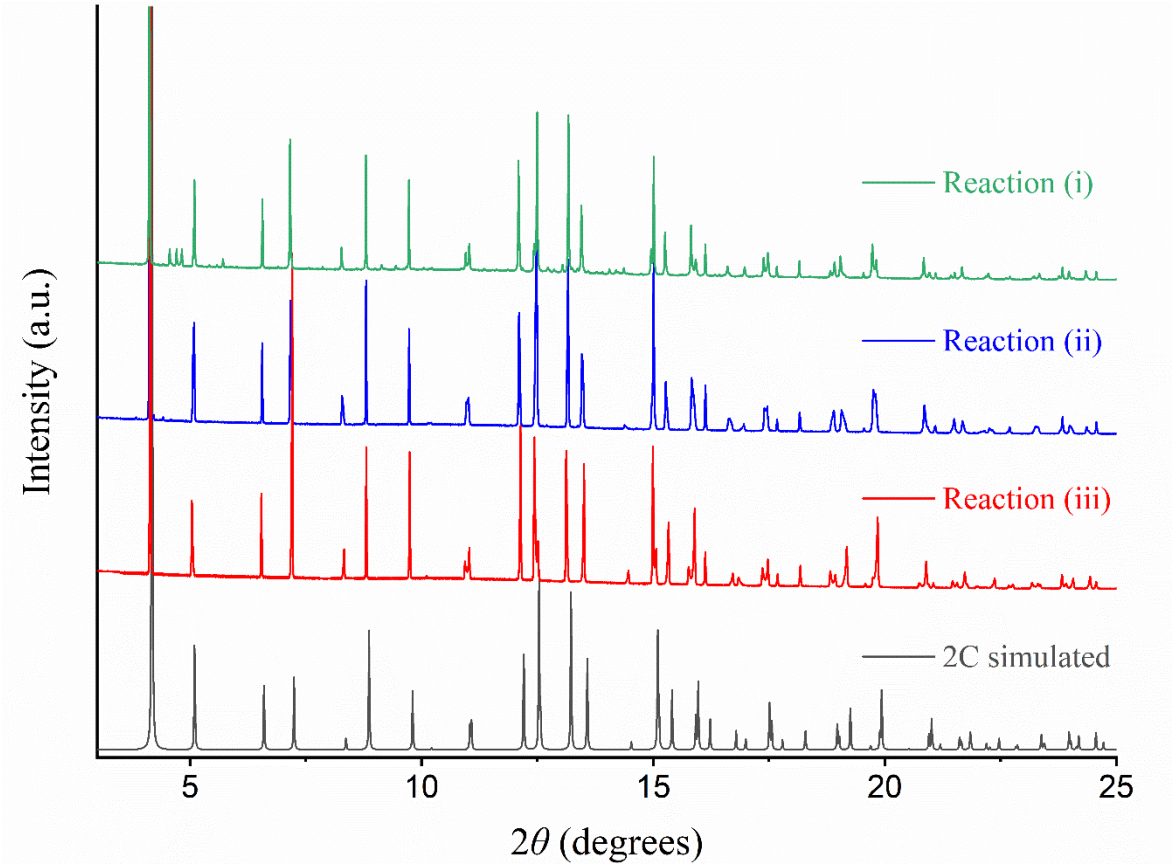

Figure 2.19 Comparison of the synchrotron powder X-ray diffraction patterns obtained for the bulk crystalline products of reactions (i), (ii) and (iii) with a simulated powder X-ray diffraction pattern of compound 2C.

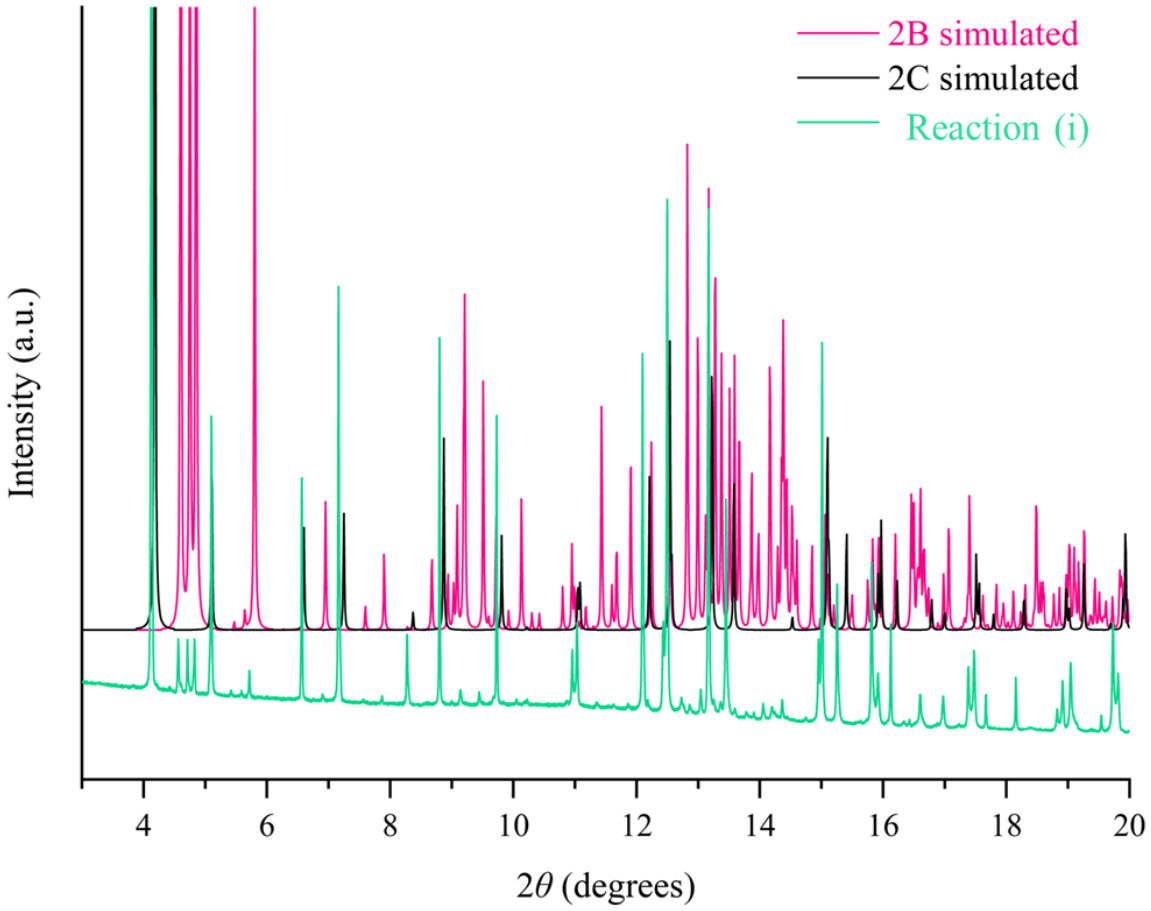

Figure 2.20 Comparison of the synchrotron powder X-ray diffraction pattern obtained for the bulk product from reaction (i) with simulated powder X-ray diffraction patterns of 2B and 2C. The pattern for the bulk product from reaction (i) is stacked below the simulated patterns for clarity. Peaks from reaction (i) align with peaks from both simulated patterns.

2.2.2.4 Compound 2E – [Rb(ctcH$_6$)]Cl·solvate (6,3) network

When RbCl and ctc are combined in the same conditions that yielded 2B, and the RbCl:ctc ratio is ≥ 1, square, colourless plate-like crystals of composition [Rb(ctcH$_6$)]Cl·solvate form. Single crystal X-ray diffraction was performed, revealing a (6,3) network in which both Rb^+ cations and ctc act as 3-connecting nodes. The crystallographic structure solution of 2E from the single crystal data reveals a framework that is topologically and geometrically identical to 2C. In 2E, attempts to model any guests in the channels proved unsatisfactory due to the quality of the crystallographic data. The poor quality of the data lead to elevated agreement

values. Despite the crystallographic difficulties encountered with this structure, the connectivity of the Rb^+-ctc network is clearly defined.

The experimental powder pattern of the material resultant from the reaction that yielded 2E was collected at the Australian Synchrotron. The pattern (2E actual, top in Figure 2.21, in purple) very clearly matches the simulated powder pattern for compound 2E (2E simulated, middle in Figure 2.21, in orange), indicating that under the reaction conditions reported, 2E is produced as a pure product. Specifically, the powder pattern showed no evidence of either a rubidium 'clam' product or distorted 6,3-network forming from this reaction. Further, the powder pattern for 2E also closely resembles 2C simulated (and 2C actual), providing evidence that the framework of 2E is isostructural with the framework of 2C.

Despite the shortcomings in the crystallography, estimates of atom to atom distances have been provided here for comparison with 2C, although caution should be exercised when considering these values. Within a sheet, the Rb^+–Rb^+ distance for adjacent rubidium centres is 11.97 Å, which, as expected, is shorter than the analogous Cs^+–Cs^+ distance of 12.25 Å in 2C. The closest contact between sheets within each bilayer in 2E is 3.07 Å, between catechol oxygens from adjacent sheets. As in 2C, there is extensive π-π stacking *between* the bilayered sheets, the shortest C–C distance being 3.41 Å, which is also shorter than in 2C. In the crystal structure of 2C, the O–Cs bonds are very similar in length for each of the two catechol oxygens, resulting in a reasonably symmetrical chelating interaction. In 2D, however, one oxygen atom from one catechol per Cs^+ is too far away from the Cs^+ to form a bond with the Cs^+. The O–Rb^+ bonds in 2E are 3.4 Å and 2.8 Å, therefore the arrangement is substantially less symmetrical than the chelating catechol–M^+ interactions in 2C, but more symmetrical than the non-chelating catechol–M^+ interaction in 2D.

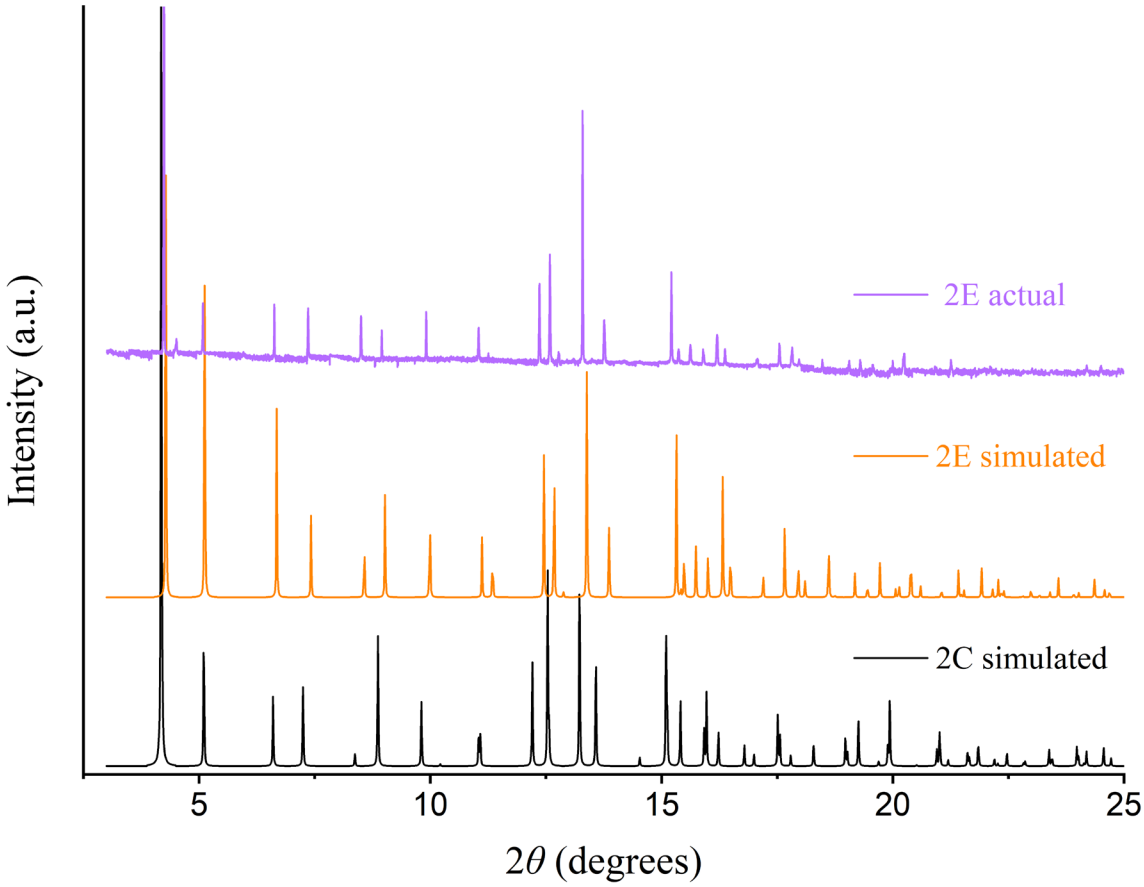

Figure 2.21 Comparison of the synchrotron powder X-ray diffraction patterns obtained for the bulk crystalline products of the reaction that produced compound 2E (2E actual) with simulated powder X-ray diffraction patterns of compound 2C (2C simulated) and 2E (2E simulated).

2.2.2.5 Concluding remarks concerning compounds 2A – 2E

In summary, the chemistry of ctc with caesium, both in acidic and basic conditions, is rich and produces a wide variety of topologically and geometrically distinct compounds. While some interesting analogous structures have been obtained with rubidium, caesium more reliably forms compounds with ctc under the conditions investigated in this work and reported in the literature.

2.2.3 Chemistry of ctc with group 2 metal cations

A set of side-by-side experiments was conducted with a view to investigating the structural diversity of crystals formed from the combination of alkali and alkaline earth metal cations with ctc. Reactions were performed under conditions similar to those that yielded the 'neutral' Cs^+ clams (compound 2A). Reactions with calcium, strontium and barium chlorides resulted in the formation of three unique assemblies, $[Ca_2(ctcH_4)_2(MeOH)_4]\cdot MeOH$ (2F), $[Sr(ctcH_4)(H_2O)_4]\cdot MeOH\cdot 2H_2O$ (2G) and $[Ba_2(ctcH_4)_2(H_2O)_7(MeOH)_2]\cdot MeOH\cdot 3H_2O$ (2H), while reactions with alkali metal chlorides and with magnesium chloride, under similar conditions, did not result in crystalline precipitate suitable for X-ray diffraction analysis (Table 2.5). In the reactions indicated in Table 2.5, 0.065 mmol of $ctcH_6$ was combined with 0.033 mmol of metal chloride in methanol and exposed to ammonia vapour.

Table 2.5 Summary of the results of experiments with group 1 and 2 metal chlorides with ctc under analogous conditions to those that yielded 2A.

Metal chloride (MCl_x)	**Reaction product**	**Structure**
LiCl	No crystalline precipitate	–
NaCl	No crystalline precipitate	–
KCl	No crystalline precipitate	–
RbCl	No crystalline precipitate	–
$MgCl_2\cdot 6H_2O$	No crystalline precipitate	–
$CaCl_2\cdot 2H_2O$	Colourless crystalline plates	2F
$SrCl_2\cdot 6H_2O$	Colourless crystalline precipitate and some brown amorphous precipitate	2G
$BaCl_2\cdot 2H_2O$	Colourless crystalline precipitate and some brown amorphous precipitate	2H

2.2.3.1 Compound 2F – $[Ca_2(ctcH_4)_2(MeOH)_4]\cdot MeOH$

The combination of $ctcH_6$ with Ca^{2+} ions results in a neutral, dimeric assembly (an M_2L_2 metallocycle) of formula $[Ca_2(ctcH_4)_2(MeOH)_4]$, shown in Figure 2.22, which crystallises with methanol in the triclinic crystal system. In the crystal structure, each Ca^{2+} is hexacoordinate with a distorted octahedral geometry, in which the metal ion is chelated by 2 catecholate moieties from different ctc units, and also coordinated to two *cis*-methanol molecules. The Ca^{2+} centres have opposite absolute configurations.

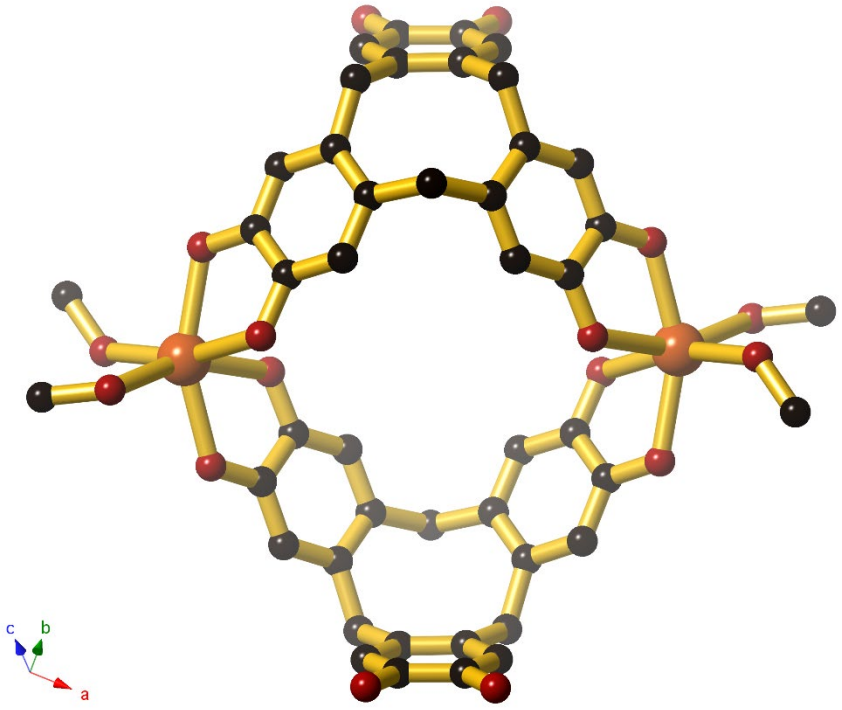

Figure 2.22 A ball and stick representation of the [2+2] metallocycle in 2F. The Ca^{2+} centre (orange sphere) on the left has Λ configuration and the Ca^{2+} centre at right has Δ configuration.

Each metallocycle participates in 16 hydrogen bonds (including four to non-coordinated methanol molecules, plus an additional two via the coordinated methanol molecules), through which it forms part of a sheet that runs parallel to the crystallographic *a* and *b* axes. In the

sheet, each metallocycle is surrounded by eight structurally related metallocycles. Each metallocycle is hydrogen bonded to all of its eight neighbouring metallocycles in the sheet. One coordinated methanol from a neighbouring metallocycle is directed into the bowl of each ctc, such that every ctc bowl is occupied. This can be seen in Figure 2.23, in which methanol molecules (in yellow) from metallocycles to the left and right of the central blue metallocycle are shown to point into the bowls of the blue metallocycle.

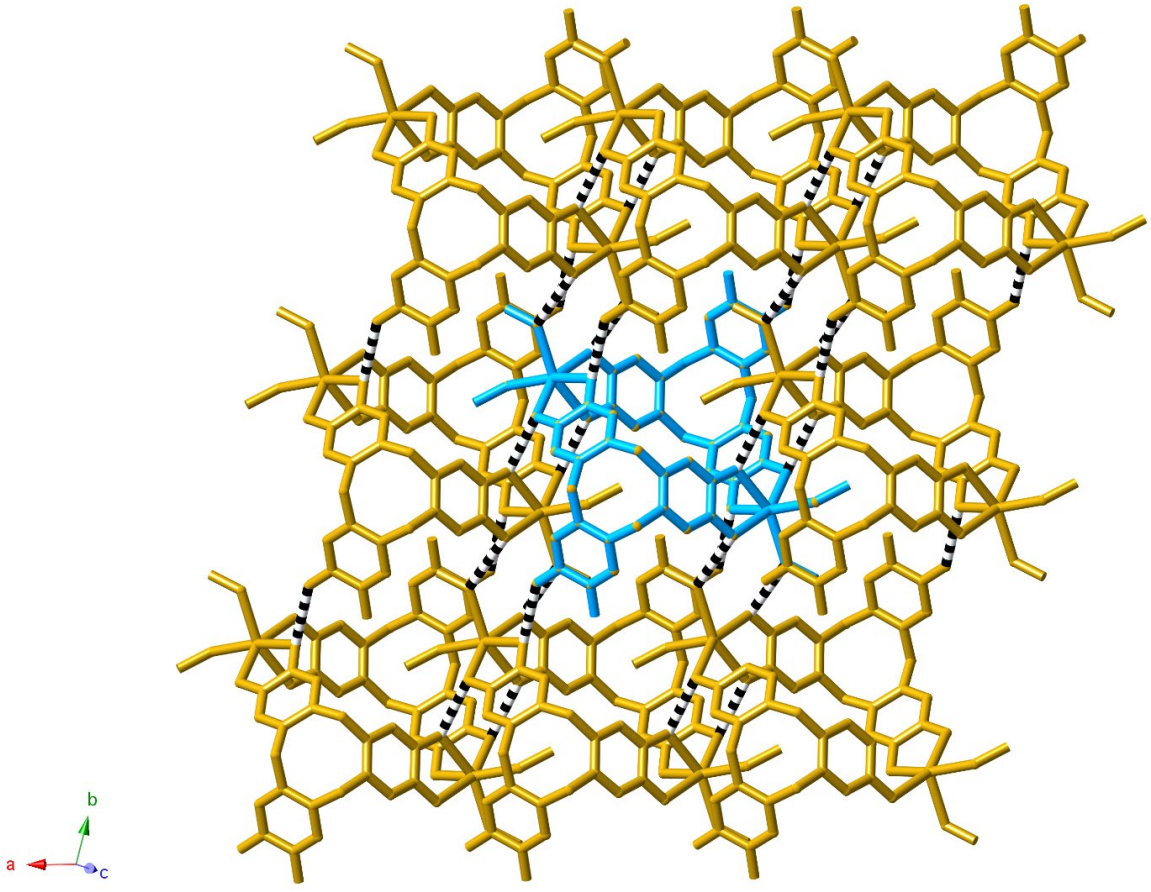

Figure 2.23 A stick representation of one hydrogen bonded sheet in 2F. In blue is shown one M_2L_2 metallocycle and, in yellow, the eight metallocycles around it. The black-and-white striped connections represent hydrogen bonds between metallocycles. The four hydrogen bonds per metallocycle to methanol molecules are not shown. Hydrogen atoms have been omitted for clarity.

The sheets in 2F lie directly above and below each other in the crystal structure, but are not connected to the sheets above or below through hydrogen bonds (Figure 2.24).

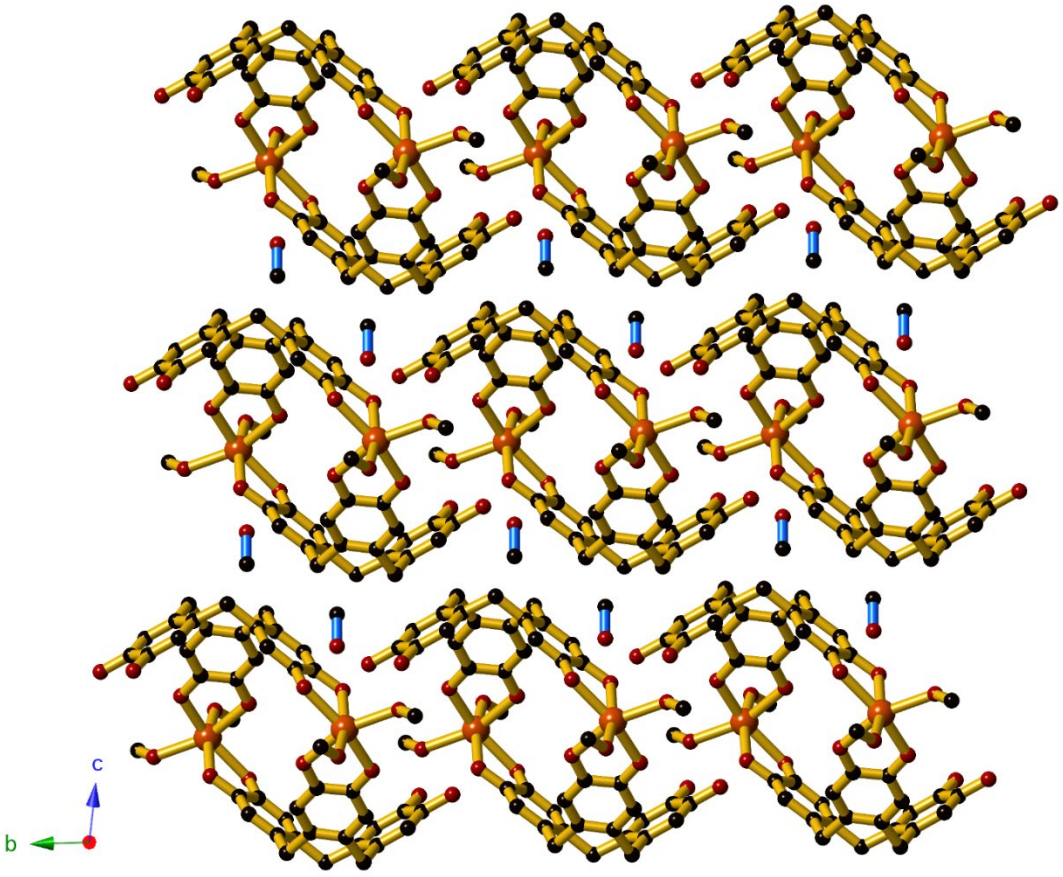

Figure 2.24 A ball and stick view of three sheets in the crystal structure of 2F. Between the sheets are methanol molecules (in blue). Half of the methanol molecules between the sheets form hydrogen bonds with the sheet above them (these have their oxygen atoms, in red, directed upwards) and the other half form hydrogen bonds to the sheet below. Hydrogen atoms and hydrogen bonds have been omitted for clarity.

2.2.3.2 Compound 2G – $[Sr(ctcH_4)(H_2O)_4]\cdot MeOH\cdot 2H_2O$

In compound 2G the anion $ctcH_4^{2-}$ binds through two of its catechol moieties to Sr^{2+} ions in a 1:1 ratio, to give sinusoidal chains (Figure 2.25) within a compound of formula $[Sr(ctcH_4)(H_2O)_4]\cdot MeOH\cdot 2H_2O$. All strontium ions in a chain lie on a line and the intra-chain Sr^{2+}–Sr^{2+} separation is 9.50 Å.

Each Sr^{2+} ion is octacoordinated, chelated by two catecholate units (Sr^{2+}–O distances ≈ 2.6 Å) and also coordinated to four water molecules (Sr^{2+}–O distances ≈ 2.6 Å), in a distorted square antiprismatic coordination environment, typical for strontium. The ctc units in each chain are related by mirror glides.

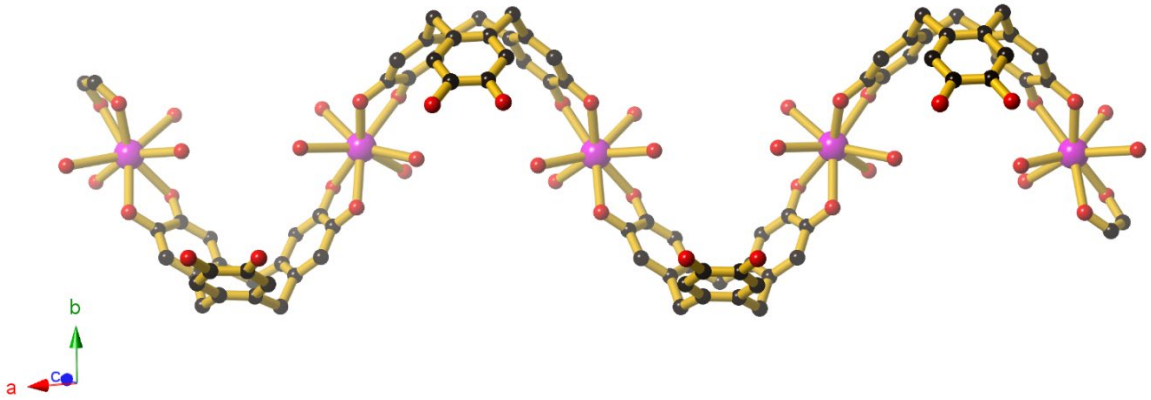

Figure 2.25 A ball and stick representation of the 1D-chain comprising $ctcH_4^{2-}$, Sr^{2+} (pink spheres) and H_2O molecules present in compound 2G. Hydrogen atoms have been omitted for clarity.

One hydroxyl group of each non-chelating catechol unit forms a hydrogen bond to a chelating catecholate unit of a neighbouring chain. Chelating catecholate units (which are only singly deprotonated) also form hydrogen bonds to chelating catecholates from neighbouring chains. Each chain participates in these hydrogen bonding interactions with two adjacent chains from the same plane, resulting in hydrogen bonded sheets (Figure 2.26).

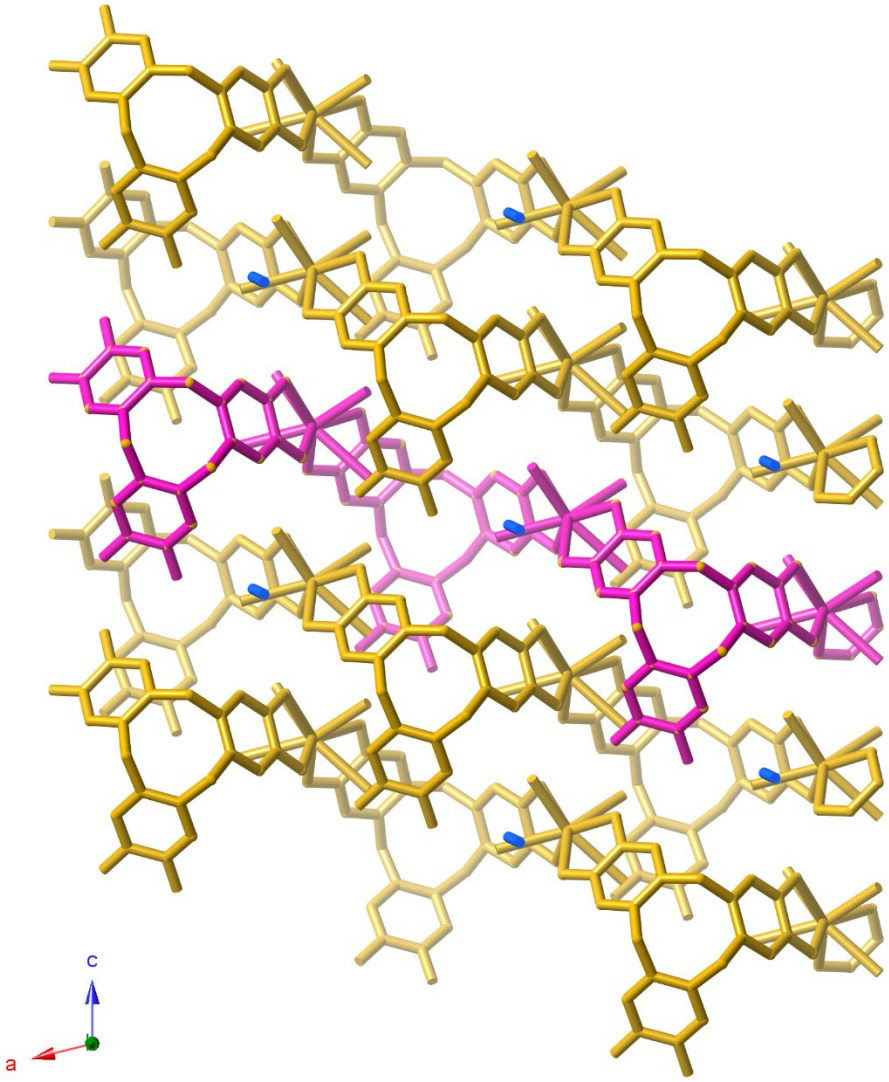

Figure 2.26 A stick representation of one hydrogen bonded sheet in 2G. Highlighted in pink is one of the neutral $ctcH_4^{2-}$–Sr chains. Methanol molecules above the chain are shown with blue bonds. Hydrogen atoms have been omitted for clarity.

The sheets do not form hydrogen bonds with each other and stack in an ABAB arrangement, with the closest contacts between sheets occurring between aromatic carbon atoms (C–C distance ≈ 3.66 Å). Methanol molecules are present between the sheets and form hydrogen bonds to catecholate oxygen atoms. The 3-dimensional structure of 2G, shown in Figure 2.27,

resembles the structure of 2F, despite the fact that the metal–ctc units in 2G form chains as opposed to discrete metallocycles.

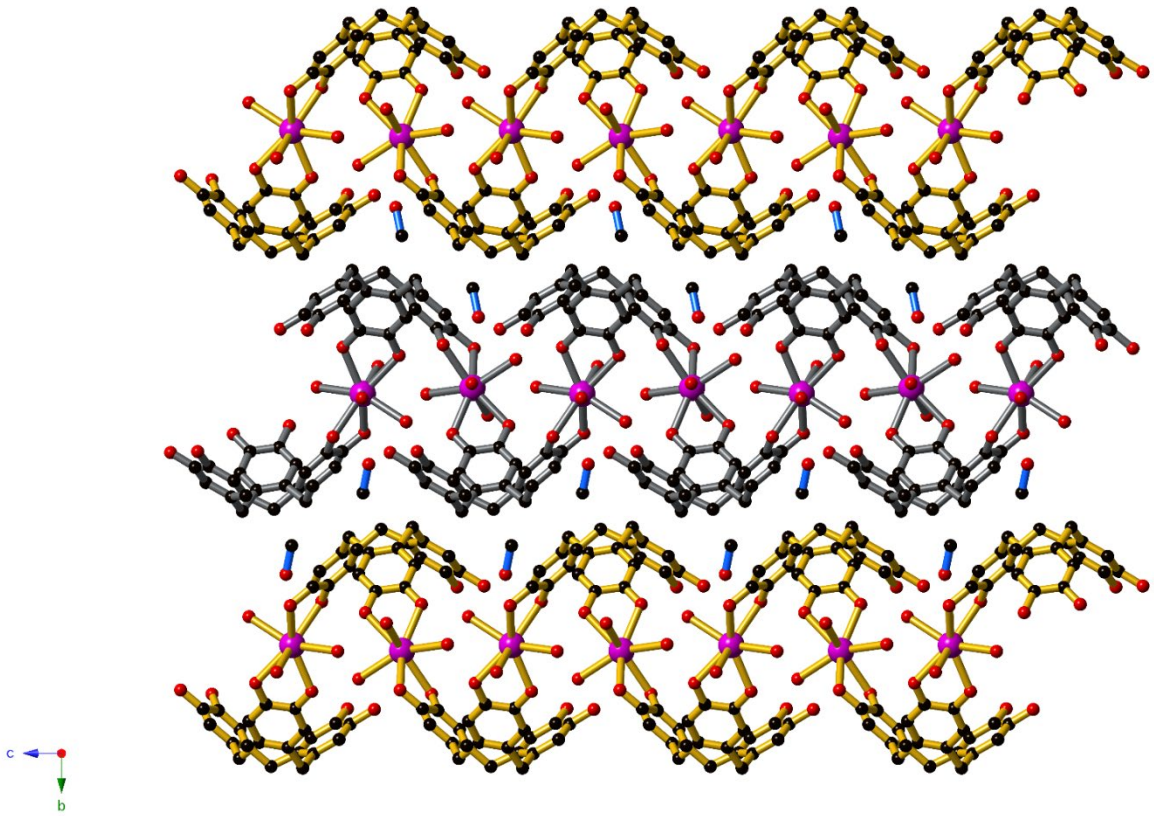

Figure 2.27 A ball and stick representation of the ABAB arrangement of sheets in 2G. Between the sheets are methanol molecules (in blue). Half of the methanol molecules between the sheets form hydrogen bonds with the sheet above them (these have their oxygen atoms, in red, directed upwards) and the other half form hydrogen bonds to the sheet below. Hydrogen atoms and hydrogen bonds have been omitted for clarity.

2.2.3.3 Compound 2H – $[Ba_2(ctcH_4)_2(H_2O)_7(MeOH)_2]\cdot MeOH\cdot 3H_2O$

In compound 2H, which has the formula $[Ba_2(ctcH_4)_2(H_2O)_7(MeOH)_2]\cdot MeOH\cdot 3H_2O$, two crystallographically distinct $ctcH_4^{2-}$ units each bind through two of their catechol moieties to two crystallographically distinct Ba^{2+} ions, to form what may be considered to be an open

clam-type structure (Figure 2.28). Both barium ions are chelated by two ctc units and coordinated by four water molecules in addition to a disordered methanol in a nonacoordinate environment. Two of the water molecules on each barium cation are crystallographically disordered. Two ordered water molecules on each Ba^{2+} centre, indicated by pink bonds (Figures 2.29 and 2.30), form bridges between two crystallographically distinct barium centres from adjacent clams. These Ba^{2+}–O–Ba^{2+} bridges connect each barium–ctc open clam to an adjacent open clam.

As a result of both barium centres in an open clam participating in this bridging, each open clam is attached to four other open clams, i.e. two per Ba^{2+}, which results in a 2D-sheet structure (Figure 2.31), reminiscent of those in 2F and 2G. Figure 2.32 shows that the sheets stack in an ABAB arrangement, similar to the sheets in 2G. Coordinated methanol molecules from a barium in one open clam project into the bowl of an adjacent open clam, as in 2F.

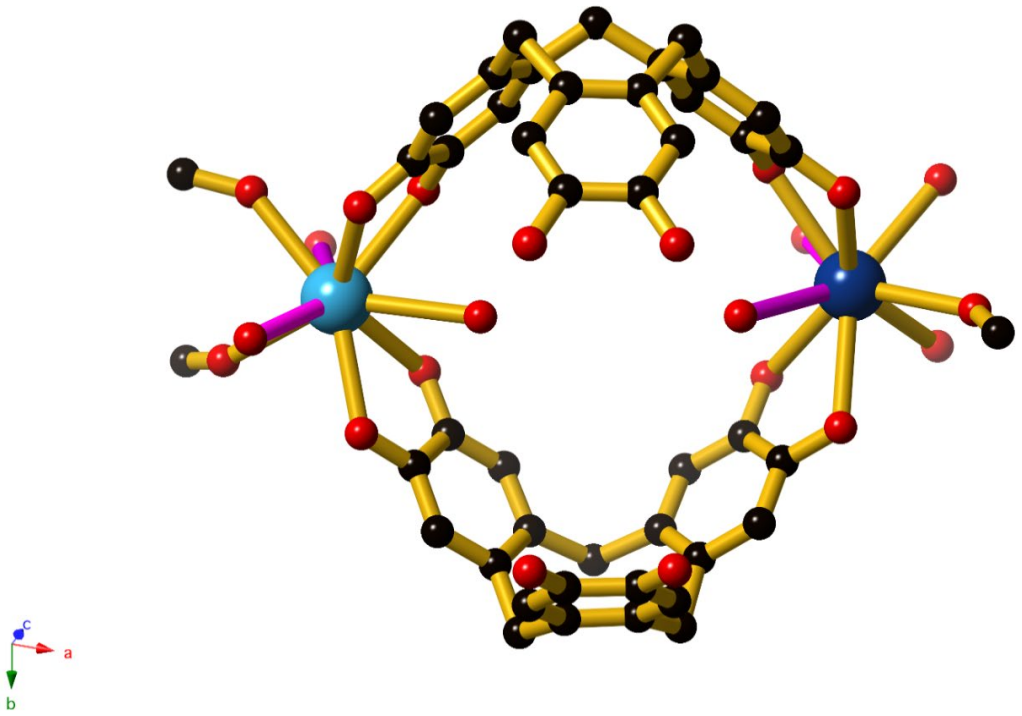

Figure 2.28 A ball and stick representation of a single barium–ctc open clam unit in 2H. The blue spheres (one light, one dark) each represent one of the crystallographically distinct Ba^{2+} cations. The water molecules connected to the barium centres by pink bonds form bridges to barium centres from adjacent barium–ctc open clams. For clarity, only one crystallographic position of the disordered water and methanol molecules has been shown. Hydrogen atoms have been omitted for clarity.

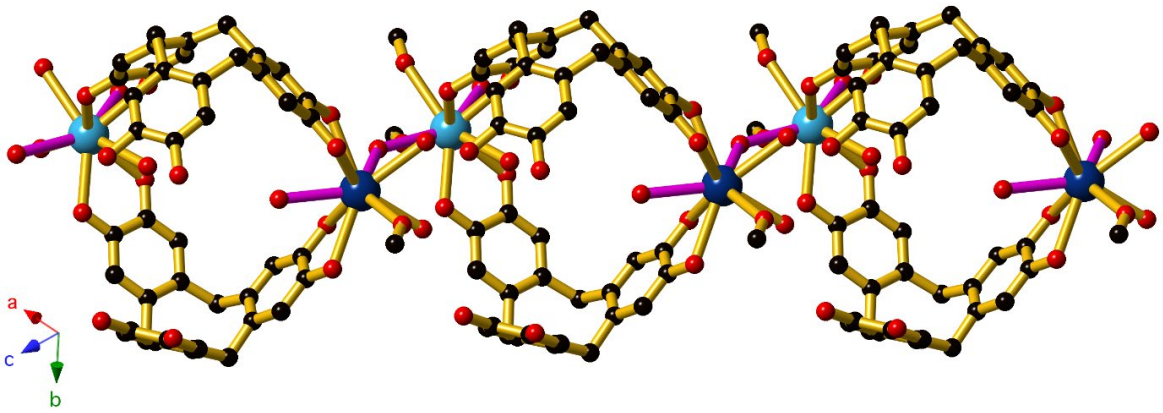

Figure 2.29 A ball and stick representation of a chain of barium–ctc open clams in 2H. The blue spheres (one light, one dark) each represent one of the crystallographically distinct Ba^{2+} cations. Water molecules bridging the two types of Ba^{2+}cations are shown. The bonds between these cations and water molecules are shown in pink. For clarity, only one crystallographic position of the disordered water and methanol molecules has been shown. Hydrogen atoms have been omitted for clarity.

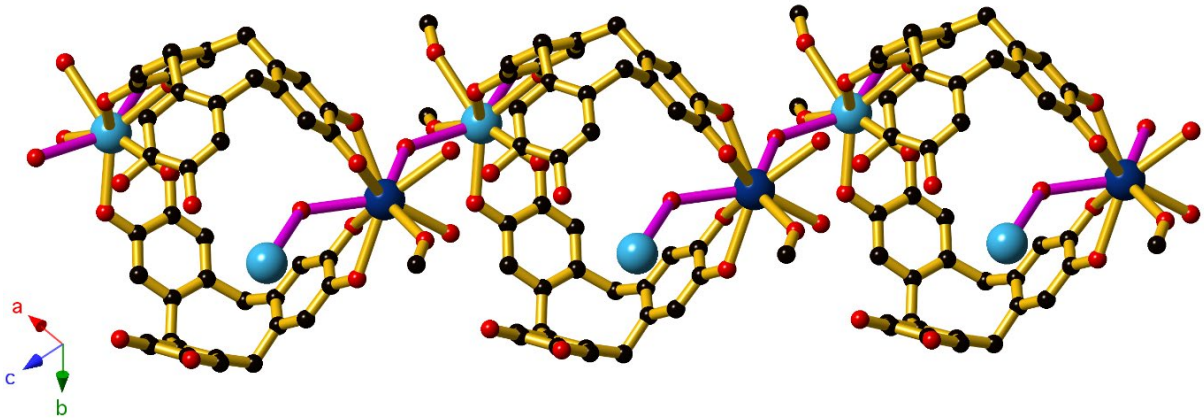

Figure 2.30 A ball and stick representation of a chain of barium–ctc open clams in 2H. The blue spheres (one light, one dark) each represent one of the crystallographically distinct Ba^{2+} cations. Each type of $Ba^{2+}$is bridged to two of the other type by a water molecule. The bonds between these cations and water molecules are shown in pink. The light blue barium centres projecting out of the page form part of other open clams within a 2D sheet. For clarity, only one crystallographic position of the disordered water and methanol molecules has been shown. Hydrogen atoms have been omitted for clarity.

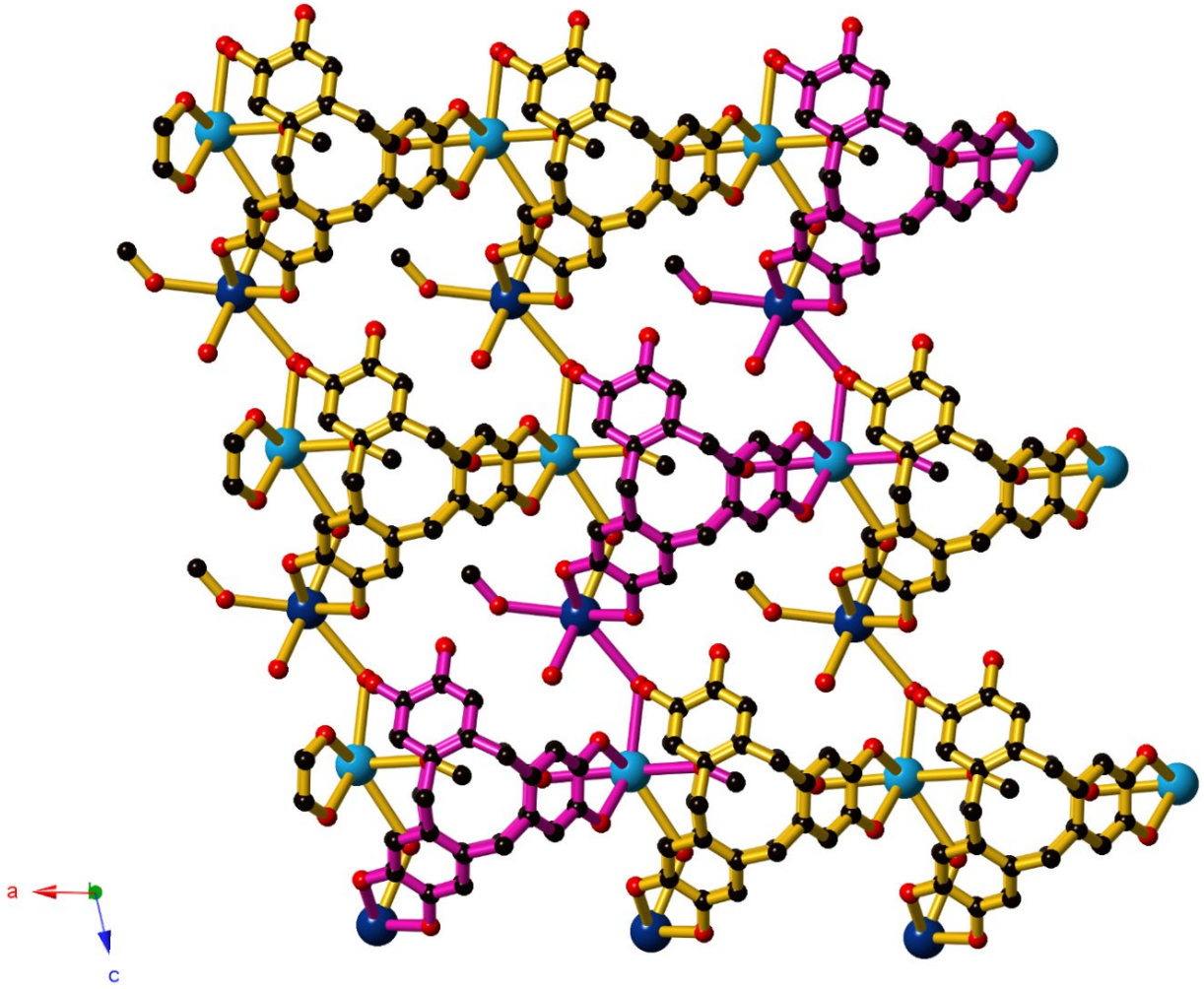

Figure 2.31 A ball and stick representation of one sheet in 2H. The pink 'chain' represents an extension of the chain of Ba^{2+} cations shown in Figure 2.29. For clarity, only one crystallographic position of the disordered water and methanol molecules has been shown. Hydrogen atoms and hydrogen bonds have been omitted for clarity.

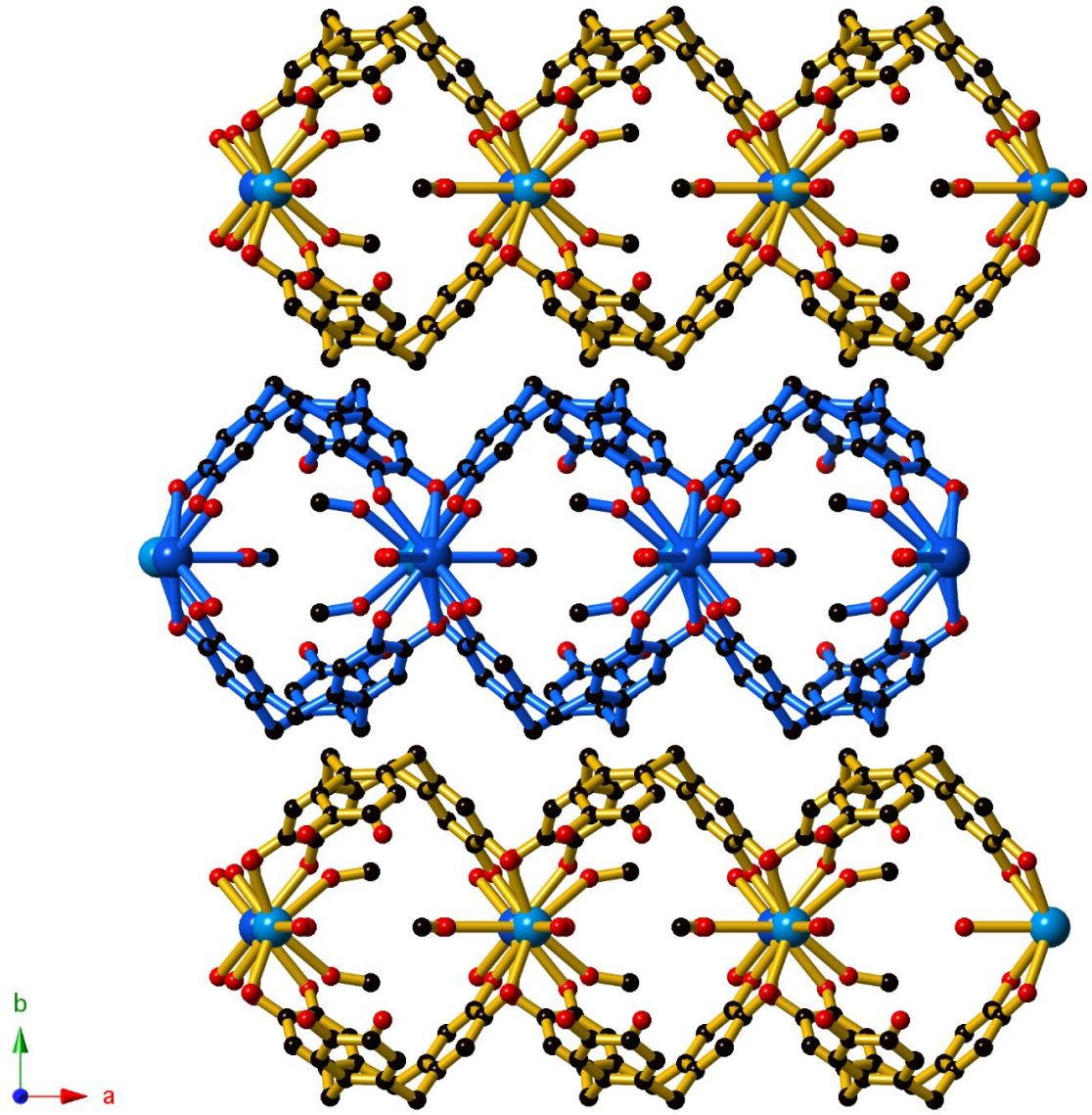

Figure 2.32 A ball and stick representation of the ABAB stacking of sheets in 2H. For clarity, only one crystallographic position of the disordered water and methanol molecules has been shown. Hydrogen atoms have been omitted for clarity.

2.2.3.4 Concluding remarks concerning 2F-2H

The combination of ctc with group 2 cations under the same conditions that yielded 2A resulted in the formation of three unique compounds which were characterised by X-ray crystallography. These compounds each contain ctc units bound through only two of their three arms to form metal–ligand complexes of different dimensionalities. Despite this, each

of the three compounds contain stacked sheets that appear remarkably alike and have a similar chemical composition, despite the significant difference in their intra-sheet connectivity. Of the three compounds, one contains ctc–metal cation oligomers that are connected by hydrogen bonds to form a sheet (2F), one contains ctc–metal cation 1D chains that are also connected by hydrogen bonds to form a sheet (2G), and one contains a ctc–metal cation sheet containing bridging water ligands.

This study, which was conducted with a view to investigating the binding modes (if any) of ctc to group 2 metal cations, revealed that stacked sheet structures with solvent filled cavities can be generated. Notably, this study supported the hypothesis that group 2 metal cations preferentially bind to the catechol oxygen atoms of ctc, as opposed to occupying the ctc bowl and/or interacting with the aromatic groups of ctc, as do the larger, softer, alkali metal cations.

2.2.4 Ctc compounds containing caesium and a group 1 or II metal cation

Small and large group 1 cations have been shown to interact differently with ctc. An opportunity to investigate the structure directing role of alkali metal cations in the formation of supramolecular assemblies and the potential structural diversity of the resultant assemblies arises from the combination of ctc with two types of group 1 cation in solution.

Also of interest are solid state compounds that form when ctc is combined with a mixture of group 1 and 2 metal cations. As illustrated by compounds 2F – 2H, ctc can bind to group 2 metal cations to form sheets. It is of interest to determine if such assemblies are still formed when Cs^+, which is known to have a strong affinity for ctc, is able to compete with the group 2 metal cations (which have a higher charge and therefore greater electrostatic attraction to ctc anions).

A compound synthesised through the deliberate combination of ctc with Cs^+ and Sr^{2+}, $Cs_3[CsSr(ctc)]\cdot$solvate (2I), is reported below. A compound obtained when Cs^+ and Li^+ were combined with ctc, $Cs_8[Li_4(ctcH_3)_4]\cdot 15.5H_2O$ (metallocycle 2J), is also described. Both compounds have connectivities that are related to commonly encountered network topologies; the (10,3)-a and diamond nets, respectively.

2.2.4.1 Compound 2I – $Cs_3[CsSr(ctc)]\cdot$solvate (10,3)-a network

A set of side-by-side experiments was conducted with a view to probing the structural diversity of solid state products formed from the reaction of alkaline earth metal cations with ctc and caesium cations. In these experiments (Table 2.6), 0.065 mmol of $ctcH_6$ was dissolved in ethanol. 1.5 molar equivalents of group 2 metal cation chloride salt was added to the solution and an aqueous solution containing 12 mole equivalents of $CsOH\cdot H_2O$ was layered

beneath. The reactions with calcium and barium chlorides did not result in crystalline precipitate suitable for X-ray diffraction analysis under these conditions (Table 2.6), nor did an analogous set of reactions containing CsOAc instead of CsOH. The reaction with strontium chloride and caesium hydroxide, however, led to the formation of a compound of formula Cs_3[CsSr(ctc)]·solvate, whose topology is that of a (10,3)-a network. The half-clam motif is present in this compound, which has caesium cations in the bowls of each ctc^{6-}, however, unlike in the (6,3) nets 2C and 2D, the ctc ligands are not coordinated to Cs^+ cations, instead they chelate Sr^{2+} cations.

Table 2.6 A summary of a set of side-by-side experiments conducted to investigate the outcome of combining ctc with multiple group 1 and 2 cations.

Metal halide (MCl_x)	Metal hydroxide (MOH)	Product
$CaCl_2.2H_2O$	$CsOH.H_2O$	–
$SrCl_2.6H_2O$	$CsOH.H_2O$	2I
$BaCl_2.2H_2O$	$CsOH.H_2O$	–

In compound 2I, each Sr^{2+} centre is chelated by three ctc anions in a distorted octahedral coordination environment (Figure 2.33). The crystal structure determination indicates one of two possible enantiomorphs of this compound, in which all the Sr^{2+} centres have the Δ configuration. All Sr^{2+} centres in 2I are crystallographically equivalent. Each of these centres can be considered a 3-connecting unit. It is expected that the bulk product represents a racemic mixture of the two enantiomorphs. In the other enantiomorph, all Sr^{2+} centres would have the Λ configuration.

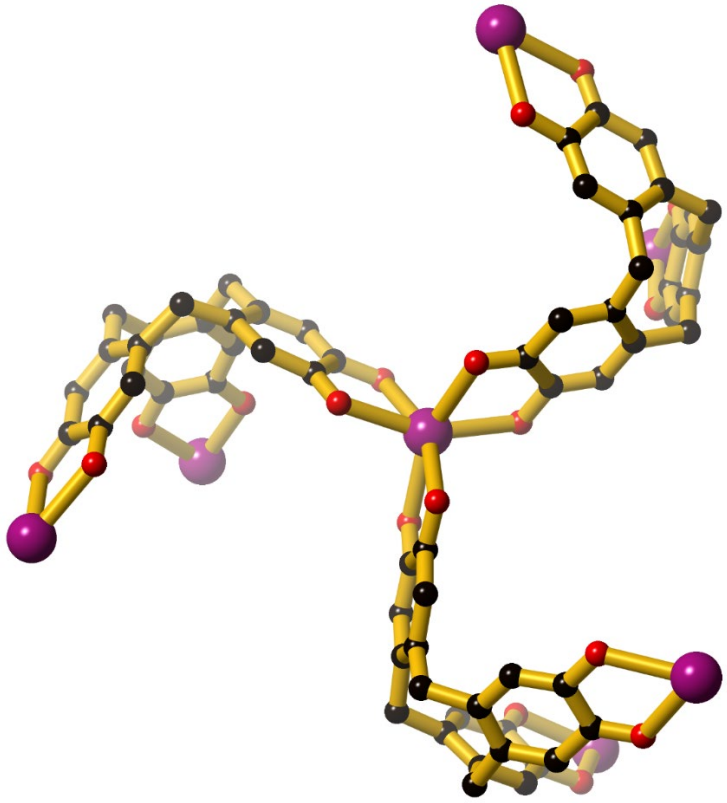

Figure 2.33 A ball and stick representation of part of the (10,3)-a network in 2I, showing the coordination environment around a Sr^{2+} centre (pink sphere), which has the Δ configuration. Hydrogen atoms have been omitted for clarity.

Each crystallographically equivalent ctc^{6-} unit in 2I chelates three Sr^{2+} centres (Figure 2.34) through its three catecholate 'arms' and, as with the Sr^{2+} centres, can be considered a 3-connecting node in the extended network of 2I.

There are two crystallographically distinct types of Cs^{+} cation in the crystal structure of 2I. As observed in all other reported crystal structures of ctc containing Cs^{+}, there is a Cs^{+} cation occupying the bowl of the ctc^{6-} that interacts with all three of the internal aromatic surfaces of the bowl. The other type of Cs^{+} is located outside the ctc bowl, but also interacts with the ctc^{6-} aromatic faces. There are three of this second type of Cs^{+} per ctc^{6-}.

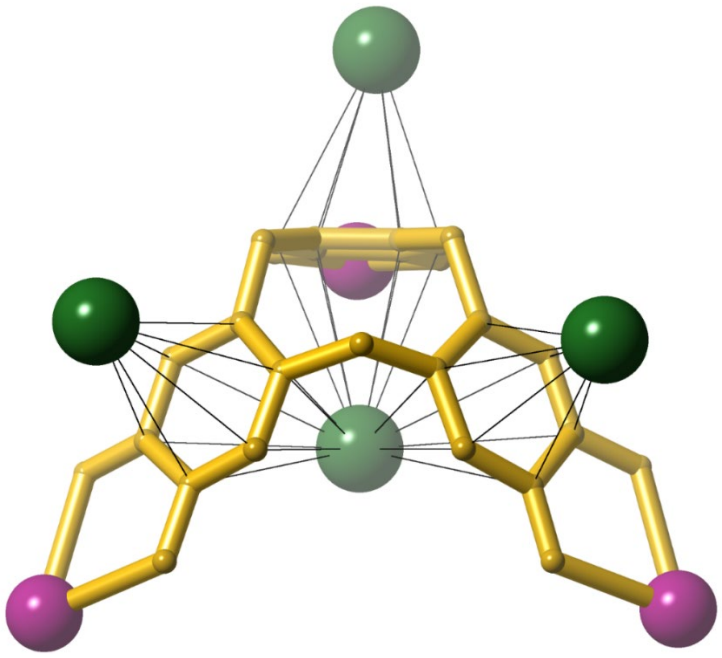

Figure 2.34 A ball and stick figure showing the ctc^{6-}–Sr^{2+} interactions and the two types of ctc^{6-}–Cs^{+} interactions in compound 2I. The ctc chelates three Sr^{2+} cations (pink). The two crystallographically distinct types of Cs^{+} cations in 2I are shown, and their interactions with the ctc^{6-} aromatic rings are represented by thin black connections. One type of Cs^{+} sits in the bowl of the ctc^{6-} and interacts with all three of the aromatic rings of the ctc^{6-}. The other type of Cs^{+} is located outside the ctc bowl and interacts with the external aromatic faces of the ctc^{6-}. Hydrogen atoms have been omitted for clarity.

The Sr^{2+} centres show a significant distortion from ideal octahedral geometry. As discussed in chapter 1 of this thesis, a feature of the (10,3)-a net is that the shortest path from a node back to itself is a ten membered circuit, that is, it contains ten bridges and passes through ten nodes. In 2I, ten catecholate 'arms' of ctc ligands can be considered the bridges. Half of the 'nodes' are represented by Sr^{2+} cations whilst the other half are represented by ctc^{6-} ligands. For simplicity, in this topological analysis, the Cs^{+} cations are not considered as a node, nevertheless it is convenient given the location of the of the Cs^{+} ion in the ctc^{6-} bowl to consider its location as the central point of the 3-connecting ctc^{6-} unit in a representation of Sr-ctc topology. A skeleton of the (10,3)-a net can thus be constructed by plotting connections

between the Sr^{2+} centres and the corresponding Cs^{+} cations (those in the bowl of the ctc^{6-} to which the Sr^{2+} is bonded), as shown in Figure 2.35.

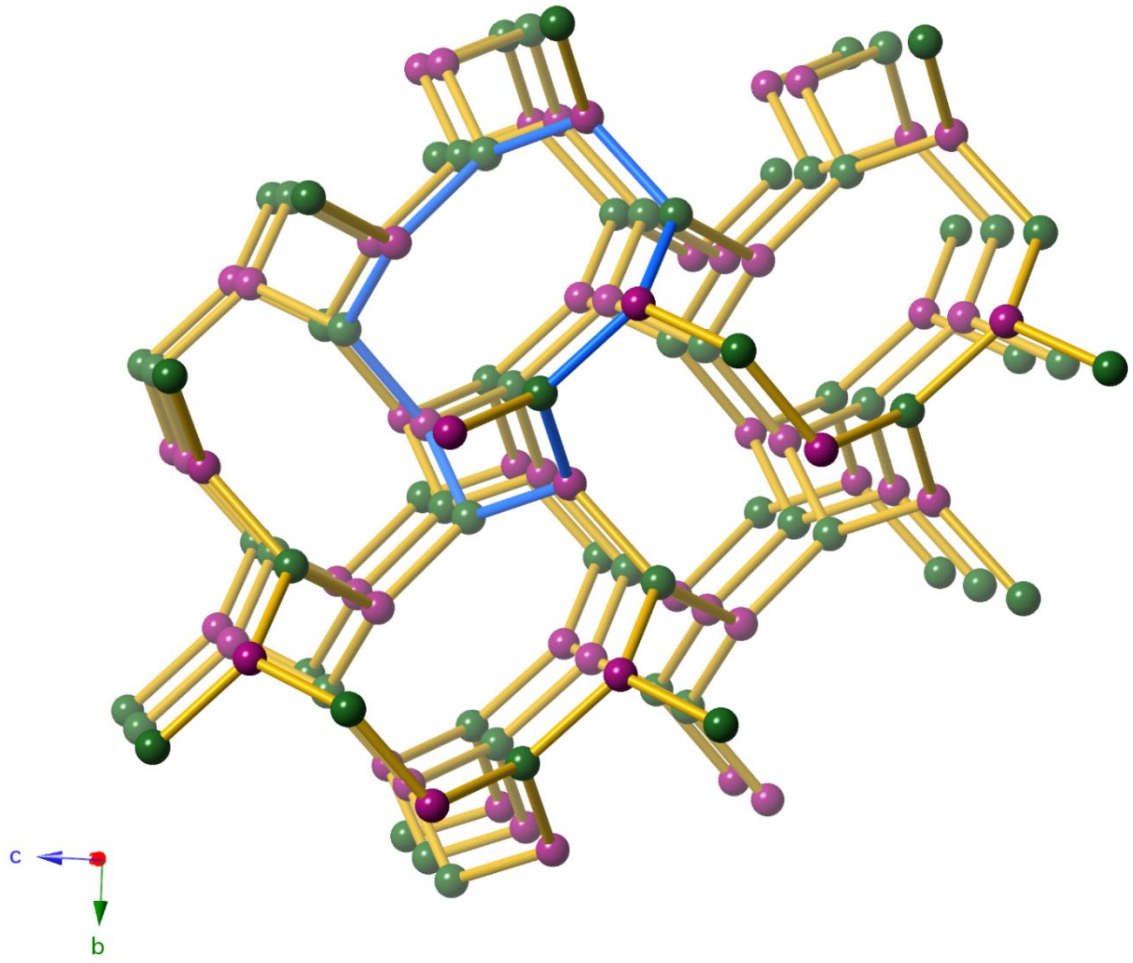

Figure 2.35 A skeletal representation of the (10,3)-a network in 2I. Pink and green spheres represent Sr^{2+} and Cs^{+} cations respectively, and indicate the nodes. The Cs^{+} cations are used as an approximation for the centre of the ctc^{6-} ligands. A ten-membered circuit is indicated in blue.

The (10,3)-a net is a commonly encountered 3D network, which, in its most symmetrical form, has cubic symmetry and is inherently chiral. It appears identical when viewed down its

crystallographic *a*, *b*, and *c* axes. A view of the network at a slight angle to the *a*-axis is shown in Figure 2.36, in which the Cs^+ cations in the ctc^{6-} bowls are shown.

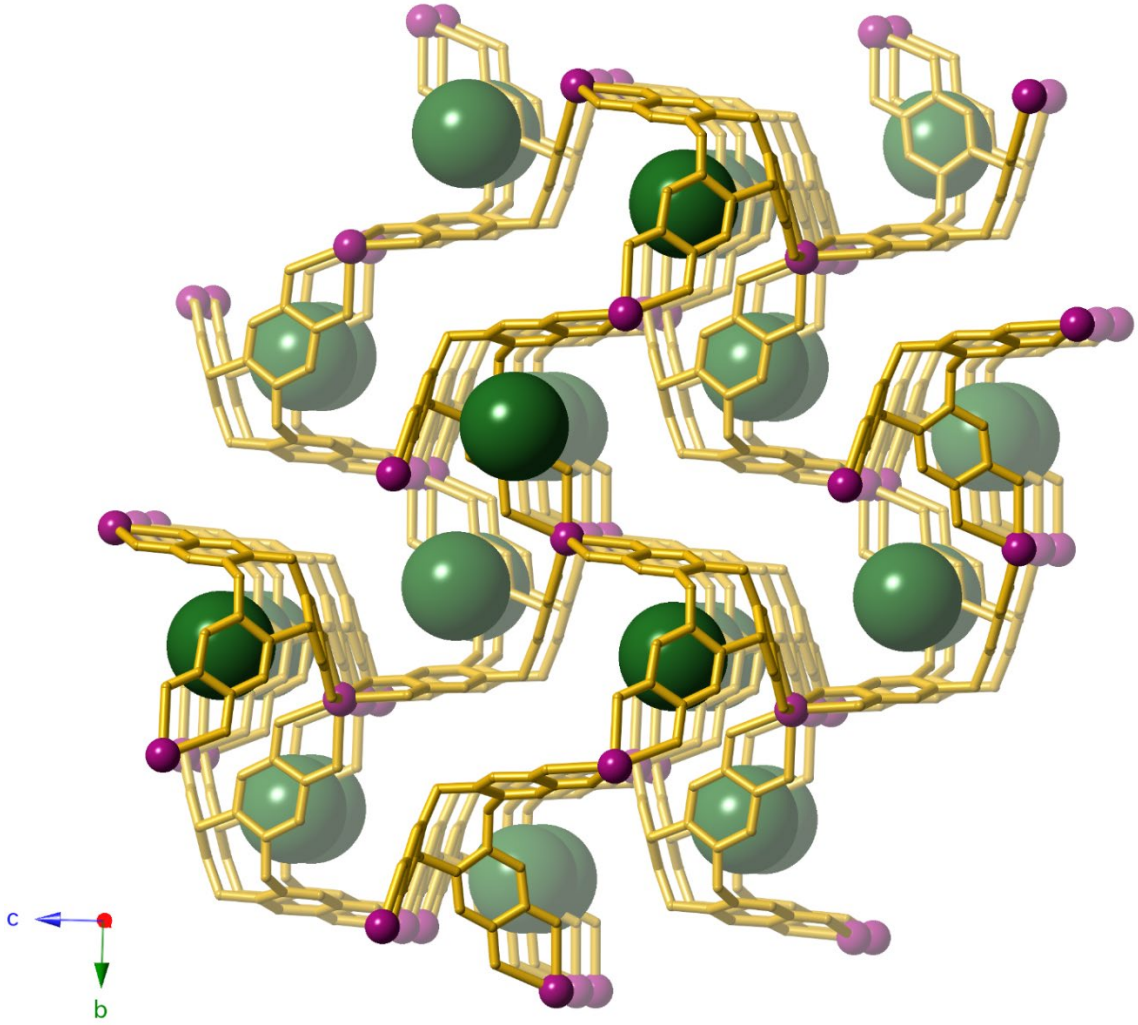

Figure 2.36 A ball and stick representation of the (10,3)-a network present in 2I. The small pink spheres represent Sr^{2+} cations whilst the larger green cations represent the Cs^+ centres in the bowls of each ctc. Additional Cs^+ counterions, solvent molecules and hydrogen atoms have been omitted for clarity.

3D networks with ctc previously reported by our group have bridging water ligands connecting tetrahedral coordination cages. Other 3D networks, such as the PtS-type network in 2A, consist of discrete metal-ligand complexes connected through hydrogen bonding interactions. As a result of the shape of the ctc ligand, most reported compounds containing

this molecule (including those in this thesis) contain discrete oligomers, 1D chains or 2D sheets. Compound 2I represents a rare example of a 3D coordination polymer in which ctc is the only ligand present.

2.2.4.2 Compound 2J – $Cs_6[Cs_2Li_4(ctcH_3)_4]\cdot 15.5H_2O$ metallocycle

A compound of formula $Cs_6[Cs_2Li_4(ctcH_3)_4]\cdot 15.5H_2O$, 2J, containing a square shaped M_4L_4 metallocycle was synthesized by diffusing a CsOH solution into a solution of $ctcH_6$ and $LiNO_3$ in aqueous methanol. As indicated in Figure 2.37 the metallocycle is composed of four $ctcH_3^{3-}$ ligands, each of which serves as a right-angle bridge between two lithium cations. Each of the four lithium cations is located halfway along an edge of the metallocycle and is chelated by two $ctcH_3^{3-}$ catecholate groups in a distorted tetrahedral environment. The point group of the metallocycle is D_{2d}, making it achiral.

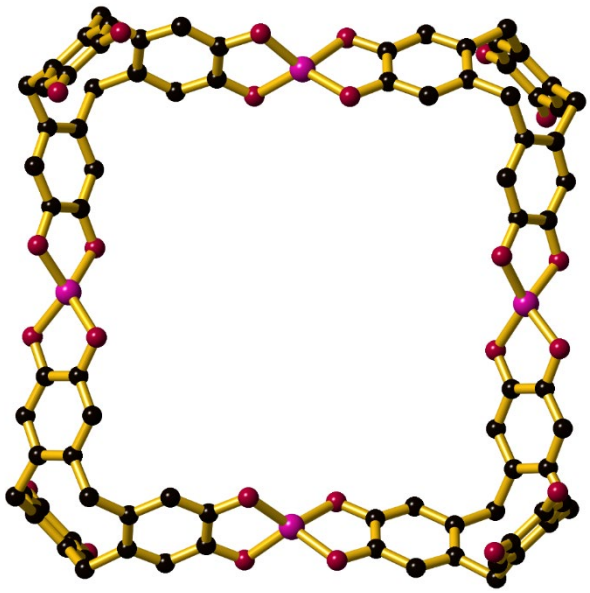

Figure 2.37 A ball and stick representation of the $[Li_4(ctcH_3)_4]^{8-}$ metallocycle in 2J. Pink spheres represent Li^+ cations, which are each chelated by two ctc units in a distorted tetrahedral environment. The non-chelating catechols from two of the ctc units (bottom left and top right) project into the page, whereas the non-chelating catechols from the other two ctc units project out of the page. Hydrogen atoms have been omitted for clarity.

The third catechol group from each of the four ctc ligands is not chelated to a lithium centre but rather remains doubly protonated and participates in hydrogen bonding interactions with a ctc unit from an adjacent metallocycle. Two additional disordered protons on coordinated catechol groups also form hydrogen bonds to the same ctc unit for a total of 6 hydrogen bonds between the pair of ctc units (Figure 2.38). Encapsulated between the hydrogen bonded ctc units is a Cs^+, forming a full clam-type interaction between adjacent metallocycles. The protonated catechol moieties on each metallocycle alternate in orientation (up, down, up, down) therefore each metallocycle is bonded to four others, two above and two below (Figure 2.39).

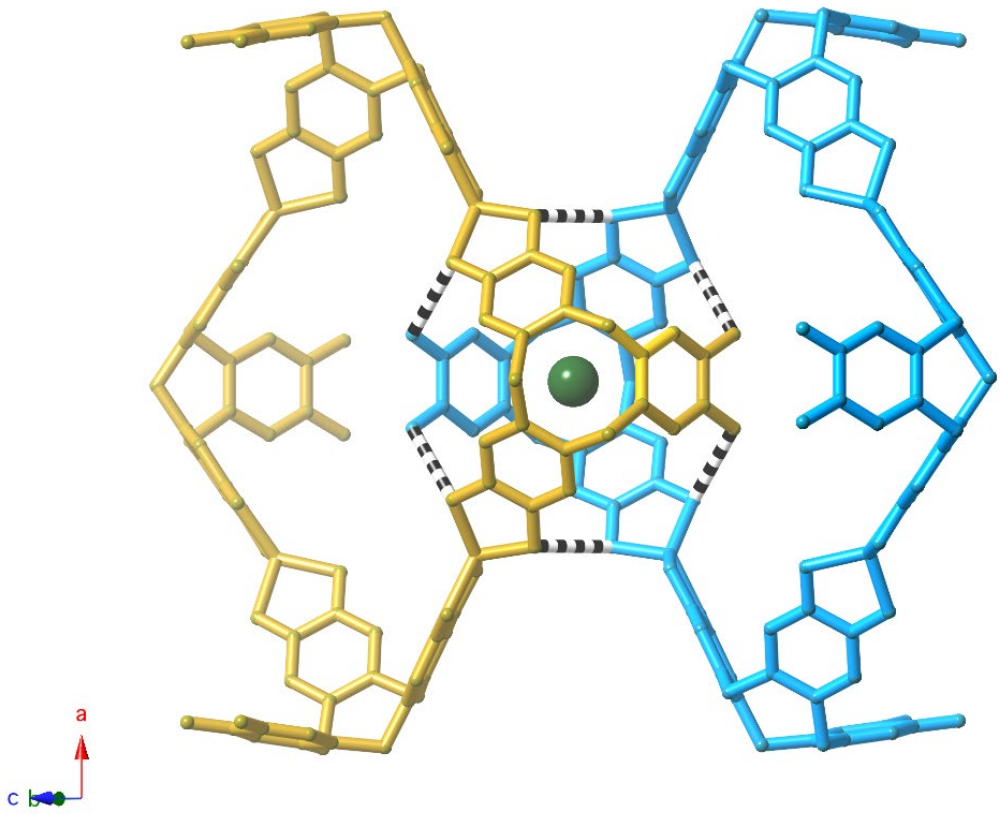

Figure 2.38 A ball and stick representation of two metallocycles (one yellow, one blue) in 2J participating in a clam type interaction with each other. The Cs^+ cation at the centre of the clam is represented by a green sphere. Hydrogen atoms have been omitted for clarity.

Each metallocycle can be considered as a distorted tetrahedral node due to the four ctc–Cs^+–ctc clam-type interactions. This connectivity between metallocycles gives rise to a 3-dimensional structure which is topologically related to that of diamond. Additional disordered Cs^+ counter cations are present in the crystal structure and interact with the outer aromatic faces of the $ctcH_3^{3-}$ units. Disordered solvent molecules are also present in the crystal structure (not shown in Figure 2.39).

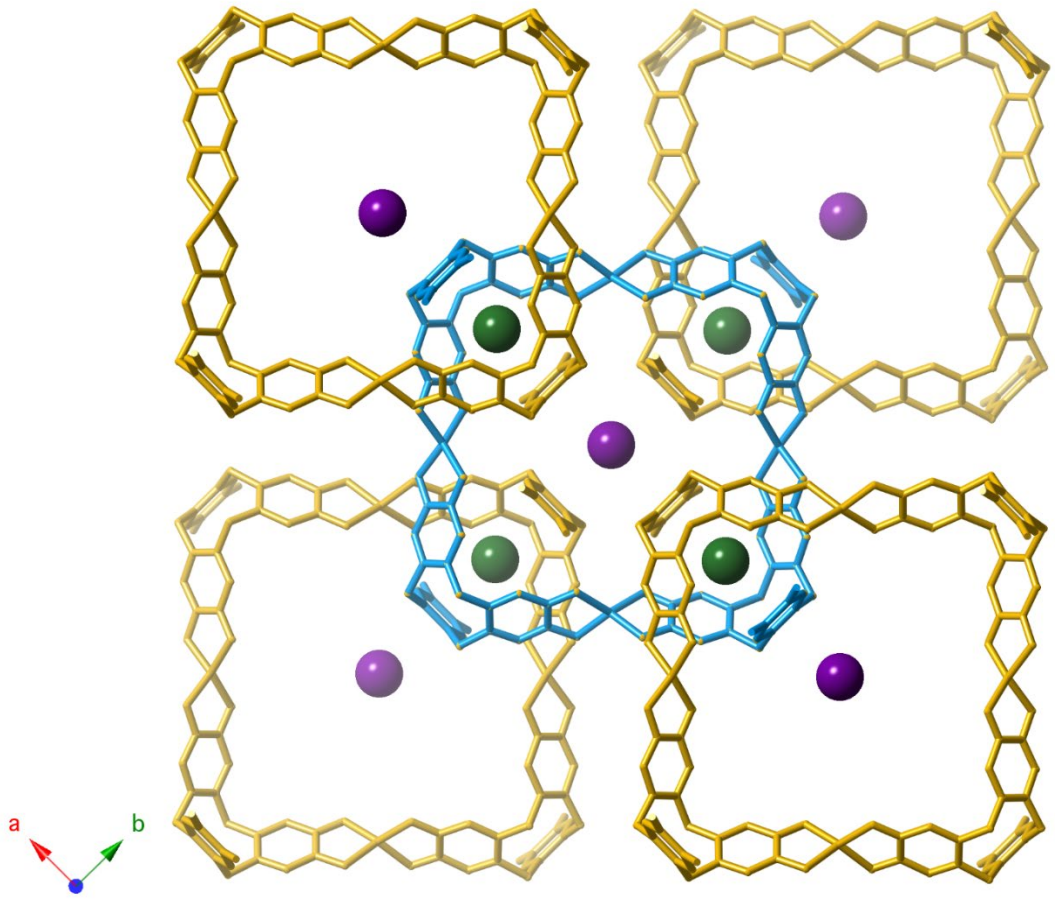

Figure 2.39 A ball and stick representation of a single metallocycle (blue) participating in four clam-type interactions with the metallocycles adjacent to it. Two of the metallocycles (bottom left and top right) lie beneath the plane of the central metallocycle while the other two (top left and bottom right) lie above. Green spheres represent Cs^+ cations in clams and purple spheres represent Cs^+ cations present outside of clams. Hydrogen atoms have been omitted for clarity.

Interestingly, one type of Cs^+ cation lies at the centre of each metallocycle, as shown in Figure 2.39, and interacts with four aromatic faces, each from one of the four adjacent metallocycles. Because these Cs^+ cations represent the central point of each metallocycle, they accurately indicate the positions of metallocycles relative to each other. When each of these centres is shown connected to the centres of the adjacent metallocycles, the 3D network described in the topological analysis is able to be simply visualised, in a manner similar to that presented for compound 2I. One adamantane unit within the diamond-type network in 2J is represented in Figure 2.40.

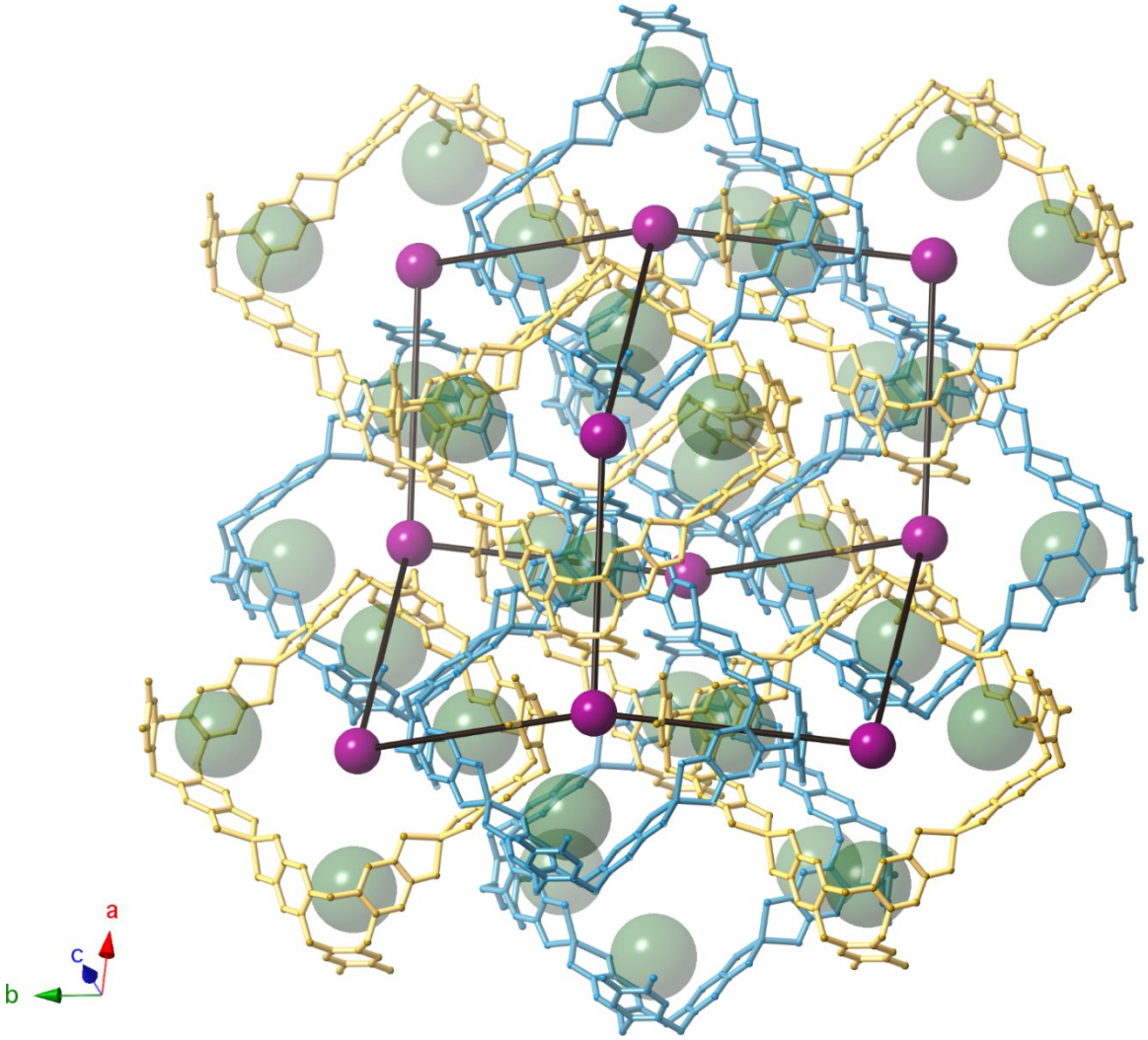

Figure 2.40 A representation of the adamantane unit in 2J. The small purple spheres represent Cs^+ cations that lie at the centre of each metallocycle and interact with the aromatic faces of four catechol units (each from metallocycles adjacent to the first). The black lines linking the Cs^+ cations that lie at the centre of each metallocycle show that the metallocycles lie in a diamond type arrangement, as indicated by the single adamantane unit shown.

2.3 Concluding remarks

This research has shown that there is extensive structural diversity in systems arising from the combination of ctc with group 1 and 2 metal cations, and in particular the Cs^+ cation. This structural diversity likely arises from the multiple available binding modes of group 1 and 2 metal cations, and the general preference of the larger alkali metal cations for the aromatic surfaces of the ctc bowl over both dioxolene-oxygen atoms and solvent molecules. Due to the weaker binding affinity of alkali metal cations than, for example, transition metal cations, as well as their less well defined coordination numbers and geometries,[40] a number of different structures were able to be obtained in which the same cation played a different role. Cs^+ preferentially interacts with the aromatic faces of the ctc bowl, which is not surprising given that it is a soft metal cation, and especially given that similar associations have been seen in Cs^+-calixarene complexes. In some cases, however, Cs^+ was able to bind to three catechol units in a hexa- or pentacoordinate environment, reflective of the non-directional nature of coordination to group 1 metal cations.

The work reported in this chapter gives valuable insight into the chemistry of ctc with the Cs^+ cation, and also provides useful insights and data for collaborators studying such host–guest systems in the gas phase and in computational studies. The research has also prompted the continued investigation of the uptake of Cs^+, in the work described in chapter 5 of this thesis.

The studies reported in this chapter have been extended upon to include the use of tetrahedral anaions and the results of these investigations form the basis of chapter 3.

2.4 Experimental Details

Compound 2A – $H_z[Cs(ctcH_x)(ctcH_y)]$ clam: CsCl (11 mg, 0.065 mmol) was dissolved in water (9 mL) and added to a solution of $ctcH_6$ (48 mg, 0.13 mmol) in methanol (9 mL). Undissolved solid was removed via gravity filtration after which ammonia vapour was allowed to diffuse into the solution. Light yellow crystals suitable for X-ray diffraction studies formed within a day. The crystals were filtered and washed with copious amounts of water, then acetone and dried at the pump. Space group: $P4_2/ncm$. Analysis: found (%): C 57.9, H 4.3, Cs 15.6; calcd (%): C 58.3, H 4.1, Cs 15.5.

Compound 2B – $[Cs(ctcH_6)_2]Cl\cdot EtOH$ cationic clam: $ctcH_6$ (48 mg, 0.13 mmol) and CsCl (5.5 mg, 0.0325 mmol) were dissolved in EtOH (12 mL). *ca.* 5 drops of concentrated HCl was added to the suspension. The reaction mixture was irradiated with microwaves for 15 minutes at 120 °C, with 30 seconds of pre-stirring. The intense yellow solution was allowed to cool to room temperature and slowly evaporate until crystal formation occurred. The small, colourless crystals were collected on a glass frit, and a 'shard-like' crystal was collected for X-ray diffraction analysis. Space group: *P*-1. Yield and elemental analysis: unable to be determined as this compound formed as part of a mixture with 2C, as confirmed through synchrotron powder X-ray diffraction.

Compound 2C – $[Cs(ctcH_6)]Cl\cdot 0.5EtOH$ (6,3) network: $ctcH_6$ (48 mg, 0.13 mmol) and CsCl (11 mg, 0.065 mmol) were dissolved in EtOH (12 mL). *ca.* 5 drops of concentrated HCl was added to the suspension. The reaction mixture was irradiated with microwaves for 15 minutes at 120 °C, with 30 seconds of pre-stirring. The intense yellow solution was allowed to cool to room temperature and slowly evaporate until crystal formation occurred. A light-yellow block-like crystal was selected for single crystal X-ray diffraction analysis. The bulk

crystalline material, which was collected on a glass frit for further analysis appears to lose ethanol and uptake water from the atmosphere upon isolation from the mother liquor, as indicated by the elemental analysis. Space group: *P*-3*m*1. Yield: 22.3 mg, 30%. Analysis: found (%): C 44.2, H 3.9 N < 0.30; calcd (%): C 44.2 H 3.9 for $[Cs(ctc)]Cl{\cdot}2H_2O$.

Compound 2D – [Cs(ctcH$_6$)]Cl·EtOH (6,3) network: $ctcH_6$ (48 mg, 0.13 mmol) was dissolved in EtOH (6 mL) and to this solution was added CsCl (22 mg, 0.13 mmol) in EtOH (6 mL). *ca.* 5 drops of concentrated HCl was added to the suspension. The reaction mixture was irradiated with microwaves for 15 minutes at 120 °C, with 30 seconds of pre-stirring. The intense yellow solution was allowed to cool to room temperature and 6 mL aliquots were left to crystallise undisturbed. The light-yellow rod-like crystals were collected on a glass frit. Space group: $P2_1/c$. Yield (for reaction product that is predominantly 2C): 40.2 mg. Elemental analysis and percentage yield calculations for this compound was unable to be performed, as the major product in bulk material resultant from the reaction was compound 2C, as confirmed through synchrotron powder X-ray diffraction.

Compound 2E – [Rb(ctcH$_6$)]Cl·0.5EtOH (6,3) network: $ctcH_6$ (48 mg, 0.13 mmol) and RbCl (15.7 mg, 0.13 mmol) was dissolved in EtOH (12 mL). *ca.* 5 drops of concentrated HCl was added to the suspension. The reaction mixture was irradiated with microwaves for 15 minutes at 120 °C, with 30 seconds of pre-stirring. The intense yellow solution was allowed to cool to room temperature and slowly evaporate until square, colourless plates formed. The bulk crystalline material, which was collected on a glass frit for further analysis appears to lose ethanol and uptake water from the atmosphere upon isolation from the mother liquor, as indicated by the elemental analysis. Space group: *P*-3*m*1. Yield: 4.3 mg, 6%. Analysis: found (%): C 49.1, H 3.5, N < 0.30; calcd (%): C 49.0 H 4.1 for $[Rb(ctc)]Cl{\cdot}1.5H_2O$.

Compound 2F – $[Ca_2(ctcH_4)_2(MeOH)_4]\cdot MeOH$: $ctcH_6$ (24 mg, 0.065 mmol) was dissolved in MeOH (3 mL) and filtered to remove any undissolved solid (commonly the methanol solvate of ctc), if necessary. To this solution was added $CaCl_2\cdot 2H_2O$ (5 mg, 0.033 mmol) in H_2O (3 mL). The reaction vessel was covered in parafilm and NH_3 vapour was then diffused into the solution through a pin hole in the film and the solution turned dark brown. Formation of colourless plates occurred within one week. The crystals were collected on a glass frit and washed with MeOH. The bulk material appears to lose methanol and uptake water from the atmosphere upon isolation from the mother liquor, as indicated by the elemental analysis. Space group: *P*-1. Yield: 11.4 mg, 71%. Analysis: found (%): C 48.0, H 4.4, N 0.6; calcd (%): C 48.3, H 5.6 for $[Ca_2(ctcH_4)_2]\cdot 13H_2O$.

Compound 2G – $[Sr(ctcH_4)(H_2O)_4]\cdot MeOH\cdot 2H_2O$: $ctcH_6$ (24 mg, 0.065 mmol) was dissolved in MeOH (3 mL) and filtered to remove undissolved solid (commonly the methanol solvate of ctc), if necessary. To this solution was added $SrCl_2.6H_2O$ (9 mg, 0.033 mmol) in H_2O (3 mL). The reaction vessel was covered in parafilm and NH_3 vapour was diffused into the solution through a pin hole in the film and the solution turned dark brown. Formation of dark yellow plates and brown powder occurred within one week (see image in supporting information). The mixture was collected on a glass frit and washed with MeOH. The bulk material appears to lose methanol and uptake water from the atmosphere upon isolation from the mother liquor, as indicated by the elemental analysis. Space group: $P2_1/c$. Yield (mixture of crystalline and powder material): 7.8 mg, 41%. Analysis: found (%): C 42.8, H 4.7, N 0.5; calcd (%): C 43.0, H 5.3 for $[Sr(ctcH_4)(H_2O)_4]\cdot 3.5H_2O$.

Compound 2H $[Ba_2(ctcH_4)_2(H_2O)_7(MeOH)_2]\cdot MeOH\cdot 3H_2O$: $ctcH_6$ (24 mg, 0.065 mmol) was dissolved in MeOH (3 mL) and filtered to remove undissolved solid (commonly the

methanol solvate of ctc), if necessary. To this solution was added $BaCl_2 \cdot 2H_2O$ (8 mg, 0.033 mmol) in H_2O (3 mL). The reaction vessel was covered in parafilm and NH_3 vapour was then diffused into the solution through a pin hole in the film and the solution turned dark brown**.** Formation of dark yellow plates and brown powder occurred within one week. The mixture was collected on a glass frit and washed with MeOH. The bulk material appears to lose methanol and uptake water from the atmosphere upon isolation from the mother liquor, as indicated by the elemental analysis. Space group: $P2_1/m$. Yield (mixture of crystalline and powder material): 12.7 mg, 60%. Analysis: found (%): C 39.8, H 3.7, N < 0.30; calcd (%): C 39.8, H 3.7 for $[Ba_2(ctc)_2] \cdot 15H_2O$.

Compound 2I – $Cs_3[CsSr(ctc)]$·solvate (10,3)-a network: $ctcH_6$ (24 mg, 0.065 mmol) was dissolved in EtOH (3 mL) and to this solution was added $SrCl_2 \cdot 6H_2O$ (26 mg, 0.0975 mmol) in H_2O (2 mL). $CsOH \cdot H_2O$ (131 mg**,** 0.78 mmol) dissolved in H_2O (1 mL) was layered beneath this solution and left to crystallise as colourless plates. Space group: $P2_13$. Difficulties were encountered in collecting a bulk product for further analysis.

Compound 2J – $Cs_6[Cs_2Li_4(ctcH_3)_4] \cdot 15.5H_2O$ metallocycle: Crystals suitable for X-ray diffraction studies were obtained by liquid/liquid diffusion. A solution of $LiNO_3$ (13.5 mg, 0.20 mmol) in water (1 mL) was added to $ctcH_6$ (24 mg, 0.065mmol) partially dissolved in MeOH (1 mL). An aqueous solution (3 mL) of $CsOH \cdot H_2O$ (262 mg, 1.56 mmol) was layered below. The solution was left to stand under a nitrogen atmosphere. Large colourless crystals formed overnight. The crystals were filtered after several days, quickly washed with acetone and dried at the pump. Space group: $I4_1/amd$. Analysis: found (%): C 35.6 H 3.4; calcd (%): C 35.9, H 3.2.

2.5 Crystallographic Details

2.5.1 General data collection and refinement details

Data for 2A – 2J were collected as per the following procedures:

A single crystal suitable for X-ray crystallography was removed from the mother liquor and immediately immersed in protective oil. The crystal was mounted on a loop and placed in a stream of N_2 flowing from an Oxford CryoStream at 130 K.[41] Intensity data were collected using the phi and omega scan technique with or CuKα radiation on a SuperNova, Dual Source, Atlas diffractometer, XtaLAB Synergy, Dualflex, HyPix diffractometer or an Xcalibur Sapphire3 diffractometer.

Crystal structure solutions were obtained by direct methods using the SHELXS-2013[42] or SHELXT programs[43] (refer to CIFs in appendix for structure specific information). Structures were thereafter refined using the SHELXL-2014/7 program using a full-matrix least-squares refinement based on F^2.[44] Absorption corrections were applied using the SADABS or Gaussian techniques.[45]

Crystallographic terminology is detailed in Chapter 7.

Compound 2A – H_z[Cs(ctcH_x)(ctcH_y)] clam:

Single crystal X-ray diffraction analysis was performed using CuKα radiation on a yellow block-like crystal that was mounted on a loop. The data indicated that the crystal possessed tetragonal symmetry. A satisfactory structure solution was obtained in the space group $P4_2/ncm$. All non-hydrogen framework atoms were clearly defined and refined with anisotropic displacement parameters. All hydrogen atoms were placed at geometrically

estimated positions, with the exception of the hydrogen atom located at the special position between four clams, H44. This hydrogen atom was assigned in the same manner as the framework atoms and refined with isotropic displacement parameters.

Compound 2B – [Cs(ctcH$_6$)$_2$]Cl·EtOH cationic clam:

Single crystal X-ray diffraction analysis was performed using CuKα radiation on a colourless plate-like crystal that was mounted on a loop. The data indicated that the crystal possessed triclinic symmetry. A satisfactory structure solution was obtained in the space group *P*-1. All non-hydrogen framework atoms and solvent atoms were clearly defined and refined with anisotropic displacement parameters. All hydrogen atoms were placed at geometrically estimated positions. The X-ray data indicated that within a given unit cell, either a chloride counterion or methanol molecule was present, with both chloride and ethanol molecules occupying the same location within the cell. The chloride and ethanol molecules were modelled over the same site and each were assigned half occupancy.

Compound 2C – [Cs(ctcH$_6$)]Cl·0.5EtOH (6,3) network:

Single crystal X-ray diffraction analysis was performed using CuKα radiation on a colourless rod-like crystal that was mounted on a loop. The data indicated that the crystal possessed trigonal symmetry. A satisfactory structure solution was obtained in the space group *P*-3*m*. All non-hydrogen framework atoms and solvent atoms were clearly defined and refined with anisotropic displacement parameters. All hydrogen atoms were placed at geometrically estimated positions. The crystal data indicated the presence of large channels with electron density found within. A chloride anion within the channel could be modelled and refined with anisotropic displacement parameters. Residual peaks of electron density within the

framework channel, attributed to solvent molecules, were apparent in the difference map. The solvent could not be modelled satisfactorily and the SQUEEZE routine from the crystallographic program *PLATON* was employed to produce a modified data set in which the solvent contribution (22 electrons occupying 99 $Å^3$) from the structure factors was removed. The electron density removed is consistent with ½ an ethanol molecule per unit formula.

Compound 2D – [Cs(ctcH$_6$)]Cl·EtOH (6,3) network:

Single crystal X-ray diffraction analysis was performed using CuKα radiation on a colourless polyhedral crystal that was mounted on a loop. The data indicated that the crystal possessed monoclinic symmetry. A satisfactory structure solution was obtained in the space group $P2_1/c$. All non-hydrogen framework atoms and solvent atoms were clearly defined and refined with anisotropic displacement parameters. All hydrogen atoms were placed at geometrically estimated positions, except for the catechol hydrogen atoms, which were manually assigned and refined with isotropic displacement parameters.

Compound 2F – [Ca$_2$(ctcH$_4$)$_2$(MeOH)$_4$]·MeOH:

Single crystal X-ray diffraction analysis was performed using CuKα radiation on a colourless prismatic crystal that was mounted on a loop. The data indicated that the crystal possessed triclinic symmetry. A satisfactory structure solution was obtained in the space group *P*-1. All non-hydrogen framework atoms and solvent atoms were clearly defined and refined with anisotropic displacement parameters. All hydrogen atoms were placed at geometrically estimated positions, except for the catechol hydrogen atoms, which were manually assigned refined with isotropic displacement parameters.

Compound 2G – $[Sr(ctcH_4)(H_2O)_4]\cdot MeOH\cdot 2H_2O$:

Single crystal X-ray diffraction analysis was performed using CuKα radiation on a brown plate-like crystal that was mounted on a loop. The data indicated that the crystal possessed monoclinic symmetry. A satisfactory structure solution was obtained in the space group $P2_1/c$. The non-hydrogen ctc, Sr and methanol atoms were clearly defined and refined with anisotropic displacement parameters. All assigned hydrogen atoms were placed at geometrically estimated positions. Refinement of coordinated water molecules with anisotropic displacement parameters proved unsatisfactory and were refined with isotropic displacement parameters. The remaining electron density was attributed to two disordered water molecules.

Compound 2H – $[Ba_2(ctcH_4)_2(H_2O)_7(MeOH)_2]\cdot MeOH\cdot 3H_2O$:

Single crystal X-ray diffraction analysis was performed using CuKα radiation on an orange plate-like crystal that was mounted on a loop. The data indicated that the crystal possessed monoclinic symmetry. A satisfactory structure solution was obtained in the space group $P2_1/m$. All non-hydrogen framework atoms and solvent atoms were clearly defined and refined with anisotropic displacement parameters. All hydrogen atoms were placed at geometrically estimated positions, except the catechol hydrogen atoms, which were manually assigned and refined with fixed O-H separations and isotropic placement parameters.

Compound 2I – $Cs_3[CsSr(ctc)]\cdot$solvate (10,3)-a network:

Single crystal X-ray diffraction analysis was performed using CuKα radiation on a colourless octahedral crystal that was mounted on a loop. The data indicated that the crystal possessed cubic symmetry. A satisfactory structure solution was obtained in the space group $P2_13$. All

non-hydrogen ctc, Sr and Cs atoms were clearly defined and refined with anisotropic displacement parameters. Water oxygen atoms coordinated to caesium cations were refined with isotropic displacement parameters. All ctc hydrogen atoms were placed at geometrically estimated positions. Hydrogen atoms associated with coordinated water molecules could not be satisfactorily modelled.

Compound 2J – $Cs_6[Cs_2Li_4(ctcH_3)_4]\cdot 15.5H_2O$ metallocycle:

Single crystal X-ray diffraction analysis was performed using CuKα radiation on a colourless block-like crystal that was mounted on a loop. The data indicated that the crystal possessed tetragonal symmetry. A satisfactory structure solution was obtained in the space group $14_1/amd$. All non-hydrogen framework atoms were clearly defined and refined with anisotropic displacement parameters. Water oxygen atoms coordinated to caesium cations were refined with isotropic displacement parameters. Caesium atoms Cs2, Cs3 and Cs4 were disordered and modelled based upon electron density in the difference map. All ctc hydrogen atoms were placed at geometrically estimated positions, except for catechol hydrogen atom H3, which was manually assigned with a fixed O-H separation and isotropic displacement parameters.

2.5.2 Crystallographic Tables

Table 2.7 Crystal data and structure refinement for compound 2A

Empirical formula	$C_{42}H_{35}CsO_{12}$	
Formula weight	864.61	
Temperature	130(1) K	
Wavelength	1.54184 Å	
Crystal system	Tetragonal	
Space group	*P*42/*n c m*	
Unit cell dimensions	*a* = 17.4558(2) Å	α= 90°.
	b = 17.4558(2) Å	β= 90°.
	c = 10.7146(2) Å	γ = 90°.
Volume	3264.79(10) $Å^3$	
Z	4	
Density (calculated)	1.759 Mg/m^3	
Absorption coefficient	9.492 mm^{-1}	
F(000)	1752	
Crystal size	0.1348 × 0.0939 × 0.0713 mm^3	
Theta range for data collection	3.581 to 73.960°.	
Index ranges	-15 ≤ h ≤ 21, -21 ≤ k ≤ 21, -13 ≤	
	l ≤ 8	
Reflections collected	6621	
Independent reflections	1706 [*R*(int) = 0.0285]	
Completeness to theta = 67.684°	100.0 %	
Absorption correction	Gaussian	
Max. and min. transmission	0.618 and 0.462	
Refinement method	Full-matrix least-squares on F^2	
Data / restraints / parameters	1706 / 0 / 132	
Goodness-of-fit on F^2	1.296	
Final *R* indices [*I*>2sigma(*I*)]	*R*1 = 0.0589, *wR*2 = 0.1159	
R indices (all data)	*R*1 = 0.0601, *wR*2 = 0.1163	
Largest diff. peak and hole	0.382 and -0.458 e.$Å^{-3}$	

Crystal data and structure refinement for compound 2B

Empirical formula	$C_{44}H_{42}ClCsO_{13}$	
Formula weight	947.13	
Temperature	130(1) K	
Wavelength	1.54184 Å	
Crystal system	Triclinic	
Space group	*P*-1	
Unit cell dimensions	a = 10.2531(5) Å	α= 69.526(5)°.
	b = 10.3497(7) Å	β= 66.344(4)°.
	c = 10.4277(5) Å	γ = 76.753(5)°.
Volume	944.45(10) $Å^3$	
Z	1	
Density (calculated)	1.665 Mg/m^3	
Absorption coefficient	8.913 mm^{-1}	
F(000)	482	
Crystal size	0.288 × 0.148 × 0.047 mm^3	
Theta range for data collection	4.585 to 67.490°.	
Index ranges	$-12 \le h \le 12$, $-12 \le k \le 11$, $-12 \le l \le 12$	
Reflections collected	6101	
Independent reflections	3410 [R(int) = 0.0221]	
Completeness to theta = 67.490°	99.9 %	
Absorption correction	Gaussian	
Max. and min. transmission	0.845 and 0.299	
Refinement method	Full-matrix least-squares on F^2	
Data / restraints / parameters	3410 / 30 / 294	
Goodness-of-fit on F^2	1.064	
Final R indices [I>2sigma(I)]	$R1$ = 0.0346, $wR2$ = 0.0937	
R indices (all data)	$R1$ = 0.0346, $wR2$ = 0.0937	
Largest diff. peak and hole	1.408 and -0.984 e.$Å^{-3}$	

Crystal data and structure refinement for compound 2C

Empirical formula	$C_{22}H_{21}ClCsO_{6.50}$	
Formula weight	557.75	
Temperature	130(1) K	
Wavelength	1.54184 Å	
Crystal system	Trigonal	
Space group	*P*-3*m*1	
Unit cell dimensions	*a* = 12.2517(6) Å	α= 90°.
	b = 12.2517(6) Å	β= 90°.
	c = 8.6972(4) Å	γ = 120°.
Volume	1130.58(12) $Å^3$	
Z	2	
Density (calculated)	1.638 Mg/m^3	
Absorption coefficient	14.189 mm^{-1}	
F(000)	554	
Crystal size	0.15 × 0.029 × 0.013 mm^3	
Theta range for data collection	4.167 to 73.743°.	
Index ranges	$-15 \le h \le 11$, $-13 \le k \le 14$, $-10 \le l \le 5$	
Reflections collected	2652	
Independent reflections	866 [*R*(int) = 0.0825]	
Completeness to theta = 67.684°	100.0 %	
Absorption correction	Semi-empirical from equivalents	
Max. and min. transmission	1.00000 and 0.80043	
Refinement method	Full-matrix least-squares on F^2	
Data / restraints / parameters	866 / 0 / 53	
Goodness-of-fit on F^2	1.112	
Final *R* indices [*I*>2sigma(*I*)]	*R*1 = 0.0670, *wR*2 = 0.1765	
R indices (all data)	*R*1 = 0.0899, *wR*2 = 0.2034	
Largest diff. peak and hole	1.087 and -1.203 e.$Å^{-3}$	

Crystal data and structure refinement for compound 2D

Empirical formula	$C_{23}H_{24}ClCsO_7$	
Formula weight	580.78	
Temperature	130(1) K	
Wavelength	1.54184 Å	
Crystal system	Monoclinic	
Space group	$P2_1/c$	
Unit cell dimensions	a = 8.80580(10) Å	α= 90°.
	b = 11.2672(2) Å	β= 91.8820(10)°.
	c = 22.3500(4) Å	γ = 90°.
Volume	2216.30(6) $Å^3$	
Z	4	
Density (calculated)	1.741 Mg/m^3	
Absorption coefficient	14.527 mm^{-1}	
F(000)	1160	
Crystal size	0.175 × 0.123 × 0.065 mm^3	
Theta range for data collection	3.958 to 67.481°.	
Index ranges	$-10 \le h \le 6$, $-11 \le k \le 13$, $-25 \le l \le 26$	
Reflections collected	8184	
Independent reflections	3997 [R(int) = 0.0184]	
Completeness to theta = 67.481°	100.0 %	
Absorption correction	Gaussian	
Max. and min. transmission	0.476 and 0.189	
Refinement method	Full-matrix least-squares on F^2	
Data / restraints / parameters	3997 / 0 / 314	
Goodness-of-fit on F^2	1.094	
Final R indices [I>2sigma(I)]	$R1$ = 0.0220, $wR2$ = 0.0554	
R indices (all data)	$R1$ = 0.0233, $wR2$ = 0.0560	
Largest diff. peak and hole	0.498 and -0.637 e.$Å^{-3}$	

Crystal data and structure refinement for compound 2F

Empirical formula	$C_{48}H_{56}Ca_2O_{18}$	
Formula weight	1001.08	
Temperature	130(1) K	
Wavelength	1.54184 Å	
Crystal system	Triclinic	
Space group	*P*-1	
Unit cell dimensions	*a* = 9.3122(7) Å	α= 93.167(5)°.
	b = 10.9878(7) Å	β= 105.515(6)°.
	c = 11.8692(7) Å	γ = 105.238(6)°.
Volume	1118.72(14) Å^3	
Z	1	
Density (calculated)	1.486 Mg/m^3	
Absorption coefficient	2.898 mm^{-1}	
F(000)	528	
Crystal size	0.309 × 0.117 × 0.050 mm^3	
Theta range for data collection	3.901 to 72.471°.	
Index ranges	-11 ≤ h ≤ 11, -13 ≤ k ≤ 13, -12 ≤ l ≤ 14	
Reflections collected	7753	
Independent reflections	4362 [R(int) = 0.0535]	
Completeness to theta = 67.684°	99.9 %	
Absorption correction	Gaussian	
Max. and min. transmission	0.942 and 0.755	
Refinement method	Full-matrix least-squares on F^2	
Data / restraints / parameters	4362 / 1 / 322	
Goodness-of-fit on F^2	1.099	
Final R indices [I>2sigma(I)]	*R*1 = 0.0754, *wR*2 = 0.2215	
R indices (all data)	*R*1 = 0.0874, *wR*2 = 0.2282	
Largest diff. peak and hole	0.893 and -0.516 e.Å^{-3}	

Crystal data and structure refinement for compound 2G

Empirical formula	$C_{22}H_{30}O_{13}Sr$	
Formula weight	590.08	
Temperature	130(1) K	
Wavelength	1.54184 Å	
Crystal system	Monoclinic	
Space group	$P2_1/c$	
Unit cell dimensions	a = 9.1958(2) Å	α= 90°.
	b = 24.7334(4) Å	β= 104.074(2)°.
	c = 10.89060(10) Å	γ = 90°.
Volume	2402.64(7) $Å^3$	
Z	4	
Density (calculated)	1.631 Mg/m^3	
Absorption coefficient	3.737 mm^{-1}	
F(000)	1216	
Crystal size	0.474 × 0.153 × 0.036 mm^3	
Theta range for data collection	3.574 to 73.965°.	
Index ranges	-11 ≤ h ≤ 11, -28 ≤ k ≤ 30, -9 ≤ l ≤ 13	
Reflections collected	9658	
Independent reflections	4733 [R(int) = 0.0292]	
Completeness to theta = 67.684°	99.9 %	
Absorption correction	Gaussian	
Max. and min. transmission	0.872 and 0.463	
Refinement method	Full-matrix least-squares on F^2	
Data / restraints / parameters	4733 / 0 / 309	
Goodness-of-fit on F^2	1.022	
Final R indices [I>2sigma(I)]	$R1$ = 0.0523, $wR2$ = 0.1431	
R indices (all data)	$R1$ = 0.0558, $wR2$ = 0.1472	
Largest diff. peak and hole	1.890 and -0.779 e.$Å^{-3}$	

Crystal data and structure refinement for compound 2H

Empirical formula	$C_{45}H_{64}Ba_2O_{25}$	
Formula weight	1279.64	
Temperature	130(1) K	
Wavelength	1.54184 Å	
Crystal system	Monoclinic	
Space group	$P2_1/m$	
Unit cell dimensions	a = 9.1694(1) Å	α= 90°.
	b = 25.3748(3) Å	β= 103.895(1)°.
	c = 10.8617(1) Å	γ = 90°.
Volume	2453.26(5) $Å^3$	
Z	2	
Density (calculated)	1.732 Mg/m^3	
Absorption coefficient	13.181 mm^{-1}	
F(000)	1292	
Crystal size	0.313 × 0.136 × 0.084 mm^3	
Theta range for data collection	3.484 to 78.114°.	
Index ranges	-11 ≤ h ≤ 11, -31 ≤ k ≤ 31, -11 ≤ l ≤ 13	
Reflections collected	23097	
Independent reflections	5298 [R(int) = 0.0454]	
Completeness to theta = 67.684°	100.0 %	
Absorption correction	Gaussian	
Max. and min. transmission	0.671 and 0.122	
Refinement method	Full-matrix least-squares on F^2	
Data / restraints / parameters	5298 / 15 / 391	
Goodness-of-fit on F^2	1.048	
Final R indices [I>2sigma(I)]	$R1$ = 0.0435, $wR2$ = 0.1141	
R indices (all data)	$R1$ = 0.0450, $wR2$ = 0.1154	
Largest diff. peak and hole	2.680 and -2.740 e.$Å^{-3}$	

Crystal data and structure refinement for compound 2I

Empirical formula	$C_{84}H_{240}Cs_{16}O_{108}Sr_4$	
Formula weight	5455.79	
Temperature	130(1) K	
Wavelength	1.54184 Å	
Crystal system	Cubic	
Space group	$P2_13$	
Unit cell dimensions	a = 16.5051(4) Å	α= 90°.
	b = 16.5051(4) Å	β= 90°.
	c = 16.5051(4) Å	γ = 90°.
Volume	4496.3(3) Å^3	
Z	1	
Density (calculated)	2.015 Mg/m^3	
Absorption coefficient	27.279 mm^{-1}	
F(000)	2640	
Crystal size	0.12 × 0.09 × 0.07 mm^3	
Theta range for data collection	3.787 to 73.639°.	
Index ranges	-13 ≤ h ≤ 9, -20 ≤ k ≤ 2, -16 ≤ l ≤ 11	
Reflections collected	3958	
Independent reflections	2558 [R(int) = 0.0341]	
Completeness to theta = 67.684°	99.9 %	
Absorption correction	Gaussian	
Max. and min. transmission	0.31 and 0.146	
Refinement method	Full-matrix least-squares on F^2	
Data / restraints / parameters	2558 / 0 / 128	
Goodness-of-fit on F^2	1.119	
Final R indices [I>2sigma(I)]	$R1$ = 0.0786, $wR2$ = 0.1928	
R indices (all data)	$R1$ = 0.0825, $wR2$ = 0.1967	
Absolute structure parameter	0.033(11)	
Largest diff. peak and hole	2.006 and -1.728 e.Å^{-3}	

Crystal data and structure refinement for compound 2J

Empirical formula	$C_{84}H_{104}Cs_8Li_4O_{48}$	
Formula weight	2972.71	
Temperature	130(1) K	
Wavelength	1.54184 Å	
Crystal system	Tetragonal	
Space group	$I4_1/amd$	
Unit cell dimensions	a = 27.2957(4) Å	α= 90°.
	b = 27.2957(4) Å	β= 90°.
	c = 16.6075(8) Å	γ = 90°.
Volume	12373.5(7) $Å^3$	
Z	4	
Density (calculated)	1.596 Mg/m^3	
Absorption coefficient	18.822 mm^{-1}	
F(000)	5776	
Crystal size	0.1461 × 0.1040 × 0.0800 mm^3	
Theta range for data collection	3.238 to 67.989°.	
Index ranges	$-32 \le h \le 31$, $-24 \le k \le 32$, $-19 \le l \le 11$	
Reflections collected	11018	
Independent reflections	2957 [R(int) = 0.0331]	
Completeness to theta = 67.684°	99.9 %	
Absorption correction	Gaussian	
Max. and min. transmission	0.337 and 0.100	
Refinement method	Full-matrix least-squares on F^2	
Data / restraints / parameters	2957 / 7 / 197	
Goodness-of-fit on F^2	1.104	
Final R indices [I>2sigma(I)]	$R1$ = 0.0694, $wR2$ = 0.2132	
R indices (all data)	$R1$ = 0.0812, $wR2$ = 0.2264	
Largest diff. peak and hole	1.417 and -0.836 e.$Å^{-3}$	

2.6 References

[1] Z. Liu, S. K. M. Nalluri, J. F. Stoddart, *Chem. Soc. Rev.* **2017**, *46*, 2459–2478.

[2] C. J. Pedersen, *J. Am. Chem. Soc.* **1967**, *89*, 7017–7036.

[3] Nobel Media AB 2018, "The Nobel Prize in Chemistry 1987," can be accessed under https://www.nobelprize.org/prizes/chemistry/1987/summary/, **2014**.

[4] C. J. Pedersen, *J. Am. Chem. Soc.* **1970**, *92*, 391–394.

[5] E. Kauffmann, J. Lehn, J. Sauvage, *Helv. Chim. Acta* **1976**, *59*, 1099–1111.

[6] D. J. Cram, *Angew. Chemie Int. Ed. English* **1986**, *25*, 1039–1057.

[7] A. Ikeda, S. Shinkai, *Chem. Rev.* **1997**, *97*, 1713–1734.

[8] S. A. Vignon, T. Jarrosson, T. Iijima, H. R. Tseng, J. K. M. Sanders, J. F. Stoddart, *J. Am. Chem. Soc.* **2004**, *126*, 9884–9885.

[9] K. Vellingiri, K. H. Kim, A. Pournara, A. Deep, *Prog. Mater. Sci.* **2018**, *94*, 1–67.

[10] M. A. Olatunji, M. U. Khandaker, H. N. M. E. Mahmud, Y. M. Amin, *RSC Adv.* **2015**, *5*, 71658–71683.

[11] D. Alby, C. Charnay, M. Heran, B. Prelot, J. Zajac, *J. Hazard. Mater.* **2018**, *344*, 511–530.

[12] M. J. Hardie, C. L. Raston, *Cryst. Growth Des.* **2001**, *1*, 53–58.

[13] C. J. Sumby, J. Fisher, T. J. Prior, M. J. Hardie, *Chem. - A Eur. J.* **2006**, *12*, 2945–2959.

[14] H. A. Fogarty, P. Berthault, T. Brotin, G. Huber, H. Desvaux, J. P. Dutasta, *J. Am. Chem. Soc.* **2007**, *129*, 10332–10333.

[15] T. Brotin, J.-P. P. Dutasta, *Chem. Rev.* **2009**, *109*, 88–130.

[16] M. J. Hardie, *Isr. J. Chem.* **2011**, *51*, 807–816.

[17] M. J. Li, C. H. Huang, C. C. Lai, S. H. Chiu, *Org. Lett.* **2012**, *14*, 6146–6149.

[18] T. Brotin, R. Montserret, A. Bouchet, D. Cavagnat, M. Linares, T. Buffeteau, *J. Org. Chem.* **2012**, *77*, 1198–1201.

[19] J. J. Henkelis, C. J. Carruthers, S. E. Chambers, R. Clowes, A. I. Cooper, J. Fisher, M. J. Hardie, *J. Am. Chem. Soc.* **2014**, *136*, 14393–14396.

[20] J. J. Henkelis, M. J. Hardie, *Chem. Commun. (Camb).* **2015**, *51*, 11929–43.

[21] J. D. Brown, *Synthesis & HyperCEST Testing of CTV Derivatives: A Bowl Shaped Compound That Encapsulates Xenon*, University of Rhode Island, **2015**.

[22] D. Xia, Y. Li, K. Jie, B. Shi, Y. Yao, *Org. Lett.* **2016**, *18*, 2910–2913.

[23] D. Zhang, A. Martinez, J.-P. P. Dutasta, *Chem. Rev.* **2017**, *117*, 4900–4942.

[24] F. L. Thorp-Greenwood, G. T. Berry, S. S. Boyadjieva, S. Oldknow, M. J. Hardie, *CrystEngComm* **2018**, *20*, 3960–3970.

[25] J. T. Yu, Z. Chen, J. Sun, Z. T. Huang, Q. Y. Zheng, *J. Mater. Chem.* **2012**, *22*, 5369–5373.

[26] S. C. Di-, J. A. Hyatt, E. N. Duesler, D. Y. Curtin, I. C. Paul, *J. Org. Chem.* **1980**,

45, 5074–5079.

[27] K. Kataoka, T. D. James, Y. Kubo, *J. Am. Chem. Soc.* **2007**, *129*, 15126–15127.

[28] B. F. Abrahams, N. J. Fitzgerald, T. A. Hudson, R. Robson, T. Waters, *Angew. Chem. Int. Ed. Engl.* **2009**, *48*, 3129–32.

[29] B. F. Abrahams, B. A. Boughton, N. J. FitzGerald, J. L. Holmes, R. Robson, *Chem. Commun.* **2011**, *47*, 7404.

[30] B. F. Abrahams, N. J. FitzGerald, R. Robson, *Angew. Chemie - Int. Ed.* **2010**, *49*, 2896–2899.

[31] J. Zhen, S. Ding, W. Wang, J. Liu, J. Sun, Z. Huang, Q. Zheng, *Chinese J. Chem.* **2016**, *34*, 783–787.

[32] J. L. Holmes, B. F. Abrahams, A. Ahveninen, B. A. Boughton, T. A. Hudson, R. Robson, D. Thinagaran, *Chem. Commun.* **2018**, *54*, 11877–11880.

[33] M. J. Hardie, R. Ahmad, C. J. Sumby, *New J. Chem.* **2005**, *29*, 1231–1240.

[34] B. H. Toby, R. B. Von Dreele, *J. Appl. Crystallogr.* **2013**, *46*, 544–549.

[35] J.-C. Chambron, M. Meyer, *Chem. Soc. Rev.* **2009**, *38*, 1663–1673.

[36] P. T. Lee, J. E. Thomson, A. Karina, C. Salter, C. Johnston, S. G. Davies, R. G. Compton, *Analyst* **2015**, *140*, 236–242.

[37] E. P. Serjeant, B. Dempsey, *Ionisation Constants of Organic Acids in Aqueous Solution*, Pergamon Press, **1979**.

[38] A. F. Wells, *Three-Dimensional Nets and Polyhedra*, John Wiley & Sons, Ltd, New York, **1977**.

[39] A. L. Spek, *Acta Crystallogr. Sect. C Struct. Chem.* **2015**, *71*, 9–18.

[40] A. Inthasot, S.-T. Tung, S.-H. Chiu, *Acc. Chem. Res.* **2018**, *51*, 1324–1337.

[41] J. Cosier, A. M. Glazer, *J. Appl. Crystallogr.* **1986**, *19*, 105–107.

[42] G. M. Sheldrick, *Acta Crystallogr. Sect. A Found. Crystallogr.* **2008**, *64*, 112–122.

[43] G. M. Sheldrick, *Acta Crystallogr. Sect. A Found. Adv.* **2015**, *71*, 3–8.

[44] G. M. Sheldrick, *Acta Crystallogr. Sect. C Struct. Chem.* **2015**, *71*, 3–8.

[45] *CrysAlisPro 1.171.40.36a, Rigaku Oxford Diffraction/Agilent Technol. UK Ltd* **2018**.

[46] J. L. Holmes, Supramolecular Structures of Cyclotricatechylene, MSc Thesis, The University of Melbourne, **2011**.

Chapter 3 Cyclotricatechylene cubes with group I metal cations and oxyanions

Contents

3.1 Introduction

Research by the Robson-Abrahams group into compounds involving cyclotricatechylene and alkali metals has resulted in the generation of a range of structurally diverse compounds. Such diversity has arisen from varying the reaction conditions, predominantly the choice of metal cation and the pH of the reaction solution. The ability of the cyclotricatechylene molecule to bind metal centres, either through aromatic surfaces or oxygen atoms, and to participate in hydrogen bonding has allowed the cavitand to form a wide range of supramolecular assemblies. The compounds reported thus far have been generated with group I and II metal halide salts (with the exception of compound 2I, the $Cs_8[Li_4(ctcH_3)_4]\cdot 15.5H_2O$ metallocycle, which employed a nitrate salt), with hydroxide present as a base. There appears however, to be great scope for extending the types of structures formed by incorporating other anions besides halides into the reaction mixture.

Prior to the synthesis of compounds described in chapter 2, exploratory work performed by a previous student in the candidate's research group, Mr Steven Russell, found that the combination of four $ctcH_6$ units with a mixture of alkali metal cations (M^+, where $M^+ = K^+$ with Cs^+ or Rb^+) generated cage-like "$M_4ctc_4H_n$" units within highly symmetric cubic crystal structures. In addition to the cage, the crystal structure showed sulphate or phosphate anions associating with cage windows through hydrogen bonds. Other alkali metal ions occupy space within the cage whilst external metal cations are coordinated by six acetone molecules. Although the early work conducted by Mr Russell succeeded in indicating the formation of these fascinating cubic structures he never completed his investigations. At the conclusion of his work the identity of the alkali metal ions in the various sites within the cubic unit cells was uncertain as was the level of protonation of the cyclotricatechylene. Furthermore, the

synthetic approach employed by Mr Russell generally yielded crystals which were not of sufficient quality for accurate crystal structure determinations. It must be emphasised that these comments are not criticisms of Mr Russell's work but merely reflect the fact that he never had the opportunity to bring this work to an appropriate conclusion.

With the primary aim of resolving the structural ambiguities relating to the identity of the metal ions, the protonation level of the cyclotricatechylene and the contents of the cage, a synthetic and structural investigation of this system was undertaken. It was hoped that the formation of cleaner products and better quality crystals would lead to improved characterisation of this unusual class of materials. Herein, four cyclotricatechylene molecular cage assemblies are reported, each of which contains a mixture of alkali metal ions as well as tetrahedral oxyanions, either phosphate or sulfate.

3.2 Results

3.2.1 Compound 3A – $[Cs((CH_3)_2CO)_6][Cs_4K_4(ctcH_6)_4(H_2O)_8](PO_4)_3 \cdot 6H_2O$

When $ctcH_6$ is combined with K_2HPO_4 and CsOH in aqueous acetone, large colourless crystals separate from the solution overnight. Single crystal X-ray diffraction analysis performed on a suitable crystal revealed a cage compound of formula $[Cs((CH_3)_2CO)_6][Cs_4K_4(ctcH_6)_4\,(H_2O)_8](PO_4)_3 \cdot 6H_2O$. The compound possesses particularly high symmetry and crystallises in the cubic space group *P*-43*m*. The high symmetry reflects the presence of a range of complementary interactions between the six different components.

The crystal structure determination clearly indicated that it was in fact the potassium ion that formed the alkali metal ion–cyclotricatechylene cage. The metallocage consists of four K^+

ions and four cyclotricatechylene molecules. Despite the coordination of the catechol groups the oxygen atoms remain protonated. Within the cage, each of the four K^+ ions is bound to three catechol groups, with the six hydroxyl oxygen atoms forming a plane; the K^+ ion sits just above the plane of the six oxygen atoms. The K^+ ion is also bound to a pair of *trans* water molecules which are oriented towards the centre and away from the centre of the cage. Thus, each K^+ ion is in an eight-coordinate hexagonal bipyramidal environment, similar to the geometry seen in some uranyl cages described in chapter 4. The coordination environment of the K^+ ion in the $[K_4(ctcH_6)_4(H_2O)_8]^{4+}$ cage can be seen in Figure 3.1.

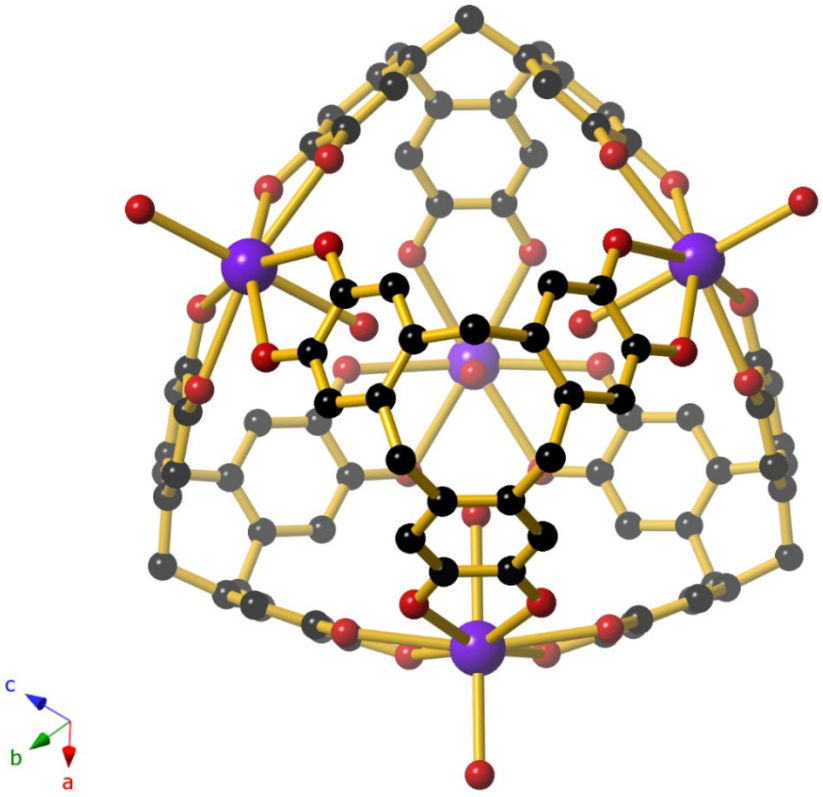

Figure 3.1 A ball and stick representation of the molecular cage of formula $[K_4(ctcH_6)_4(H_2O)_8]^{4+}$ in 3A. Purple spheres represent K^+ centres; red spheres, oxygen; black spheres, carbon. Hydrogen atoms have been omitted for clarity.

Inspection of the crystallographic model of the cage reveals that it possesses an approximately tetrahedral geometry, with $ctcH_6$ units forming the vertices and the K^+ ions located at the centres of the triangular faces of the tetrahedron. Despite the resemblance to a tetrahedron, from a topological perspective the cage is best described as a cube. A cube consists of eight 3-connecting vertices and in the cage both the $ctcH_6$ and the K^+ ions act as vertices, even though the cage edges (represented by catechol groups) are not orthogonal to each other at the K^+ centres. The topological relationship with the cube is apparent from inspection of Figure 3.2.

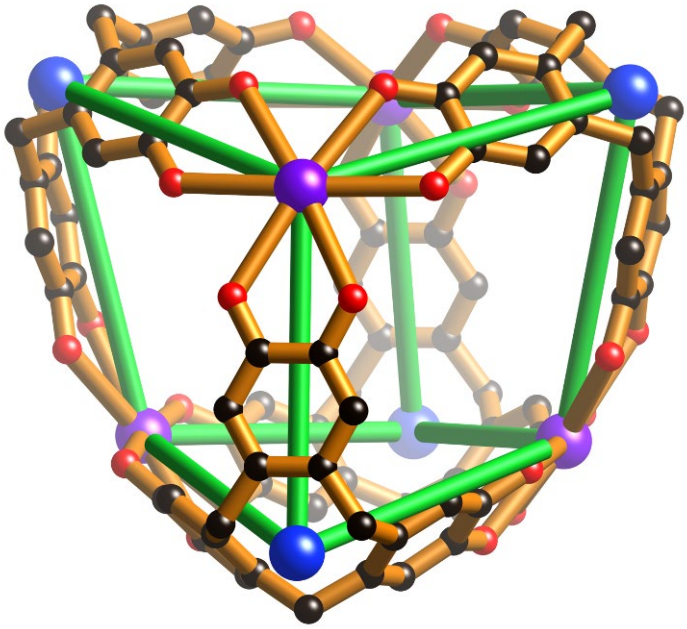

Figure 3.2 The structure of the $[K_4(ctcH_6)_4(H_2O)_8]^{4+}$ cage in 3A indicating the topological relationship with the cube (green connections); the four K^+ centres (purple) and the four $ctcH_6$ molecules (represented by blue spheres) each represent 3-connecting nodes. Hydrogen atoms have been omitted for clarity.

The metallocage has six windows, with each window corresponding to a face of the 'cube'. A phosphate ion is located in each window where it forms four crystallographically equivalent hydrogen bonds ($O{-}H{\cdots}OPO_3$ = 2.59 Å) to the four hydroxyl groups located in each window. Figure 3.3 shows ball and stick representations of the six PO_4^{3-} ions located in

the windows of the $[K_4(ctcH_6)_4(H_2O)_8]^{4+}$ cage. A space filling representation of the cube is shown in Figure 3.4, which shows that the tetrahedral anion is an ideal size and shape for the cage windows. The external oxygen atoms of each phosphate anion interact in a similar manner with another cage as indicated in Figure 3.5. With each phosphate linking a pair of cages through hydrogen bonds, each cage is connected to six other cages within a primitive cubic network of cages.

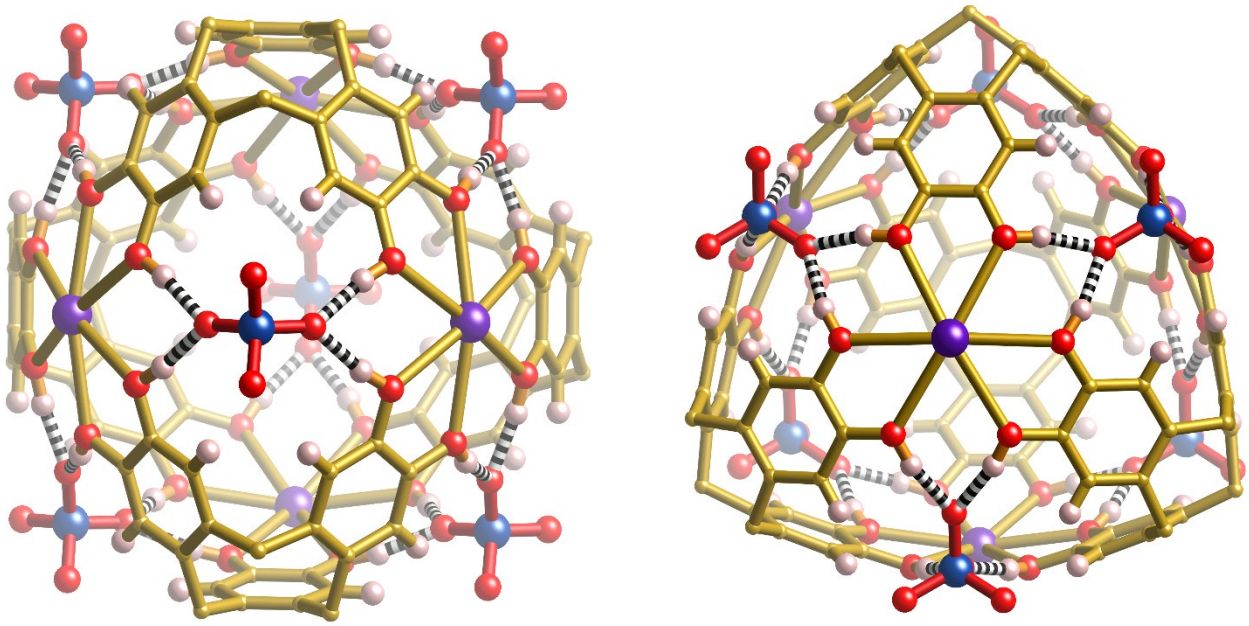

Figure 3.3 Two views of the $[K_4(ctcH_6)_4(H_2O)_8]^{4+}$ cage in 3A along with the six associated phosphate anions. Ball and stick representations of the cage showing each phosphate forming four equivalent hydrogen bonds with the hydroxyl groups of the $ctcH_6$ units. The orientation of the cage shown at right corresponds to the orientation in the space filling model shown in Figure 3.4. Hydrogen bonds are indicated by striped cylinders. Coordinated water molecules and methylene hydrogen atoms have been omitted for clarity.

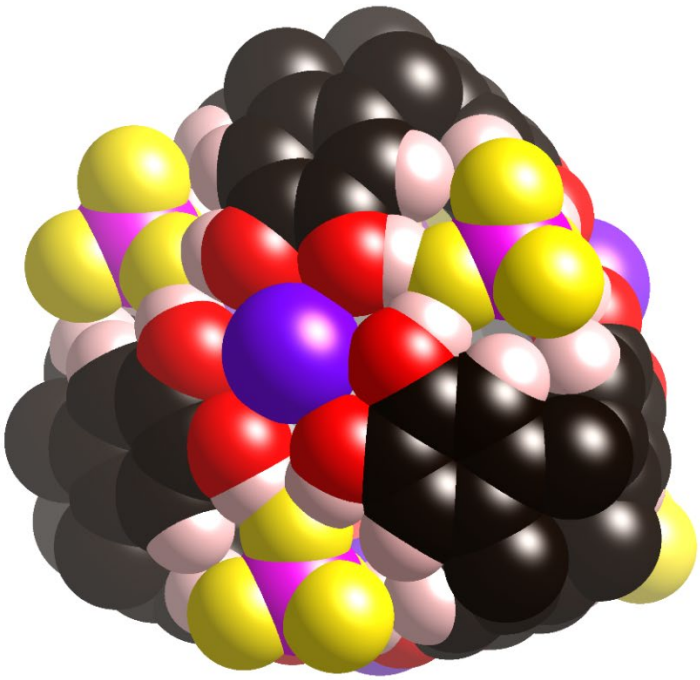

Figure 3.4 A space filling representation of the $[K_4(ctcH_6)_4(H_2O)_8]^{4+}$ cage in 3A, with its six associated phosphate anions, highlighting the size and shape complementarity of the anion with the cage windows. Phosphate oxygen atoms are represented by yellow spheres. Methylene hydrogen atoms and coordinated water molecules have been omitted for clarity.

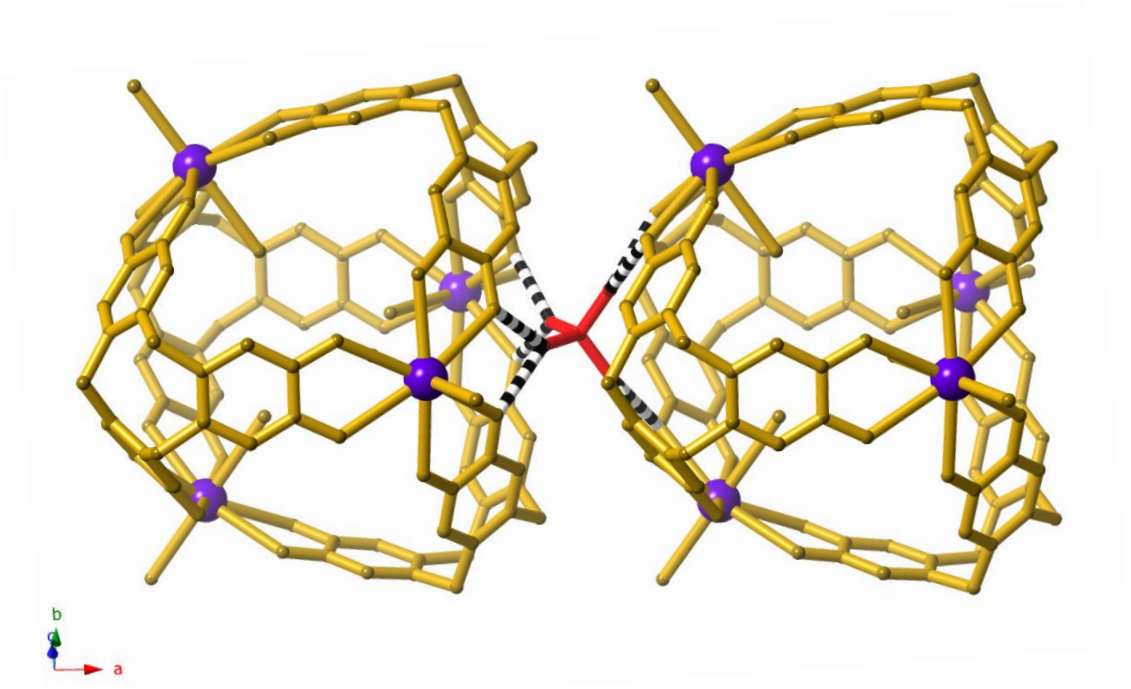

Figure 3.5 A ball and stick representation of a pair of cages in 3A linked by a hydrogen bonded phosphate anion (red). Each cage links to six equivalent cages through a bridging phosphate anion, via the interaction shown. Hydrogen bonds are represented by black and white striped cylinders. Hydrogen atoms have been omitted for clarity.

The inside of each cage is occupied by Cs^+ cations and water molecules. Despite being fully protonated and also associating with three K^+ ions, each cyclotricatechylene unit hosts a Cs^+ centre within its bowl-type cavity. The closest contact between the Cs^+ and the $ctcH_6$ is 3.52 Å. The location of the Cs^+ ion is similar to that previously observed in clam and metallocage structures with ctc. Although the cage is cationic, the shortest Cs^+–$ctcH_6$ distance is slightly shorter than the corresponding distances in various anionic tetrahedral cages:

- 3.66 Å in $[Mn_6(OH)_3(ctc)_4]^{12-}$, (CCDC ID: TUWWUE),[1]
- 3.58 Å in $[(VO)_6(ctc)_4]^{12-}$, (CCDC ID: TUWXEP),[1] and
- 3.61 Å compound 5B $[(PhSi)_6(ctc)_4]^{6-}$ (CCDC ID: ADUZOR)[2].

Six symmetry-related water molecules are also present inside the cage with each bound to a pair of Cs^+ ions as indicated in Figure 3.6.

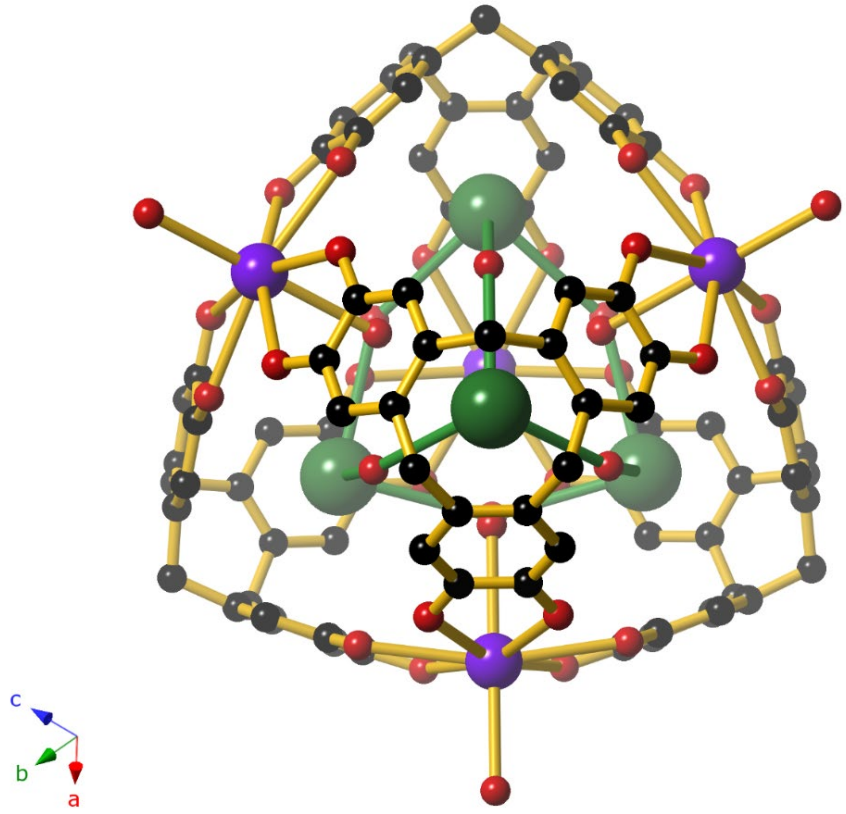

Figure 3.6 A ball and stick representation of the cage in 3A along with the Cs^+ ions and water molecules located inside the cage. Purple spheres represent K^+ centres. The four green spheres in the four ctc bowls represent Cs^+ cations. Each of the Cs^+ cations bridges to three others via water molecules, as indicated by the green bonds. Hydrogen atoms have been omitted for clarity.

An additional monocation, per cage, is required for charge balance and this is situated outside the cage. The cation is a Cs^+ ion which is located at the origin of the primitive cubic unit cell and is bound by six symmetry related acetone molecules (Figure 3.7). This is a rare coordination environment for not only Cs^+ ions, but metal cations in general, with only a few examples of hexa-acetone metal cations appearing in the Cambridge Structural Database (CSD[3]).[4–7] While some examples of six acetone molecules binding to alkali metal cations have been reported for clusters of more than one alkali metal cation, only two discrete $[M((CH_3)_2CO)_6]^{x+}$ complexes have been reported: 1) in the complex salt hexakis(acetone)-

magnesium bis((μ$_2$-iodo)-iodo-copper(I))[8] and 2) in a Ni–Cu carbide carbonyl cluster with hexakis(acetone)-nickel(II) cations.[9]

The examples that do appear in the database show a bend at the carbonyl oxygen atom, however in the structure described here, the Cs^+–O=C angle is 180° with the carbonyl group oriented along each of the crystallographic axes. The carbonyl oxygen does have a thermal ellipsoid which is elongated in a direction normal to the Cs^+–O bond. This is suggestive of disorder for the oxygen atom however attempts to model the carbonyl oxygen over a pair of symmetry related sites were unsuccessful.

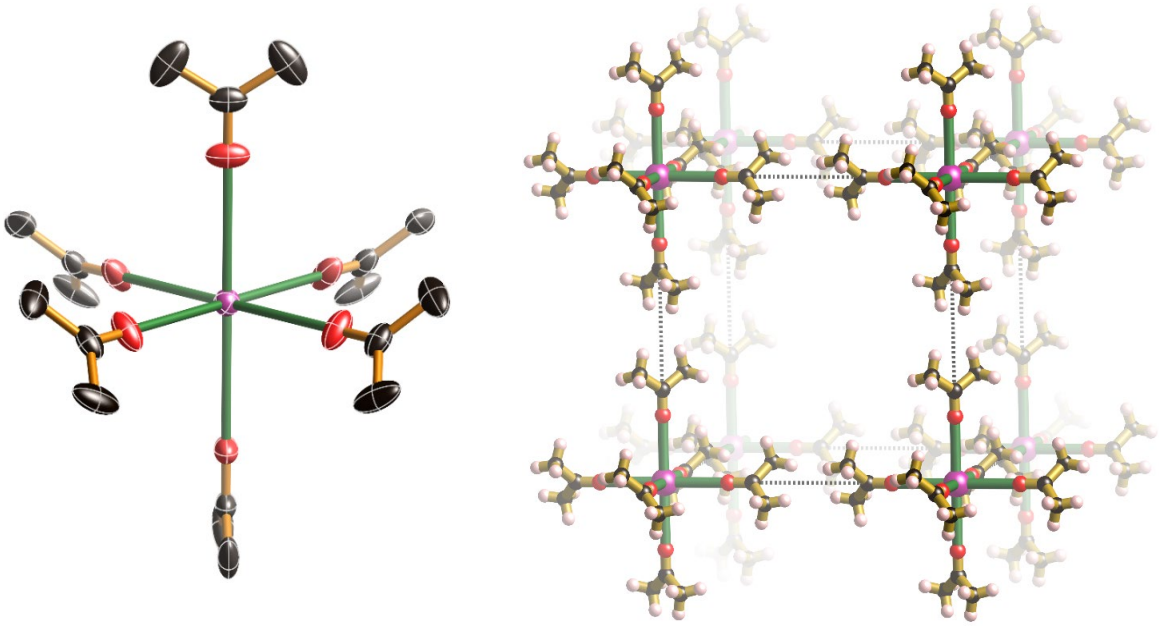

3.7 Representations of the $[Cs((CH_3)_2CO)_6]^+$ complex in 3A. Left: A single complex with atoms represented by thermal ellipsoids at the 50% probability level. Right: Eight $[Cs((CH_3)_2CO)_6]^+$ complexes located at the vertices of the cubic unit cell, which is indicated by dotted lines.

Figure 3.7 (right) shows the $[Cs((CH_3)_2CO)_6]^+$ located at the vertices of the primitive cubic unit cell with the acetone molecules lying along the direction of the crystallographic axes. Close contact is made between methyl hydrogen atoms of coordinated acetone molecules

belonging to two neighbouring $[Cs((CH_3)_2CO)_6]^+$ complexes located on the unit cell edge. The figure shows that the planes of the acetone molecules that approach the mid-point of the unit cell edge are rotated 90° relative to each other.

Figure 3.8 shows the relative positions of the cage, the anions and the eight surrounding $[Cs((CH_3)_2CO)_6]^+$ complexes. The middle of the unit cell corresponds to the centre of the cage and is situated on a site of -43*m* symmetry. At this point, four 3-fold axes converge, each of which passes through a K^+ ion of the cage, the 3-fold axis of a $ctcH_6$ molecule and an internal Cs^+ ion. The anions are located on positions of -42*m* symmetry in the centre of each face where they are able to serve as hydrogen bonded bridges between pairs of cages. The $[Cs((CH_3)_2CO)_6]^+$ units are located at the vertices of the unit cell with each lying on a site of -43*m* symmetry and surrounded by eight cages.

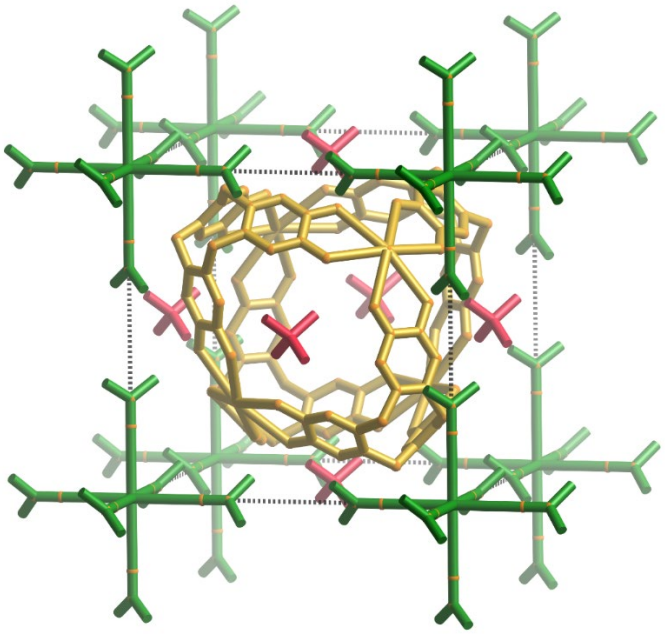

Figure 3.8 A stick representation of the unit cell of 3A showing the location of the $[Cs((CH_3)_2CO)_6]^+$ complexes (green), the cage (gold) and the phosphate anions (red). Hydrogen atoms and coordinated water molecules have been omitted for clarity.

Further appreciation of the size complementarity between the cage units and the $[Cs((CH_3)_2CO)_6]^+$ units can be gained by inspection of Figure 3.9 which provides a representation of the void volume in 3A when the $[Cs((CH_3)_2CO)_6]^+$ units are excluded. This volume is equivalent to approximately 22% of the crystal volume. Figure 3.9 shows brown contours that indicate the void space between the $\{[Cs_4K_4(ctcH_6)_4(H_2O)_8](PO_4)_3 \cdot 6H_2O\}^-$ units after removal of the $[Cs((CH_3)_2CO)_6]^+$ ions from the crystallographic model. The cages can be seen to make close face-to-face contact, with the phosphate anions effectively fusing them together, leaving no discernable void between them. Small channels can be seen to run parallel to the *a*, *b*, and *c* axes (as indicated by red, green and blue lines). The void in and around the intersection of the three perpendicular channels is the perfect size and geometry to accommodate an octahedral metal complex such as the $[Cs((CH_3)_2CO)_6]^+$ ion. The channels can be seen to widen slightly near the midpoint of each cell, corresponding to the position of the methyl groups of the acetone ligands. Small voids (ca. 0.3% of unit cell volume) can also be seen at the centre of each cage. Void volumes were calculated with the Mercury program using the contact surface (probe radius of 1.2 Å and approx. grid spacing of 0.7 Å).[10]

Figure 3.9 A representation of four unit cells in 3A. The brown contours indicate the void space between the $\{[Cs_4K_4(ctcH_6)_4(H_2O)_8](PO_4)_3{\cdot}6H_2O\}^-$ units after removal of the $[Cs((CH_3)_2CO)_6]^+$ ions at the corners of each cell. The $[K_4(ctcH_6)_4(H_2O)_8]^{4+}$ framework cage unit is shown in blue; intracage guests and PO_4^{3-} anions are shown in magenta.

3.2.2 Compound 3B – $[Rb((CH_3)_2CO)_6][Rb_6K_2(ctcH_6)_4(H_2O)_8](PO_4)_3{\cdot}6H_2O$

Compound 3B, of formula $[Rb((CH_3)_2CO)_6][Rb_6K_2(ctcH_6)_4(H_2O)_8](PO_4)_3{\cdot}6H_2O$, was synthesised by combining $ctcH_6$ with K_2HPO_4 and RbOH in aqueous acetone. Single crystal structure analysis indicates a very similar structure to compound 3A. Compounds 3A and 3B adopt the same space group (*P*-43*m*) and have similar unit cell dimensions, a = 14.2376(2) Å for 3B and a = 14.2581(2) Å for 3A. The main difference between the two structures is the incorporation of Rb^+ in place of all of the Cs^+ cations and some of the K^+ cations. Only two of the metal cations that form part of the cage in 3B are K^+ cations, rather than all four, with

the other two centres being Rb^+ cations. The K^+ and Rb^+ cations that form part of the cage are substitutionally disordered with each other.

Another minor difference, which is associated with the smaller radius of the Rb^+ ion, is the disorder of the water molecules inside the cage. Unlike in 3A, the water molecules are unable to symmetrically bridge the internal alkali metal cations.

3.2.3 Compound 3C – $[Cs((CH_3)_2CO)_6][CsK_4(ctcH_6)_4(H_2O)_8](SO_4)_3 \cdot 9H_2O$

When cyclotricatechylene is combined with $KHSO_4$ and CsOH in aqueous acetone, crystals of composition $[Cs((CH_3)_2CO)_6][CsK_4(ctcH_6)_4(H_2O)_8](SO_4)_3 \cdot 9H_2O$, compound 3C, are formed. The crystals adopt the same space group as 3A and 3B (*P*-43*m*), while the cell dimensions for 3C (*a* = 14.396(2) Å) are slightly longer than that of 3A (*a* = 14.2581(2) Å). The cubes pack in the same arrangement as in 3A and 3B and have $[Cs((CH_3)_2CO)_6]^+$ units located on each of the corners of the unit cell.

There are two significant differences between 3A and 3C. Firstly, the phosphate anions have been replaced with sulphate anions. Despite the difference in charge, there is little difference in the way the two anions interact with the $ctcH_6$ molecules. Like each of the phosphate anions in 3A and 3B, each sulphate anion in 3C forms four hydrogen bonds to hydrogen atoms on ctc units on one cage, as shown in Figure 3.10, and four equivalent hydrogen bonds to an adjacent cage.

The second significant difference relates to the number of cations inside each cage. In order to achieve charge balance, following the incorporation of dianionic sulfate anions in place of

the trianionic phosphate anions, the number of internal Cs^+ cations is reduced from four to one. The Cs^+ ion inside the cage is located in the bowl-like cavity of one of the four $ctcH_6$ molecules. Preservation of the cubic symmetry requires this Cs^+ ion to be disordered over the four sites that were fully occupied by Cs^+ ions in 3A. In the crystallographic refinement of the structure, the best refinement was achieved when each of these symmetry-related sites is refined with 25% occupancy by Cs^+ and 75% occupancy by an oxygen atom of a water molecule. In addition to the internal water coordinated to the K^+ ions of the cage, the contents of each cage include nine water molecules and one Cs^+ cation. Three of the water molecules occupy positions within the $ctcH_6$ bowls. The six remaining water molecules lie between the guests in the four bowls and are each disordered over two positions. This disorder arises from the disorder associated with the Cs^+ cation and water molecules in the $ctcH_6$ bowls, with water–Cs^+ interactions being longer than the corresponding water–water interactions.

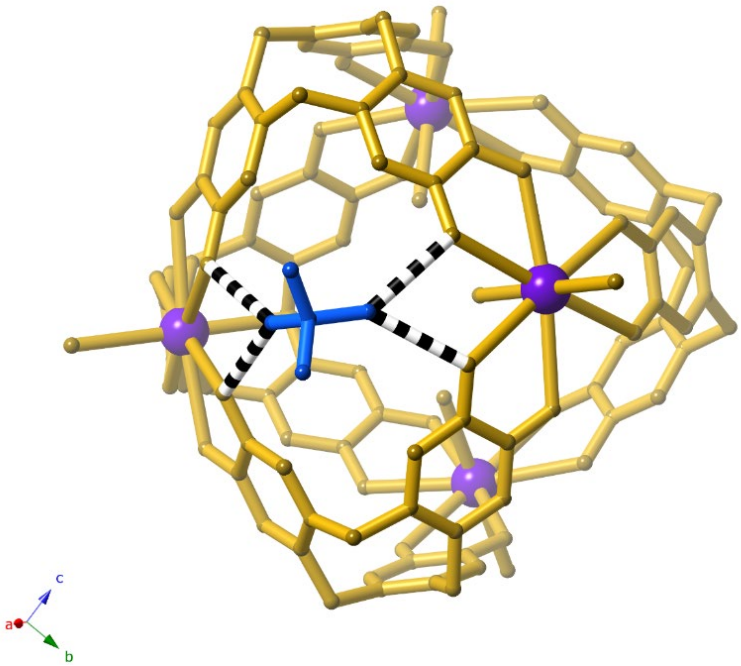

Figure 3.10 A ball and stick representation of the cage in 3C showing the four hydrogen bonds (black and white striped bonds) between the protonated catechol units of the cage and one of the six associated SO_4^{2-} anions (blue). Purple spheres represent K^+ centres. Hydrogen atoms have been omitted for clarity.

3.2.4 Compound 3D – $[Rb((CH_3)_2CO)_6][Rb_3K_2(ctcH_6)_4(H_2O)_8](SO_4)_3 \cdot 9H_2O$

The final member of the family of compounds described in this chapter has the composition $[Rb((CH_3)_2CO)_6][Rb_3K_2(ctcH_6)_4(H_2O)_8](SO_4)_3 \cdot 9H_2O$ (3D). Compound 3D is the rubidium analogue of 3C, in which the cage itself is formed from four ctc ligands, two K^+ and two Rb^+ cations as with compound. One Rb^+ centre is located inside each cage and another is located outside each cage and is bound by six acetone molecules. As with 3C the Rb^+ ion inside each cage is disordered over four symmetry related sites. The Rb^+ is substitutionally disordered with the water molecules, analogous to the arrangement in 3B. The unit cell dimensions of 3D are similar to that found for the Cs^+ analogue, 3C, with a = 14.395 Å.

3.3 Discussion

The thesis introduction discussed the theme of complementarity in the context of supramolecular chemistry and crystal engineering. The presence of certain favourable interactions between different components can lead to the self-assembly of both discrete and extended chemical systems which commonly exhibit high symmetry. The family of compounds described in this chapter represent examples with a high level of complementarity arising from the combination of a remarkable six ionic or molecular building blocks: potassium ions, either rubidium or caesium ions, either phosphate or sulphate anions, acetone, water and the neutral cyclotricatechylene molecule. Together these units associate through a variety of primary and secondary interactions to yield beautifully symmetrical crystalline materials. A summary of the composition of the four crystalline materials is presented in Table 3.1

Table 3.1 Summary of compositions for compounds 3A-3D

Structure component	**3A**	**3B**	**3C**	**3D**
M_4ctc_4; M =	$K^+ \times 4$	$Rb^+ \times 2$; $K^+ \times 2$	$K^+ \times 4$	$Rb^+ \times 2$; $K^+ \times 2$
Internal cage cations	$Cs^+ \times 4$	$Rb^+ \times 4$	$Cs^+ \times 1$	$Rb^+ \times 1$
$[M(acetone)_6]^+$; M =	Cs^+	Rb^+	Cs^+	Rb^+
Anion	PO_4^{3-}	PO_4^{3-}	SO_4^{2-}	SO_4^{2-}

The cationic $[M_4(ctcH_6)_4(H_2O)_8]^{4+}$ cage is common to all four structures and is, to the best of the candidate's knowledge, the first example of a cationic metal-cyclotricatechylene coordination cage. Not surprisingly the catechol oxygen atoms prefer to associate with the K^+ centres rather than the larger Cs^+ ions. The K^+ ion is large enough to accommodate six of the catechol oxygen atoms in equatorial coordination sites and complete its coordination environment with two *trans* water molecules.

Given the coordination of the catechol oxygen atoms, the high degree of protonation of the cyclotricatechylene can be explained by the complementary interactions that occur between the hydroxyl groups and the oxygen atoms of the tetrahedral anion. The cage windows, with their four hydroxyl groups, are ideally set up to bind to a pair of oxygen atoms of a tetrahedral anion which provides a link between pairs of cages and thus leads to the cubic arrangement of the $[M_4(ctcH_6)_4(H_2O)_8]^{4+}$ complexes. It is interesting to note that essentially the same structure is formed when either phosphate or sulphate is used as the tetrahedral anion. Remarkably, the structure is able to adapt to the lower charged anion, sulphate, by incorporating fewer cations (Rb^+ or Cs^+) inside the cage. In regard to the location of the internal alkali metal ions, it is noted that the metal ion occupies a similar position to that observed in a range of other cyclotricatechylene assemblies. These structures represent further examples of the clear affinity Cs^+ and Rb^+ cations have for the aromatic surfaces of the bowl-like cavity of cyclotricatechylene.

Perhaps the most unusual aspect of the structures is the coordination of Cs^+ or Rb^+ ions by six acetone molecules. This was particularly surprising, given that the crystals were obtained from an aqueous acetone mixture and under these circumstances a hydrated alkali metal cation would seem much more likely. Close inspection of the crystal structure, however,

provides insight into the reason the metal ion is associated with acetone rather than water. As shown in Figure 3.8, each $[K_4(ctcH_6)_4(H_2O)_8]^{4+}$ in compound 3A is surrounded by eight $[Cs((CH_3)_2CO)_6]^+$. Four of the eight $[Cs((CH_3)_2CO)_6]^+$ units form close associations with the cyclotricatechylene ligands while the other four are located near hydrated K^+ ions of the cage. The two types of associations are indicated in Figure 3.11. The $[Cs((CH_3)_2CO)_6]^+$ located at the top left of the unit cell depicted in Figure 3.11 has three acetone molecules in a face-to-face arrangement with aromatic rings of the cyclotricatechylene. The separation between the two planes is ~3.5 Å. Another aromatic ring from a diagonally adjacent symmetry related cage is located on the other side of each acetone and thus each acetone is neatly sandwiched between a pair of catechol groups. The $[M((CH_3)_2CO)_6]^+$ located at the bottom right hand side of the unit cell depicted in Figure 3.11 has the coordinated water molecule lying snugly in between a trio of coordinated acetone molecules. In this arrangement the methyl hydrogen atoms are able to form C−H···O interactions (~3.34 Å) with the oxygen atoms of the cyclotricatechylene, in what is considered to be a relatively weak but still important structure directing interaction.[11,12] Thus, there is elegant complementarity between the $[Cs((CH_3)_2CO)_6]^+$ cations and the cage. Furthermore, by coincidence, the spacing between $[Cs((CH_3)_2CO)_6]^+$ cations along the edge of the unit cell, where pairs of coordinated acetone molecules make van der Waals contact with each other, matches the separation of the centres of neighbouring cages which are bridged by the tetrahedral anions.

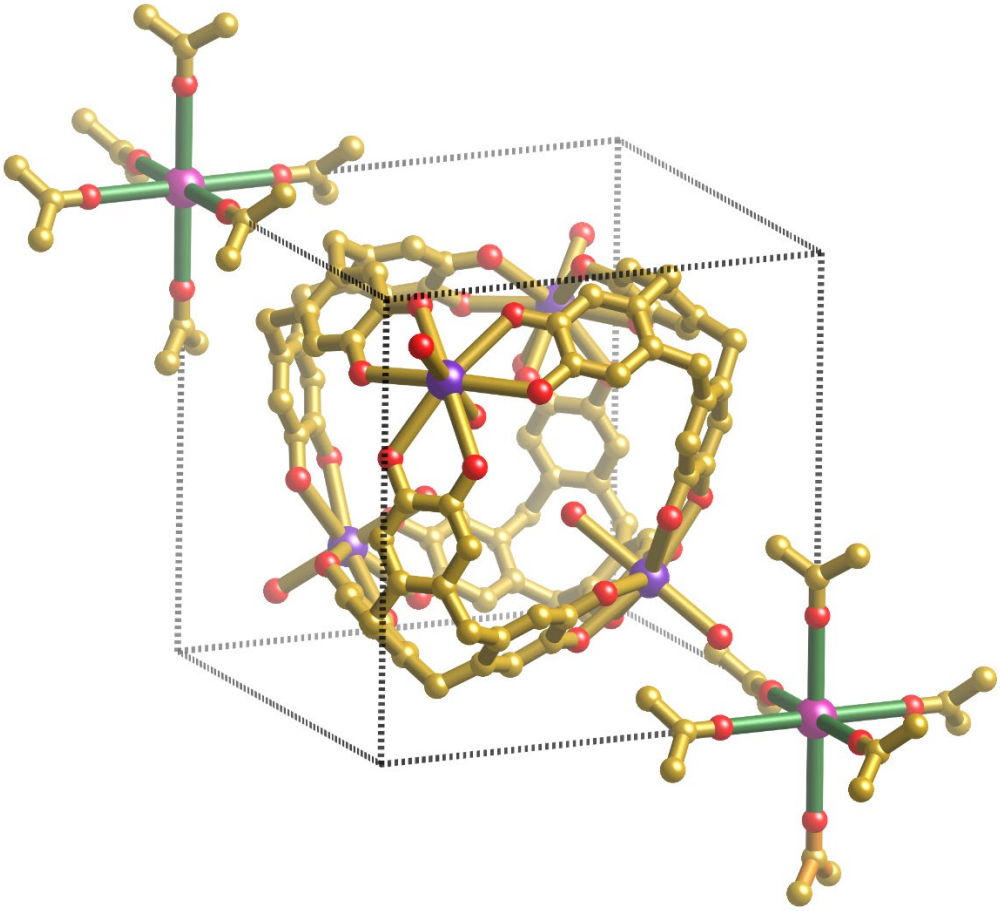

Figure 3.11 A representation of the cage in 3A along with a pair of $[Cs((CH_3)_2CO)_6]^+$ which illustrates the two ways the Cs^+ complex interacts with the cage. At the top corner of the unit cell three acetone molecules are parallel with the aromatic rings of the top $ctcH_6$ unit; at the bottom corner the coordinated water molecule sits snugly between coordinated acetone molecules.

3.4 Concluding Remarks

In summary, the aim of the work in providing a clean synthesis and full structural characterisation of the cubic compounds has been achieved with the ambiguities arising from the early preliminary work having been resolved. In addition, a detailed analysis of the manner in which the six components interact with each other to generate the highly symmetric crystalline products has been undertaken.

Many of the highly complementary interactions that exist in the family of compounds described in this chapter take advantage of the symmetric cyclotricatechylene molecule's tendency to participate in three types of interaction: metal coordination through the oxygen atoms, hydrogen bonding through the hydroxyl groups and association with alkali metal cations through metal cation–π interactions. Although the ability of the cyclotricatechylene to participate in all of these types of interaction simultaneously has been recognised before, it seems unlikely that the structures described in this chapter could have been predicted. Clearly serendipity has played a key role in the generation of the materials. Although the initial structure was never intended, the results presented provide a foundation for extending the family of compounds that may be generated. For example, it may be possible, by taking into consideration the internal dimensions of the cage, to incorporate organic cations of an appropriate size or shape; or perhaps other octahedral metal complexes could be included in place of the $[M((CH_3)_2CO)_6]^+$ complex ion. It would not be surprising to discover that similar structures could be generated by using other tetrahedral anions. In this respect, the four structures presented in this chapter may represent a foundation for generating a large number of highly symmetric, structurally related compounds.

3.5 Experimental Details

Compound 3A – $[Cs((CH_3)_2CO)_6][Cs_4K_4(ctcH_6)_4(H_2O)_8](PO_4)_3 \cdot 6H_2O$: $ctcH_6$ (24 mg, 0.065 mmol) was dissolved in acetone (3 mL). To this was added K_2HPO_4 (14.8 mg, 0.065 mmol) in H_2O (1 mL) followed by $CsOH \cdot H_2O$ (9.7 mg 0.065 mmol) in H_2O (2 mL). Colourless polyhedral crystals formed overnight. A suitable crystal was chosen for single crystal X-ray diffraction analysis. The bulk crystalline material was collected on a glass frit. Yield = 30.5 mg, 51.5% Analysis: found (%): C 39.6, H 4.49; calcd (%): C 38.8, H 4.3.

Compound 3B – $[Rb((CH_3)_2CO)_6][Rb_6K_2(ctcH_6)_4(H_2O)_8](PO_4)_3 \cdot 6H_2O$: $ctcH_6$ (24 mg, 0.065 mmol) was dissolved in acetone (3 mL). To this was added K_2HPO_4 (14.8 mg, 0.065 mmol) in H_2O (1 mL) followed by RbOH (6.7 mg, 0.065 mmol) in H_2O (2 mL). Colourless polyhedral crystals formed overnight. A suitable crystal was chosen for single crystal X-ray diffraction analysis. The synthesis initially produced a satisfactory amount of crystalline material, with no byproduct observable on visual inspection. However, the bulk material from all samples of this compound lost crystallinity upon or before collection and was unable to be sent for elemental analysis. Yield > 1 mg.

Compound 3C – $[Cs((CH_3)_2CO)_6][CsK_4(ctcH_6)_4(H_2O)_8](SO_4)_3 \cdot 9H_2O$: $ctcH_6$ (24 mg, 0.065 mmol) was dissolved in acetone (3 mL). To this was added $KHSO_4$ (8.9 mg, 0.065 mmol) in H_2O (1 mL) followed by $CsOH \cdot H_2O$ (9.7 mg, 0.065 mmol) in H_2O (2 mL). A suitable crystal was chosen for single crystal X-ray diffraction analysis. The bulk crystalline material was remade to measure the yield. When the procedure was repeated as above, only 1 mg of bulk product was obtained. However, a sample was also produced by layering the aqueous CsOH layer beneath the acetone layer. The crystalline product of this procedure was

collected on a glass frit. Yield = 19.0 mg, 41% Analysis: found (%): C 45.4, H 5.1; calcd (%): C 43.8, H 5.0.

Compound 3D – $[Rb((CH_3)_2CO)_6][RbK_4(ctcH_6)_4(H_2O)_8](SO_4)_3 \cdot 9H_2O$: $ctcH_6$ (24 mg, 0.065 mmol) was dissolved in acetone (3 mL). To this was added $KHSO_4$ (8.9 mg, 0.065 mmol) in H_2O (1 mL) followed by RbOH (6.7 mg, 0.065 mmol) in H_2O (2 mL). The bulk material, which discoloured when left in its mother liquor, was collected on a glass frit. Yield = 17.0 mg, 39% Analysis: found (%): C 64.5, H 5.2; calcd (%):C 44.8, H 5.2. The discrepancy in calculated and actual elemental analysis is likely due to the collected material having a different composition to the crystalline material due to degradation over time as indicated by the discolouration. The bulk material also contained powder which could not be unambiguously identified as compound 3D.

3.6 Crystallographic Details

3.6.1 General data collection and refinement details

Data for 3A – 3D were collected as per the following procedures:

A single crystal suitable for X-ray crystallography was removed from the mother liquor and immediately immersed in protective oil. The crystal was mounted on a loop and placed in a stream of N_2 flowing from an Oxford Cryosystem CryoStream at 100 K.[13] Intensity data were collected using the phi and omega scan technique with MoKα (3A and 3B) or CuKα (3C and 3D) radiation on a Rigaku XtaLAB Synergy-S diffractometer.

Crystal structure solutions were obtained by direct methods using the SHELXT program.[14] Structures were thereafter refined using the SHELXL-2014/7 program using a full-matrix

least-squares refinement based on F^2.[15] Absorption corrections were applied using the SADABS or Gaussian techniques.[16]

Crystallographic terminology is detailed in Chapter 6.

Compound 3A – $[Cs((CH_3)_2CO)_6][Cs_4K_4(ctcH_6)_4(H_2O)_8](PO_4)_3 \cdot 6H_2O$: Single crystal X-ray diffraction analysis was performed using MoKα radiation on a yellow polyhedral crystal that was mounted on a loop. The data indicated that the crystal possessed cubic symmetry. A satisfactory structure solution was obtained in the space group *P*-43*m*. All non-hydrogen framework atoms and solvent atoms were clearly defined and refined with anisotropic displacement parameters. The acetone carbonyl oxygens have thermal ellipsoids slightly elongated in a direction normal to the Cs^+–O bond, which suggests disorder for the oxygen atom, however attempts to model the oxygen over a pair of symmetry related sites were unsuccessful. All hydrogen atoms were placed at geometrically estimated positions.

Compound 3B – $[Rb((CH_3)_2CO)_6][Rb_6K_2(ctcH_6)_4(H_2O)_8](PO_4)_3 \cdot 6H_2O$: Single crystal X-ray diffraction analysis was performed using MoKα radiation on a colourless polyhedral crystal that was mounted on a loop. The data indicated that the crystal possessed cubic symmetry. A satisfactory structure solution was obtained in the space group *P*-43*m*. All non-hydrogen framework atoms and solvent atoms were clearly defined and refined with anisotropic displacement parameters. The substitutionally disordered Rb^+ and K^+ centres that formed part of the $[Rb_2K_2(ctcH_6)_4(H_2O)_8]^{4+}$ cage were constrained to be on the same position, each at 50% occupancy and with equal thermal parameters. All hydrogen atoms were placed at geometrically estimated positions.

Compound 3C – $[Cs((CH_3)_2CO)_6][CsK_4(ctcH_6)_4(H_2O)_8](SO_4)_3 \cdot 9H_2O$: Single crystal X-ray diffraction analysis was performed using CuKα radiation on a yellow polyhedral crystal that was mounted on a loop. The data indicated that the crystal possessed cubic symmetry. A satisfactory structure solution was obtained in the space group *P*-43*m*. All non-hydrogen framework atoms and solvent atoms were clearly defined and refined with anisotropic displacement parameters. The substitutionally disordered Cs^+ and H_2O guests within the $[K_4(ctcH_6)_4(H_2O)_8]^{4+}$ cage were constrained to be on the same position, Cs^+ at 25% occupancy and H_2O at 75% occupancy, with equal thermal parameters. All hydrogen atoms were placed at geometrically estimated positions.

Compound 3D – $[Rb((CH_3)_2CO)_6][Rb_3K_2(ctcH_6)_4(H_2O)_8](SO_4)_3 \cdot 9H_2O$: Single crystal X-ray diffraction analysis was performed using CuKα radiation on a yellow polyhedral crystal that was mounted on a loop. The data indicated that the crystal possessed cubic symmetry. A satisfactory structure solution was obtained in the space group *P*-43*m*. All non-hydrogen framework atoms and solvent atoms were clearly defined and refined with anisotropic displacement parameters. The substitutionally disordered Rb^+ and K^+ centres that formed part of the $[Rb_2K_2(ctcH_6)_4(H_2O)_8]^{4+}$ cage were constrained to be on the same position, each at 50% occupancy and with equal thermal parameters. The substitutionally disordered Rb^+ and H_2O guests within the $[Rb_2K_2(ctcH_6)_4(H_2O)_8]^{4+}$ cage were constrained to be on the same position, Rb^+ at 25% occupancy and H_2O at 75% occupancy, with equal thermal parameters. All hydrogen atoms were placed at geometrically estimated positions.

3.6.2 Crystallographic Tables

Crystal data and structure refinement for compound 3A

Empirical formula	$C_{102}H_{134}Cs_5K_4O_{55}P_3$
Formula weight	3153.94
Temperature	100(1) K
Wavelength	0.71073 Å
Crystal system	Cubic
Space group	*P* -4 3 *m*
Unit cell dimensions	*a* = 14.2581(2) Å
Volume	2898.58(12) $Å^3$
Z	1
Density (calculated)	1.807 mg/cm^3
Absorption coefficient	1.841 mm^{-1}
F(000)	1582
Crystal size	0.117 × 0.095 × 0.052 mm^3
Theta range for data collection	2.474 to 30.757°.
Index ranges	$-19 \le h \le 14$, $-20 \le k \le 7$, $-18 \le l \le 19$
Reflections collected	7781
Independent reflections	1481 [*R*(int) = 0.0411]
Completeness to theta = 25.242°	99.7 %
Absorption correction	Gaussian
Max. and min. transmission	1.000 and 0.833
Refinement method	Full-matrix least-squares on F^2
Data / restraints / parameters	1481 / 18 / 82
Goodness-of-fit on F^2	1.068
Final *R* indices [*I*>2sigma(*I*)]	*R*1 = 0.0355, *wR*2 = 0.0898
R indices (all data)	*R*1 = 0.0382, *wR*2 = 0.0911
Absolute structure parameter	-0.049(13)

Crystal data and structure refinement for compound 3B

Empirical formula	$C_{102}H_{134}K_2O_{55}P_3Rb_7$
Formula weight	3009.48
Temperature	100(1) K
Wavelength	0.71073 Å
Crystal system	Cubic
Space group	*P* -4 3 *m*
Unit cell dimensions	*a* = 14.2376(2) Å
Volume	2886.1(1) $Å^3$
Z	1
Density (calculated)	1.732 mg/cm^3
Absorption coefficient	3.156 mm^{-1}
F(000)	1528
Crystal size	0.256 × 0.223 × 0.137 mm^3
Theta range for data collection	2.478 to 33.384°.
Index ranges	$-14 \le h \le 22$, $-21 \le k \le 15$, $-16 \le l \le 13$
Reflections collected	8768
Independent reflections	1725 [*R*(int) = 0.0433]
Completeness to theta = 25.242°	99.7 %
Absorption correction	Gaussian
Max. and min. transmission	1.000 and 0.534
Refinement method	Full-matrix least-squares on F^2
Data / restraints / parameters	1725 / 17 / 86
Goodness-of-fit on F^2	1.046
Final *R* indices [*I*>2sigma(*I*)]	*R*1 = 0.0613, *wR*2 = 0.1689
R indices (all data)	*R*1 = 0.0737, *wR*2 = 0.1765
Absolute structure parameter	0.00(3)

Crystal data and structure refinement for compound 3C

Empirical formula	$C_{102}H_{138}Cs_2K_4O_{57}S_3$
Formula weight	2794.52
Temperature	100(1) K
Wavelength	1.54184 Å
Crystal system	Cubic
Space group	*P* -4 3 *m*
Unit cell dimensions	*a* = 14.3955(17) Å
Volume	2983.2(11) $Å^3$
Z	1
Density (calculated)	1.556 mg/cm^3
Absorption coefficient	7.344 mm^{-1}
F(000)	1440
Crystal size	0.14 × 0.11 × 0.0 mm^3
Theta range for data collection	3.070 to 78.157°.
Index ranges	$-18 \le h \le 18$, $-18 \le k \le 18$, $-17 \le l \le 18$
Reflections collected	64422
Independent reflections	1261 [*R*(int) = 0.0568]
Completeness to theta = 67.684°	100.0 %
Absorption correction	Gaussian
Max. and min. transmission	0.761 and 0.481
Refinement method	Full-matrix least-squares on F^2
Data / restraints / parameters	1261 / 20 / 85
Goodness-of-fit on F^2	1.048
Final *R* indices [*I*>2sigma(*I*)]	*R*1 = 0.0679, *wR*2 = 0.1700
R indices (all data)	*R*1 = 0.0681, *wR*2 = 0.1702
Absolute structure parameter	0.00(2)

Crystal data and structure refinement for compound 3D

Empirical formula	$C_{102}H_{134}K_2O_{55}Rb_4S_3$
Formula weight	2756.34
Temperature	100(1) K
Wavelength	1.54184 Å
Crystal system	Cubic
Space group	*P* -4 3 *m*
Unit cell dimensions	*a* = 14.395(1) Å
Volume	2982.8(1) $Å^3$
Z	1
Density (calculated)	1.534 mg/cm^3
Absorption coefficient	Gaussian
F(000)	1420
Crystal size	0.341 × 0.276 × 0.212 mm^3
Theta range for data collection	3.070 to 77.766°.
Index ranges	$-18 \le h \le 15$, $-18 \le k \le 17$, $-18 \le l \le 18$
Reflections collected	64279
Independent reflections	1260 [*R*(int) = 0.0447]
Completeness to theta = 67.684°	100.0 %
Absorption correction	Gaussian
Max. and min. transmission	0.166 and 3.986
Refinement method	Full-matrix least-squares on F^2
Data / restraints / parameters	1260 / 42 / 85
Goodness-of-fit on F^2	1.072
Final *R* indices [*I*>2sigma(*I*)]	*R*1 = 0.0877, *wR*2 = 0.2269
R indices (all data)	*R*1 = 0.0877, *wR*2 = 0.2269
Absolute structure parameter	-0.01(8)

3.7 References

[1] B. F. Abrahams, N. J. FitzGerald, R. Robson, *Angew. Chemie - Int. Ed.* **2010**, *49*, 2896–2899.

[2] J. L. Holmes, B. F. Abrahams, A. Ahveninen, B. A. Boughton, T. A. Hudson, R. Robson, D. Thinagaran, *Chem. Commun.* **2018**, *54*, 11877–11880.

[3] C. R. Groom, I. J. Bruno, M. P. Lightfoot, S. C. Ward, *Acta Crystallogr. Sect. B Struct. Sci. Cryst. Eng. Mater.* **2016**, *72*, 171–179.

[4] O. Hiemisch, D. Henschel, P. G. Jones, A. Blaschette, *Z. Anorg. Chem. Allg. Chem.* **1996**, *622*, 829–836.

[5] K. Kirakci, P. Kubát, M. Kučeráková, V. Šícha, H. Gbelcová, P. Lovecká, P. Grznárová, T. Ruml, K. Lang, *Inorganica Chim. Acta* **2016**, *441*, 42–49.

[6] S. A. Adonin, E. V. Peresypkina, M. N. Sokolov, V. P. Fedin, *Russ. J. Coord. Chem. Khimiya* **2014**, *40*, 867–870.

[7] S. A. Adonin, M. N. Sokolov, A. I. Smolentsev, S. G. Kozlova, V. P. Fedin, *Dalt. Trans.* **2013**, *42*, 9818–9821.

[8] M. Hoyer, H. Hartl, *Zeitschrift fur Anorg. und Allg. Chemie* **1992**, *612*, 45–50.

[9] A. Bernardi, I. Ciabatti, C. Femoni, M. C. Iapalucci, G. Longoni, S. Zacchini, *Dalt. Trans.* **2013**, *42*, 407–421.

[10] C. F. Macrae, P. R. Edgington, P. McCabe, E. Pidcock, G. P. Shields, R. Taylor, M. Towler, J. van de Streek, *J. Appl. Crystallogr.* **2006**, *39*, 453–457.

[11] G. R. Desiraju, *Chem. Commun.* **2005**, 2995–3001.

[12] T. Steiner, *Chem. Commun.* **1997**, 727–734.

[13] J. Cosier, A. M. Glazer, *J. Appl. Crystallogr.* **1986**, *19*, 105–107.

[14] G. M. Sheldrick, *Acta Crystallogr. Sect. A Found. Adv.* **2015**, *71*, 3–8.

[15] G. M. Sheldrick, *Acta Crystallogr. Sect. C Struct. Chem.* **2015**, *71*, 3–8.

[16] *CrysAlisPro 1.171.40.36a, Rigaku Oxford Diffraction/Agilent Technol. UK Ltd* **2018**.

Chapter 4 Anionic cage assemblies with cyclotricatechylene containing vanadyl and uranyl cations

Contents

4.1 Introduction

Our group's research into cage assemblies of ctc was motivated by geometric considerations of the bowl-shaped ctc unit, which offered the prospect of providing metallocage assemblies when combined with appropriate metal ions. As described in chapter 1 of this thesis, the hexamethyl analogue of ctc, ctv, and a large family of ctv derivatives have been successfully incorporated into metallocage assemblies. Despite this, to the best of our knowledge, ctc had not been utilised in metallocage synthesis in a similar manner prior to the commencement of the work in our group. The absence of ctc-derived metallocages in the literature was particularly surprising given that ctc incorporates the catechol functionality. As detailed in chapter 1, the literature provides numerous examples of *bis*- and *tris*-catecholates strongly and predictably binding to *d*- and *f*-block metal cations to form a variety of 1D, 2D and 3D architectures, and, as such, ctc might reasonably be expected to do the same.

Work within our group over the last decade has indicated that several transition metal cations, as well as the actinide uranium (as UO_2^{2+}), in combination with ctc have the propensity to form cage-type assemblies. When combined with such metals under basic conditions, even in the presence of group 1 metal cations such as Cs^+ and Li^+, ctc has been shown to chelate the *d*- and *f*-block metal cations preferentially.[1,2]

Previous research in the Robson-Abrahams group succeeded in the isolation and structural characterisation of several anionic $[M_6(ctc)_4]^{n-}$ cages of tetrahedral geometry (M = Cu^{2+}, VO^{2+}, Mn^{2+} and Co^{2+})[1–4], a Cu^{II}-based example of which is shown in Figure 4.1. In the $[M_6(ctc)_4]^{n-}$ metallocage, the four ctc^{6-} ligands are located at the vertices of a regular tetrahedron, while the transition metal cations are positioned on the midpoint of each of the

six edges of the tetrahedron. Each metal centre is chelated by two catecholate units, the oxygen atoms from which form an O_4-plane. In a perfect regular tetrahedron, the edges meet at an angle of 60° at the vertices, however, the geometry of the catecholate 'arms' that form the edges of the tetrahedron is incompatible with the required 60° angle, despite the ability of the ctc ligand to flex slightly. In order to form a tetrahedral cage, bowing of the edges of the tetrahedron is necessary, and as a result, the metal centres on each edge lie slightly above the catecholate O_4-plane. The tetrahedral cages in this family, in their most symmetrical form, have four equivalent three-fold axes that each pass through the apex of a ctc ligand and the centre of the face on the opposite side of the cage.

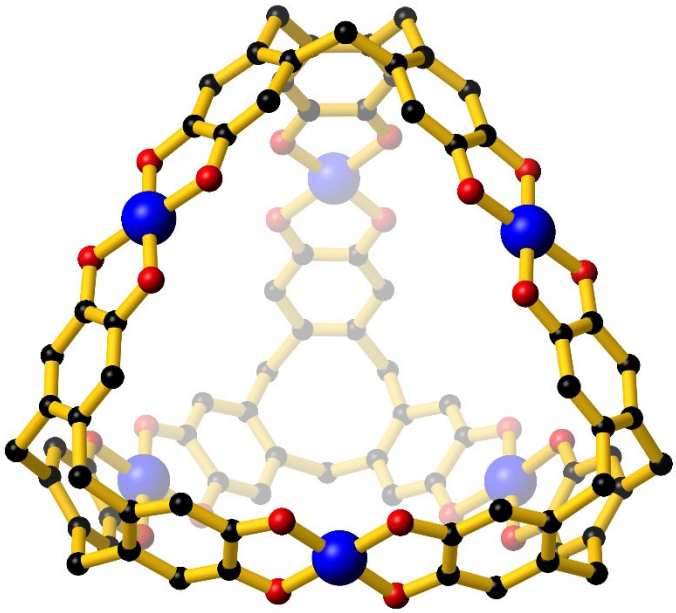

Figure 4.1 A ball and stick representation of an $[M_6(ctc)_4]^{n-}$ molecular tetrahedron from the family of tetrahedra reported by the Robson-Abrahams group. Hydrogen atoms have been omitted for clarity.

Despite the cages in this family all sharing the same framework connectivity, the 3D packing of the cages in the respective crystals shows considerable variation. Some of the crystalline

compounds possess high symmetry whilst others pack in less symmetrical arrangements. This variation appears to be dependent on three factors:

1) the identity and preferred geometry of the *d*-block metal cation,

2) the counterions present in the crystal structure and

3) the solvent used in the synthesis of the compound.

To the candidate's knowledge, no other $[M_6(ctc)_4]^{n-}$ molecular tetrahedra with *d*-block metal cations have been reported by researchers outside our group. Table 4.1 summarises information regarding the composition and crystallographic details of the molecular tetrahedra synthesised in the group prior to the commencement of the work reported in this thesis.

Table 4.1 Summary of the composition and crystallographic details of the $[M_6(ctc)_4]^{n-}$ molecular tetrahedra synthesised in the Robson-Abrahams group.

Composition	Crystal system	Space group	Unit cell
$(NMePent_3)_6Na_8[Cu_6(ctc)_4]I_2 \cdot solv$[1]	cubic	*Fd*-3*m*	a = 36.6111(5) Å
$(NMePent_3)_6Li_8[Cu_6(ctc)_4]I_2 \cdot solv$[4]	cubic	*Fd*-3*m*	a = 36.4073(15) Å
$(PPh_4)_{3.5}Li_{8.5}[Cu_6(ctc)_4] \cdot solv$[4]	triclinic	*P*-1	a = 20.1291(5) Å, b = 21.6436(5) Å, c = 25.4466(6) Å α = 101.099(2)°, β = 108.040(2)°, γ = 105.157(2)°
$(PPh_4)_{3.5}K_{8.5}[Cu_6(ctc)_4] \cdot solv$[4]	triclinic	*P*-1	a = 19.9822(3) Å, b = 21.4428(2) Å, c = 25.4764(4) Å α = 101.2630(10)°, β = 108.0510(10)°, γ = 105.8770(10)°
$Ca_6[(VO)_6(ctc)_4] \cdot solv$[2]	tetragonal	$I4_1/a$	a = 21.1696(7) Å, c = 47.577(2) Å
$Cs_8Na_4[(VO)_6(ctc)_4] \cdot solv$[2]	cubic	*I*-43*d*	a = 37.9956(4) Å
$Mg_6[(VO)_6(ctc)_4] \cdot solv$[2]	cubic	*P*-43*n*	a = 31.6182(2) Å

$Rb_{11}Na_4[Co_6(OH)_3(ctc)_4]\cdot solv$[2]	cubic	*Fm*-3*m*	a = 35.5734(9) Å
$Cs_{10}Na_5[Mn_6(OH)_3(ctc)_4]\cdot solv$[2]	cubic	*Fm*-3*m*	a = 36.5356(8) Å
$Na_6[(Mn_6(H_2O)_3)_6(dioxane)_3(ctc)_4]\cdot solv$[3]	cubic	*Pm*-3*m*	a = 20.6956(5) Å
$(PMePh_3)_3Na_3[(Mn_6(H_2O)_3)_6(dioxane)_3(ctc)_4]\cdot solv$[3]	trigonal	*R*-3*m*	a = 30.4081(8) Å, c = 41.8550(9) Å

The results presented in Table 4.1 indicate that the counterions impact significantly on the arrangement of cages in the crystal structure, but in the case where $MePPh_3^+$ was present in the reaction mixture, a different connectivity was found for the cage that crystallised with ctc and the vanadyl cation (VO^{2+}) (not included in Table 4.1). While the vanadyl cation has been incorporated into tetrahedral cages[2], in one instance it was incorporated into a large, anionic $[(VO)_9(ctc)_6]^{18-}$ trigonal prismatic assembly in a compound of formula $Na_{10}(PMePh_3)_8[(VO)_9(ctc)_6]\cdot$solvate. The compound crystallised with triclinic symmetry and a satisfactory structure determination was achieved in the space group *P*-1. In the $[(VO)_9(ctc)_6]^{18-}$ cage, the V^{IV} centres adopt the same square pyramidal geometry as when they are incorporated into $[(VO)_6(ctc)_4]^{6-}$ tetrahedral assemblies (Figure 4.2, left). While in the $[(VO)_6(ctc)_4]^{6-}$ cages, all six oxo-groups associated with the V^{IV} centres project outward, in the $[(VO)_9(ctc)_6]^{18-}$ trigonal prismatic cage, three of the nine oxo-groups project inwards; these three centres are located at the central 'belt' of the trigonal prism, as shown at right in Figure 4.2.

Whereas, in the tetrahedral assemblies the vanadyl cations are located at the vertices of a regular octahedron, in the trigonal prismatic assembly the vanadyl centres are in a tricapped trigonal prismatic arrangement.

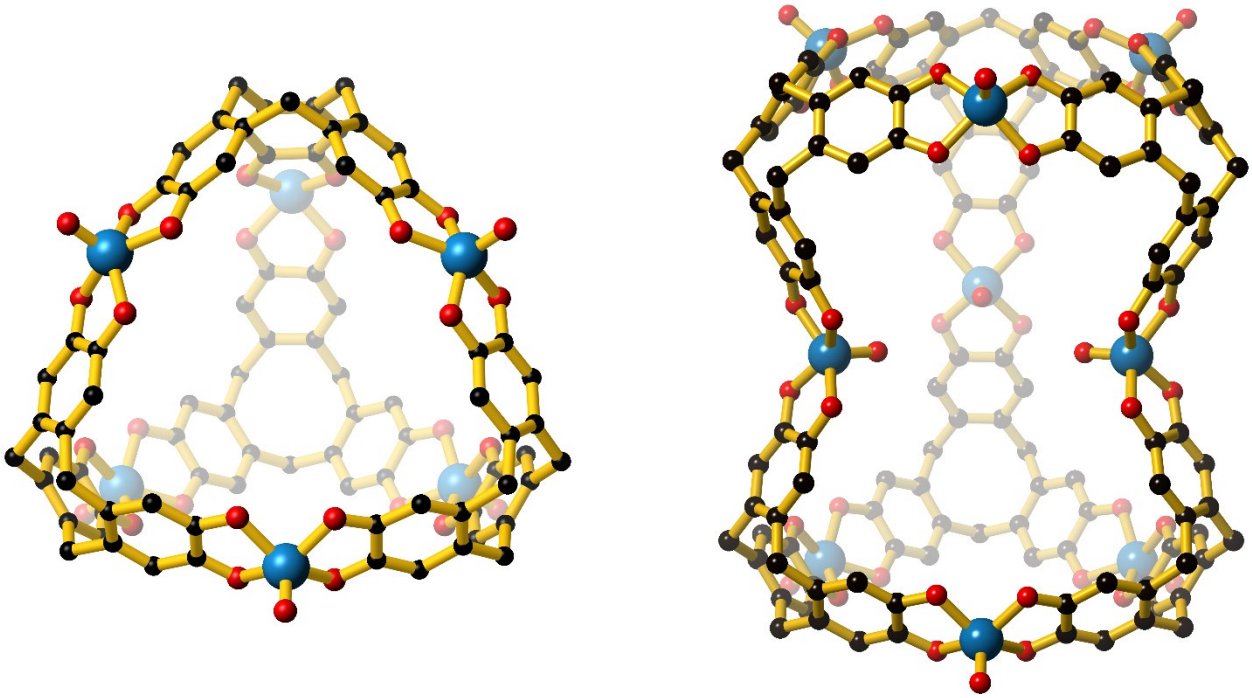

Figure 4.2 Left: A ball and stick representation of a $[(VO)_6(ctc)_4]^{12-}$ molecular tetrahedron from the family of tetrahedra reported by the Robson-Abrahams group. Right: A ball and stick representation of the $[(VO)_9(ctc)_6]^{18-}$ molecular trigonal prism. V^{IV} centres are represented by teal spheres. Hydrogen atoms have been omitted for clarity.

In addition to the trigonal prism, molecular tetrahedra, and the alkali metal-based cages, 3A – 3D, reported in chapter 3 of this thesis, a variety of other cage assemblies have also been obtained during our previous research.

The uranyl cation (UO_2^{2+}) is a linear moiety, which is able to adopt a range of coordination geometries. Commonly encountered coordination geometries include square-, pentagonal-, hexagonal- and heptagonal bipyramidal arrangements (see Figure 4.3 for examples) in which there are four, five, six or seven donor atoms, respectively, coordinated to the U^{VI} centre, orthogonal to the O=U=O plane.[5,6] Additionally, the uranyl cation displays interesting coordination behaviour when precipitated from alkaline environments, often precipitating in clusters containing oxo, hydroxo, peroxo and aqua ligands.[5–8]. Small clusters of uranyl cations, such as those shown in Figure 4.3, can act as two, three or four connecting centres,

that can be chelated by up to four ctc ligands. Due to the formation of these clusters, as well as the various geometries available to the mono-uranyl cation, a range of topologically and geometrically distinct assemblies may be generated when uranyl ions are combined with ctc. In this regard it should be noted that the chelation of uranyl cations by *mono*- and *bis*(catechol)-based ligands has been reported.[9–11] Given the proven ability of catechol(ate)s to chelate the uranyl centre, the combination of uranyl cations with ctc under basic conditions with a variety of counterions has been explored by our group over the last decade.

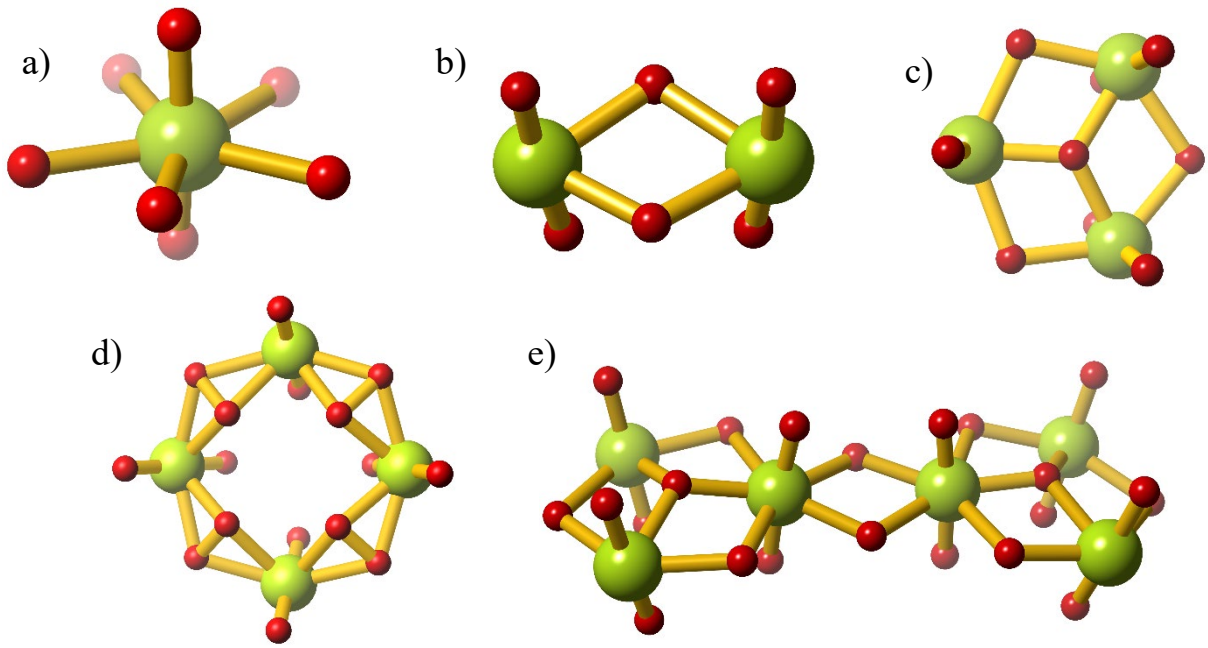

Figure 4.3 Selected examples of the uranyl cation in different coordination environments and small clusters. U^{VI} centres are represented by lime spheres; oxygen atoms by red spheres. Examples b) – e) show the core of uranyl clusters with some coordination sites left vacant. a) The uranyl cation in a pentagonal bipyramidal coordination environment; b) a dimer of uranyl cations bridged by a pair of oxygen atoms typically from hydroxo ligands; c) a trimer of uranyl cations bridged by a μ_3-O^{2-} anion and each bridged to each other by an oxygen atom typically from a hydroxo ligand; d) a tetramer of uranyl cations, each of which is bridged to two neighbouring uranium centres by *bis*-bidentate peroxo ligands; e) a hexamer of uranyl centres in which a dimer of the trimer c), in which the trimers are bridged in the same manner as the uranyl centres in b).

Preliminary investigations in which ctc was combined with the uranyl cation and NaOH yielded a large molecular 'cube' (Figure 4.4) in a compound of formula $Na_{24}[(UO_2(H_2O))_{12}(ctc)_8]\cdot$solvate.[3] In this $[(UO_2)_{12}(ctc)_8]^{24-}$ cube, each uranyl cation is chelated by two ctc ligands, and also bonded to an aqua ligand, in a pentagonal bipyramidal

coordination environment. The ctc ligand does not in fact possess the required geometry to form the vertices of a cube, as the vectors that run through the centres of 'arms' of the ctc intersect with each other at an angle that is less than 90°. Consequently, the ctc ligands are rotated such that the catecholate arms do not project down the edges of a regular cube. Instead, the catecholate units project into the faces of the cube where they chelate the U^{VI} centre such that the two catechol units are not diametrically opposed to each other (Figure 4.5), and therefore two uranyl centres are positioned on each face of the cube.

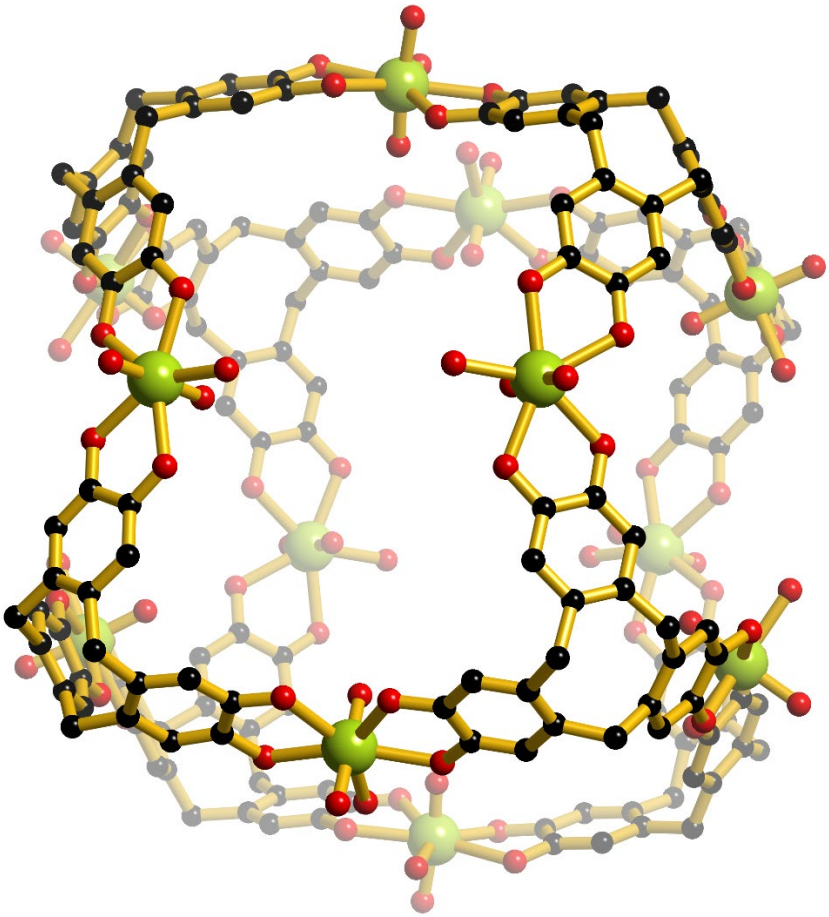

Figure 4.4 A ball and stick representation of the $[(UO_2)_{12}(ctc)_8]^{24-}$ molecular cube in the compound of formula $Na_{24}[(UO_2(H_2O))_{12}(ctc)_8]\cdot$solvate. Uranyl cations are represented by lime spheres. Hydrogen atoms have been omitted for clarity.

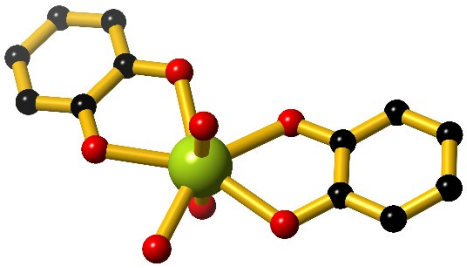

Figure 4.5 A ball and stick representation of the pentagonal bipyramidal coordination environment of the uranyl cations in $Na_{24}[(UO_2(H_2O))_{12}(ctc)_8]\cdot$solvate. Two catecholate moieties coordinate the U^{VI} centre around the equatorial plane, such that they approach more closely on one side of the metal centre than the other. An aqua ligand is present in the same plane as the catechols, which is orthogonal to the plane of the two trans oxo-ligands.

Subsequent to the generation of the $[(UO_2(H_2O))_{12}(ctc)_8]^{24-}$ cube, the candidate generated a variety of uranyl-based molecular cage compounds during her MSc[4], as summarised in Table 4.2.

Table 4.2 Summary of the selected compositional and crystallographic details of the uranyl-based assemblies synthesised by the candidate during her MSc in the Robson-Abrahams group.

Composition	Crystal system	Space group	Description of assembly	Uranyl cations present as
$Na_{12}[(UO_2(H_2O))_6(ctc)_4]\cdot$ solv[4]	Hexagonal	*P*-62*m*	**M_6L_4** 'half cube'	Pentagonal bipyramidal centres
$Cs_{14}Li_{10}[(UO_2(H_2O))_6$ $(ctc)_6]\cdot$solv[4]	Monoclinic	$P2_1/n$	**$M_{12}L_8$** cube	Pentagonal bipyramidal centres
$Cs_{18}Li_{10}[(UO_2(H_2O))_6$ $(ctcH)_6]\cdot$solv[4]	Hexagonal	*R*3*c*	**M_6L_6** hexagonal prism	Pentagonal bipyramidal centres
$Li_6MePPh_3[UO_2(H_2O))_6$ $(O)(ctc)_3]\cdot$solv*[4]	Trigonal	*P*-3*c*1	**$(M_3)M_3L_4$** tetrahedron	Uranyl trios and pentagonal bipyramidal centres
$Na_{11}Cs_8[(UO_2)_3(H_2O)_3$ $(O)_4(ctc)_4]\cdot$solv*[4]	Orthorhombic	*Pnnm*	**$(M_3)_3L_4$** cube	Uranyl trios
$Li_{40}[(UO_2)_{16}(O_2)_{12}(ctc)_8]\cdot$ solv[4]	Tetragonal	$P4_2/ncm$	**$(M_4)_2(M_2)_4L_8$** 'hourglass'	Peroxide bridged dimers and peroxide bridged tetramers
$Li_{48}[(UO_2)_4((O_2)_4)_6(ctc)_8]$ $\cdot$solv[4]	Orthorhombic	*I*4*mmm*	**$(M_4)_6L_8$** 'nanosphere'	Peroxide bridged tetramers

* The identity of the bridging oxygen atoms in these assemblies was unclear, and those species assigned as aqua ligands (on the basis of charge balance) in the trios are possibly hydroxo ligands. Consequentially, additional counterions may also be present.

The generation of the structures detailed above indicated the combination of ctc with *d*- and *f*-block metal cations to be a rich vein of research which we were encouraged to further explore.

Our investigations into molecular cage assemblies containing the cyclotricatechylene ligand with vanadyl and uranyl units was therefore continued with a view to the following:

1) examining the scope of cage-like units that can be formed

2) investigating the effect of countercations on cage connectivity and packing

3) improving the structural characterisation of cage species with large, solvent filled voids

Hereafter are reported examples of a vanadyl tetrahedron (4A) and a $[(VO)_9(ctc)_6]^{18-}$ trigonal prismatic assembly (4B). This is followed by four uranyl-based assemblies (4C – 4F); two cages in the $[(UO_2(H_2O))_{12}(ctc)_8]^{24-}$ family, followed by two assemblies of ctc containing uranyl clusters. The chapter concludes with an unexpected cubic network in which $UO_2Zn(OAc)_4$ was used a reactant.

4.2 Results and discussion

4.2.1 Vanadium-based cages with cyclotricatechylene

4.2.1.1 Compound 4A – $Cs_8[(VO)_6Cs_4(ctc)_4]\cdot 123H_2O$

To investigate the effect of alkali metal cations on cage packing, the reaction of ctc and the vanadyl cation in combination with CsOH was performed in aqueous acetone. X-ray diffraction analysis of green crystals that separated from the reaction revealed the presence of the previously observed $[(VO)_6(ctc)_4]^{12-}$ metallocage. With the absence of organic and other alkali metal ions, the compound $Cs_8[(VO)_6Cs_4(ctc)_4]\cdot 123H_2O$ (4A) crystallised. Unlike other examples of vanadyl-based cages only Cs^+ serves as the sole countercation for the cage. The crystal adopts the high symmetry cubic space group *I*-43*d* (a = 37.9039(6) Å). Interestingly, the compound has an almost identical packing arrangement to that found for the cages in $Cs_8Na_4[(VO)_6(ctc)_4]\cdot$solvate which had been previously reported by our group.[12] This similarity is reflected in the cubic unit cell edge length of 37.9956(4) Å for the Cs/Na analogue.

As in $Cs_8Na_4[(VO)_6(ctc)_4]\cdot$solvate, Cs^+ cations occupy the ctc bowls within the tetrahedra whilst cations, some of which are disordered, as well as disordered solvent molecules lie in the inter-cage regions of the crystal. In many of the examples of ctc assemblies in which there are external Cs^+ cations, the large Cs^+ cation associates with the outer aromatic faces of the ctc units of the cages. In contrast, in 4A the external Cs^+ counterions are bound to vanadyl oxo-groups and catecholate oxygens. These interactions link the cages together into a 3D network, as shown in Figure 4.6.

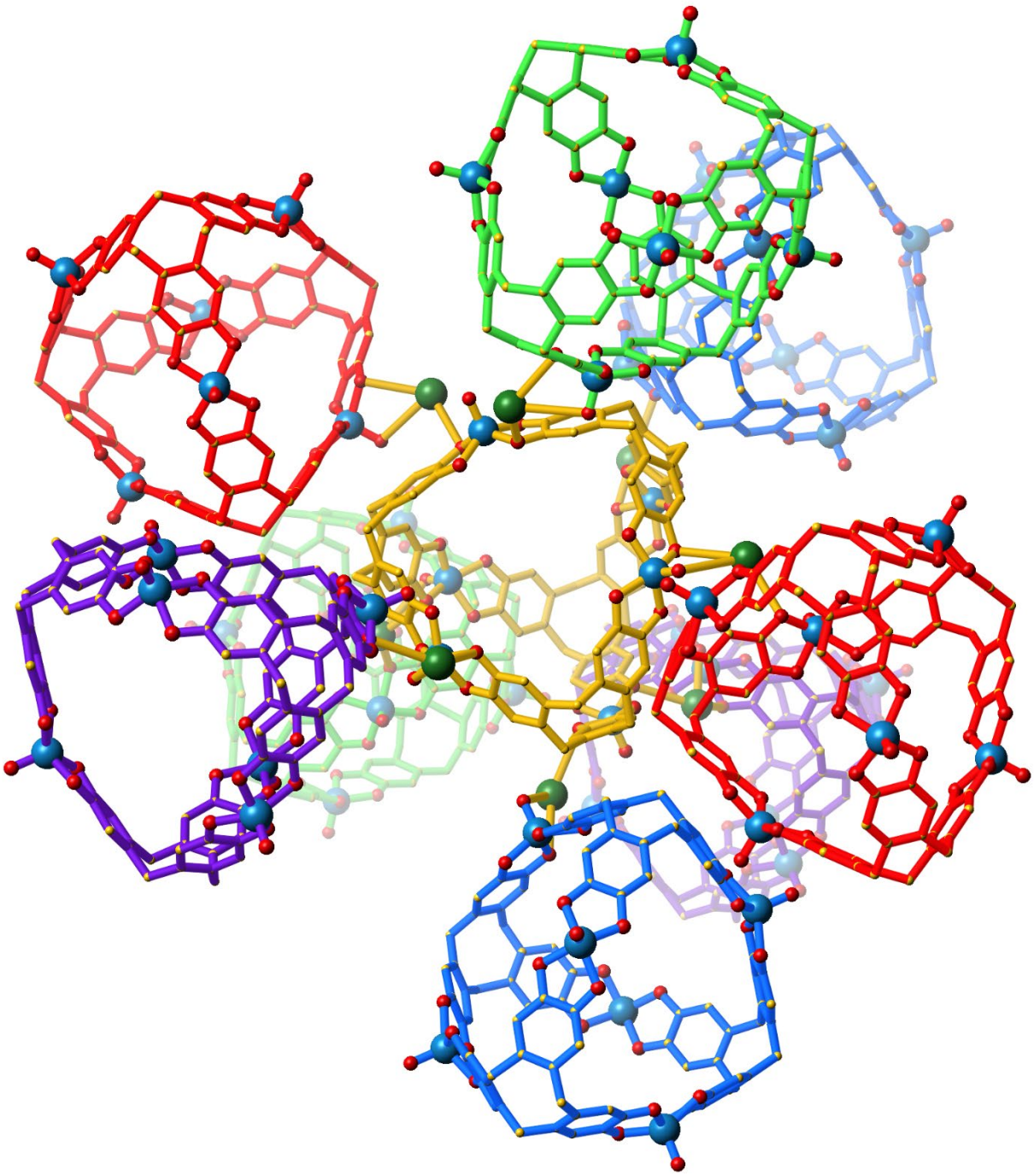

Figure 4.6 A ball and stick representation of $[(VO)_6(ctc)_4]^{12-}$ metallocages bridged by Cs^+ cations (green) in 4A. The central tetrahedron, in yellow, is bridged to eight surrounding tetrahedra. The Cs^+ cations are crystallographically disordered and are only shown in one of two closely located positions. Cages of a single colour are related to each other by translation. Hydrogen atoms have been omitted for clarity.

One of the aims of the research presented in this chapter was to determine to what extent particular cations exert a structure directing influence on the arrangement of molecular cage assemblies in their crystal structures. Dr. Nicholas FitzGerald, who originally characterised the $Cs_8Na_4[(VO)_6(ctc)_4]$·solvate compound, asserted that the Na^+ cations did not appear to impact upon the packing of the cages in the crystal structure and preferred to associate with solvent molecules rather than directly with the cages. The validity of such an assertion regarding the structural role of Na^+ ions is difficult to assess but the fact that an almost identical packing arrangement is obtained for both compounds lends support to the claim that the identity of external group 1 cations appears to have little influence. Despite extensive efforts it was not possible to obtain crystals of the compound, $Na_{12}[(VO)_6(ctc)_4]$·solvate. The structure of this compound, should it indeed form, would provide further insight into the effect of using only Na^+ cations on the packing of the tetrahedral cages.

4.2.1.2 Compound 4B – $Cs_4(MePPh_3)_8[(VO)_9Cs_6(ctc)_6]\cdot 74H_2O$

With a view to investigating formation conditions required for the $[(VO)_9(ctc)_6]^{18-}$ trigonal prism, ctc was combined with the vanadyl cation, the $MePPh_3^+$ cation and CsOH. X-ray analysis of the resultant crystalline material revealed the presence of the $[(VO)_9(ctc)_6]^{18-}$ trigonal prism in a compound of formula $Cs_4(PMePh_3)_8[(VO)_9Cs_6(ctc)_6]\cdot 74H_2O$ (4B). The trigonal prism in 4B crystallises in the same space group as the analogous compound containing Na^+ cations. The compounds have similar cell dimension, but 4B has a slightly smaller unit cell, perhaps somewhat surprisingly, given the presence of larger cations (Cs^+ rather than Na^+) in the crystal structure.

Within the interior of trigonal prism in 4B are six Cs^+ cations, which occupy the electron rich ctc bowls, as shown at left in Figure 4.7. An additional Cs^+ cation was found to be located in

one face of a cage, bridging between two of the convergent oxo-groups and coordinated to two additional water molecules. Charge balance in the compound is achieved by the inclusion of three additional, crystallographically disordered Cs^+ cations per cage and eight $MePPh_3^+$cations. Residual electron density within and between cages was attributed to the disordered Cs^+ cations and disordered water molecules which are also present in the crystal structure. The arrangement of $MePPh_3^+$ cations around the trigonal prism is indicated at right in Figure 4.7. The organic cations participate in four types of aromatic interactions which appear to have an important structure directing influence in the compound (shortest C–C separations given in parentheses): 1) aromatic face-to-face interactions with catecholate units from ctc (3.49 Å); 2) edge of cation-to-face of catecholate units of ctc (3.39 Å); 3) aromatic face of cation-to-ctc methylene proton (3.85 Å); 4) cation-cation face-to-face interactions (3.60 Å).

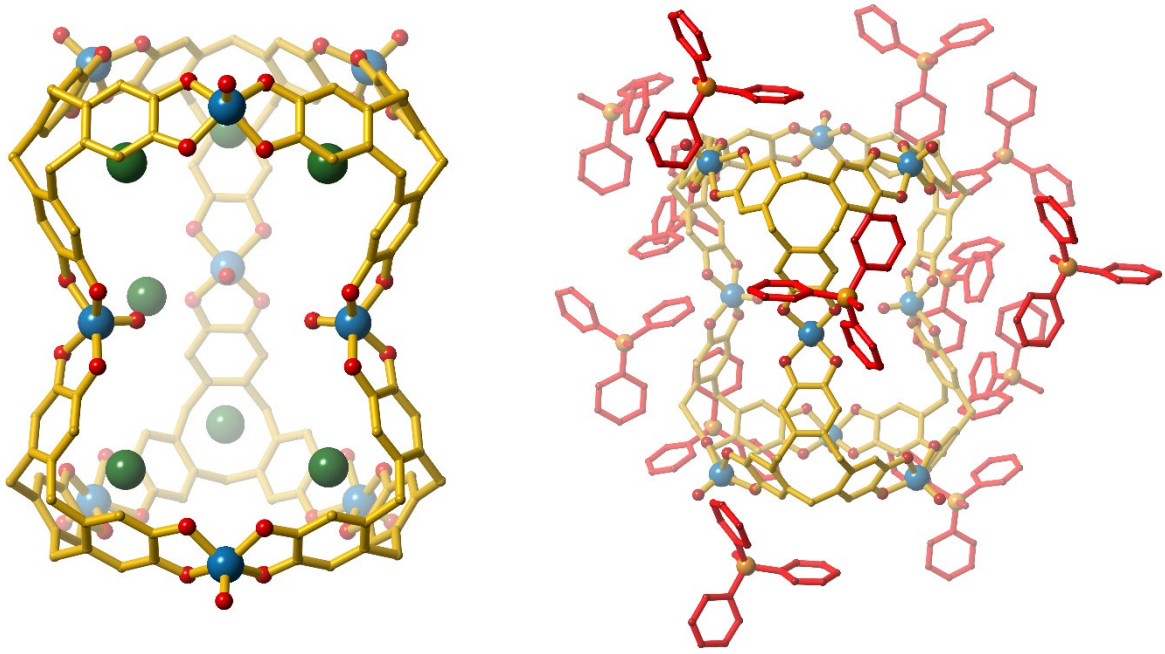

Figure 4.7 Ball and stick representations of, Left: the $[Cs[(VO)_9Cs_6(ctc)_6]]^{11-}$ trigonal prism in 4B, with Cs^+ cations represented by green spheres and V^{IV} centres represented by blue spheres; Right: the arrangement of $MePPh_3^+$ cations (in red) around a cage in 4B. Hydrogen atoms have been omitted for clarity.

In the 3D crystal structure of 4B the trigonal prisms are arranged in layers that are parallel to the *a*-*b* plane, as shown in Figure 4.8. Figure 4.9 shows two of the sheets, one in blue and one in yellow. Within the sheets the trigonal prisms are stacked in columns. Between the columns, both within and between the sheets are located the $MePPh_3^+$ cations. Single phenyl groups from one type of $MePPh_3^+$ cation lie between the trigonal prisms from a single column and for interactions with each of them.

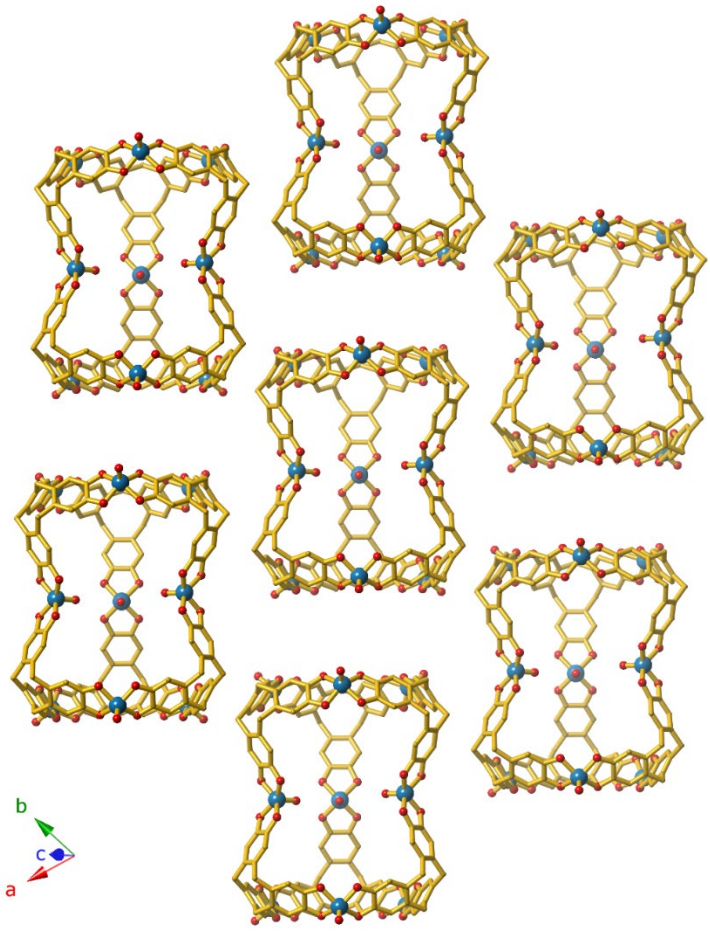

Figure 4.8 A ball and stick representation of one layer of $[(VO)_9(ctc)_6]^{18-}$ trigonal prisms which lie parallel to the *a*/*b* plane, in compound 4B. Cations, solvent molecules and hydrogen atoms have been omitted for clarity.

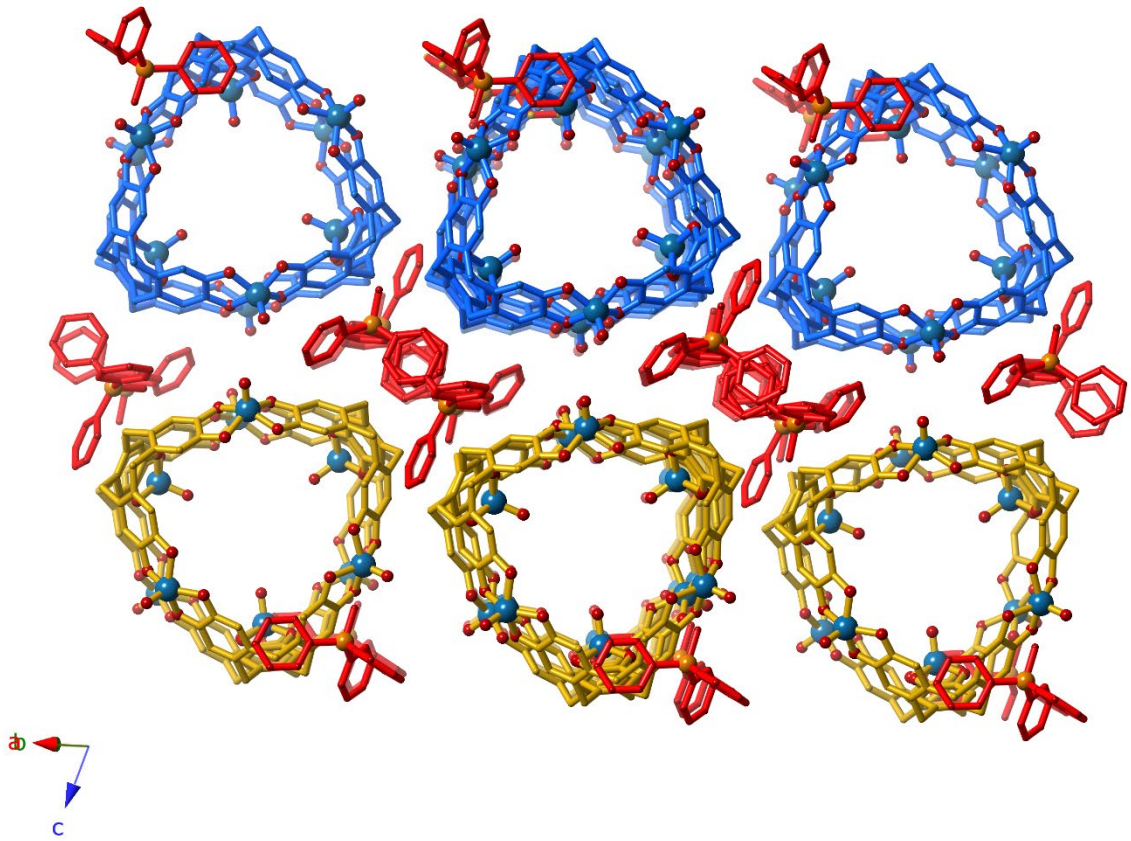

Figure 4.9 A view of the arrangement of $MePPh_3^+$ cations, in red, surrounding trigonal prisms in six columns of trigonal prisms in compound 4B. Blue and yellow colouring indicates trigonal prisms in different layers, each layer being parallel to the *a*/*b* plane. Cs^+ cations, solvent molecules and hydrogen atoms have been omitted for clarity.

The formation of $[(VO)_9(ctc)_6]^{18-}$ trigonal prisms in 4B from a solution containing $MePPh_3^+$ cations suggests that the presence of $MePPh_3^+$ cations is important for either or both of the formation of $[(VO)_9(ctc)_6]^{18-}$ trigonal prismatic assemblies or the crystallisation of the assemblies in preference to tetrahedra. A third $[(VO)_9(ctc)_6]^{18-}$ trigonal prismatic assembly, with the Li^+ and the $MePPh_3$ cations, was also identified by the candidate during her PhD research, however the X-ray crystallographic data for his compound was not of sufficient quality to be included in this thesis. At the time of writing, additional investigations into the formation conditions of tetrahedral and trigonal prismatic assemblies of ctc and their characterisation are being continued in the Robson-Abrahams group.

4.2.2 Uranyl-based cages of cyclotricatechylene

The combination of ctc with the uranyl cation has yielded a wide assortment of metallocages, listed in Table 4.2, which clearly demonstrates that investigation of assemblies formed from these two components is a particularly rich vein of research in the field of supramolecular chemistry. This work has been extended with a view to providing better characterisation of some these cages in addition to further exploring the structural diversity of uranyl-ctc assemblies.

4.2.2.1 Compound 4C – $Na_{24}[(UO_2(H_2O))_{12}(ctc)_8]\cdot 175H_2O$

As indicated in the introduction, the compound $Na_{24}[(UO_2(H_2O))_{12}(ctc)_8]\cdot$solvate was originally synthesised and characterised using X-ray crystallography by Dr. Nicholas FitzGerald during his PhD candidature in the Robson-Abrahams group. The cube-like cage, was formed from the combination of uranyl sulfate and $ctcH_6$ in the presence of NaOH. The crystal structure, determined by Dr FitzGerald, was solved and refined in the trigonal space group *R*-3 and clearly indicated the presence of the $[(UO_2(H_2O))_{12}(ctc)_8]^{24-}$ metallocube (Figure 4.4.) with Na^+ cations providing the charge balance. Difficulties in obtaining a homogeneous product limited the ability to characterise the material. During the candidate's MSc, further study of the reaction that yielded the metallocube (Scheme 4.1) identified the co-crystallisation of hexagonal plates of composition $Na_{12}[(UO_2(H_2O))_6(ctc)_4]\cdot$solvate containing 'half-cubes', which are compositionally equivalent to one half of the $[(UO_2(H_2O))_{12}(ctc)_8]^{24-}$ metallocube (as indicated in Table 4.2).

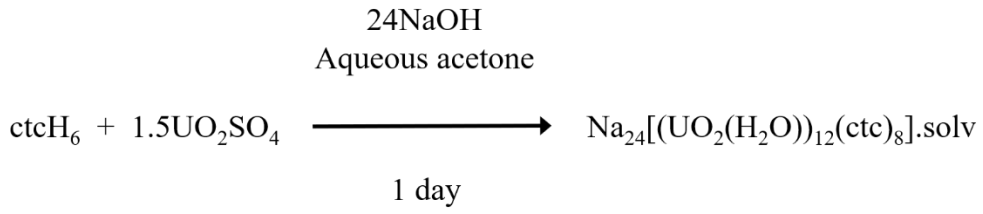

Scheme 4.1 Synthesis of original $Na_{24}[(UO_2(H_2O))_{12}(ctc)_8]$·solvate crystals with trigonal symmetry.

Difficulties were encountered both by Dr FitzGerald and the candidate in the characterisation of bulk products of the uranyl-ctc systems. In particular, microanalyses of bulk precipitates, typically showed significantly lower amounts of carbon than that expected for the uranyl-ctc assemblies.

The bulk product from the reaction that yields the product described in Scheme 4.1 (and the 'half cube' analogue which has the same empirical formula) was collected for elemental analyses during the both the candidate's MSc and PhD. The analytical results are presented in Table 4.3; in each case the amount of carbon is lower than expected.

It is proposed that the analysed samples contain small quantities of uranyl-based contaminants, which lead to a discrepancy between calculated and experimentally determined proportions of elements. Literature investigations revealed that the uranyl cation has the propensity to precipitate from alkaline solution as polyoxometalate-type clusters, particularly in the presence of alkali metal cations.[7,13] Evidence of contamination with such products is provided by the observation of small amounts of amorphous yellow material in the reaction product. Although this material was separated out manually using a needle under a microscope, a small amount of remaining uranium-based side product could significantly impact upon the elemental analysis of the product, particularly given the high atomic mass of uranium. Additional characterisation experiments were performed, including synchrotron powder X-ray diffraction on products formed from XPS on single crystals of 4C, TGA of 4A

and ICP-OES of sodium and uranium content in the compound. Unfortunately, these experiments did not provide additional information, but are included in the thesis appendix. A number of attempts were also made to completely eliminate the yellow side product from the reaction (Table 4.4).

Table 4.3 Results of elemental analyses of the bulk crystalline product from reactions that yielded the cube present in 4C with Na^+ counterions.

Attempt	**C %**	**H %**	**Na %** (ICP-OES)
1	19.18	3.48	7.96
2	19.10	2.90	8.77
3	19.49	2.38	-
4	16.02	2.82	-
5	17.43	3.08	-
Average	18.24	2.93	8.37
Calcd (solv free)	29.30	1.76	8.01
Calcd (84 H_2O solvent)	24.08	3.18	6.58

Table 4.4 $Na_{24}[(UO_2(H_2O))_{12}(ctc)_8]$·solvate purification attempts.

Technique	**Result**
Manual separation with a needle under a microscope, dry and under mother liquor	Contaminants stick to crystals and cannot all be separated. Low carbon % in elemental analysis
Recrystallisation from water/acetone and from water followed by solvent evaporation.	Yellow crystals which have been identified as uranyl-peroxide 'balls' with sodium counter cations. Similar results obtained when recrystallizing from other organic solvents

Density separation with dichloromethane (a layer of the original reaction mixture layered above dichloromethane) with and without sonication.	Oily substance forms on sonication. Without sonication eventually solution becomes yellow (apparent break down of crystals - further investigation required)
Density separation with reaction mixture layered above CS_2	Some crystals separated to bottom of flask but only a small proportion before aggregated amorphous precipitate also separates.
Crystals washed with glacial acetic acid (aqueous acid cannot be used because crystals are water soluble) on a glass frit	Fine grey precipitate remains. IR suggests it is NaOAc. Filtrate is a yellow colour, indicative of the presence of the uranyl cation.
Detergent bubbled through original solution and acetone/water solution with filtered crystals	Most solid remained at bottom of flask. No discrimination between crystalline species and side product.
Centrifugation of reaction mixture of large crystals followed by acetone wash repeated several times.	Sample still has mismatching elemental analysis.
Various reactions performed involving alteration of base/pH, solvent, reagents etc. to avoid side products	Unsuccessful, either due to no product formation or the presence of amorphous material.

Despite being unable to eliminate the yellow side product that is thought to have been the reason for the mismatching elemental analysis, the series of purification experiments detailed in Table 4.4 yielded two interesting results:

i) A crystal structure containing a uranyl-based polyoxometalate and

ii) a new synthesis and crystal structure solution for the original compound of formula $Na_{24}[(UO_2(H_2O))_{12}(ctc)_8]\cdot$solvate.

When the bulk product from the reaction shown is scheme 4.1 was recrystallised from a minimum of a 1:1 mixture of acetone and water and allowed to evaporate, a compound containing a discrete polyoxometallate cluster of formula

$[Na_{14}(UO_2)_{24}(H_2O)_8(O_2)_{24}(OH)_{24}]^{10-}$ was identified (Figure 4.10). The compound does not contain ctc. The $[Na_{14}(UO_2)_{24}(H_2O)_8(O_2)_{24}(OH)_{24}]^{10-}$ cluster in the compound is composed of twenty-four 3-connecting uranyl cations of hexagonal bipyramidal geometry. These are bridged by peroxo- and hydroxo-groups. The anionic cage, which may be described as an 'actinyl peroxide nanosphere' is, from a topological perspective, a truncated octahedron, which contains six of the uranyl-peroxide tetramers shown in Figure 4.3 d).

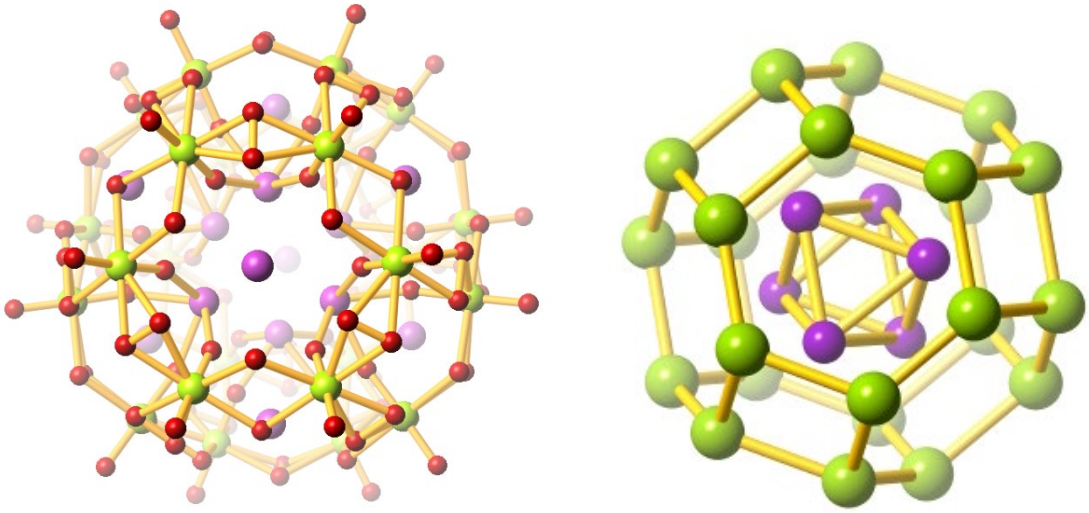

Figure 4.10 Left: A view of the $[Na_{14}(UO_2)_{24}(H_2O)_8(O_2)_{24}(OH)_{24}]^{10-}$ anionic nanoball that highlights the presence of peroxo-bridged uranyl clusters. Green spheres represent U^{VI} centres and purple spheres represent Na^+ which can be seen in the hexagonal faces of the sphere and within the sphere binding to oxo-groups. Right: A ball and stick representation of the nanosphere in which all oxygen atoms have been omitted for clarity. This view shows the octahedron of Na^+ cations (purple) at the centre of the cluster and shows the three-connecting nature of the uranyl centres. Na^+ cations present of the faces of the cluster have been omitted for clarity.

The nanosphere has six square and eight hexagonal faces. Six sodium counter cations are present within the sphere and each interact with four oxo-groups from the uranyl ions that form the corners of single square face. Na^+ ions are also present in the plane of each of the six hexagonal faces. The clusters pack in a body centered cubic arrangement with additional counter cations located between the spheres. Crystal structures containing the $[(UO_2)_{24}(H_2O)_8(O_2)_{24}(OH)_{24}]^{24-}$ species with Na^+ and Li^+ were reported by Nyman and co-

workers in 2012[14] and in a review of uranyl peroxide nanoclusters by Burns and co-workers, the $[(UO_2)_{24}(O_2)_{24}(OH)_{24}]^{24-}$ unit has been reported to form at high concentrations of Na^+ and uranyl cations (c.a. 35 000 ppm).[15]

The significance of the $Na_{10}[Na_{14}(UO_2)_{24}(H_2O)_8(O_2)_{24}(OH)_{24}]\cdot$solvate species in this body of work is that it has been identified crystallographically as the crystalline product in several attempts to recrystallize the original $Na_{24}[(UO_2(H_2O))_{12}(ctc)_8]\cdot$solvate cubes, 4F, described above. This is not confirmation that the nanosphere species is the side product observed in many reaction mixtures containing the uranyl cation, particularly given the many other possible nanosphere clusters exist and may precipitate preferentially depending on reaction conditions. Nevertheless, the formation of this anion in this current work suggests that polyoxometallate formation involving uranyl-based species may be readily occurring in many of the reaction mixtures. Additional support for this assertion comes from the identification of crystals of this compound in a reaction of $ctcH_6$ with NaOH and alloxan in aqueous solution that was left undisturbed for more than a year. Crystallographic details relating to $Na_{10}[Na_{14}(UO_2)_{24}(H_2O)_8(O_2)_{24}(OH)_{24}]\cdot 176H_2O$ (from the dataset obtained from the reaction containing $ctcH_6$ with NaOH and alloxan in aqueous solution) are recorded in the appendix.

As indicated previously, visual inspection using a microscope of the solids that are formed when uranyl is combined with ctc under basic conditions often indicate a homogeneous crystalline product along with a small amount of a fine precipitate. On other occasions very small amounts of aggregated yellow precipitate can be identified (see appendix for an example of this). These unidentified materials may indeed be polyoxometallates related to the structurally characterised $[Na_{14}(UO_2)_{24}(H_2O)_8(O_2)_{24}(OH)_{24}]^{10-}$ anion.

In order to eliminate the formation of side products completely, the reaction was repeated with numerous variations, including under more dilute and less alkaline conditions. When a reaction was performed according to scheme 4.2, large brown rods formed over several months.

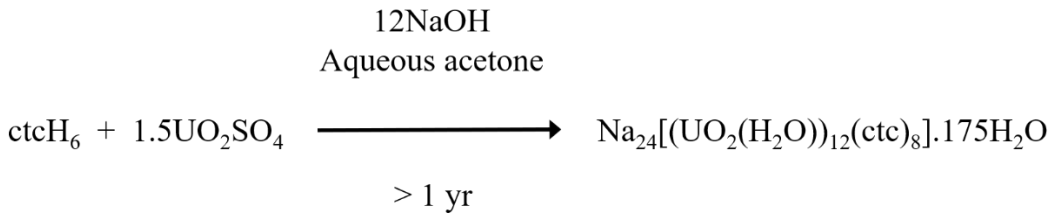

Scheme 4.2 Synthesis of $Na_{24}[(UO_2(H_2O))_{12}(ctc)_8]\cdot 175H_2O$ crystals with cubic symmetry.

Single crystal X-ray analysis revealed the presence of the same molecular cubes of composition $[(UO_2(H_2O))_{12}(ctc)_8]^{24-}$ (Figure 4.4) with Na^+ countercations, as in 4C. These crystals were identified to have cubic symmetry and a satisfactory solution and refinement was achieved in space group *Fm-3* (a = 34.325 Å). There is only one crystallographically distinct uranium cation in this system, whereas there are two are present in Dr FitzGerald's $[(UO_2(H_2O))_{12}(ctc)_8]^{24-}$ which is a consequence of the lower symmetry. Close analysis of the two structures reveals a very similar arrangement of the $[(UO_2(H_2O))_{12}(ctc)_8]^{24-}$ cages in the crystal but in the case of Dr FitzGerald's structure the crystallographic 3-fold axes are restricted to only one direction whereas crystals of 4C prepared by the candidate possess considerably higher symmetry. It seems likely that different degrees of solvation are responsible for the differences in crystal symmetry.

Given the difficulties associated with modelling crystal structures of weakly diffracting crystals with large, solvent filled voids, attempts were directed towards generating molecular cubes with organic cations that might instead occupy these spaces.

4.2.2.2 Compound 4D – $Li_{24}(MePPh_3)_6[(UO_2(H_2O))_{12}(ctc)_8]Br_6 \cdot 147H_2O$

A $[(UO_2(H_2O))_{12}(ctc)_8]^{24-}$ cube with an organic counter cation (Figure 4.11) was serendipitously, rather than deliberately, generated when $ctcH_6$, LiOH, $UO_2(NO_3)$ and $Mn(OAc)_2$ were combined in aqueous dioxane. The original intention of the experiment was to generate a mixed metal cation assembly. When crystals of hexagonal symmetry from the reaction were analysed using X-ray diffraction, an extremely well-defined compound, 4D, of formula $Li_{24}(MePPh_3)_6[(UO_2(H_2O))_{12}(ctc)_8]Br_6 \cdot 147H_2O$ was revealed. The cubes in 4D share the same connectivity as those in 4C.

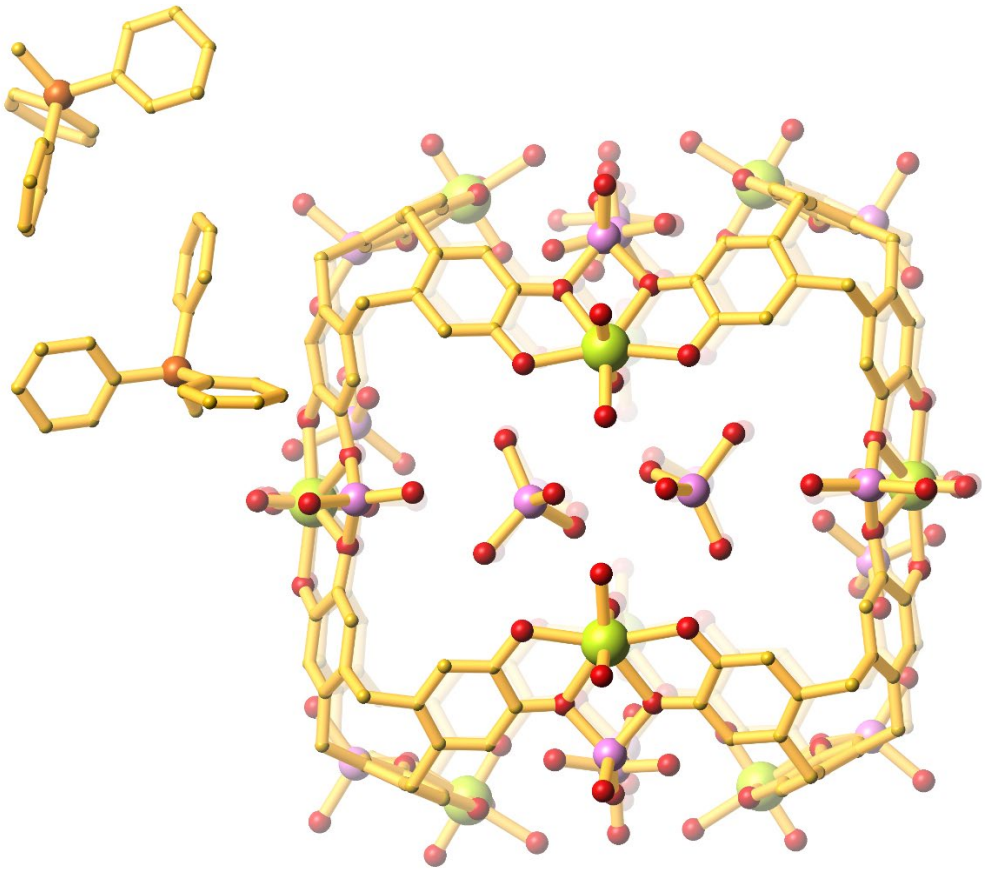

Figure 4.11 A ball and stick representation of the $[(UO_2(H_2O))_{12}(ctc)_8]^{24-}$ cube in 4D. $MePPh_3^+$ countercations are shown interacting with each other and with methylene hydrogen atoms on the ctc. Li^+ cations (pink) in the faces of the cage are each surrounded by four oxygen atoms. Li^+ cations adjacent to the U^{VI} centres (green) interact with two catecholate oxygens and two water molecules.

As shown in Figure 4.11, in each face of the cube there are two crystallographically distinct Li^+ cations, in tetrahedral environments, coordinated by four aqua ligands each. These aqua ligands hydrogen bond to nearby aqua ligands associated with uranyl cations as well as to aqua ligands coordinated to adjacent Li^+ cations.

Two additional Li^+ cations are found on each face. Each of these Li^+ cations binds to two catecholate oxygen atoms – one from each of the two ctc molecules that chelates a uranyl centre – and is located on the opposite side of the uranyl centre from the coordinated water

molecule. The Li^+ centres have their coordination spheres completed by two aqua ligands each. These aqua ligands also hydrogen bond to those associated with the Li^+ cations in the cage faces. Hydrogen bonding between aqua ligands on the lithium cations and water molecules that are located between the cages appear to both hold the lithium cations in position and 'stitch' the anionic cages together.

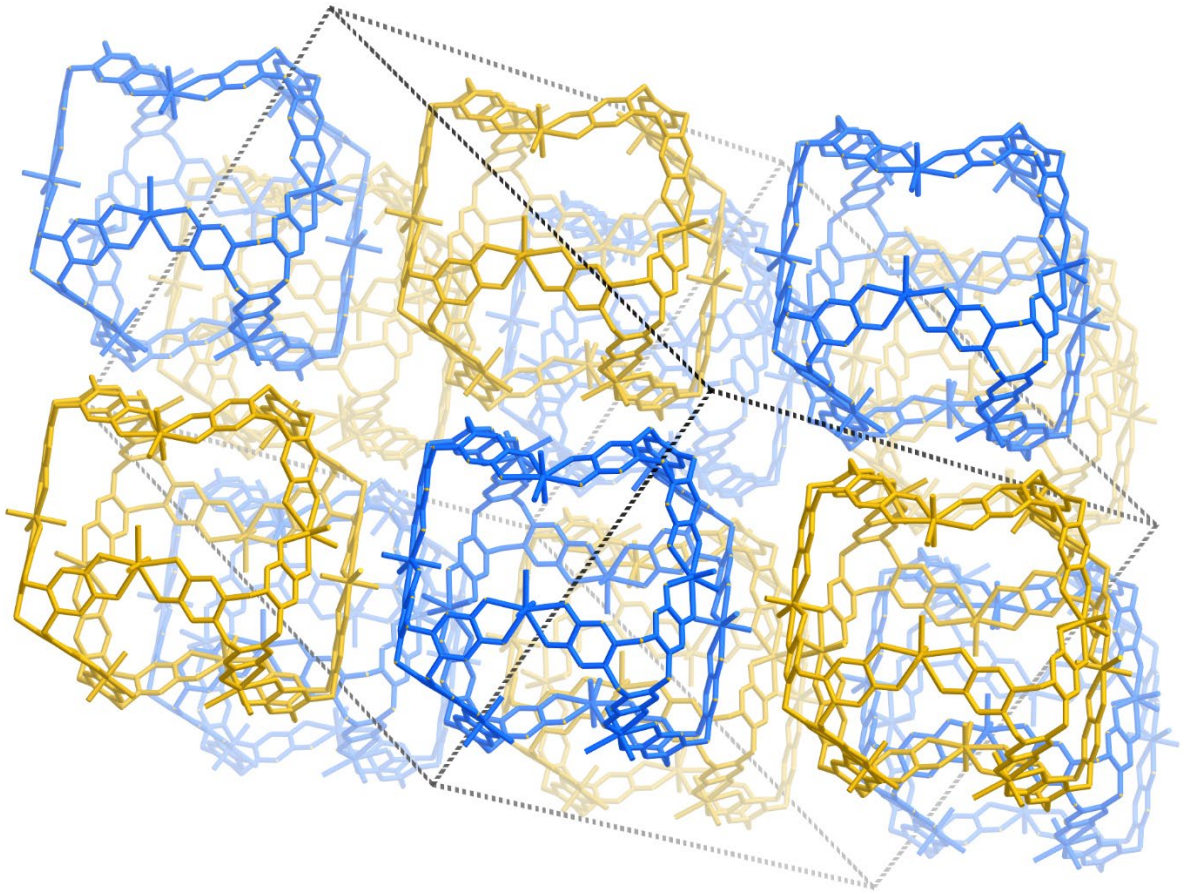

Figure 4.12 A stick representation of the face-to-face arrangement of cubes in the unit cell of compound 4D. Hydrogen atoms, solvent molecules and counterions have been omitted for clarity.

Compound 4D contains slightly offset cubes that pack such that their faces are parallel (Figure 4.12), in a crystal structure which contains significantly less empty space than 4C. $MePPh_3^+$ cations and disordered Br^- are present in the spaces between cubes where eight cubes converge at their corners, essentially one of each associated with each corner of the

cage. The $MePPh_3^+$ cations participate in edge-to-face aromatic interactions with each other, as shown in Figure 4.13 Left and Right, as well as interacting with the ctc methylene protons from the cube in both an edge-to-face and face-to-face manner (Figure 4.13, Left, and Figure 4.14).

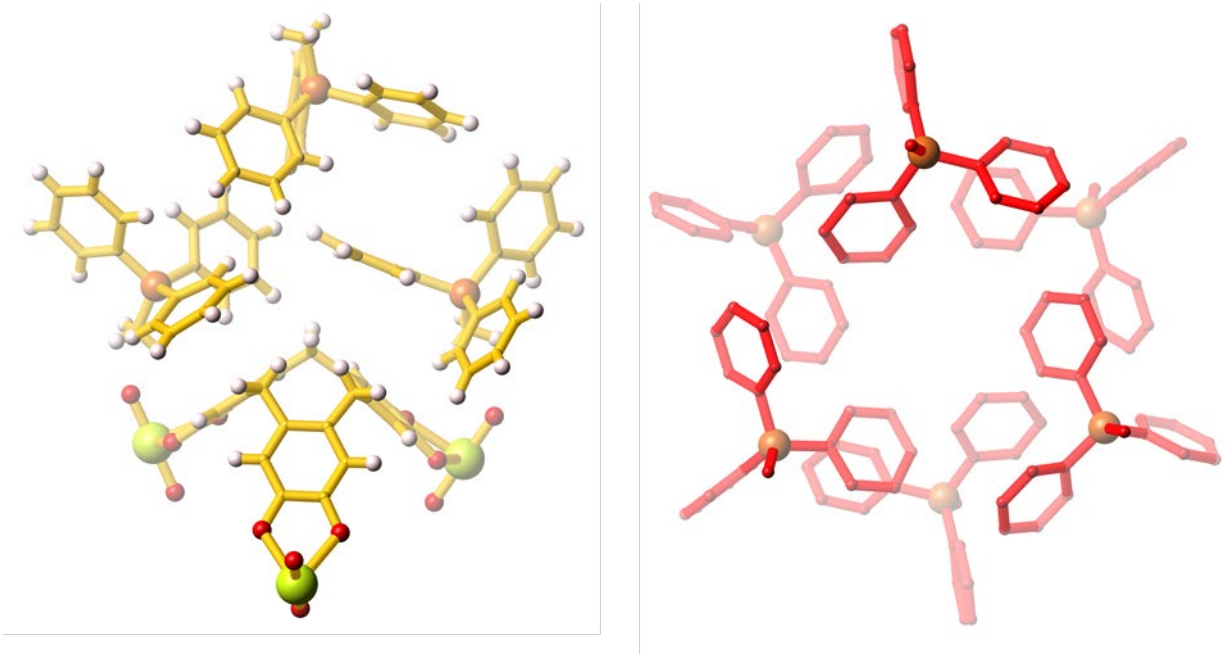

Figure 4.13 Ball and stick representations of the aromatic interaction present in compound 4D. Left: three $MePPh_3^+$cations are shown interacting with each other, and with the methylene protons of a ctc that forms one corner of the $[(UO_2(H_2O))_{12}(ctc)_8]^{24-}$ metallocube. Right: aromatic interactions between six adjacent $MePPh_3^+$cations in the crystal structure of 4G. Green spheres represent U^{VI} centres; Orange, phosphorus. At right, hydrogen atoms have been omitted for clarity.

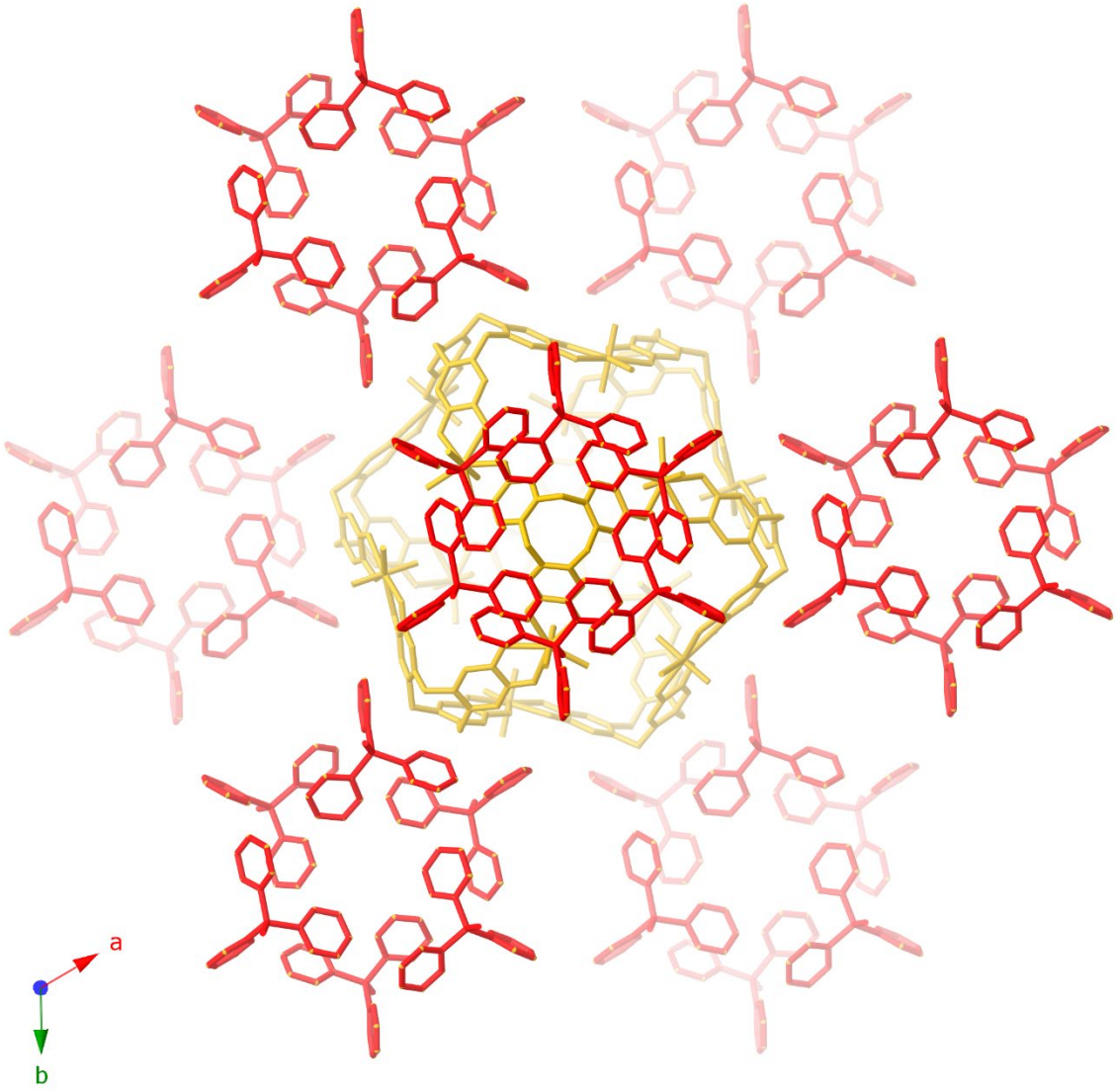

Figure 4.14 A stick representation of the arrangement of $MePPh_3^+$cations (red) adjacent to the corners of the $[(UO_2(H_2O))_{12}(ctc)_8]^{24-}$ metallocube (yellow) in 4G. Hydrogen atoms and the cations behind the cage have been omitted for clarity.

Compound 4D, containing Br^- counterions, is one of a growing number of double salts of ctc complexes which contain charged assemblies and contain both countercations and counteranions. Other examples include $(NMePent_3)_6Na_8[Cu_6(ctc)_4]I_2\cdot solvate$[1] and the silicon-based tetrahedron reported in chapter 5 of this thesis.

A remarkable feature of this compound is that well defined Li^+ cations were able to be identified so close to uranium centres. From a crystallographic perspective this was somewhat surprising given that atoms of light elements can be difficult to identify so close to heavy atoms of heavy elements such as uranium.

Numerous attempts were made to generate compound 4D in the absence of $Mn(OAc)_2$. These experiments did not yield crystals containing 4D. The candidate performed an experiment analogous to that which yielded Dr. FitzGerald's cubes, in which $ctcH_6$ was combined with the uranyl cation and $MePPh_3Br$ in aqueous acetone, followed by treatment with lithium hydroxide. After a week, this experiment yielded hexagonal crystals of formula $Li_6MePPh_3[UO_2(H_2O))_6(O)(ctc)_3]\cdot$solvate that contain a cage of tetrahedral geometry, with a single uranyl trio. This compound was reported in the candidate's MSc thesis.[4] The generation of the various uranyl clusters appears to be a key factor in the uranyl-based assembly obtained. Despite systematic investigations that varied concentrations of reagents and also their stoichiometry, a clear pattern was not observed in relation to reaction conditions governing the types of uranyl cluster and cage compound formed.

The connectivity of the components within the cubes is the same in compounds 4C, 4D and in the cube synthesised by Dr FitzGerald. While the three cubes are very similar in dimensions, they differ slightly. In Dr Fitzgerald's example, the distance between diametrically opposed uranium centres is 19.71 or 20.44 Å; in 4C, in which the cube has higher symmetry, the distance between uranium centres in each diametrically opposed pair is 19.09 Å; in 4D the distance between diametrically opposed uranium centres is 18.58 or 19.23 Å.

4.2.2.3 Compound 4E – $Cs_{12}[Cs_2(UO_2)_3(O)(OH)_3(ctc)]_4 \cdot 24H_2O$

A compound containing four uranyl trimers was crystallised from an aqueous acetone solution of $ctcH_6$, $UO_2(NO_3)_2$ and CsOH, X-ray analysis of the brown crystals revealed molecular cubes of composition $[(UO_2)_3(O)(OH)_3(ctc)]_4^{20-}$ (Figure 4.15, Left) in a crystal of formula $Cs_{12}[Cs_2(UO_2)_3(O)(OH)_3(ctc)]_4 \cdot 24H_2O$, compound 4E.

The cube, represented in Figure 4.15 is fundamentally different to the uranyl-based cubes, 4C and 4D described above. The cubes in 4E more closely resemble the cubes in 3A – 3D, reported in chapter 3 of this thesis. In 4E, as in 3A – 3D, four of the eight 3-connected "vertices" of the cube correspond to ctc ligands. However, whereas in 3A - 3D, alkali metal ions fulfil the role of the four remaining 3-connected vertices, tri(uranyl) clusters occupy each of the four remaining vertices in 4E. A comparison of the two structures showing the similarities and differences is presented in Figure 4.16.

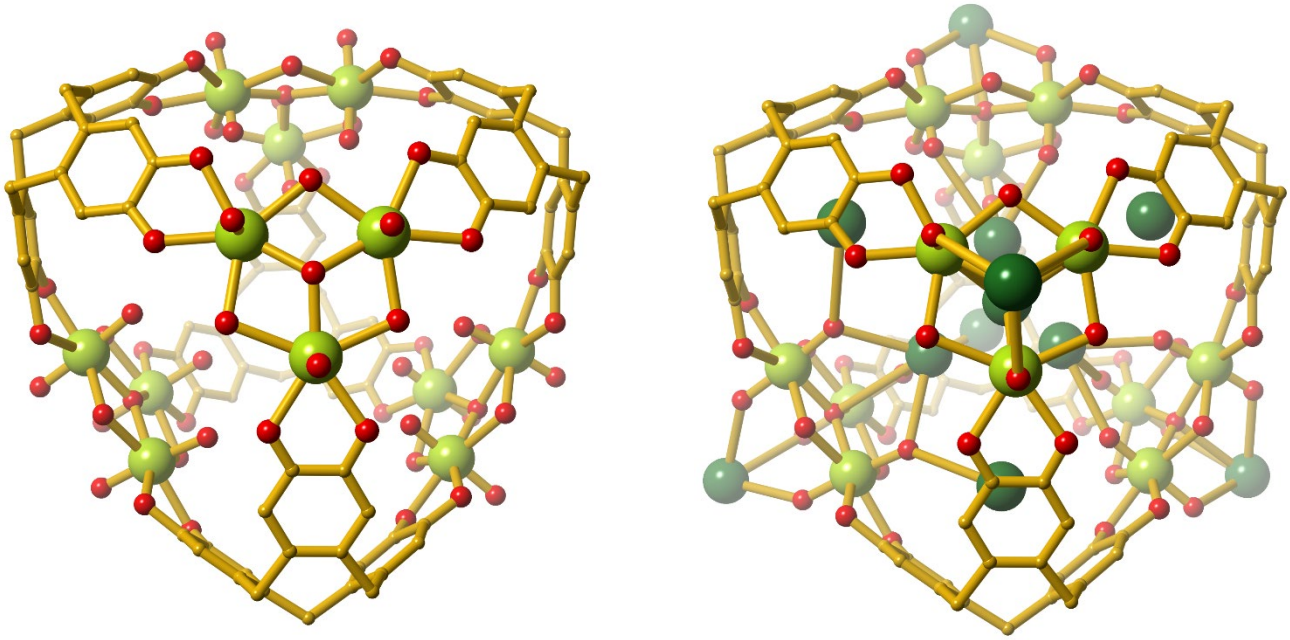

Figure 4.15 Ball and stick representations of the $[(UO_2)_3(O)(OH)_3(ctc)]_4^{20-}$ cage in 4E, Left: without and Right: with the associated Cs^+ cations (dark green spheres). Hydrogen atoms have been omitted for clarity.

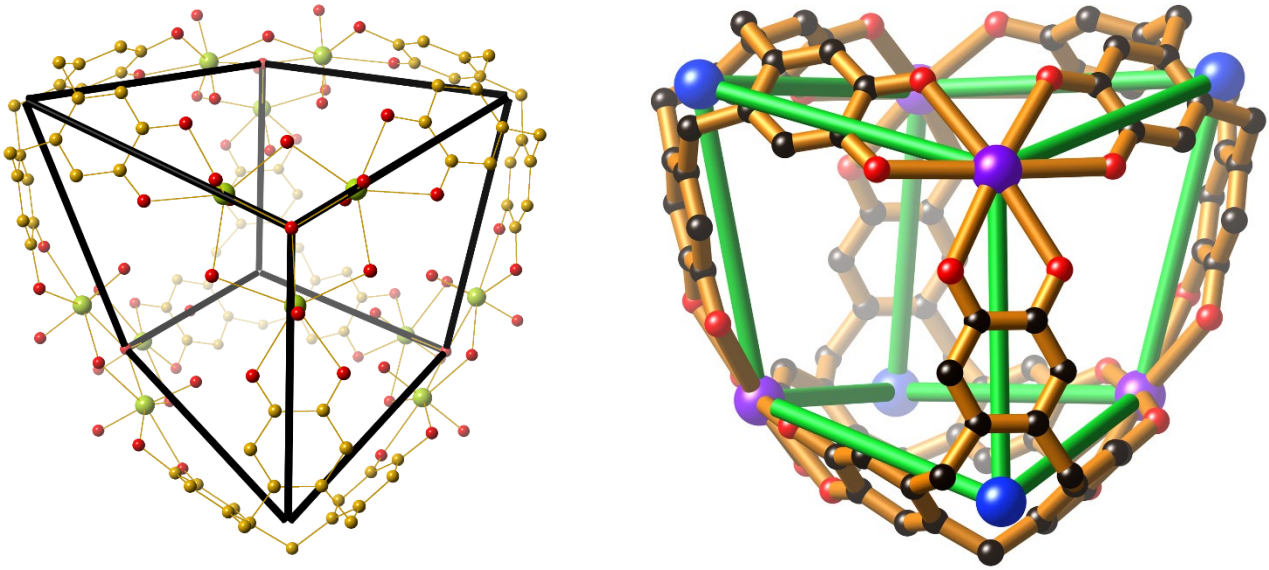

Figure 4.16 A comparison of the metallocubes in Left: 4E and Right: 3A, indicating the similarity in connectivity and geometry of the frameworks of the two assemblies. Hydrogen atoms have been omitted for clarity.

In 4E, a crystallographic 3-fold axis passes through the oxo ion of one of the triuranyl units, while the remaining three units are crystallographically related by 3-fold symmetry. The linear O=U=O groups in each trimer are close to perpendicular to the mean plane of the three U centres, however they are not perfectly parallel with each other. For the triuranyl cluster located on the 3-fold axis, the internal U=O bonds diverge sightly inside the cage while the external U=O bonds converge to a small extent. In the remaining three triuranyl units (related by 3-fold symmetry), the internal U=O converge slightly inside the cage while the external U=O bonds exhibit a small degree of divergence.

Each triuranyl unit is associated with a pair of Cs^+ ions, one located inside the cage and the other outside the cage. Each Cs^+ cation is bound to a trio of oxo uranyl groups as indicated in Figure 4.15 (right). In addition, four Cs^+ cations associate with the internal aromatic surfaces of the cage as has been previously observed in cages formed from four ctc anions. Thus, a total of twelve Cs^+ ions, eight internal and four external, are closely associated with each cage. The cube in 4E represents an unusual example of a cage in which the number of internal Cs^+ ions exceeds the number of ctc ligands from which the cage is formed.

In addition to the aforementioned twelve Cs^+ cations associating closely with each cage, further Cs^+ ions are located between the anionic $\{[Cs_3(UO_2)_3(O)(OH)_3(ctc)]_4\}^{8-}$ assemblies. Some disorder of these Cs^+ cations is apparent, however there are well defined O–Cs^+–O interactions between cations and catecholate oxygen atoms and bridging water molecules that fuse the cages together (Figure 4.17).

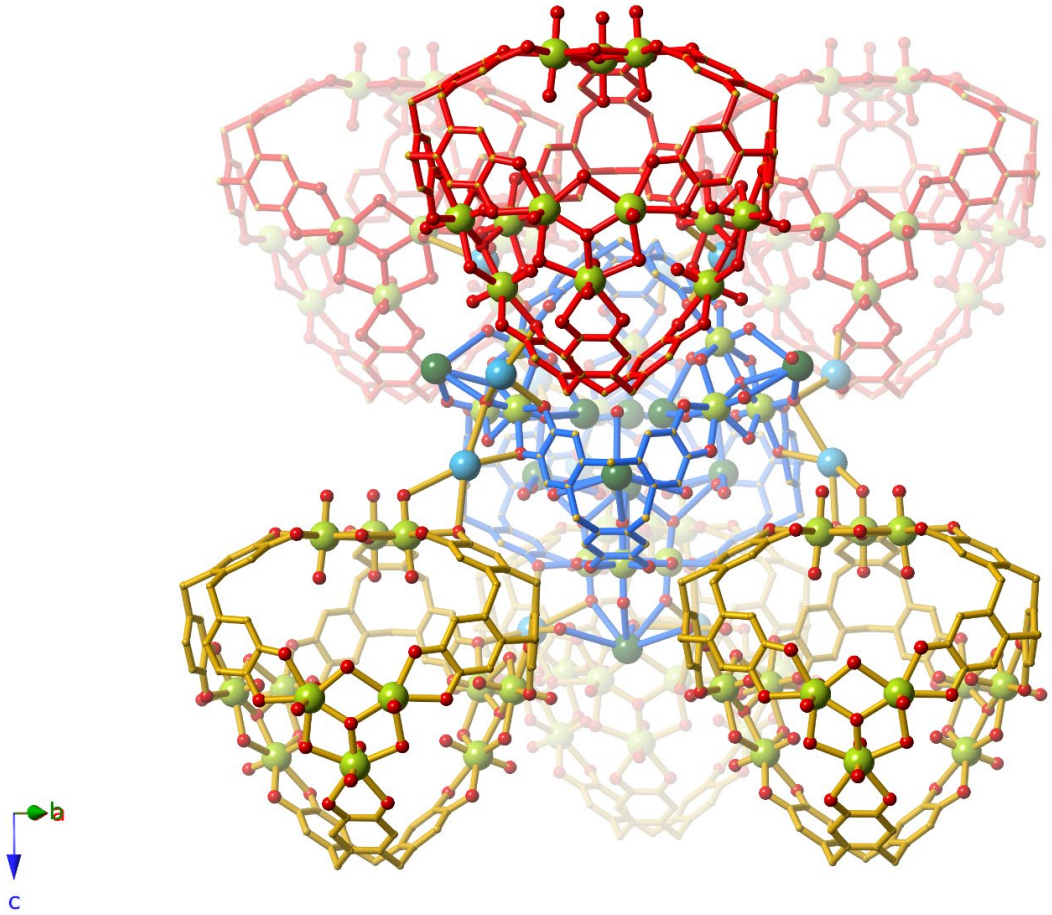

Figure 4.17 A ball and stick representation of the ABC packing of metallocubes in 4E. Green spheres indicate Cs^+ cations within the ctc bowls and coordinated to three oxo-groups of each trimer, each belonging to only one cage. Blue spheres represent one type of bridging Cs^+ cation that connects each cage to the six cages that surround it in an octahedral arrangement. Hydrogen atoms, solvent molecules and additional Cs^+ countercations have been omitted for clarity.

4.2.2.4 Compound 4F – $Cs_{10}Na_{19}[CsNa_{0.5}(UO_2)_{10}(O)_2(OH)_8(H_2O)_2(ctc)_4]_2 \cdot 195H_2O$

Hollow, "semi-ellipsoidal" shaped assemblies (shown in Figure 4.18) of formula $[CsNa_{0.5}(UO_2)_{10}(O)_2(OH)_8(H_2O)_2(ctc)_4]^{16-}$ form in a compound of formula $Cs_{10}Na_{19}[CsNa_{0.5}(UO_2)_{10}(O)_2(OH)_8(H_2O)_2(ctc)_4]_2 \cdot 195H_2O$, 4F, when $ctcH_6$ and the uranyl cation are combined with Na^+ and Cs^+ cations.

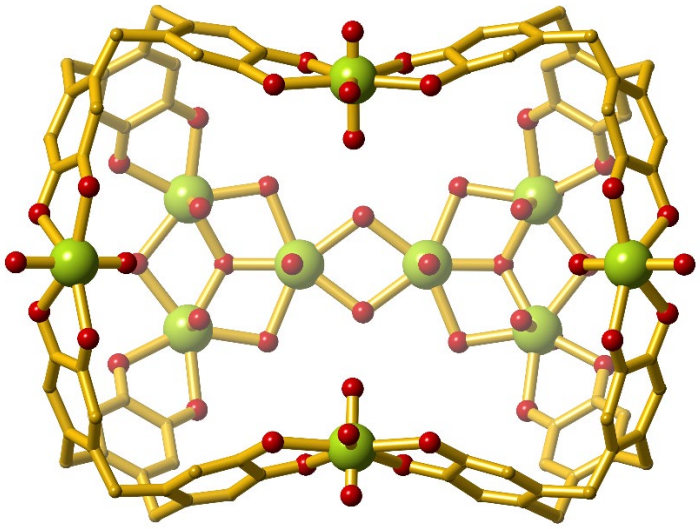

Figure 4.18 A view into the cavity of the $[(UO_2)_{10}(O)_2(OH)_8(H_2O)_2(ctc)_4]^{16-}$ semi-ellipsoid, present in the crystal structure of $Cs_{10}Na_{19}[CsNa_{0.5}(UO_2)_{10}(O)_2(OH)_8(H_2O)_2(ctc)_4]_2 \cdot 195H_2O$, 4F. Uranyl centres are represented by fluoro green spheres. Hydrogen atoms have been omitted for clarity.

The semi-ellipsoids are composed of two triuranyl units which each have a central μ_3-oxo group. Pairs of uranyl groups, within each triuranyl unit, are bridged by μ_2 oxygen atoms from hydroxide anions (Figure 4.19). The triuranyl units are geometrically similar to those present in 4E. Two bridging μ_2 hydroxo ligands link the trimers together to form a hexauranyl unit. Four of the six uranyl centres are chelated by catecholate units from four separate ctc ligands. Each of these ctc ligands also binds to a pair of uranyl groups on the rim of the ctc bowl, two of which are in a pentagonal bipyramidal coordination environment, and two of which are in a distorted octahedral environment.

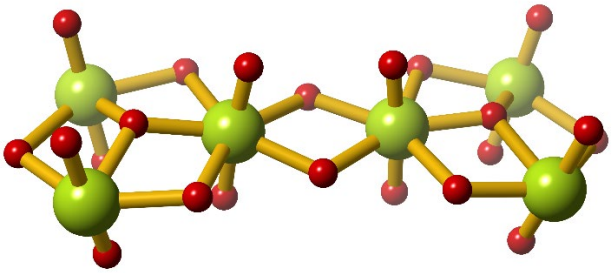

Figure 4.19 A ball and stick representation of the 'dimer of trimers' in the hexauranyl unit of formula $[((UO_2OH)_3(O))_2(OH)_2]$ present in the semi ellipsoid in 4F. Hydrogen atoms have been omitted for clarity.

As previously seen in uranyl-based ctc assemblies, alkali metal cations play important roles in the arrangement of anionic supramolecular species within the crystal structure. In 4F, Na^+ ions interact with three converging oxo groups of each trimer, which extend into the interior of the semi-ellipsoid. Also within the interior of the semi-ellipsoid is a third Na^+ ion, located equidistant between the two others. Not surprisingly, a Cs^+ cation associates with each of the four electron-rich bowls of the ctc ligands.

In addition to the Cs^+ cations within the ctc bowls, additional Cs^+ cations interact with the three divergent oxo groups, located outside each semi-ellipsoid, as shown in Figure 4.20. These exterior Cs^+ cations form a bridge between two adjacent semi-ellipsoids resulting in the generation of a dimer as indicated in Figure 4.21. Thus, each Cs^+ is bound to oxo groups from six uranyl units. In addition, the μ_3 oxo centre, which is slightly pyramidal, forms an interaction with the bridging Cs^+ cation as indicated in Figure 4.21. The two semi-ellipsoids in the dimer are further cemented together by bonds between the oxo groups and a Na^+ cation located equidistant from the four oxo groups. An octahedral environment of this central Na^+ cation is completed by a pair of *trans* water molecules.

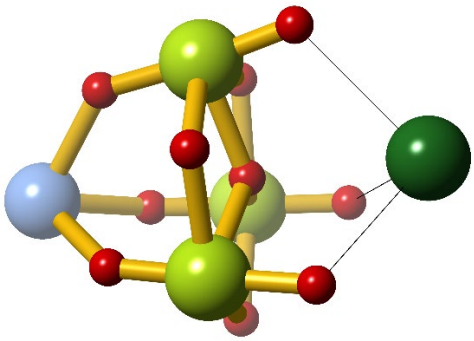

Figure 4.20 A ball and stick representation of the Na^+ (blue) and Cs^+ (dark green) cation interactions with the oxo groups in a trimer from 4F. Hydrogen atoms have been omitted for clarity.

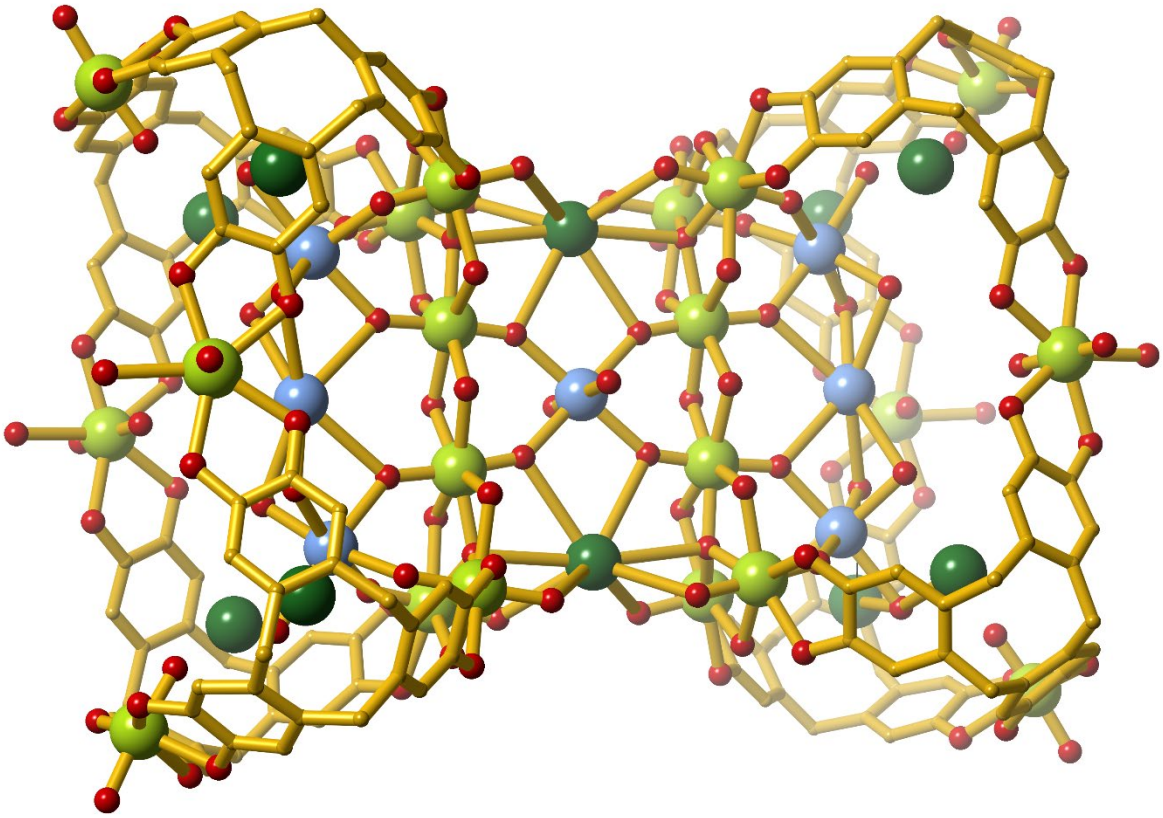

Figure 4.21 A ball and stick representation of the dimer of the two crystallographically equivalent semi-ellipsoids in 4F, showing the two bridging Cs^+ cations in dark green. Additional Na^+ (blue) and Cs^+ cations associated with the assembly are also show. Cations and solvent molecules located between dimers and hydrogen atoms have been omitted for clarity.

In the 3D crystal structure, dimers form sheets fused together by interactions with Cs^+ cations, as shown in Figure 4.22. Each dimer is bonded to four others in this manner. The sheets of dimers, which lie perpendicular to the crystallographic *c*-axis, stack atop each other in an ABAB arrangement, illustrated in figure 4.23, where each sheet is rotated 90° relative to the other.

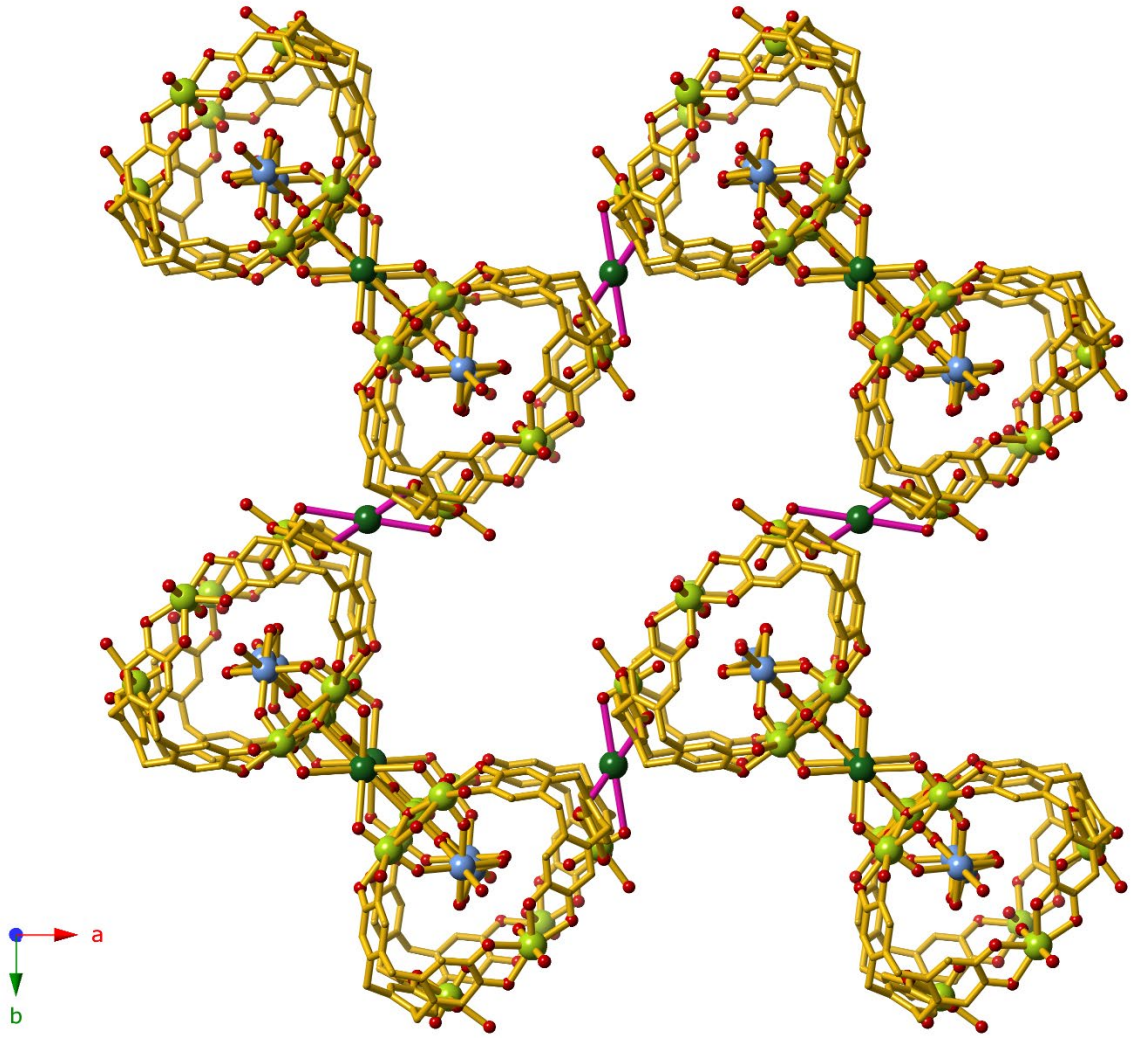

Figure 4.22 A ball and stick representation of one sheet of dimers of semi-ellipsoids in 4F. Pink connections indicate bonds to Cs^+ cations that bridge between the dimers to connect them in the sheet. Hydrogen atoms have been omitted for clarity.

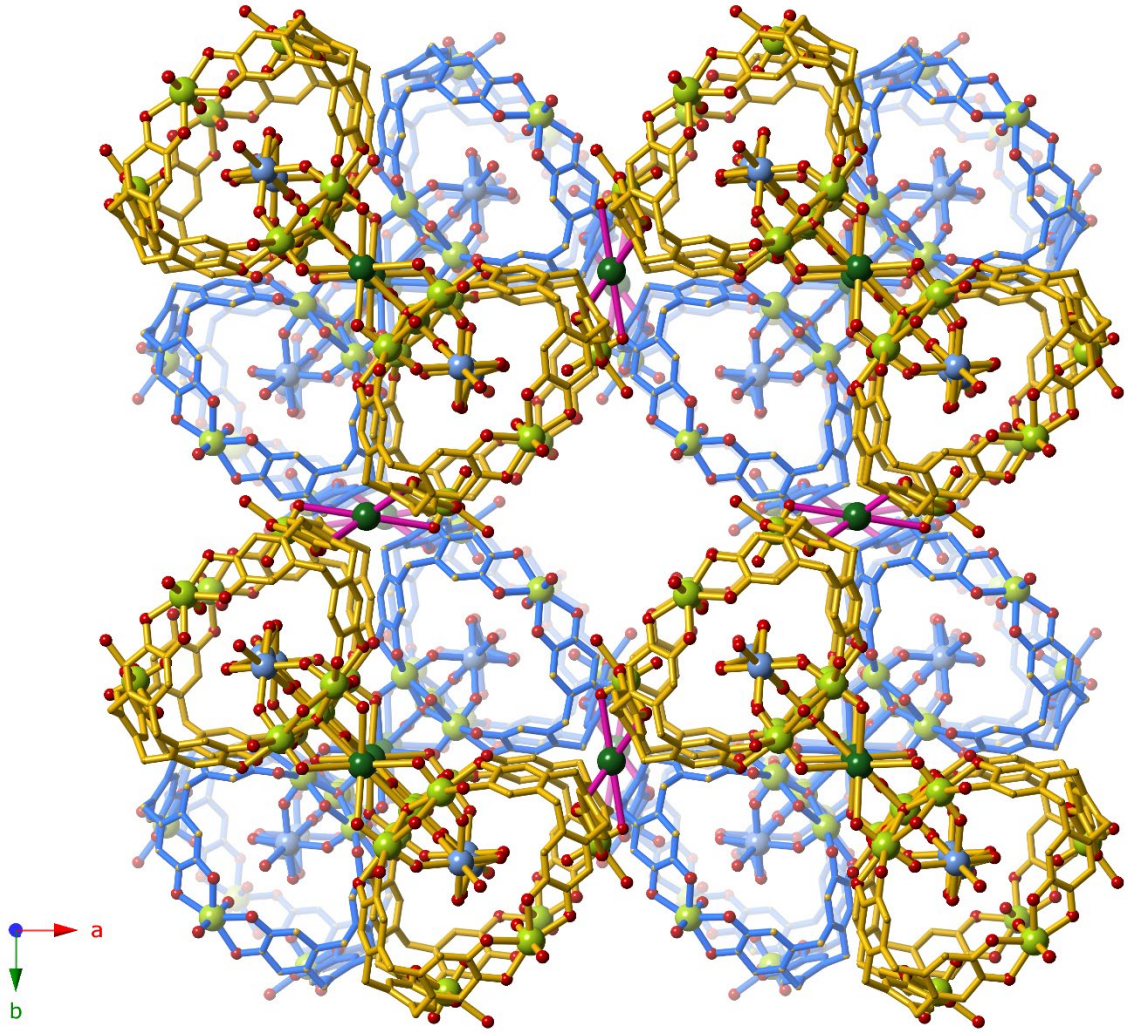

Figure 4.23 A ball and stick representation of two sheet of dimers of semi-ellipsoids in 4F, one in blue and the other in yellow, indicated the AB packing in the crystal structure. Pink connections indicate bonds to Cs^+ cations that bridge between the dimers to connect them in the sheet. Hydrogen atoms have been omitted for clarity.

4F is a structurally fascinating and unusual uranyl-based assembly. A search of the Cambridge crystallographic database indicates that the 'dimer-of-trimers' motif has never been reported (either with aqua or hydroxo ligands) in a crystal structure containing organic ligands. Despite a thorough literature search, the candidate could not identify the motif in any inorganic assemblies either.

4.2.3 A zinc-based tetrahedral cage with cyclotricatechylene

4.2.3.1 Compound 4G – $Cs_{11}[Zn_6(OH)_3Cs_4(ctc)_4]\cdot 88H_2O$

In the investigation of uranyl assemblies, UO_2SO_4 or $UO_2(NO_3)_2$ were commonly used as sources of the uranyl ion. In addition to stocks of these uranyl salts, our laboratory possessed a mixed metal-uranyl compound of composition $UO_2Zn(OAc)_4$. Given the wide variety unusual assemblies that had been generated from the combination of uranyl ions with ctc in the presence of alkali metal cations, it was of interest to determine if the incorporation of other metal ions, such as Zn^{2+} could yield further exotic species. The ready availability of the mixed metal salt, $UO_2Zn(OAc)_4$, provided a relatively simple opportunity to determine whether a U-Zn supramolecular assembly could be easily generated. Rather than obtaining crystals of a compound containing the uranyl cation, the first ever ctc-Zn^{II} molecular tetrahedron was obtained.

An anionic metallocage of composition $[Zn_6(ctc)_4]^{12-}$ was identified within a crystalline compound of formula $Cs_{11}[Zn_6(OH)_3Cs_4(ctc)_4]\cdot 54.5H_2O$ (4G). The cage exhibits a similar connectivity to that of the vanadyl-based cage in 4A. Each Zn^{II} centre in the cage is in a square pyramidal coordination environment, as is the case with the analogous Co^{II} and Mn^{II}-based molecular tetrahedra, as well as the VO^{2+}-based tetrahedron shown at left in Figure 4.2. As with the Co^{II} and Mn^{II}-based molecular tetrahedra, previously reported within the group,[2] each crystallographically equivalent tetrahedron in 4G is directly connected to six adjacent tetrahedra via Zn–O–Zn linkages, in which the oxygen atom belongs to a μ_2 hydroxo ligand. Figure 4.24 shows one such connection between two adjacent tetrahedra.

As in 4A, within each anionic tetrahedral cage are four Cs^+ cations which occupy each of the four ctc bowls, as shown in Figure 4.24. In addition to the internal cations, four Cs^+ cations

lie between each pair of adjacent cages. Two of these Cs^+ cations (those in front of and behind the hydroxo ligand in the figure) are crystallographically identical and lie equidistant between the two cages, where they form close interactions with aromatic faces from both tetrahedra (shortest Cs^+–C separation = 3.27 Å). The coordination environment of these cations is completed by three equatorial aqua ligands.

In the previously reported Co^{II} and Mn^{II} analogues, Rb^+ and Cs^+ cations, respectively, occupy similar positions between the cages. The main difference between 4G and past examples of the hydroxo-bridged tetrahedral assemblies of ctc is that in 4G, only Cs^+ countercations are present, whereas the Co^{II} and Mn^{II} compounds each had Na^+ countercations present, in addition to either Rb^+ or Cs^+.

4G crystallises in the same space group, *Fm*-3*m*, as the Co^{II} and Mn^{II} examples, which each have α-Po (simple cubic) connectivity. Figure 4.25 indicates that the cages in 4B share the same α-Po connectivity, wherein each cage is linked to six adjacent cages in an octahedral arrangement.

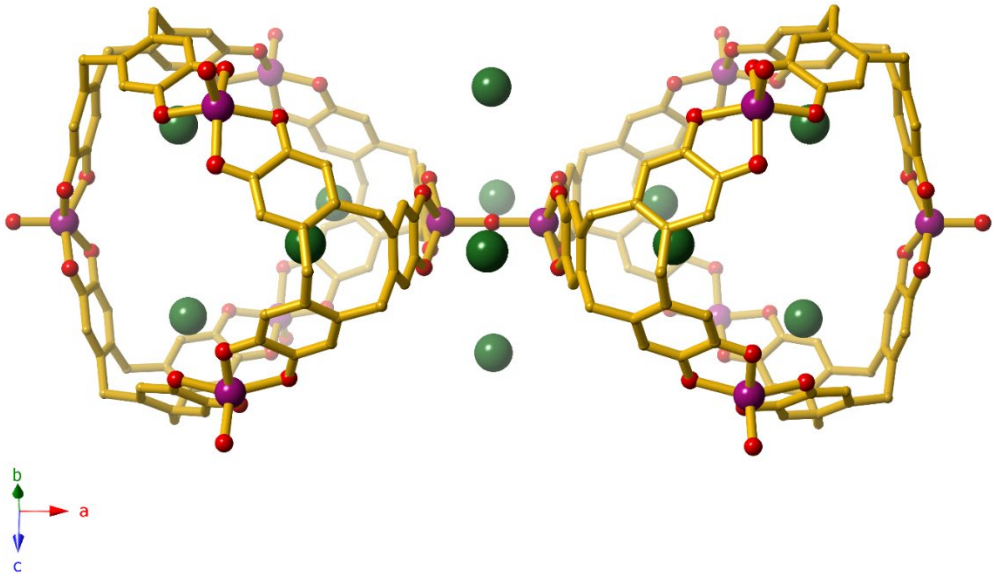

Figure 4.24 A ball and stick representation of two hydroxo-bridged molecular tetrahedra of formula $[Zn_6(OH)_3Cs_4(ctc)_4]^{15-}$ cages in compound 4G. shown in blue. Zn^{II} centres are shown as magenta spheres. Hydrogen atoms have been omitted for clarity.

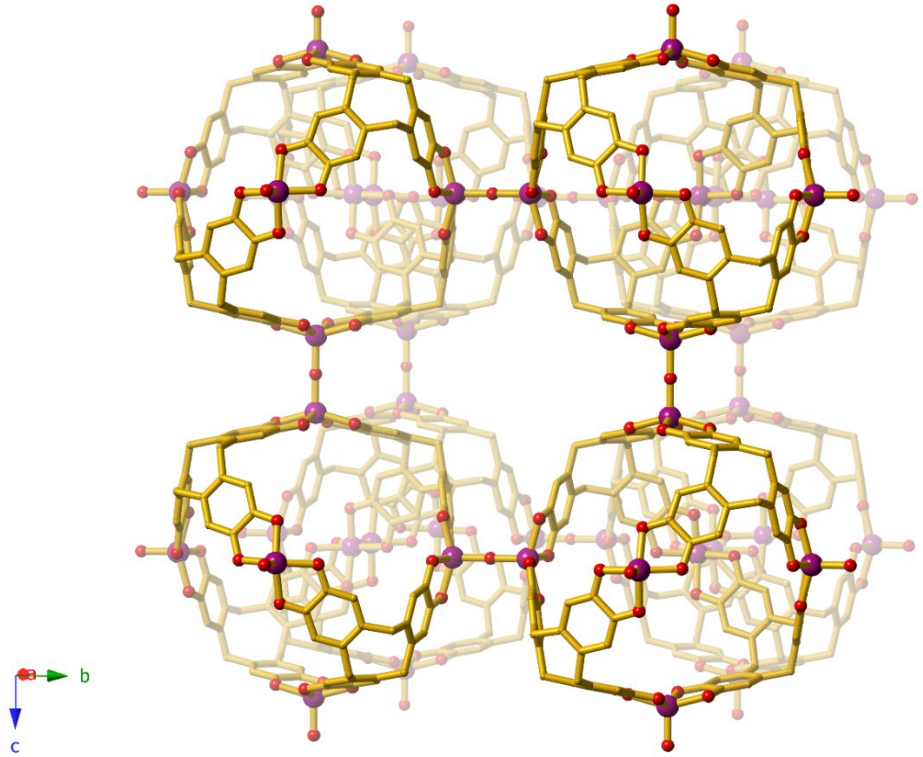

Figure 4.25 A ball and stick representation of the arrangement of the molecular tetrahedra in 4G. The cages form a 3D network which displays the connectivity of α-Po. Zn^{II} centres are shown as magenta spheres. Hydrogen atoms have been omitted for clarity.

It is perhaps unsurprising that Zn^{II}, which is an oxophilic cation with an ability to adopt square pyramidal coordination geometries, forms hydroxo bridges between tetrahedra.

In related work, Ni^{II}, which can also adopt a square pyramidal coordination geometry, was selected as a candidate to generate molecular tetrahedra that could coordinate to nitrogen donor ligands. Despite multiple attempts, crystallographic data of sufficient quality could not be obtained for crystals of a compound containing Ni^{II} and 4-styryl pyridine co-ligands. Experimental and structural details are included in the appendix to demonstrate proof-of-concept.

4.3 Concluding remarks

Chapter 4 largely focused on the generation of cage-like assemblies formed by the combination of vanadyl or uranyl ions with ctc in its hexaanionic form. In the case of the vanadyl cation, the formation of 4A, in which a tetrahedron of composition $[(VO)_6(ctc)_4]^{12-}$ was obtained, is unsurprising as this anion has been formed on numerous occasions with a range of countercations. From a geometrical perspective, the 5-coordinate square pyramidyl geometry of the V^{IV} ion would appear to be particularly well-suited to the formation of the tetrahedron because it allows the mean planes of the catecholate units bound to the V^{IV} centres to be slightly inclined to each other. This arrangement results in a reduction of the internal strain of the tetrahedron that would exist if the catecholate units were coplanar.

A similar 5-coordinate geometry for the vanadyl cation found for the tetrahedron is also apparent in the the trigonal prism ($[(VO)_9(ctc)_6]^{18-}$). This is only the second time the trigonal prism has been formed. Whilst the square pyramidal geometry of the vanadyl group is compatible with the formation of the trigonal prism ($[(VO)_9(ctc)_6]^{18-}$), entropic factors would appear to favour the tetrahedron, with the assembly of 15 components required in the case of the trigonal prism (9 vanadyl groups and 6 ctc^{6-} anions) versus 10 components in the case of the tetrahedron (6 vanadyl groups and 4 ctc^{6-} anions). This may be the reason for the apparent dominance with respect to the formation of tetrahedra. Care must be exercised in using such simplistic thermodynamic arguments because they fail to take into account the role countercations may play as structure-directing agents in the assembly of the cages. In this regard it is worth noting that both examples of trigonal prism formation have occurred in the presence of the methyltriphenylphosphonium cations.

A much wider variety of assemblies have been obtained when the uranyl ion has been employed. In all cases investigated, the oxo groups on the uranium have been in the expected *trans* arrangement leaving equatorial sites available for catecholate groups or oxygen atoms of aqua ligands or peroxo, hydroxo or oxo anions. The work has succeeded in generating two further examples of large cubic assemblies of composition $\{[UO_2(H_2O)]_{12}(ctc)_8\}^{24-}$. The ability of uranyl groups to readily form a variety of anionic aggregates involving up to six uranyl groups has resulted in considerable diversity in the cage-like assemblies.

A common theme running through the chapter is the association of Cs^+ ion with the cage-like assemblies. Cs^+ ions have been commonly found in the ctc bowls where they interact with the electron-rich aromatic surfaces of the catecholate groups. In the case of uranyl aggregates, parallel oxo groups bound to closely separated uranium centres have allowed chelation of not only Cs^+ cations, but smaller cations such as Na^+ as well.

A clear deficiency of the work described in this chapter relates to the characterisation of the uranyl-based systems. Despite considerable work devoted towards purification of the uranyl-ctc assemblies it was not possible to obtain satisfactory microanalyses to support the crystallographic work. Presumably, it is the co-precipitation of small quantities of uranyl oxo/hydroxo species that are formed not only in the initial reaction but also in subsequent recrystallisation attempts that prevent isolation of pure compounds. Time constraints have prevented further efforts by the candidate to characterise these assemblies to a point where they would be suitable for publication in the scientific literature; further work in the group is seeking to resolve issues relating to the characterisation of these assemblies. Nevertheless, the structural work has succeeded in identifying a range of fascinating supramolecular

species that may be formed from the combination of uranyl groups and the hexaanion of cyclotricatechylene.

4.4 Experimental Details

Compound 4A – $Cs_8[(VO)_6Cs_4(ctc)_4]\cdot 123H_2O$

$ctcH_6$ (24 mg, 0.065 mmol) was dissolved in acetone (1.5 mL). To this solution was added $VOSO_4$ (14.3 mg, 0.0975 mmol) dissolved in H_2O (1 mL) followed by $CsOH\cdot H_2O$ (262 mg, 1.56 mmol) in H_2O (1 mL). Green irregular rod-type crystals suitable for X-ray diffraction separated from solution after 1–2 days. Crystals were collected on a glass frit and dried at the pump. Space group: *I-43d*. Yield: 12.5 mg.

Compound 4B – $Cs_9(MePPh_3)_3[(VO)_9Cs_6(ctc)_8]\cdot 74H_2O$

$ctcH_6$ (24 mg, 0.065 mmol) was dissolved in acetone (3 mL). To this solution was added $VOSO_4$ (14.3 mg, 0.0975 mmol) dissolved in H_2O (1 mL) followed by $MePPh_3Br$ (230 mg, 0.65 mmol) in H_2O (1 mL). $CsOH\cdot H_2O$ (262 mg, 1.56 mmol) in H_2O (1 mL) was layered beneath ths solution. Crystalline green hexagonal prismatic rods suitable for X-ray diffraction separated from solution after several days. Crystals were collected on a glass frit and dried at the pump. Space group: *P*-1. Yield: 2 mg (dry, 5%). X-ray powder diffraction was performed on the bulk material, but no diffraction was observed. Visual inspection of the material indicated that crystallinity had been lost, likely as a result of solvent loss on removal from mother liquor.

Compound 4C – $Na_{24}[(UO_2(H_2O))_{12}(ctc)_8]\cdot 175H_2O$

$ctcH_6$ (24 mg, 0.065 mmol) was dissolved in acetone (3 mL). To this solution was added UO_2SO_4 (42 mg, 0.0975 mmol) in H_2O (2 mL), followed by NaOH (31.4 mg, 0.78 mmol) H_2O (1 mL). The solution was left undisturbed for several months after which time, brown

crystals suitable for X-ray diffraction were found. Space group: *Fm*-3. The compound has also been obtained from analogous reaction mixtures with 62.8 mg of NaOH and in reaction mixtures where the sulphate salt of the uranyl cation was substituted with the nitrate salt. Reactions in this family were found to contain a mixture of solid products. Maximum recorded yield of solid products = 16 mg.

Compound 4D - $Li_{24}(MePPh_3)_6[(UO_2(H_2O))_{12}(ctc)_8]Br_6 \cdot 147H_2O$

$ctcH_6$ (24 mg, 0.065 mmol) was dissolved in 1,4-dioxane (3 mL). To this solution was added $MePPh_3Br$ (116 mg, 0.325 mmol) followed by $UO_2(NO_3)_2 \cdot 6H_2O$ (24.6 mg, 0.049 mmol) in H_2O (0.5 mL), $Mn(OAc)_2$ (8.4 mg, 0.049 mmol) in H_2O (0.5 mL) and an additional 1 mL of H_2O. Finally LiOH (37.4 mg, 1.56 mmol) was added in H_2O (1 mL). After several days very dark brown polyhedral separated from solution and a suitable crystal was chosen for X-ray diffraction experiments. No further analysis was performed.

Compound 4E– $Cs_{12}[Cs_2(UO_2)_3(O)(OH)_3(ctc)]_4 \cdot 24H_2O$

$ctcH_6$ (24 mg, 0.065 mmol) was dissolved in acetone (3 mL). To this solution was added $UO_2(NO_3)_2 \cdot 6H_2O$ (33 mg, 0.065 mmol) and $Sc(NO_3)_3$ (15 mg, 0.065 mmol) in H_2O (2 mL). Beneath this solution was layered and $CsOH \cdot H_2O$ (262 mg, 1.56 mmol) H_2O (1 mL). Crystals suitable for X-ray diffraction separated after several days and a suitable single crystal was selected for X-ray diffraction experiments. Space group: $P4_2/mcm$.

Compound 4F – $Cs_{10}Na_{19}[CsNa_{0.5}(UO_2)_{10}(O)_2(OH)_8(H_2O)_2(ctc)_4]_2 \cdot 195H_2O$

$ctcH_6$ (24 mg, 0.065 mmol) was dissolved in acetone (3.5 mL). To this solution was added CsCl (25 mg, 0.15 mmol), $UO_2(NO_3)_2 \cdot 6H_2O$ (38.6 mg, 0.0975 mmol) and alloxan (20 mg,

0.125 mmol) in H_2O (1.5 mL). Beneath this solution was layered NaOH (62.4 mg, 1.56 mmol) in H_2O (1 mL). Very dark brown polyhedral crystals separated from solution after several weeks. A suitable single crystal was selected for X-ray diffraction experiments.

Compound 4G – $Cs_{11}[Zn_6(OH)_3Cs_4(ctc)_4]\cdot 88H_2O$

$ctcH_6$ (24 mg, 0.065 mmol) was dissolved in acetone (3 mL). To this solution was added $UO_2Zn(OAc)_4$ (31.6 mg, 0.065 mmol) dissolved in H_2O (1 mL) followed by $MePPh_3Br$ (116 mg, 0.325 mmol) in H_2O (1 mL). Beneath this solution was layered $CsOH\cdot H_2O$ (262 mg, 1.56 mmol). in H_2O (1 mL). Small colourless crystalline cubes suitable for X-ray diffraction separated from solution within a week. Space group: *Fm*-3*m*. The crystal structure solution indicated that no $MePPh_3^+$ was present in the compound. Attempts that were made to characterise very small crystals that formed from an analogous reaction with no $MePPh_3Br$ present were unsuccessful and as such no further analysis was performed.

4.5 Crystallographic Details

4.5.1 General data collection and refinement details

Data for 4A – 4G were collected as per the following procedures:

A single crystal suitable for X-ray crystallography was removed from the mother liquor and immediately immersed in protective oil. The crystal was mounted on a loop and placed in a stream of N_2 flowing from an Oxford CryoStream at 130 K.[16] Intensity data were collected using the phi and omega scan technique with or CuKα radiation on a SuperNova, Dual Source, Atlas diffractometer, XtaLAB Synergy, Dualflex, HyPix diffractometer or an Xcalibur Sapphire3 diffractometer.

Crystal structure solutions were obtained by direct methods using the SHELXS-2013[17] or SHELXT programs[18] (refer to CIFs in appendix for structure specific information). Structures were thereafter refined using the SHELXL-2014/7 program using a full-matrix least-squares refinement based on F2.[19] Absorption corrections were applied using the SADABS or Gaussian techniques.[20]

Crystallographic terminology is detailed in Chapter 7.

Compound 4A – $Cs_8[(VO)_6Cs_4(ctc)_4]\cdot 123H_2O$

Single crystal X-ray diffraction analysis was performed using CuKα radiation on a green rod-like crystal that was mounted on a loop. The data indicate that the crystal possessed cubic symmetry. A satisfactory structure solution and refinement was achieved in the space group *I*-43*d*. All non-hydrogen framework atoms were clearly defined and refined with anisotropic displacement parameters. All framework hydrogen atoms were placed at geometrically estimated positions and refined with isotropic displacement parameters. Crystallographically

disordered Cs^+ cations, Cs2A–Cs2B and oxygen atoms of assigned solvent molecules O1w and O2w were refined with isotropic displacement parameters.

The crystal data indicates the presence of large regions with electron density found within. Residual peaks of electron density within the framework, attributed to Cs^+ cations and solvent molecules, were apparent in the difference map. The solvent could not be modelled satisfactorily and the SQUEEZE routine from the crystallographic program *PLATON* was employed to produce a modified data set in which the solvent contribution (12,428 electrons occupying 27,613 $Å^3$ per unit cell) from the structure factors was removed. The electron density removed is consistent with 6 Cs^+ ions and 123 water molecules per tetrahedron.

Compound 4B – $Cs_4(PMePh_3)_8[(VO)_9Cs_6(ctc)_6]\cdot 74H_2O$

Single crystal X-ray diffraction analysis was performed using CuKα radiation on a green plate-like crystal that was mounted on a loop. The data indicate that the crystal possessed triclinic symmetry. A satisfactory structure solution was solution and refinement was achieved in the space group *P*-1. All non-hydrogen framework, Cs and methyltriphenylphosphonium atoms were clearly defined and refined with anisotropic displacement parameters. Cs^+-coordinated solvent molecules O52 and O53 were refined with isotropic displacement parameters. All hydrogen atoms were placed at geometrically estimated positions and refined with isotropic displacement parameters.

The crystal data indicates the presence of large intra- and extra-cage open space with electron density found within. Residual peaks of electron density within the framework channel, attributed to further solvent molecules, were apparent in the difference map. The solvent could not be modelled satisfactorily and the SQUEEZE routine from the crystallographic

program *PLATON* was employed to produce a modified data set in which the solvent contribution (2,347 electrons occupying 7,065 $Å^3$ per unit cell) from the structure factors was removed.

Compound 4C – $Na_{24}[(UO_2(H_2O))_{12}(ctc)_8]\cdot 175H_2O$

Single crystal X-ray diffraction analysis was performed using CuKα radiation on a black rhombic prism shaped crystal. The X-ray data indicate that the crystal possessed cubic symmetry and a satisfactory structure solution was solution and refinement was achieved in the space group *Fm*-3. All framework atoms that make up the uranyl-ctc assembly were clearly defined and, except for atoms O4 and O6, were refined with anisotropic displacement parameters. The countercations Na1, Na2 and Na3 were also clearly defined and refined with isotropic displacement parameters. The elevated thermal parameters for Na1 are likely due to the atom occupying large void regions that exist between the uranyl-ctc assemblies. All ctc hydrogen atoms were placed at geometrically estimated positions and refined with isotropic displacement parameters. The hydrogen atoms located on the uranium-coordinated water molecule (O6), were not assigned. The crystal data indicate the presence of regions of open space with electron density found within. Residual peaks of electron density within the framework, attributed to additional solvent molecules, were apparent in the difference map. The solvent could not be modelled satisfactorily and the SQUEEZE routine from the crystallographic program *PLATON* was employed to produce a modified data set in which the solvent contribution (6,992 electrons occupying 21,896 $Å^3$ per unit cell) from the structure factors was removed. The electron density removed is consistent with 175 water molecules per cube.

Compound 4D - $Li_{24}(MePPh_3)_6[(UO_2(H_2O))_{12}(ctc)_8]Br_6 \cdot 147H_2O$

Single crystal X-ray diffraction analysis was performed using CuKα radiation on a black block-like crystal. The X-ray data indicate that the crystal possessed trigonal symmetry and a satisfactory structure solution was obtained in the space group *R*-3. All framework atoms that make up the uranyl-ctc assembly were clearly defined and refined with anisotropic displacement parameters. The oxygen atom of the ctc-bowl water molecule, along with the methyltriphenylphosphonium and hydrated Li^+ counter cations were apparent in the difference map and could not be refined with anisotropic displacement parameters, except for atoms C108, C109, C110, C115, C116, C117, C118, C119 and the disordered oxygen atoms 9WA and 9WB. All ctc and methyltriphenyl phosphonium hydrogen atoms were placed at geometrically estimated positions and refined with isotropic displacement parameters. No hydrogen atoms located on uranium- or lithium- coordinated water molecules were assigned. The crystal data indicated the presence of regions of open space with electron density found within. Residual peaks of electron density within the framework, attributed to solvent molecules, were apparent in the difference map. The solvent could not be modelled satisfactorily and the SQUEEZE routine from the crystallographic program *PLATON* was employed to produce a modified data set in which the solvent contribution (3,235 electrons occupying 10,240 $Å^3$ per unit cell) from the structure factors was removed. The electron density removed is consistent with 108 water molecules per cube.

Compound 4E– $Cs_{12}[Cs_2(UO_2)_3(O)(OH)_3(ctc)]_4 \cdot 24H_2O$

Single crystal X-ray diffraction analysis was performed using CuKα radiation on a colourless prismatic crystal. The X-ray data indicate that the crystal possessed trigonal symmetry and a satisfactory structure solution was solution and refinement was achieved in the space group

R-3*m*. The $[(UO_2)_{12}(O)_4(OH)_{12}(ctc)_4]$ framework atoms were clearly defined and were able to be refined with anisotropic displacement parameters. All ctc hydrogen atoms were placed at geometrically estimated positions and refined with isotropic displacement parameters. OH^- and non-coordinated H_2O hydrogen atoms were not assigned. Cs^+ counter cations were apparent in the difference map and were able to be assigned, however large peaks of electron density adjacent to a number of the Cs^+ ions indicates a significant degree of disorder. Attempts to model the Cs^+ disorder resulted in an unstable refinement. The disordered arrangement of the Cs^+ ions coupled with the poorly resolved data resulted in the refined model having an elevated *R*1 value. While some non-framework water molecules, totaling 15 per cube, could be modelled, the crystal data indicated additional peaks of electron density within the framework spaces, attributed to additional solvent molecules. The solvent could not be modelled satisfactorily and the SQUEEZE routine from the crystallographic program *PLATON* was employed to produce a modified data set in which the solvent contribution (261 electrons occupying 744 $Å^3$ per unit cell) from the structure factors was removed. The electron density removed is consistent with a further 9 water molecules per cube.

Compound 4F – $Cs_{10}Na_{19}[CsNa_{0.5}(UO_2)_{10}(O)_2(OH)_8(H_2O)_2(ctc)_4]_2 \cdot 195H_2O$

Single crystal X-ray diffraction analysis was performed using CuKα radiation on a translucent, brown crystal that was block shaped. The X-ray data indicate that the crystal possessed tetragonal symmetry and a satisfactory structure solution and refinement was achieved in the space group $P4_2/mcm$. All framework atoms that make up the uranyl-ctc assembly were clearly defined and, except for atoms O5, O6, O13, O14, O15, O17, O31, O32, O34, O36, O37, C9, were refined with anisotropic displacement parameters. Crystallographically disordered Cs^+ cations, Cs3A and Cs3B were also assigned with

isotropic displacement parameters. All ctc hydrogen atoms were placed at geometrically estimated positions and refined with isotropic displacement parameters. Hydrogen atoms attributed to coordinated water molecules were not apparent in the difference map and not assigned. The crystal data indicated the presence of regions of open space with electron density found within. Residual peaks of electron density within the framework, attributed to further solvent molecules, were apparent in the difference map. The solvent could not be modelled satisfactorily and the SQUEEZE routine from the crystallographic program *PLATON* was employed to produce a modified data set in which the solvent contribution (4,131 electrons occupying 11,044 $Å^3$ per unit cell) from the structure factors was removed, corresponding to 13 Na^+ ions and 195 H_2O molecules per formula unit.

Compound 4G – $Cs_{11}[Zn_6(OH)_3Cs_4(ctc)_4]\cdot 88H_2O$

Single crystal X-ray diffraction analysis was performed using CuKα radiation on a colourless prismatic crystal that was mounted on a loop. The data indicate that the crystal possessed cubic symmetry. A satisfactory structure solution and refinement was achieved in the space group *Fm*-3*m*. All non-hydrogen framework atoms and 12 of the 15 Cs^+ ions were clearly defined and refined with anisotropic displacement parameters. All framework hydrogen atoms were placed at geometrically estimated positions and refined with isotropic displacement parameters. The crystal data indicated the presence of large spaces with electron density found within. The oxygen atoms of eight, part occupancy water molecules (totaling 51.5 H_2O per cage) could be modelled and refined with anisotropic displacement parameters. Residual peaks of electron density within the framework spaces, attributed to further solvent molecules, were apparent in the difference map. The solvent could not be

modelled satisfactorily and the SQUEEZE routine from the crystallographic program *PLATON* was employed to produce a modified data set in which the solvent contribution (4,209 electrons occupying 16,294 $Å^3$ per unit cell) from the structure factors was removed. The electron density removed is consistent with 3 Cs^+ ions and 37 water molecules per unit formula.

4.6 Crystallographic Tables

Crystal data and structure refinement for compound 4A

Empirical formula	$C_{126}H_{334}Cs_{18}O_{180}V_9$	
Formula weight	7580.75	
Temperature	130(1) K	
Wavelength	1.54184 Å	
Crystal system	Cubic	
Space group	*I*-43*d*	
Unit cell dimensions	a = 37.9039(6) Å	α= 90°.
	b = 37.9039(6) Å	β= 90°.
	c = 37.9039(6) Å	γ = 90°.
Volume	54457(3) $Å^3$	
Z	8	
Density (calculated)	1.849 Mg/m^3	
Absorption coefficient	21.930 mm^{-1}	
F(000)	29816	
Crystal size	0.33 x 0.09 x 0.05 mm^3	
Theta range for data collection	3.298 to 73.657°.	
Index ranges	$-15 \le h \le 46$, $-12 \le k \le 27$, $-8 \le l \le 45$	
Reflections collected	21330	
Independent reflections	7550 [R(int) = 0.0600]	
Completeness to theta = 67.684°	99.8 %	
Absorption correction	Semi-empirical from equivalents	
Max. and min. transmission	1.0 and 0.32	
Refinement method	Full-matrix least-squares on F^2	
Data / restraints / parameters	7550 / 0 / 297	
Goodness-of-fit on F^2	1.025	
Final R indices [I>2sigma(I)]	$R1$ = 0.0854, $wR2$ = 0.2232	
R indices (all data)	$R1$ = 0.0975, $wR2$ = 0.2399	
Absolute structure parameter	0.5	
Largest diff. peak and hole	1.433 and -0.628 e.$Å^{-3}$	

Crystal data and structure refinement for compound 4B

Empirical formula	$C_{366}H_{544}Cs_{30}O_{238}P_6V_{18}$	
Formula weight	13842.02	
Temperature	130(1) K	
Wavelength	1.54184 Å	
Crystal system	Triclinic	
Space group	*P*-1	
Unit cell dimensions	a = 20.2025(3) Å	α= 75.8670(10)°.
	b = 22.0964(2) Å	β= 75.6090(10)°.
	c = 36.6007(4) Å	γ = 69.8320(10)°.
Volume	14628.2(3) Å^3	
Z	1	
Density (calculated)	1.571 Mg/m^3	
Absorption coefficient	17.513 mm^{-1}	
F(000)	6798	
Crystal size	0.711 x 0.214 x 0.118 mm^3	
Theta range for data collection	3.087 to 76.760°.	
Index ranges	$-25 \le h \le 24$, $-27 \le k \le 27$, $-43 \le l \le 46$	
Reflections collected	157026	
Independent reflections	60772 [R(int) = 0.0370]	
Completeness to theta = 67.684°	99.9 %	
Absorption correction	Semi-empirical from equivalents	
Max. and min. transmission	1.00000 and 0.51378	
Refinement method	Full-matrix least-squares on F^2	
Data / restraints / parameters	60772 / 0 / 2232	
Goodness-of-fit on F^2	1.882	
Final R indices [I>2sigma(I)]	R1 = 0.1323, wR2 = 0.4008	
R indices (all data)	R1 = 0.1482, wR2 = 0.4258	
Largest diff. peak and hole	4.767 and -4.928 e.Å^{-3}	

Crystal data and structure refinement for compound 4C

Empirical formula	$C_{168}H_{462}Na_{24}O_{259}U_{12}$	
Formula weight	10035.47	
Temperature	130(1) K	
Wavelength	1.54184 Å	
Crystal system	Cubic	
Space group	*Fm*-3	
Unit cell dimensions	a = 34.325(1) Å	α= 90°.
	b = 34.325(1) Å	β= 90°.
	c = 34.325(1) Å	γ = 90°.
Volume	40441(5) $Å^3$	
Z	4	
Density (calculated)	1.648 Mg/m^3	
Absorption coefficient	14.495 mm^{-1}	
F(000)	19640	
Crystal size	0.11 x 0.10 x 0.04 mm^3	
Theta range for data collection	3.642 to 70.986°.	
Index ranges	$-41 \le h \le 28$, $-22 \le k \le 38$, $-13 \le l \le 38$	
Reflections collected	6940	
Independent reflections	3389 [*R*(int) = 0.0483]	
Completeness to theta = 67.684°	99.3 %	
Absorption correction	Semi-empirical from equivalents	
Max. and min. transmission	1.0 and 0.58	
Refinement method	Full-matrix least-squares on F^2	
Data / restraints / parameters	3389 / 0 / 105	
Goodness-of-fit on F^2	0.961	
Final *R* indices [*I*>2sigma(*I*)]	*R*1 = 0.0830, *wR*2 = 0.2656	
R indices (all data)	*R*1 = 0.1044, *wR*2 = 0.2872	
Largest diff. peak and hole	1.429 and -1.325 $e.Å^{-3}$	

Crystal data and structure refinement for compound 4D

Empirical formula	$C_{282}H_{498}Br_6Li_{24}O_{231}P_6U_{12}$	
Formula weight	11272.97	
Temperature	130(1) K	
Wavelength	1.54184 Å	
Crystal system	Trigonal	
Space group	*R*-3:*H*	
Unit cell dimensions	*a* = 34.7002(5) Å	α= 90°.
	b = 34.7002(5) Å	β= 90°.
	c = 32.5998(5) Å	γ = 120°.
Volume	33994(1) $Å^3$	
Z	3	
Density (calculated)	1.652 Mg/m^3	
Absorption coefficient	13.539 mm^{-1}	
F(000)	16542	
Crystal size	0.114 x 0.080 x 0.066 mm^3	
Theta range for data collection	3.084 to 73.977°.	
Index ranges	$-41 \le h \le 41$, $-33 \le k \le 43$, $-39 \le l \le 15$	
Reflections collected	25923	
Independent reflections	14778 [*R*(int) = 0.0247]	
Completeness to theta = 67.684°	99.6 %	
Absorption correction	Semi-empirical from equivalents	
Max. and min. transmission	1.000 and 0.898	
Refinement method	Full-matrix least-squares on F^2	
Data / restraints / parameters	14778 / 6 / 870	
Goodness-of-fit on F^2	1.078	
Final *R* indices [*I*>2sigma(*I*)]	*R*1 = 0.0436, *wR*2 = 0.1163	
R indices (all data)	*R*1 = 0.0528, *wR*2 = 0.1241	
Largest diff. peak and hole	2.062 and -1.515 e.$Å^{-3}$	

Crystal data and structure refinement for compound 4E

Empirical formula	$C_{84}H_{78}Cs_{20}O_{83.5}U_{12}$	
Formula weight	7938.02	
Temperature	130(1) K	
Wavelength	1.54184 Å	
Crystal system	Trigonal	
Space group	*R*-3*m*:*H*	
Unit cell dimensions	*a* = 22.8967(8) Å	α= 90°.
	b = 22.8967(8) Å	β= 90°.
	c = 65.16(1) Å	γ = 120°.
Volume	29582(5) $Å^3$	
Z	6	
Density (calculated)	2.673 Mg/m^3	
Absorption coefficient	56.324 mm^{-1}	
F(000)	20724	
Crystal size	0.3 x 0.2 x 0.1 mm^3	
Theta range for data collection	3.511 to 59.990°.	
Index ranges	$-10 \le h \le 23$, $-25 \le k \le 9$, $-73 \le l \le 64$	
Reflections collected	18578	
Independent reflections	5314 [*R*(int) = 0.0790]	
Completeness to theta = 59.990°	99.9 %	
Absorption correction	Semi-empirical from equivalents	
Max. and min. transmission	1.0 and 0.28	
Refinement method	Full-matrix least-squares on F^2	
Data / restraints / parameters	5314 / 0 / 344	
Goodness-of-fit on F^2	1.101	
Final *R* indices [*I*>2sigma(*I*)]	*R*1 = 0.1075, *wR*2 = 0.3012	
R indices (all data)	*R*1 = 0.1488, *wR*2 = 0.3376	
Largest diff. peak and hole	2.974 and -3.575 $e.Å^{-3}$	

Crystal data and structure refinement for compound 4F

Empirical formula	$C_{168}H_{413}Cs_{12}Na_{20}O_{321}U_{20}$	
Formula weight	14377.28	
Temperature	130(1) K	
Wavelength	1.54184 Å	
Crystal system	Tetragonal	
Space group	$P4_2/mcm$	
Unit cell dimensions	a = 24.6795(4) Å	α= 90°.
	b = 24.6795(4) Å	β= 90°.
	c = 35.216(1) Å	γ = 90°.
Volume	21449(1) Å^3	
Z	2	
Density (calculated)	2.226 Mg/m^3	
Absorption coefficient	29.984 mm^{-1}	
F(000)	13410	
Crystal size	0.07 x 0.05 x 0.04 mm^3	
Theta range for data collection	3.582 to 74.100°.	
Index ranges	$-30 \le h \le 21$, $-29 \le k \le 26$, $-41 \le l \le 20$	
Reflections collected	37055	
Independent reflections	11129 [R(int) = 0.0754]	
Completeness to theta = 67.684°	99.1 %	
Absorption correction	Semi-empirical from equivalents	
Max. and min. transmission	1.0 and 0.66	
Refinement method	Full-matrix least-squares on F^2	
Data / restraints / parameters	11129 / 1 / 373	
Goodness-of-fit on F^2	0.910	
Final R indices [I>2sigma(I)]	$R1$ = 0.0899, $wR2$ = 0.2468	
R indices (all data)	$R1$ = 0.1308, $wR2$ = 0.2789	
Largest diff. peak and hole	6.160 and -3.854 e.Å^{-3}	

Crystal data and structure refinement for compound 4G

Empirical formula	$C_{168}H_{352}Cs_{30}O_{230}Zn_{12}$	
Formula weight	10824.21	
Temperature	130(1) K	
Wavelength	1.54184 Å	
Crystal system	Cubic	
Space group	*Fm*-3*m*	
Unit cell dimensions	*a* = 35.9801(5) Å	α= 90°.
	b = 35.9801(5) Å	β= 90°.
	c = 35.9801(5) Å	γ = 90°.
Volume	46578 (1) $Å^3$	
Z	4	
Density (calculated)	1.544 Mg/m^3	
Absorption coefficient	19.414 mm^{-1}	
F(000)	20840	
Crystal size	0.06 x 0.03 x 0.03 mm^3	
Theta range for data collection	3.474 to 73.913°.	
Index ranges	$-38 \le h \le 44$, $-44 \le k \le 37$, $-31 \le l \le 44$	
Reflections collected	47812	
Independent reflections	2358 [*R*(int) = 0.1226]	
Completeness to theta = 67.684°	99.9 %	
Absorption correction	Semi-empirical from equivalents	
Max. and min. transmission	1.0 and 0.35	
Refinement method	Full-matrix least-squares on F^2	
Data / restraints / parameters	2358 / 0 / 78	
Goodness-of-fit on F^2	1.369	
Final R indices [*I*>2sigma(*I*)]	*R*1 = 0.1301, *wR*2 = 0.3485	
R indices (all data)	*R*1 = 0.1634, *wR*2 = 0.3836	
Largest diff. peak and hole	4.043 and -0.918 $e.Å^{-3}$	

4.7 References

[1] B. F. Abrahams, B. A. Boughton, N. J. FitzGerald, J. L. Holmes, R. Robson, *Chem. Commun.* **2011**, *47*, 7404–7406.

[2] B. F. Abrahams, N. J. FitzGerald, R. Robson, *Angew. Chemie - Int. Ed.* **2010**, *49*, 2896–2899.

[3] N. J. FitzGerald, Supramolecular Assemblies from Catechol-Based Ligands, PhD Thesis, The University of Melbourne, **2010**.

[4] J. L. Holmes, Supramolecular Structures of Cyclotricatechylene, MSc Thesis,The University of Melbourne, **2011**.

[5] S. Tsushima, A. Suzuki, *J. Mol. Struct. THEOCHEM* **2000**, *529*, 21–25.

[6] P. C. Burns, *Mineral. Mag.* **2011**, *75*, 1–25.

[7] K. E. Knope, L. Soderholm, *Chem. Rev.* **2013**, *113*, 944–994.

[8] D. L. Clark, S. D. Conradson, R. J. Donohoe, D. W. Keogh, D. E. Morris, P. D. Palmer, R. D. Rogers, C. D. Tait, *Inorg. Chem.* **1999**, *38*, 1456–1466.

[9] C. Ni, D. K. Shuh, K. N. Raymond, *Chem. Commun.* **2011**, *47*, 6392–6394.

[10] Q. Zhang, B. Jin, R. Peng, S. Lei, S. Chu, *Polyhedron* **2015**, *87*, 417–423.

[11] Q. Zhang, B. Jin, Z. Shi, X. Wang, Q. Liu, S. Lei, R. Peng, *Sci. Rep.* **2016**, *6*, 1–12.

[12] J. L. Holmes, B. F. Abrahams, A. Ahveninen, B. A. Boughton, T. A. Hudson, R. Robson, D. Thinagaran, *Chem. Commun.* **2018**, *54*, 11877–11880.

[13] M. Nyman, M. a Rodriguez, C. F. Campana, *Inorg. Chem.* **2010**, *49*, 7748–55.

[14] M. Nyman, T. M. Alam, *J. Am. Chem. Soc.* **2012**, *134*, 20131–20138.

[15] S. Hickam, S. M. Aksenov, M. Dembowski, S. N. Perry, H. Traustason, M. Russell, P. C. Burns, *Inorg. Chem.* **2018**, *57*, 9296–9305.

[16] J. Cosier, A. M. Glazer, *J. Appl. Crystallogr.* **1986**, *19*, 105–107.

[17] G. M. Sheldrick, *Acta Crystallogr. Sect. A Found. Crystallogr.* **2008**, *64*, 112–122.

[18] G. M. Sheldrick, *Acta Crystallogr. Sect. A Found. Adv.* **2015**, *71*, 3–8.

[19] G. M. Sheldrick, *Acta Crystallogr. Sect. C Struct. Chem.* **2015**, *71*, 3–8.

[20] *CrysAlisPro 1.171.40.36a, Rigaku Oxford Diffraction/Agilent Technol. UK Ltd* **2018**.

Chapter 5 A tetrahedral silicon-based assembly of cyclotricatechylene

Contents

5.1 Introduction

In the preceding chapters, cyclotricatechylene supramolecular species involving metal ions from the *s*, *d* and *f*-blocks of the periodic table have been described. In these assemblies the association between the *tris*(catechol) ligand and metal centres has included both ionic and coordinate interactions. Ionic and coordinate bonds are commonly labile and therefore discrete species in solution are often subject to exchange processes which limit the lifetime of a cage in solution. Rapid exchange of cage components is potentially problematic in cases where intra-cage chemical processes involving guest species requires the cage to remain intact for periods longer than the exchange rate of cage components.

One approach to generate more robust ctc cages that will exhibit longer lifetimes in solution is to exploit covalent interactions between the ctc anion and *p*-block elements to create assemblies that geometrically resemble the cages formed from coordinate bonds e.g. $[(VO)_6(ctc)_4]^{12-}$. In this chapter the synthesis, structure and characterisation of an anionic cage of composition, $[(PhSi)_6(ctc)_4]^{6-}$ is described in which Si–O bonds hold this 10-component assembly together.

The research described in this chapter was published in *Chemical Communications* in 2018 and the final version of the accepted manuscript is reproduced below in Sections 5.2 and 5.3. This chapter is presented in accordance with the University of Melbourne's guidelines relating to thesis submission with publication. The supporting information relating to this manuscript is presented in Sections 5.4 and 5.5.

5.2 Self-Assembly of a Si-based Cage by the Formation of 24 Equivalent Covalent Bonds

Jessica L. Holmes,[a] Brendan F. Abrahams,[a] Anna Ahveninen,[a] Berin A. Boughton,[b] Timothy A. Hudson,[a] Richard Robson[a] and Dinaiz Thinagaran[b]

a School of Chemistry, University of Melbourne, Parkville, Victoria 3010, Australia
b Metabolomics Australia, School of Biosciences, University of Melbourne, Parkville, Victoria 3010, Australia

A robust, nano-sized covalent cage, of composition, $[(PhSi)_6(ctc)_4]^{6-}$ (H_6ctc = cyclotricatechylene) has been prepared in a simple reaction in good yield. The tetrahedral anionic cage is stable in both the solid and solution state and exhibits an affinity for Cs^+ ions which bind to the internal surface of the cage.

Molecular cages have been the focus of considerable interest for their potential to encapsulate guest species,[1,2] deliver drugs[3,4] and catalyse reactions within their cavities.[5-7] Some of the most elegant cages extend back to the mid-1980s and include Cram's beautifully designed carcerands[8,9] and Saalfrank's adamantoid assembly in which four Mg^{II} centres are bridged by chelating ligands.[10] Fujita successfully used coordinate bonds in the 1990's to form a variety of nanoscale shell-like metal-ligand assemblies.[11] Since then, numerous researchers have exploited the reversibility of the coordinate bond to generate self-assembled 'metallocages'.[12-20] In contrast to covalent cages, metallocages commonly involve the assembly of a large number of components. For example, a cage of composition $Pd_{30}L_{60}$ (L = a boomerang-shaped bipyridyl ligand), yielded a sphere-like cage large enough to enclose proteins.[21] Of particular relevance to the work reported here is a family of cyclotriveratrylene-based metallocages reported by Hardie.[22] Interest in metallocages extends to properties relating to redox activity, magnetism and host behaviour.[20,23,24]

The combination of the bowl-shaped tris-catechol ligand, cyclotricatechylene ($ctcH_6$, I) with appropriate metal cations has led to the self-assembly of various metallocages e.g. the tetrahedral anionic cages, $[(VO)_6(ctc)_4]^{12-}$ and $[M_6(ctc)_4]^{12-}$ (M = Co^{2+}, Cu^{2+}).[25] A particularly interesting aspect of these cages is their affinity for large alkali metal cations i.e. caesium and rubidium, which associate with the internal aromatic surfaces of these anionic assemblies. In addition to the vanadyl example, other metal centres also yield structurally similar tetrahedral cages of composition, $[M_6(ctc)_4]^{12-}$ (M = Co^{2+}, Cu^{2+}).[25,26] The cavities of the $[M_6(ctc)_4]^{12-}$cages are large enough to encapsulate multiple molecules/ions. Difficulties in handling and purifying these compounds, especially with respect to the separation from amorphous co-precipitates, make the isolation of bulk products challenging. Furthermore, attempts to recrystallise these cage-like compounds have been, generally, unsuccessful. When the copper and vanadyl-based tetrahedra were dissolved in various solvents they were unable to be detected in electrospray ionization mass spectrometric (ESI-MS) analyses. This is possibly due to the instability of the cage in solution or a consequence of the electrospray ionization process. The general lability of coordinate bonds is known to make many metal-ligand assemblies susceptible to exchange processes.[24,27,28] The instability of many metallocages in solution impacts upon the ability to analyse such species using solution NMR and ESI-MS.[29] In order to overcome challenges associated with lability, the Fujita group has employed sophisticated characterization techniques such as cold-spray ionization mass spectrometry.[30,31] It should be recognised however that there are cages, assembled using coordinate bonds, which are robust and amenable to investigation by ESI-MS. Examples include the beautiful symmetric cages of Li and co-workers involving chelating ligands.[32-34]

Thus, whilst metal-ligand assemblies can provide outstanding examples of highly symmetric and open-type architectures, the lability of the coordinate bond can impact upon the stability of the cages in solution. Cages in which all links are covalent may be expected to be much more robust. Examples of covalent cages pertinent to this current work have been reported by the Collet, Canceill, Dutasta and Brotin groups.[35-40]

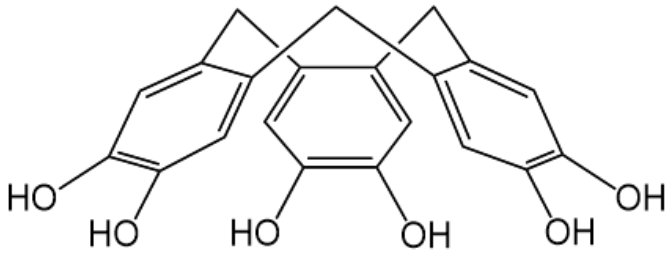

I

One approach we have begun to explore for the synthesis of cages and macrocycles is to employ tri- and tetravalent elements such as boron and silicon in place of transition metals to yield products in which all bonds are covalent. We have reported that the reaction of trimethoxyborane with the bis-catechol 3,3,3',3'-tetramethyl-1,1'-spirobisindane-5,5',6,6'-tetrol (H_4spiro) leads to the formation of macrocyclic organoborate triangles and squares.[41,42] ESI-MS analysis confirms the presence of these covalent macrocyclic species. Of particular importance to the work described here, Shea and coworkers were able to link four spiro^{4-} units into a macrocycle by reaction with phenyltriethoxysilane ($PhSi(OEt)_3$) under basic conditions.[43] On the basis of NMR, Shea proposed four pentacoordinate square pyramidal silicon centres within a molecular square of composition $[(PhSi)_4spiro_4]^{4-}$. By using a similar synthetic approach we hoped to generate covalent tetrahedral cage-like species resembling the metal-based cages described above.

Herein we report an anionic covalent cage, $[(PhSi)_6(ctc)_4]^{6-}$, structurally similar to the aforementioned tetrahedral cages. The cage was generated through the reaction of $ctcH_6$ with phenyltriethoxysilane under basic conditions and possesses the anticipated pentacoordinate square pyramidal Si^{IV} centres. The compound was formed in a yield of 51% (46.5 mg).

The assembly process involves the combination of ten components, four ctc anions and six PhSi units through the remarkable formation of 24 equivalent covalent bonds. As indicated above, there are many examples of metal-ligand cages in which large numbers of components undergo self-assembly through the coordinate bonds, however it is far less common to have so many new covalent bonds formed in the self-assembly process.

The compound, $(NEt_4)_4(HNEt_3)_4[(PhSi)_6(ctc)_4]Br_2 \cdot$solvate (solvate = DMF/EtOAc) forms as large yellow crystals, typically with dimensions of ~0.7 mm. A fragment of one such crystal was structurally characterized by single crystal X-ray diffraction, which indicated the adoption of the cubic space group, *F*-43*m*. The compound was further characterized by ESI-MS and NMR.

The $[(PhSi)_6(ctc)_4]^{6-}$ cage (Fig. 1) closely resembles the previously reported $[(VO)_6(ctc)_4]^{12-}$ metallocages, in which the vanadium centres are also 5-coordinate and the apical substituents, oxo groups, are oriented outwards.[25] In this present case a phenyl group, also oriented outwards, is bound to each silicon centre. Each of the four ctc units in this covalently bonded assembly has been fully deprotonated at its phenolic oxygen atoms and serves as a vertex of the tetrahedron. A Si^{IV} centre is located at the midpoint of each edge of the tetrahedron and acts as a two-connecting bridge between the catecholate units.

The phenyl groups on the pentacoordinate silicon centres are rotationally disordered over two positions. The Si centres lie at the corners of a regular octahedron of edge length 9.5 Å. All

six Si centres are located on the surface of a sphere of diameter 13.4 Å. The diameter of the anionic molecule, defined by the maximum separation of the van der Waals surfaces of opposing phenyl groups, is 2.71 nm.

All tetrahedra are crystallographically identical, with the asymmetric unit including one sixth of a ctc^{6-} unit. The cages pack in a face centred cubic arrangement with six phenyl groups from adjacent $[(PhSi)_6(ctc)_4]^{6-}$ cages directed towards the octahedral holes.

The tetraethylammonium and triethylammonium countercations are highly disordered and cannot be unambiguously identified from the structure determination. Their presence and ratios were confirmed by ESI-MS and NMR analyses of isolated crystals that had been re-dissolved. Crystallographically disordered bromide ions (two per cage) lie between the anionic cages. A similar incorporation of halide ions was observed in the crystal structure of $Na_8[(CH_3(n\text{-}C_5H_{12})]_6[Cu_6(ctc)_4]I_2 \cdot$hydrate.

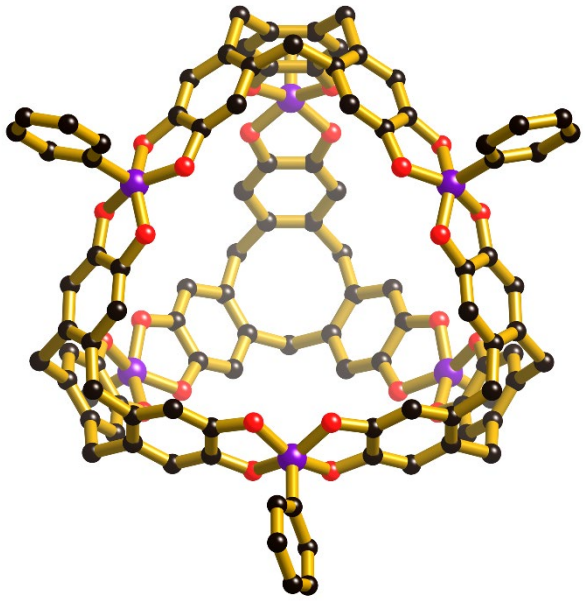

Fig. 1 A view of the $[(PhSi)_6(ctc)_4]^{6-}$ tetrahedral cage. The silicon centres are represented by purple spheres. The phenyl rings are disordered over two positions but have been represented in one orientation only. The three phenyl rings pointing into the page have been omitted for clarity, except for the phenyl carbon atom bound to the silicon. Hydrogen atoms have been also omitted for clarity.

Solution state ^{1}H NMR (d_6DMSO) spectroscopy confirms the tetraethylammonium and triethylammonium cations to be present in the crystals in the ratio of 4:4:cage. The NMR studies also showed the presence of both DMF and ethyl acetate. When the crystals were air dried on a glass frit, the ethyl acetate was lost (as indicated by NMR and TGA studies). The ^{1}H NMR spectra are consistent with the presence of the cage upon dissolution.

High resolution direct infusion ESI-FT-ICR mass spectrometry was performed in negative ionization mode using approximately 3-4 crystals of the silicon-based cage which were dissolved in < 1 mL of DMF and diluted with acetone (~10 mL). The dominant peaks correspond to [cage + $(Et_4N)_4]^{2-}$ (*m/z* 1296.49046, -2.72 ppm error) and [cage + $(Et_4N)_3]^{3-}$ (*m/z* 820.94623, 2.23 ppm error) adducts associating with four and three tetraethlyammonium cations respectively. The observed isotopic peak profiles for the [cage + $(Et_4N)_4]^{2-}$ and [cage + $(Et_4N)_3]^{3-}$ species matched very closely (mSigma 17.0 and mSigma 10.2 respectively, a measure of overall fit) to the predicted isotopic peak profiles confirming the assignment. Further, lower abundant species were observed also where one or more tetraethylammonium cations had been substituted with triethylammonium cations. In particular, the following species were apparent: [cage + $(Et_4N)_3(Et_3NH)]^{2-}$ (*m/z* 1282.47689) and [cage + $(Et_4N)_2(Et_3NH)_2]^{2-}$ (*m/z* 1268.46409) The spectra suggest that the cage prefers to associate with the tetraethylammonium ion, at least in the gas phase. The presence of the crystallographically disordered bromide anions in the crystal structure was also confirmed using MS, although there is no evidence of association with the cage.

As indicated above, mass spectrometric analysis of several ctc-derived tetrahedral metallocages, in which ligands bind to metal centres through coordinate bonds, have been performed by our group in the past without successful detection of the anionic cages. The

results reported in this current study however, provide a strong indication that mass spectrometry will be a useful tool for the study of derivatives and inclusion compounds of this type of covalent cage in the gas phase.

In order to assess the stability of the compound, crystals of the cage compound were immersed in boiling water for 30 minutes during which time the surface of the crystals showed some discolouration and the water turned a pale brown. Whilst inspection of the crystals revealed some cracking, single crystal X-ray analysis revealed the original face-centred cubic unit cell. Although the quality of the diffraction data was inferior to that of the original crystals, it was possible to obtain a crude structural solution. The crystalline material was dissolved in DMSO/MeCN and analysed by ESI-FT-ICR mass spectrometry with dominant peaks associated with the species, $[\text{cage} + (Et_4N)_3]^{3-}$ and $[\text{cage} + (Et_4N)_2]^{2-}$ (Fig. S7 and Table S2). Clearly the cage is remarkably robust, a feature that may allow its use as a host molecule in a wide variety of applications.

Cyclotricatechylene in either its coordinated form or in its various protonated forms exhibits a clear affinity for Cs^+ ions, which commonly associate with the internal surface of the aromatic rings that form the bowl-like cavity.[25,44] Although crystals of $(NEt_4)_4(HNEt_3)_4[(PhSi)_6(ctc)_4]Br_2\cdot$solvate are insoluble in water, the relatively large inter-cage spaces prompted an investigation to determine if Cs^+ ions could permeate through the solvent filled regions of the crystal and perhaps associate with the cyclotricatechylene units. When crystals of $(NEt_4)_4(HNEt_3)_4[(PhSi)_6(ctc)_4]Br_2\cdot$solvate are immersed in 2 mL of an aqueous solution containing 30 mg of CsBr for three days the crystallinity of the material is found to be preserved. Single crystal structural analysis indicates the same space group as the original crystals, with cubic cell lengths ~0.2 Å shorter than that of the original crystals.

Structure solution and refinement clearly show the $[(PhSi)_6(ctc)_4]^{6-}$ cage. Analysis of the Fourier difference maps reveals a large peak of electron density in the bowl-like cavity of each cyclotricatechylene unit within the cage. This peak was assigned as a Cs atom and its position and site occupancy were allowed to refine. Structural refinements indicated a site occupancy greater than 90% and in subsequent refinements the Cs atom was assigned full site occupancy. The Cs^+ ions are located on sites of 3*m* symmetry and associate with the aromatic carbon atoms of the cyclotricatechylene units (Cs···C 3.607-3.848 Å) as indicated in Fig. 2. Peaks of electron density lying towards the centre of the cage were assigned as oxygen atoms of disordered water molecules bound to the Cs^+ ions. Cs^+ ions are found to occupy similar sites in the related $[(VO)_6(ctc)_4]^{12-}$ cages.[25]

When the crystals soaked in the aqueous CsBr solution are dissolved in DMF and MeCN and the solution investigated using ESI-MS, a large number peaks in the spectrum are apparent indicating the presence of the cage accompanied by a variety of cations. The dominant species in the spectrum corresponds to $[cage + (Et_4N)_2 + Cs]^{3-}$. The spectrum is presented in the ESI (Fig. S9 and Table S3).

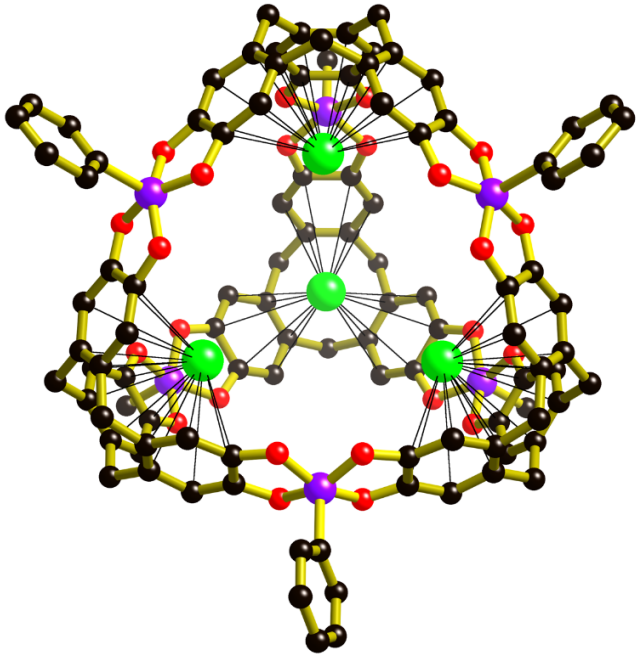

Fig. 2 The $[(PhSi)_6(ctc)_4]^{6-}$ cage with Cs^+ ions (green) located in each of the bowl-like cavities of the four ctc ligands. The fine black lines represent C···Cs contacts. Only a single orientation of each of the phenyl rings is indicated. The three phenyl rings pointing into the page have been omitted for clarity, except for the phenyl carbon atom bound to the silicon. Hydrogen atoms have also been omitted for clarity.

5.2.1 Conclusions

In summary, anionic tetrahedral assemblies are generated by covalently linking cyclotricatechylene anions with phenylsilane to form a crystalline product of composition $[(NEt_4)_4(HNEt_3)_4[(PhSi)_6(ctc)_4]Br_2 \cdot$solvate. Crystals of the compound are not only simple to synthesise and isolate but are also robust as indicated by their ability to survive in boiling water. The $[(PhSi)_6(ctc)_4]^{6-}$ cages themselves have been shown to exist in the solution state and the gas phase as indicated by NMR and mass spectrometry. The size, shape and robustness of the cage make it an outstanding candidate for further study as a host molecule for intra-cage reactions, and for guest encapsulation and exchange studies. Furthermore, the cage can be studied easily by common techniques such as NMR and mass spectrometry in order to probe its inclusion chemistry.

A potentially rich vein of future research relates to the introduction of different groups at the apical coordination site of the Si centre, which in this current work is occupied by the phenyl group. The inclusion of various groups at this site has the potential to alter the solubility of the cage, or in the case of charged groups such as alkyl pyridiniums, modify the net charge of the cage. The attachment of metal binding groups, extending outwards from the cage, may permit the cage to serve as a 6-connecting octahedral unit in a 3D coordination network. The resulting material would possess intra- and inter-cage spaces which could be expected to offer fascinating host properties. Clearly, there are outstanding opportunities for introducing a wide variety of functionality by exploiting this fifth site on the Si centre.

The authors gratefully acknowledge the financial support of the Australian research Council.

5.2.2 Conflicts of interest

There are no conflicts of interest to declare.

5.2.3 Notes and references

Crystal data for $[N(C_2H_5)_4]_4[HN(C_2H_5)_3]_4[(C_6H_5Si)_6(C_{21}H_{12}O_6)_4]Br_2 \cdot 4(C_3H_7NO) \cdot 6(C_4H_8O_2)$, $C_{220}H_{314}Br_2N_{12}O_{44}Si_6$, M = 3982.97, cubic, a = 27.9568(6) Å, U = 21850.5(14) Å^3, T = 130(1) K, space group F-43m (no. 216), Z = 4, 3975 reflections measured, 1510 unique (R_{int} = 0.0216), which were used in all calculations. The final $wR(F^2)$ was 0.2300 (all data); the final $wR(F)$ was 0.0773 ($I > 2\sigma(I)$). Crystallographic information has been deposited with the CCDC (1575718).

Crystal data for $[N(C_2H_5)_4]_4Cs_4[(C_6H_5Si)_6(C_{21}H_{12}O_6)_4]Br_2 \cdot 70H_2O$, $C_{152}H_{298}Br_2Cs_4N_4O_{94}Si_6$, M = 4545.93, cubic, a = 27.7206(7) Å, U = 21301.4(16) Å^3, T = 130(1) K, space group F-43m (no. 216), Z = 4, 5561 reflections measured, 1670 unique (R_{int} = 0.0380), which were

used in all calculations. The final $wR(F^2)$ was 0.2864 (all data); the final $wR(F)$ was 0.1023 ($I > 2\sigma(I)$). Crystallographic information has been deposited with the CCDC (1860473).

1 H. Amouri, C. Desmarets and J. Moussa, *Chem. Rev.*, 2012, **112**, 2015-2041.

2 F. Hof, S. L. Craig, C. Nuckolls and J. J. Rebek, *Angew. Chem. Int. Ed.*, 2002, **41**, 1488-1508.

3 N. Ahmad, H. A. Younus, A. H. Chughtai and F. Verpoort, *Chem. Soc. Rev.*, 2015, **44**, 9-25.

4 J. E. M. Lewis, E. L. Gavey, S. A. Cameron and J. D. Crowley, *Chem. Sci.*, 2012, **3**, 778-784.

5 M. Yoshizawa, J. K. Klosterman and M. Fujita, *Angew. Chem. Int. Ed.*, 2009, **48**, 3418-3438.

6 Y. Inokuma, M. Kawano and M. Fujita, *Nat. Chem.*, 2011, **3**, 349.

7 C. J. Hastings, M. D. Pluth, R. G. Bergman and K. N. Raymond, *J. Am. Chem. Soc.*, 2010, **132**, 6938-6940.

8 D. J. Cram, S. Karbach, Y. H. Kim, L. Baczynskyj and G. W. Kallemeyn, *J. Am. Chem. Soc.*, 1985, **107**, 2575-2576.

9 D. J. Cram and J. M. Cram, *Container Molecules and Their Guests*, *The Royal Society of Chemistry*, 1997.

10 R. W. Saalfrank, A. Stark, K. Peters and H. G. von Schnering, *Angew. Chem. Int. Ed.*, 1988, **27**, 851-853.

11 M. Fujita, *Chem. Soc. Rev.*, 1998, **27**, 417-425.

12 P. J. Stang and B. Olenyuk, *Acc. .Chem. Res.*, 1997, **30**, 502-518.

13 D. L. Caulder, R. E. Powers, T. N. Parac and K. N. Raymond, *Angew. Chem. Int. Ed.*, 1998, **37**, 1840-1843.

14 C. Brückner, R. E. Powers and K. N. Raymond, *Angew. Chem. Int. Ed.*, 1998, **37**, 1837-1839.

15 S. R. Seidel and P. J. Stang, *Acc. Chem. Res.*, 2002, **35**, 972-983.

16 D. Fiedler, R. G. Bergman and K. N. Raymond, *Angew. Chem. Int. Ed.*, 2006, **45**, 745-748.

17 T. R. Cook, Y.-R. Zheng and P. J. Stang, *Chem. Rev.*, 2013, **113**, 734-777.

18 C. J. Bruns, D. Fujita, M. Hoshino, S. Sato, J. F. Stoddart and M. Fujita, *J. Am. Chem. Soc.*, 2014, **136**, 12027-12034.

19 D. Fujita, H. Yokoyama, Y. Ueda, S. Sato and M. Fujita, *Angew. Chem. Int. Ed.*, 2015, **54**, 155-158.

20 T. R. Cook and P. J. Stang, *Chem. Rev.*, 2015, **115**, 7001-7045.

21 D. Fujita, Y. Ueda, S. Sato, H. Yokoyama, N. Mizuno, T. Kumasaka and M. Fujita, *Chem.*, 2016, **1**, 91-101.

22 M. J. Hardie, *Chem. Lett.*, 2016, **45**, 1336-1346.

23 A. Ferguson, M. A. Squire, D. Siretanu, D. Mitcov, C. Mathoniere, R. Clerac and P. E. Kruger, *Chem. Commun.*, 2013, **49**, 1597-1599.

24 M. D. Ward and P. R. Raithby, *Chem. Soc. Rev.*, 2013, **42**, 1619-1636.

25 B. F. Abrahams, N. J. FitzGerald and R. Robson, *Angew. Chem. Int. Ed.*, 2010, **49**, 2896-2899.

26 B. F. Abrahams, B. A. Boughton, N. J. FitzGerald, J. L. Holmes and R. Robson, *Chem. Commun.*, 2011, **47**, 7404-7406.

27 A. Stephenson, S. P. Argent, T. Riis-Johannessen, I. S. Tidmarsh and M. D. Ward, *J. Am. Chem. Soc.*, 2011, **133**, 858-870.

28 A. M. Najar, I. S. Tidmarsh, H. Adams and M. D. Ward, *Inorg. Chem.*, 2009, **48**, 11871-11881.

29 S. Leininger, B. Olenyuk and P. J. Stang, *Chem. Rev.*, 2000, **100**, 853-908.

30 S. Sakamoto, M. Fujita, K. Kim and K. Yamaguchi, *Tetrahedron*, 2000, **56**, 955-964.

31 K. Yamaguchi, *Mass Spec.*, 2013, **2**, S0012-S0012.

32 X.-P. Zhou, J. Liu, S.-Z. Zhan, J.-R. Yang, D. Li, K.-M. Ng, R. W.-Y. Sun and C.-M. Che, *J. Am. Chem. Soc.*, 2012, **134**, 8042-8045.

33 X.-P. Zhou, Y. Wu and D. Li, *J. Am. Chem. Soc.*, 2013, **135**, 16062-16065.

34 D. Luo, X-Z. Wang, C. Yang, X.-P. Zhou and D. Li, *J. Am. Chem. Soc.*, 2018, **140**, 118-121.

35 K. T. Holman, in *Encyclopedia of Supramolecular Chemistry*, ed. J. L. A. J. W. Steed, Marcel Dekker, New York, 2004, vol. 1, pp. 340-348.

36 T. Brotin and J.-P. Dutasta, *Chem. Rev.*, 2009, **109**, 88-130.

37 T. Brotin, V. Roy and J.-P. Dutasta, *J. Org. Chem.*, 2005, **70**, 6187-6195.

38 J. Canceill and A. Collet, *J. Chem. Soc., Chem. Commun.*, 1988, 582 —584.

39 A. Collet, J.-P. Dutasta, B. Lozach and J. Canceill, in *Topics in Current Chemistry: Supramolecular Chemistry I — Directed Synthesis and Molecular Recognition*, ed. E. Weber, Springer-Verlag, Berlin Heidelberg, 1993, pp. 103-129.

40 D. Zhang, A. Martinez and J. P. Dutasta, *Chem Rev*, 2017, **117**, 4900-4942.

41 B. F. Abrahams, B. A. Boughton, H. Choy, O. Clarke, M. J. Grannas, D. J. Price and R. Robson, *Inorg. Chem.*, 2008, **47**, 9797-9803.

42 B. F. Abrahams, D. J. Price and R. Robson, *Angew. Chem. Int. Ed.*, 2006, **45**, 806-810.

43 D. J. McCord, J. H. Small, J. Greaves, Q. N. Van, A. J. Shaka, E. B. Fleischer and K. J. Shea, *J. Am. Chem. Soc.*, 1998, **120**, 9763-9770.

44 B. F. Abrahams, N. J. FitzGerald, T. A. Hudson, R. Robson and T. Waters, *Angew. Chem. Int. Ed.*, 2009, **48**, 3129-3132.

5.3 Supporting Information

5.3.1 S1. Comments on the formulation of the cage

The covalent anionic tetrahedral cage has the formula $[(PhSi)_6(ctc)_4]^{6-}$. Whilst single crystal X-ray diffraction clearly revealed the structure and formula of the cage, other techniques have been employed to identify counterions, tetraethylammonium, triethylammonium and bromide. For example, NMR has been used to determine that the cage forms as a DMF/EtOAc solvate (see *S5. NMR spectroscopy*). The amount of solvent present varies depending on the treatment of the crystals; water is incorporated when the crystals are exposed to the atmosphere for extended periods of time.

5.3.2 S2. Instrumentation

Microwave reactor synthesis of the compound was performed using a Biotage Initiator Classic microwave reactor. Single crystal X-ray diffraction experiments were performed using a SuperNova dual source diffractometer using CuKα radiation λ = 1.5418 Å. Powder X-ray diffraction patterns were measured using a Rigaku Synergy instrument. Mass spectrometry was performed using an Agilent QTOF 6520. High resolution mass spectrometry was performed using a Bruker Daltonics (Bremen, Germany) SolariX 7 Tesla Hybrid MALDI/ESI-FT-ICR-MS. ^{1}H and ^{13}C NMR spectrometry was performed using a Varian 400 MHz NMR Spectrometer. Thermogravimetric analyses were performed using a Mettler TGA/SDTA851 apparatus. Infrared spectroscopy was performed using a Bruker Tensor FTIR 27.

5.3.3 S3. Synthesis and characterisation

Method 1

This method was used for growing crystals for single crystal X-ray diffraction. Preparation of $(NEt_4)_4(HNEt_3)_4[(PhSi)_6(ctc)_4]Br_2$·solvate: Cyclotricatechylene (H_6ctc) (192 mg, 0.52 mmol) was placed in a 10-20 mL microwave vial and dissolved in DMF (6 mL). NEt_4Br (66 mg, 0.31 mmol) in DMF (6 mL) was added to the $ctcH_6$ solution followed by $SiPh(OEt)_3$ (0.30 mL) and excess NEt_3 (ca. 16 drops). The solution was sparged with N_2 for 2 minutes then sealed and placed in a Biotage Initiator microwave reactor. The solution was heated to 100°C with stirring and held at this temperature for 15 minutes then allowed to cool to room temperature. 2 mL of the reaction mixture was decanted into a vial and exposed to EtOAc vapour for several days over which time large yellow crystals (typical dimensions between 0.5 and 1.0 mm) suitable for x-ray diffraction grew on the surface of the vial. A single crystal was taken from the mother liquor and placed directly into protective oil. Single crystal X-ray diffraction data was collected using a SuperNova diffractometer fitted with a CuKα X-ray source. The X-ray data revealed the crystals to be face centered cubic with the adoption of the space group *F*-43*m*, $a = 27.9568(6)$ Å.

In order to improve the yield, reduce solvent usage and reduce crystallization time of the compound the synthetic procedure was modified and the resultant crystalline product used for all further characterization experiments. The method described above is hereafter designated *method 1* and the modified method detailed below is *method 2.*

Method 2

Cyclotricatechylene (192 mg, 0.52 mmol) was placed in a 2-5 mL microwave vial and dissolved in DMF (4 mL). NEt_4Br (66 mg, 0.31 mmol) was then added to the $ctcH_6$ solution followed by $SiPh(OEt)_3$ (0.30 mL) and excess NEt_3 (ca. 16 drops). The solution was sparged with N_2 for 2 minutes then sealed and placed in a Biotage Initiator microwave reactor. The solution was heated to 120°C with stirring and held at this temperature for 30 minutes then allowed to cool to room temperature. The reaction mixture was distributed into 5 vials in equal aliquots before exposure to EtOAc vapour to induce crystallisation. Each aliquot contained 1.05×10^{-5} mol of the limiting reagent, $ctcH_6$.

The crystals formed from method 2 were shown to be the same as those obtained by method 1 by comparison of the powder X-ray diffraction pattern of the product from method 2 with the simulated pattern produced from the crystal structure determination obtained on a crystal produced by method 1 (Figure S5). Crystals from one aliquot were collected via vacuum filtration and dried in a stream of air. These were used for elemental and infrared analyses. Elemental analysis was performed at Campbell Microanalytical Laboratory, Chemistry Department, *Te Tari Hua Ruānuku*, University of Otago. Analysis (air dried sample prepared via method 2) $(NEt_4)_4(HNEt_3)_4[(PhSi)_6(ctc)_4]Br_2.(DMF)(H_2O)_{19}$: Calc: %C 60.1, %H 7.5, %N 3.5; Found: %C 60.1; %H 6.9; %N 3.3.

Crystals from a second aliquot were collected on a glass frit and washed with minimum EtOAc to measure the yield and ^{13}C (not shown) and ^{1}H NMR spectra of the compound. The percentage yield is based on the best approximation of the chemical formula of vacuum dried crystals $(NEt_4)_4(HNEt_3)_4[(PhSi)_6(ctc)_4]Br_2.4DMF$ (from which all the EtOAc has been removed and have not been exposed to atmospheric water vapour for an extended period of

time) as estimated by integration of the ^{1}H NMR spectrum of the dried crystals (see figure S8). The yield was 46.5 mg, 51%.

5.3.4 S4. Further crystallographic details

In the crystal structure investigated, initial refinements involved attempts to assign numerous small peaks of electron density in the difference Fourier maps to atoms of disordered cations and solvent molecules. This approach resulted in unsatisfactorily high agreement values. In response to these difficulties, the SQUEEZE[S1] routine within the crystallographic program PLATON[S2] was used to subtract the contribution of the diffuse solvent from the diffraction data and this led to an improvement in agreement values. It also provided an indication of the volume of the solvent accessible void spaces and the number of electrons in these regions. On the basis of this information as well as thermogravimetric analysis of 'wet crystals' (see *S6 Thermogravimetric analysis*) and ^{1}H NMR (see S5. *NMR spectroscopy*) the number of solvent molecules (assumed to be only DMF and EtOAc) in the unit cell was estimated. Despite the uncertainties arising from the location of solvent molecules and cations within the structure, the anionic cage, which is the focus of our interest, is clearly defined. The formula of the crystal that was crystallographically characterized was assigned as $(NEt_4)_4(HNEt_3)_4[(PhSi)_6(ctc)_4]Br_2{\cdot}(DMF)_4(EtOAc)_6$.

Crystallographic analysis of the crystals immersed in the CsBr solution revealed a similar structure to that of the parent crystals except that a Cs^+ ion was now located in each of the four corners of the $[(PhSi)_6(ctc)_4]^{6-}$ cage. Estimation of the chemical formula of the crystals was difficult because the solvent and cations occupying the inter-cage spaces could not be identified. Given that triethylammonium is likely to be more soluble in water, it was assumed for the purposes of estimating the formula of the crystals that the incorporation of Cs^+ accompanied the loss of triethylammonium to the aqueous environment upon immersion in

the CsBr solution. In addition, it was thought that the dimethylformamide and ethyl acetate would be replaced by water in the crystal. The formula of the immersed crystals therefore was tentatively assigned as $(NEt_4)_4Cs_4[(PhSi)_6(ctc)_4]Br_2{\cdot}70H_2O$. Despite the uncertainty associated with the overall formula, the crystal structure clearly indicates Cs^+ ions associating with the internal surface of the cage.

The cages in both the parent and immersed crystals pack in a face centred cubic (FCC) arrangement in which six phenyl groups from six distinct cages converge upon octahedral sites within the FCC structure as indicated in Fig. S2.

The structures were solved using SHELXT[S3] and refined using a full-matrix least squares procedure based upon F^2 (SHELXL[S4]). The solution and refinement of $(NEt_4)_4(HNEt_3)_4[(PhSi)_6(ctc)_4]Br_2{\cdot}(DMF)_4(EtOAc)_6$was performed within the WinGX system of programs[S5] whereas OLEX2[S6] was employed for $(NEt_4)_4Cs_4[(PhSi)_6(ctc)_4]Br_2{\cdot}70H_2O$.

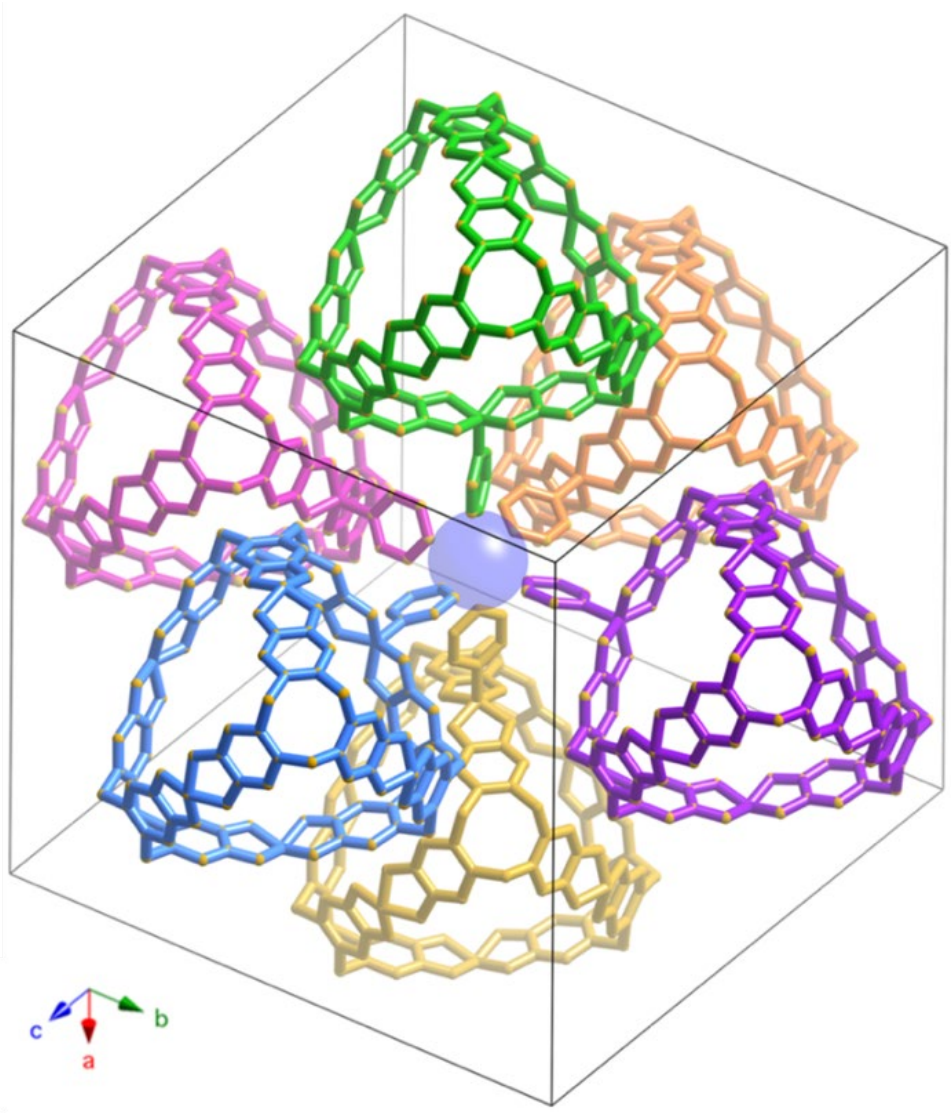

Figure S1. A representation of the packing in $(NEt_4)_4(HNEt_3)_4[(PhSi)_6(ctc)_4]Br_2 \cdot (DMF)_4(EtOAc)_6$ showing only the cages located in the middle of each face of the cubic unit cell. The translucent sphere corresponds to an octahedral site at the centre of the cell where the phenyl rings from six cages converge. Crystallographically equivalent octahedral sites are located half-way along each edge. Only one phenyl ring from each cage is depicted. The cages located at the vertices of the unit cell are not shown.

5.3.5 S5. NMR spectroscopy

^{1}H NMR spectra were collected for three samples of the compound, each with different post-synthetic treatment. The three samples are shown in Figures S3 and S4. The top sample (3) in each figure corresponds to a sample that was prepared by directly transferring multiple large single crystals directly from the mother liquor into d_6DMSO. The middle sample (2) corresponds to the bulk material collected on a glass frit without suction and washed with ethyl acetate. The bottom spectrum (1) was obtained on the bulk material that was collected on a glass frit and dried at the pump without washing with additional solvent, no heating was performed.

The distinct absence of the three characteristic ethyl acetate peaks (1.18 ppm, 1.98 ppm and 4.03 ppm) in sample 1 shows that it is easily released at room temperature. Aside from this difference, the three spectra have the same peak profile indicating that the bulk sample is the same as the single crystals. A small shift in some of the peaks is observable on loss of ethyl acetate in sample 1.

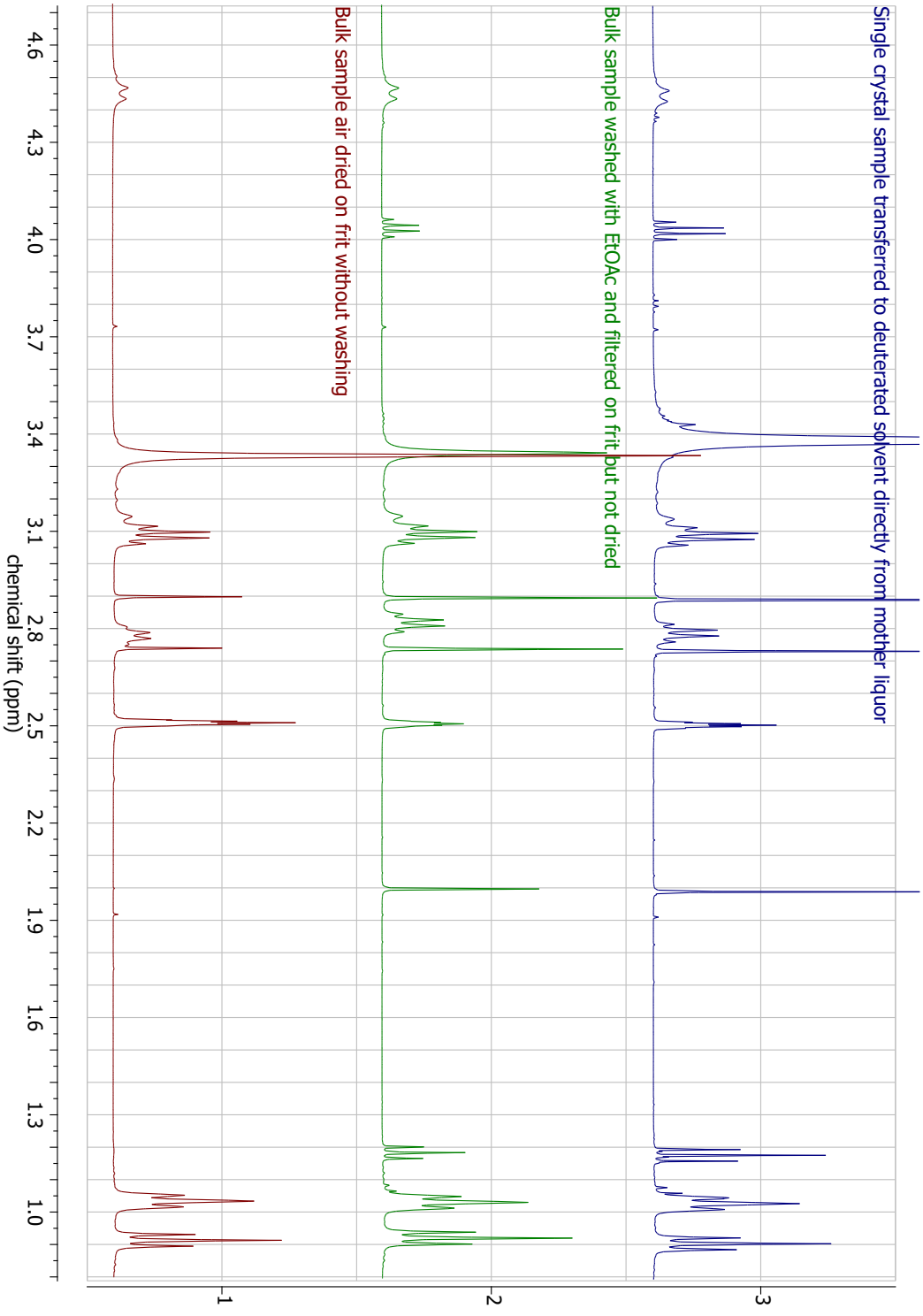

Figure S2. ^{1}H NMR 2.8-4.5 ppm for three samples of the crystals, each with different post-synthetic treatment. All samples were dissolved in and referenced to d_6DMSO. No peaks were present below 2.8 ppm or between 4.5 and 5.5 ppm.

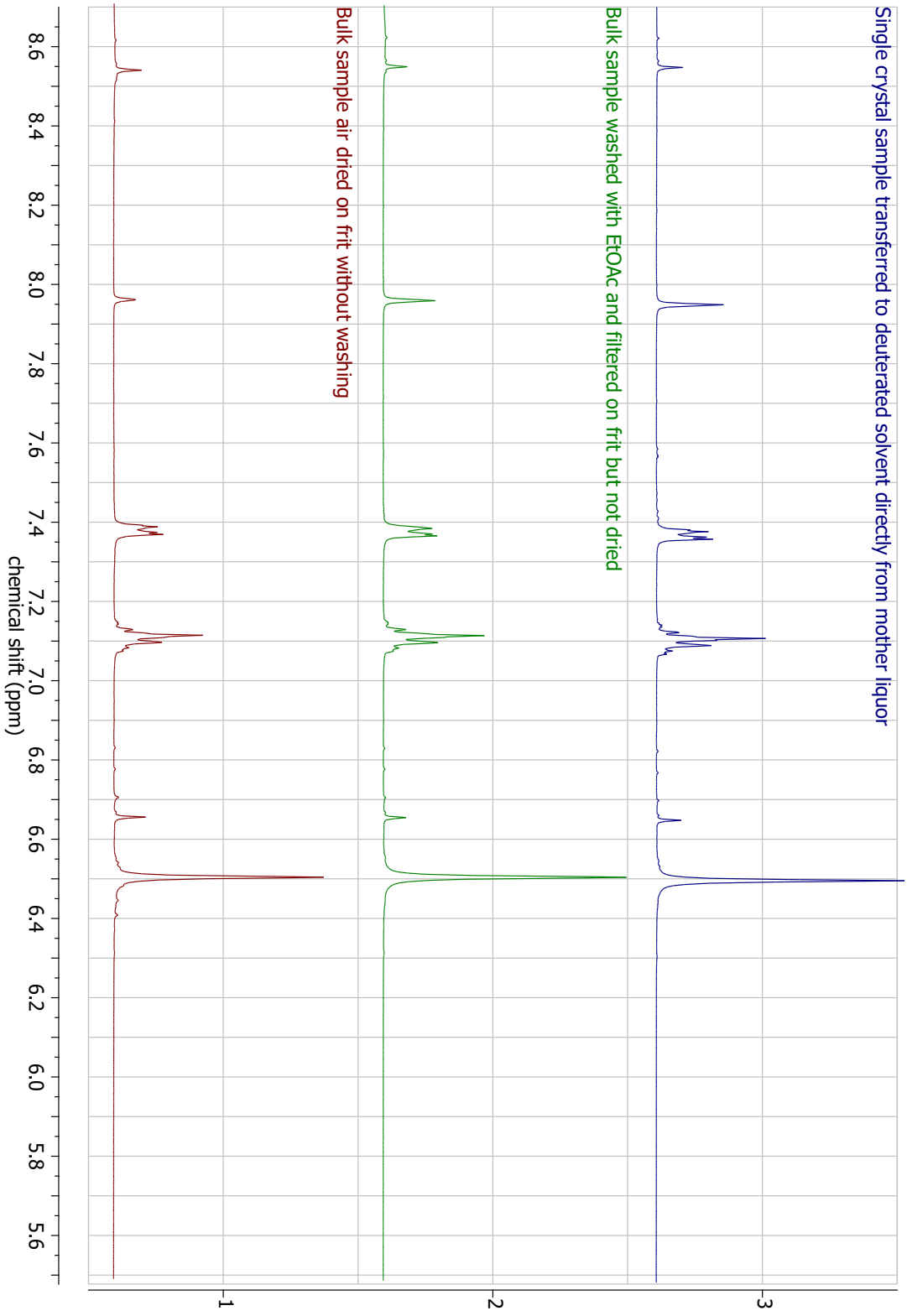

Figure S3. ^{1}H NMR 5.5 to 8.7 ppm for three samples of the compound, each with different post-synthetic treatment. All samples were dissolved in and referenced to d_6DMSO. No peaks were present above 8.7 ppm.

5.3.6 S6. Thermogravimetric analysis

Thermogravimetric analysis (TGA) of two samples of the compound was performed across a temperature range of 25-450 °C. The 'dry crystals', represented below in Figure S5 in blue, were collected on a glass frit and air was pulled through the sample for several minutes. The crystals were left for several days before TGA was performed. Though there is a small initial drop in mass as dry nitrogen was blown across the sample at 25 °C the gradient of the graph remains close to horizontal to temperatures around 250 °C indicating that most ethyl acetate is lost at room temperature. This is confirmed also by ^{1}H NMR of the dried crystals (see S5 Nuclear Magnetic Resonance Spectroscopy). Some of the mass loss below 80 °C may also correspond to water adsorbed from the atmosphere, however this has not been confirmed. The total mass loss up to 450 °C corresponds approximately to all solvent (DMF) and counterions, leaving only the cage remaining. Stability of the cage above 450 °C has not been measured.

The 'wet crystals' were prepared for analysis by filtration on a glass frit in the absence of suction, immediately before being transferred to the TGA instrument. Some solvent loss may have occurred during sample transfer and calibration of the instrument however the steeper gradient of this line indicates presence and subsequent loss of ethyl acetate (and possibly water) up to approximately 250 °C. The TGA data of the wet crystals combined with the NMR provide the basis for the estimate of the chemical formula of the single crystal used for x-ray diffraction, $(NEt_4)_4(HNEt_3)_4[(PhSi)_6(ctc)_4]Br_2{\cdot}(DMF)_4(EtOAc)_6$.

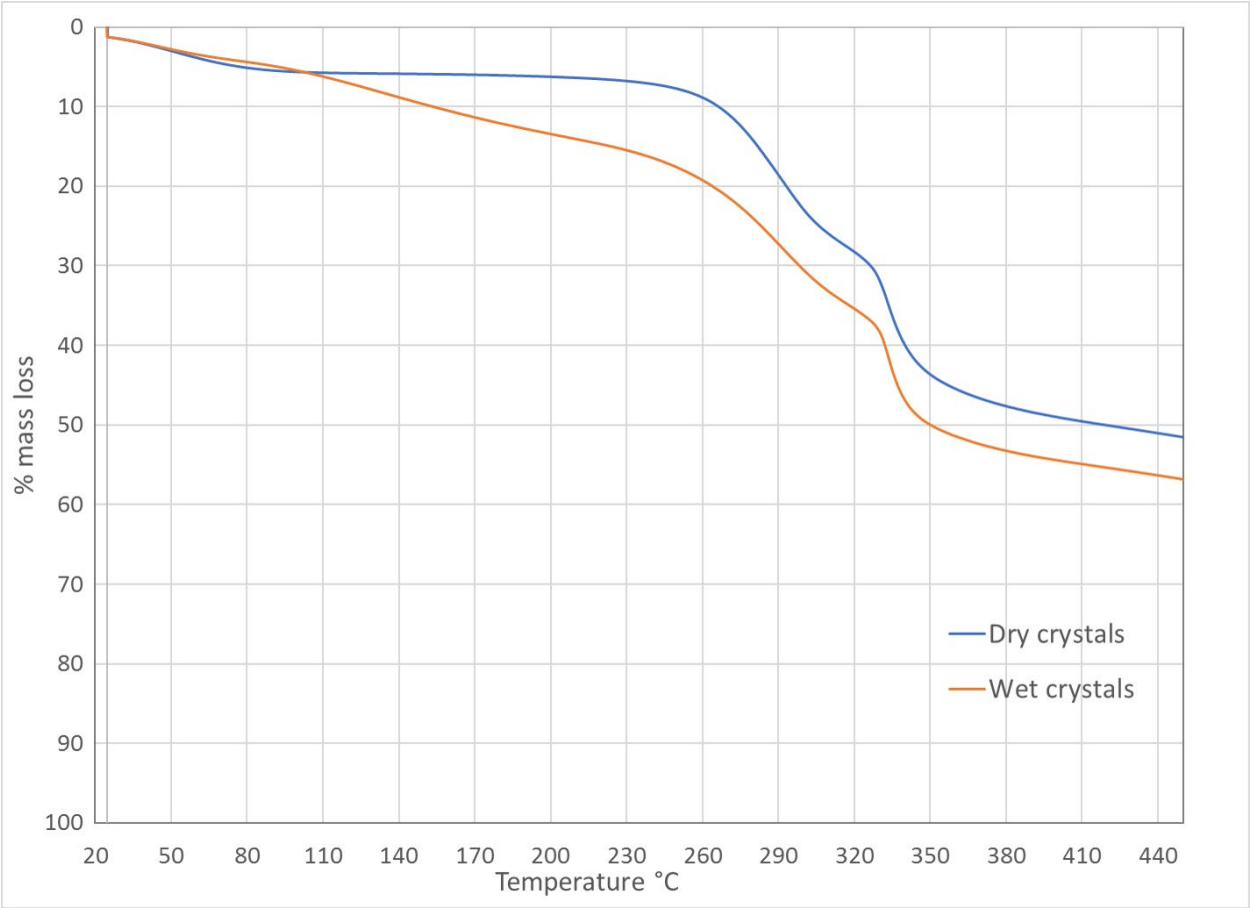

Figure S4. Thermogravimetric traces of air dried crystals that were exposed to atmosphere (blue) and crystals that were collected from their mother liquor with no vacuum and transferred directly to the instrument (orange)

5.3.7 S7. Powder Diffraction Patterns

The powder diffraction pattern for the parent compound $(NEt_4)_4(HNEt_3)_4[(PhSi)_6(ctc)_4]Br_2$.solvate (Figure S5), of the boiled crystals (Figure S6) and the crystals soaked in aqueous CsBr (Figure S7) are shown below.

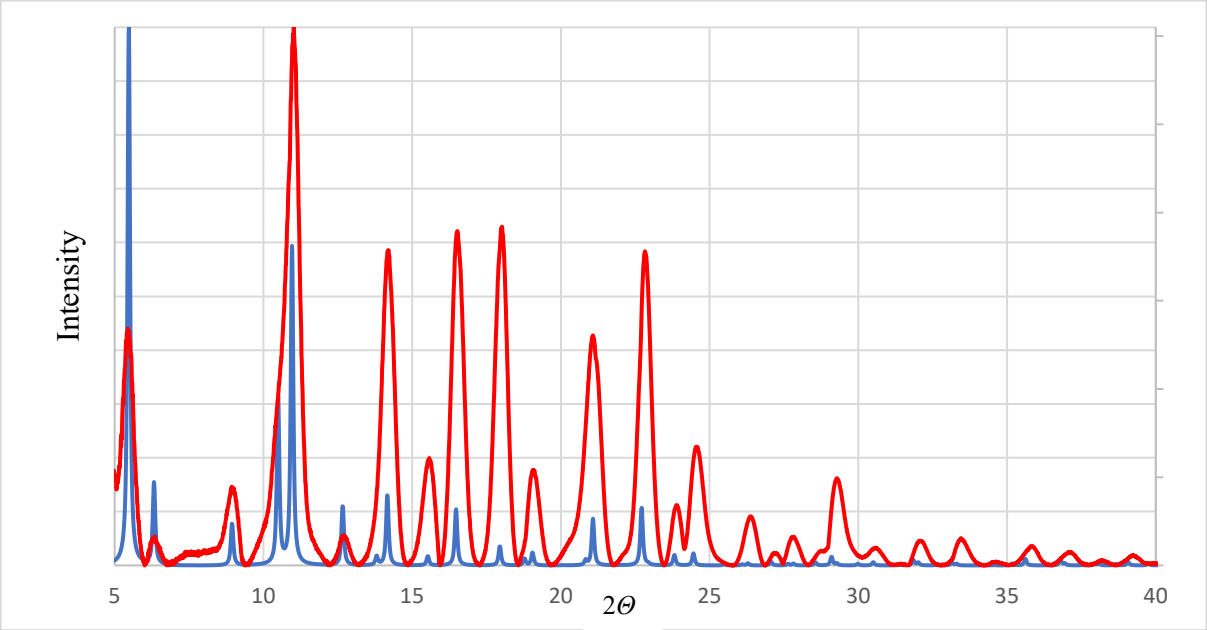

Figure S5. Calculated powder X-ray diffraction pattern of $(NEt_4)_4(HNEt_3)_4[(PhSi)_6(ctc)_4]Br_2$.solvate (blue) compared with experimental data for ground up crystals prepared via *method 2* and washed with a minimum of ethyl acetate (red).

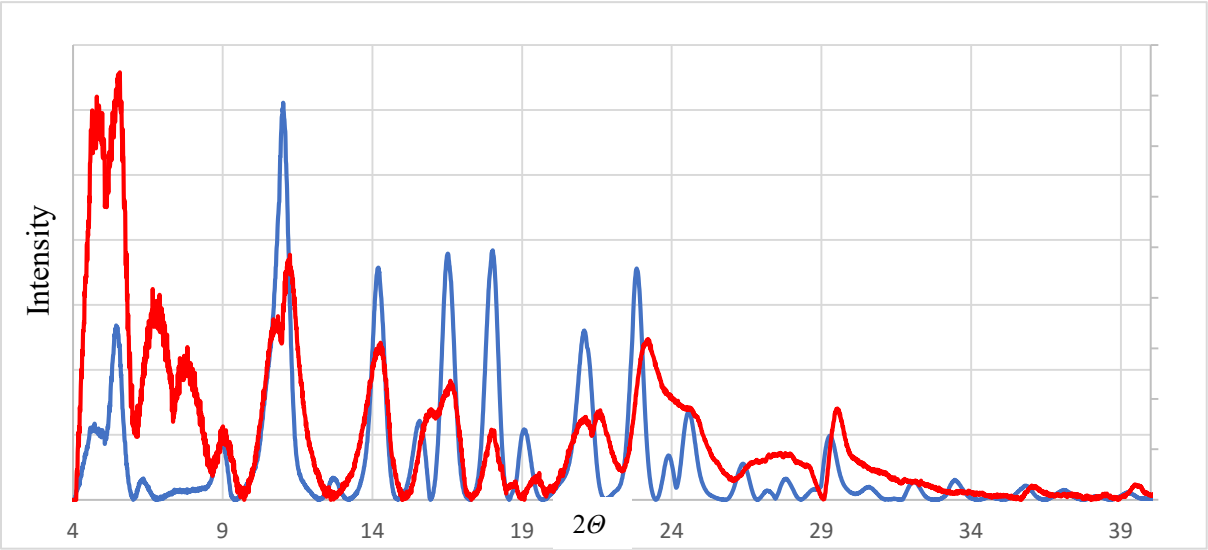

Figure S6. Observed powder diffraction patterns of $(NEt4)_4(HNEt_3)_4[(PhSi)_6(ctc)_4]Br_2$·solvate untreated (blue) and after being boiled in H_2O for 30 mins (red).

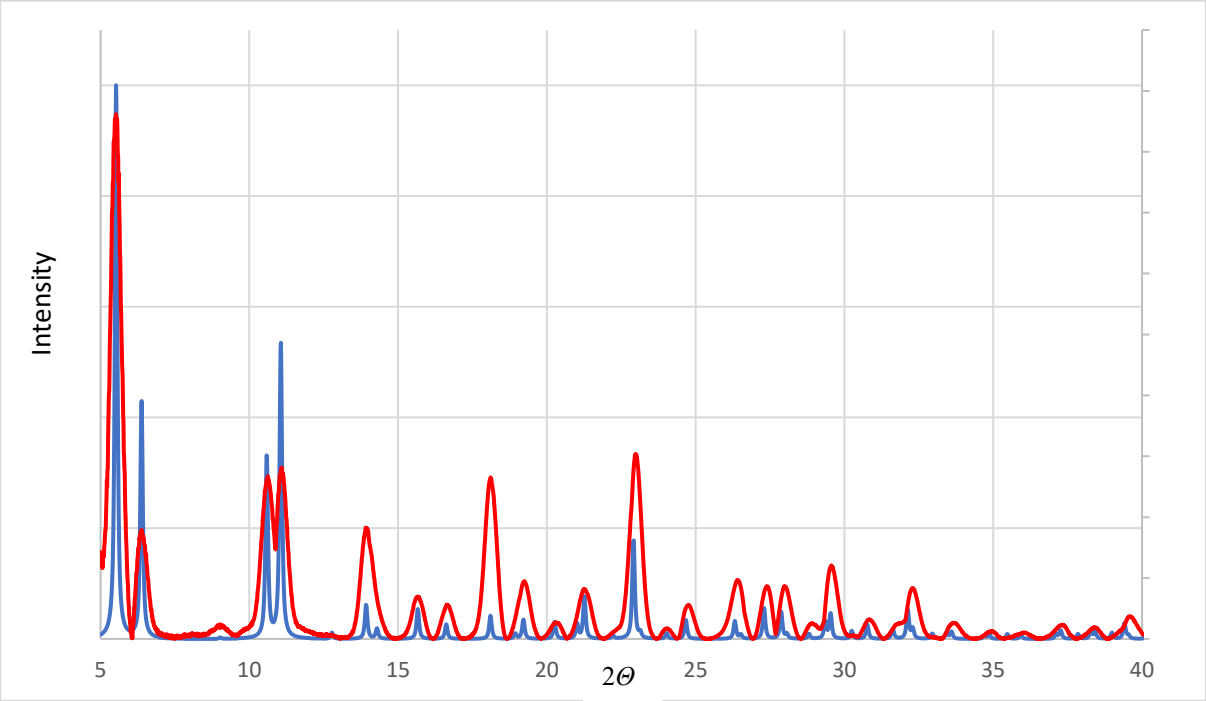

Figure S7. Calculated (blue) and observed (red) powder patterns of the Si-cage crystals, $[(NEt_4)_4Cs_4[(PhSi)_6(ctc)_4]Br_2$·solvate] after immersion in aqueous CsBr.

5.3.8 S8. ESI mass spectrometry

A Bruker Daltonics (Bremen, Germany) SolariX 7 Tesla Hybrid MALDI/ESI-FT-ICR-MS was used for high mass resolution analysis. The instrument was operated in ESI negative and positive ionisation modes with TD acquisition = 1M *m/z* 200-2000 or 4M *m/z* 53.75-3000 providing mass resolutions of 260000 and 140000 at *m/z* 400 respectively, and ESI positive ionization mode. The system was calibrated using an external calibration of ESI-TOF low concentration Tune Mix (Agilent Technologies, Santa Clara, CA, USA). Samples were infused at a rate of 2 μL min^{-1} using the syringe pump, a total of 10-20 scans were collected and averaged to generate mass spectra. The following general instrument conditions were set: capillary voltage, negative mode = 4200 V and positive mode = –4000 V; drying gas flow, 4.0 L min^{-1}; drying gas temperature, 180°C; nebulizer gas flow rate, 1.0 bar; source accumulation, 0.001 sec; ion accumulation, 0.5 sec; ion cooling time, 0.01 sec; flight time, 0.001 sec. Data were analysed using the Bruker Compass Data Analysis 4.2 (Build 383.1) software.

Unless otherwise indicated, the *m*/*z* values given refer to the base peak of on isotopologue series.

Sample preparation for ESI-MS analysis

1. $(NEt_4)_4(HNEt_3)_4[(PhSi)_6(ctc)_4]\cdot$solvate (untreated crystals)

3-4 large crystals of the compound, prepared via synthetic *method 1*, were dissolved in a minimum of DMF (<1 mL) followed by dilution with acetone (10 mL) prior to analysis.

2. $(NEt_4)_4(HNEt_3)_4[(PhSi)_6(ctc)_4]$·solvate crystals that had been immersed in boiling water

2 mg of crystals of the compound, prepared via synthetic *method 2*, were boiled in deionized water for 30 min then solution was kept at 60 °C for 7 days, then filtered, the crystals dried. 3-4 large crystals were dissolved in a minimum of DMSO (<1 mL) followed by dilution with acetonitrile (10 mL).

3. $(NEt_4)_4(HNEt_3)_4[(PhSi)_6(ctc)_4]$·solvate soaked in aqueous CsBr

1 mg of large crystals prepared via synthetic *method 2* was immersed in an aqueous CsBr solution (30 mg in 2 mL water) for 3 days, then filtered and dried. 3-4 large crystals were dissolved in DMF (1 mL) followed by dilution with acetonitrile (10 mL).

Results of ESI-MS analysis

1. $(NEt_4)_4(HNEt_3)_4[(PhSi)_6(ctc)_4]$·solvate (untreated crystals)

Figure S8 shows the full, high resolution ESI mass spectrum in negative mode.

Table S1 lists the dominant isotopologues in the full spectrum. The relative intensities of the base peaks within each of the isotopologue series are indicated as their percentage contribution to the sum of the intensities of the base peaks in each of the isotopologue series. The error (in ppm) for each species is calculated based upon the monoisotopic peak for each isotopologue series.

Figure S9 shows a portion of the spectrum in which a series of dianionic cage adducts are indicated. Figure S10 shows an enlargement of the signal corresponding to [cage + $(NEt_4)_4]^{2-}$

and a comparison with the calculated pattern. An enlargement of the signal corresponding to [cage + $(NEt_4)_3$]$^{3-}$ and a comparison with the calculated pattern is displayed in Figure S11.

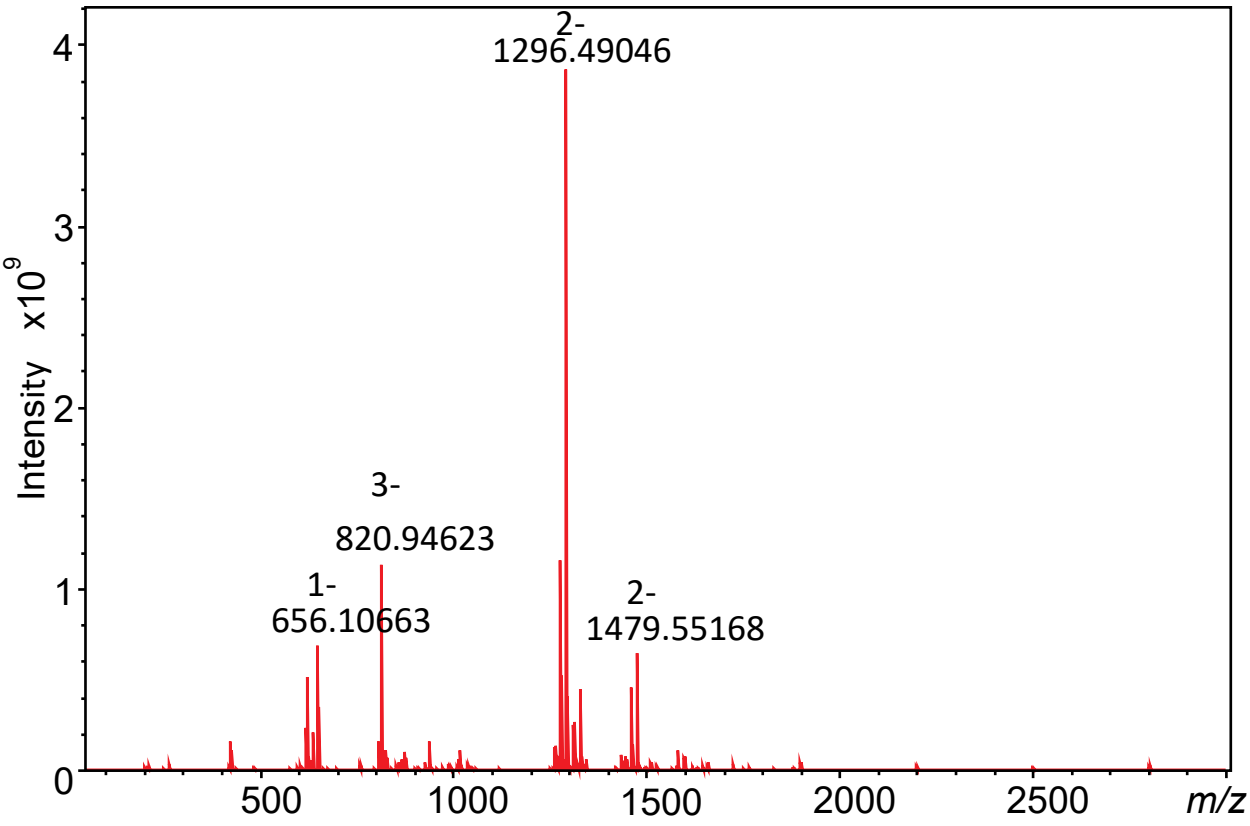

Figure S8. Full ESI-mass spectrum, in negative mode of samples obtained from the dissolution of $(NEt_4)_4(HNEt_3)_4[(PhSi)_6(ctc)_4]$·solvate crystals.

Table S1. Selected negative ionisation mode mass spectrum data for untreated crystals.

m/z **(monoisotopic peak)**	***m/z*** **(base peak)**	**Charge**	**Species**	**Mass Error (ppm)**	**%**
626.07767	628.07517	-1		-	4.93
644.02513	644.02513	-1		-	1.98
654.10885	656.10663	-1		-	6.62
810.93470	811.60256	-3	$[cage + (Et_4N)_2(HNEt_3)]^{3-}$	2.12	1.57
820.27857	820.94623	-3	$[cage + (Et_4N)_3]^{3-}$	2.23	10.94
833.20603	833.20603	-1		-	1.04
880.62603	881.62843	-3		-	10.94
942.31547	942.98363	-3		-	1.5
1020.22131	1022.21970	-1		-	1.09
1267.46585	1268.46409	-2	$[cage + (Et_4N)_2(HNEt_3)_2]^{2-}$	1.99	1.29
1281.47736	1282.47689	-2	$[cage + (Et_4N)_3(HNEt_3)]^{2-}$	-1.26	11.08
1295.49110	1296.49046	-2	$[cage + (Et_4N)_4]^{2-}$	-2.72	37
1316.00693	1317.00842	-2	$[cage + (Et_4N)_4 + MeCN]^{2-}$	-0.74	2.59
1332.02091	1333.02389	-2	$[cage + (Et_4N)_4 + DMF]^{2-}$	-0.08	4.33
1332.39625	1333.91475	-2		-	1.41
1464.53513	1465.53452	-2		-	4.36
1478.54996	1479.55168	-2		-	6.2
1583.09263	1584.59398	-2		-	1.04

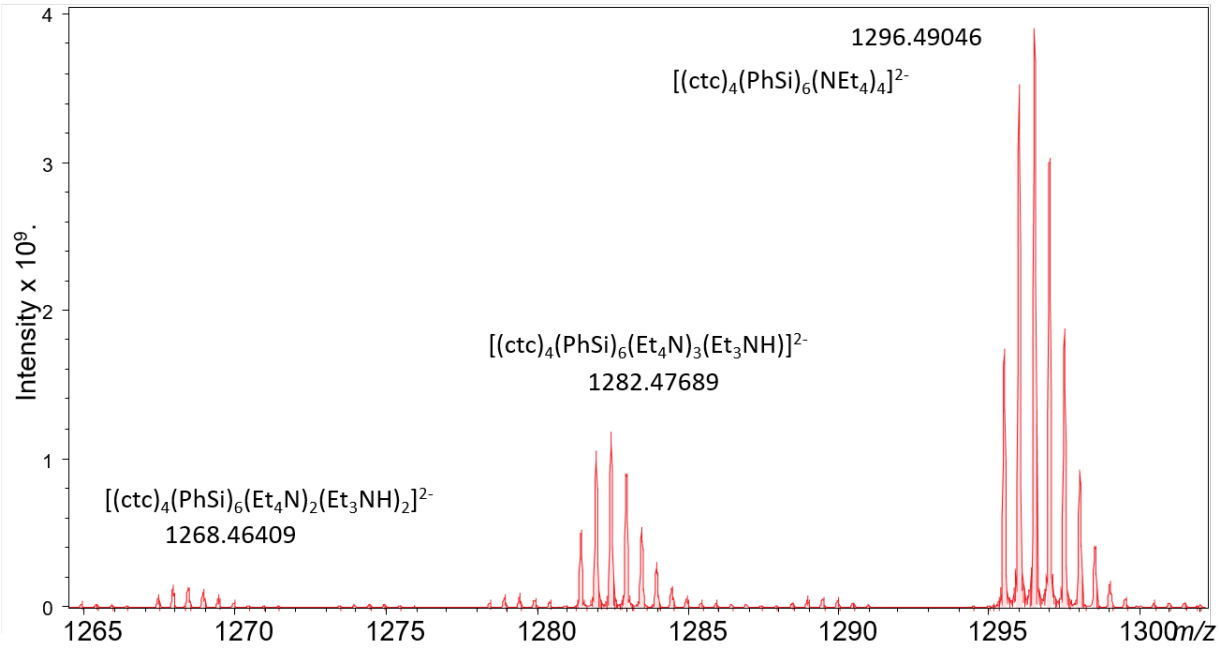

Figure S9. ESI-mass spectrum, in negative mode, of the peaks associated with [cage + $(Et_4N)_4]^{2-}$ at *m/z* 1296.49046, [cage + $(Et_4N)_3$ + $(Et_3NH)]^{2-}$ at *m/z* 1282.47896 and [cage + $(Et_4N)_2$ + $(Et_3NH)_2]^{2-}$ at *m/z* 1268.46409 from the dissolution of $[(NEt_4)_4(HNEt_3)_4[(PhSi)_6(ctc)_4]$·solvate crystals.

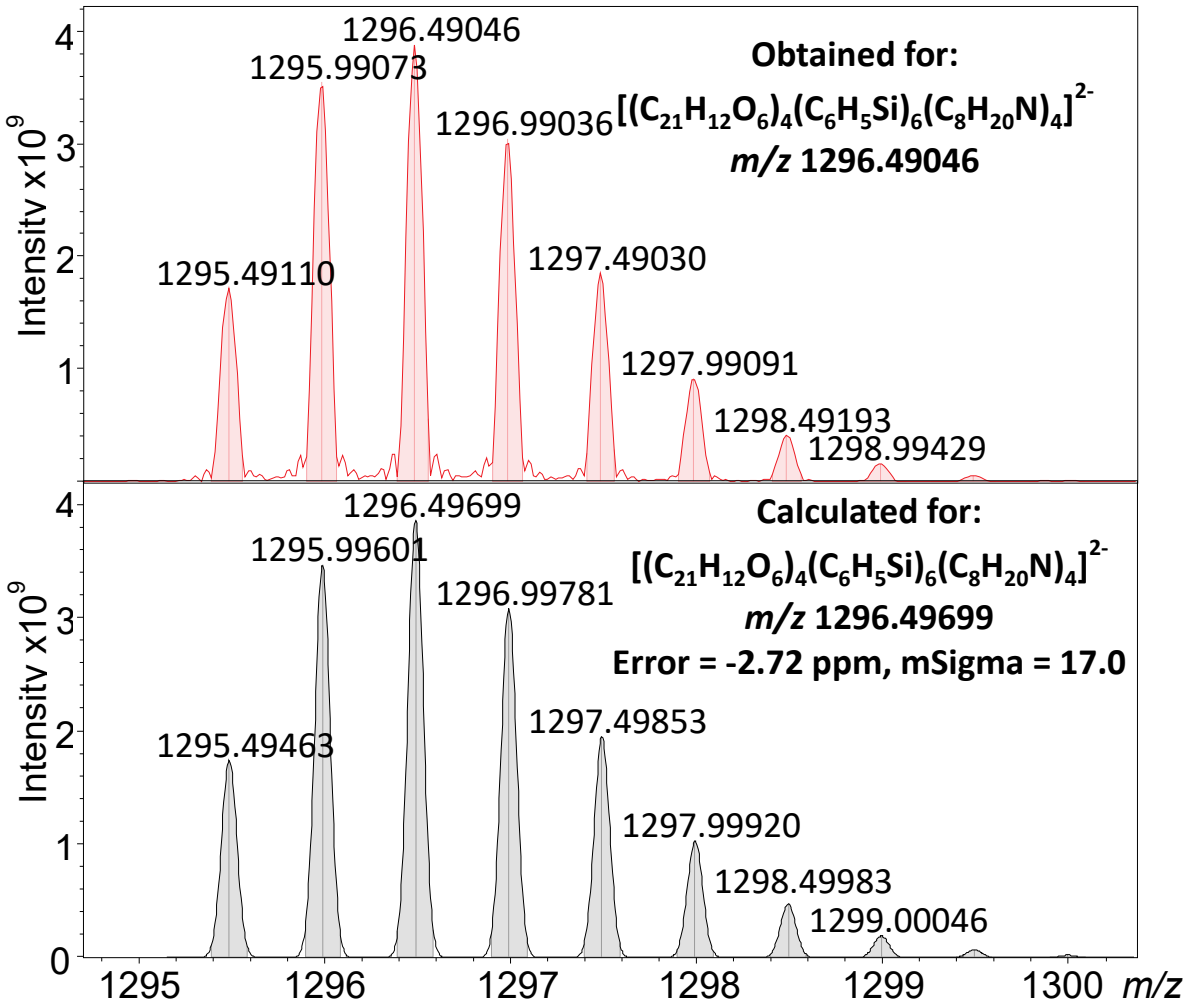

Figure S10. ESI-mass spectrum, in negative mode of the peaks associated with [cage + $(Et_4N)_4$]$^{2-}$ at *m/z* 1296.49046 from the dissolution of $[(NEt_4)_4(HNEt_3)_4[(PhSi)_6(ctc)_4]$·solvate crystals.

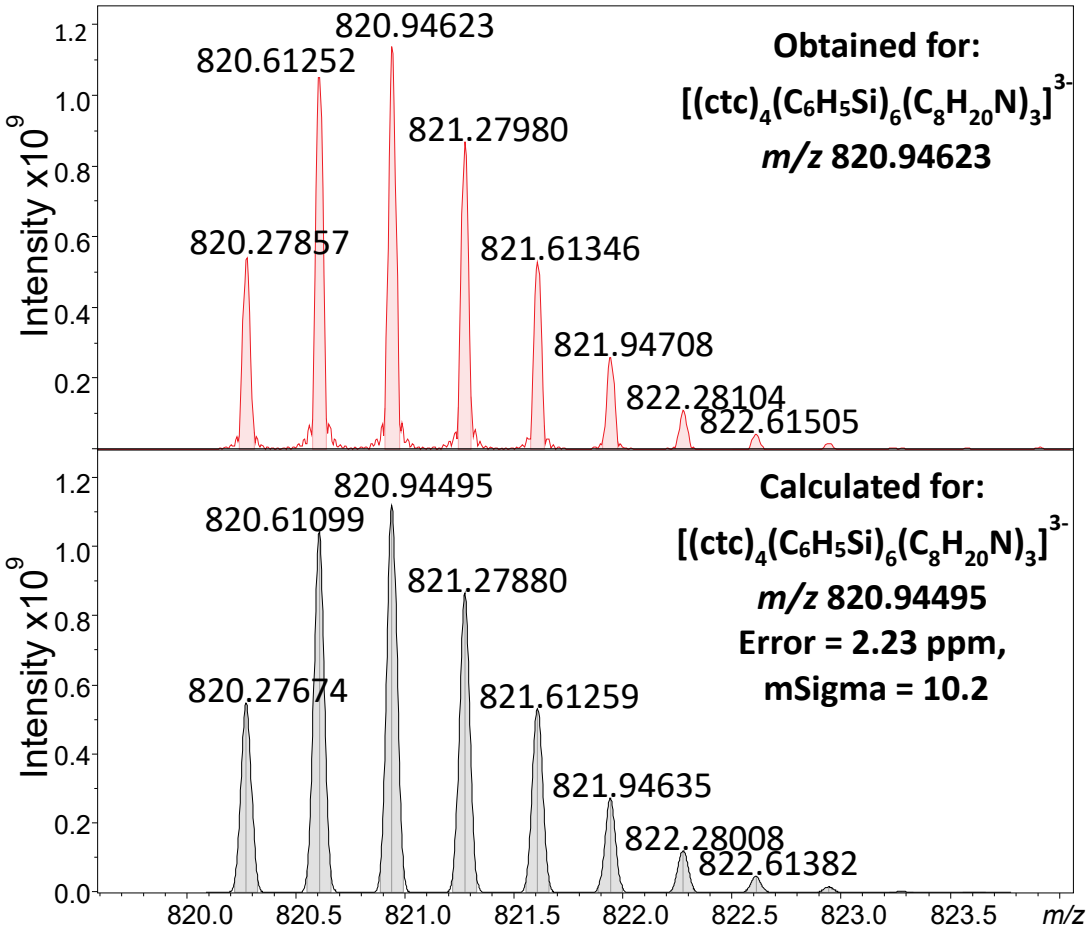

Figure S11. ESI-mass spectrum, in negative mode of the peaks associated with $[cage + (Et_4N)_3]^{3-}$ at *m/z* 820.94623 (base peak) from the dissolution of $(NEt_4)_4(HNEt_3)_4[(PhSi)_6(ctc)_4]$·solvate crystals.

2. $(NEt_4)_4(HNEt_3)_4[(PhSi)_6(ctc)_4]$·solvate crystals that had been immersed in boiling water

Figure S12 shows the full negative mode, high resolution ESI mass spectrum obtained for crystals of the compound boiled in water then dissolved in dimethylsulfoxide and diluted with acetonitrile. The dominant peak in the spectrum corresponds to $[cage + (Et_4N)_3]^{3-}$ at *m/z* 820. 820.94461. Additionally, there is a significant peak corresponding to $[cage + (Et_4N)_2]^{4-}$ at *m/z* 583.16930.

Table S2 lists the dominant isotopologues in the full spectrum. The relative intensities of the base peaks within each of the isotopologue series are indicated as their percentage

contribution to the sum of the intensities of the base peaks in each of the isotopologue series. The error (in ppm) for each species is calculated based upon the monoisotopic peak for each isotopologue series.

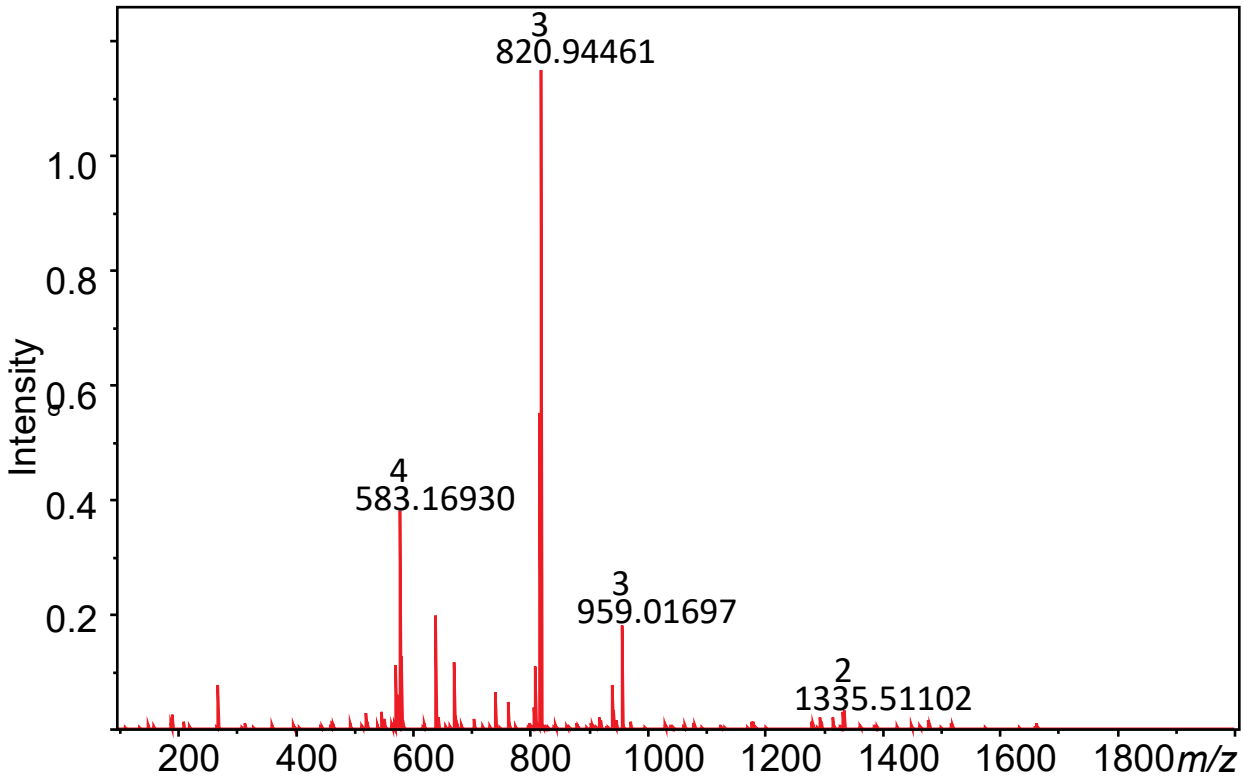

Figure S12. Full negative mode mass spectrum of the crystals that had been boiled in water prior to being dissolved in DMSO and diluted with MeCN.

Table S2. Selected negative ionisation mode mass spectrum data for crystals boiled in water prior to being dissolved in DMSO and diluted with MeCN.

m/z **(monoisotopic peak)**	***m/z*** **(base peak)**	**Charge**	**Species**	**Mass Error (ppm)**	**%**
525.88164	525.13325	-4		-	1.14
550.12908	550.37984	-4		-	1.15
575.66102	575.91153	-4	$[cage + (Et_4N)(HNEt_3)]^{4-}$	1.81	4.28
582.66875	583.16930	-4	$[cage + (Et_4N)_2]^{4-}$	1.63	14.67
641.90823	642.15815	-4		-	7.6
575.38082	575.63061	-4		-	4.5
743.22912	743.56421	-3		-	2.53
765.72434	766.22586	-2		-	1.88
810.93427	811.22759	-3	$[cage + (Et_4N)_2(HNEt_3)]^{3-}$	1.59	4.27
820.27674	820.94461	-3	$[cage + (Et_4N)_3]^{3-}$	0.00	44.49
942.31837	942.98549	-3		-	3.02
958.34956	959.01697	-3		-	7.03
1266.34775	1267.34243	-2	$[cage +(Et_4N)(HNEt_3)Na_2]^{2-}$ + DMSO + 2MeCN + H_2O*	-15.05	0.06
1281.42767	1281.92988	-2	$[cage + (Et_4N)_3(HNEt_3)]^{2-}$ *	-40.04	0.5
1295.49463	1295.99949	-2	$[cage + (Et_4N)_4]^{2-}$	0.00	0.77
1316.01536	1317.01879	-2	$[cage + (Et_4N)_4 + MeCN]^{2-}$	5.67	0.83
1335.00905	1335.51102	-2		-	1.27

* indicates assignment of species, where large mass error may be attributable to overlapping peaks in the mass spectrum.

3. Analysis of $(NEt_4)_4(HNEt_3)_4[(PhSi)_6(ctc)_4]$·solvate soaked in CsBr

Figure S13 shows the full negative mode, high resolution ESI mass spectrum of the sample obtained for crystals of the compound that had been immersed in an aqueous CsBr solution then dissolved in dimethylformamide and diluted with acetonitrile. Overlapping isotopic profiles of the cage with caesium and tetraethylammonium cations reflect the similarity in the mass of Cs^+ and NEt_4^+.

Table S3 lists the dominant isotopologues in the full spectrum. The relative intensities of the base peaks within each of the isotopologue series are indicated as their percentage

contribution to the sum of the intensities of the base peaks in each of the isotopologue series. The error (in ppm) for each species is calculated based upon the monoisotopic peak for each isotopologue series.

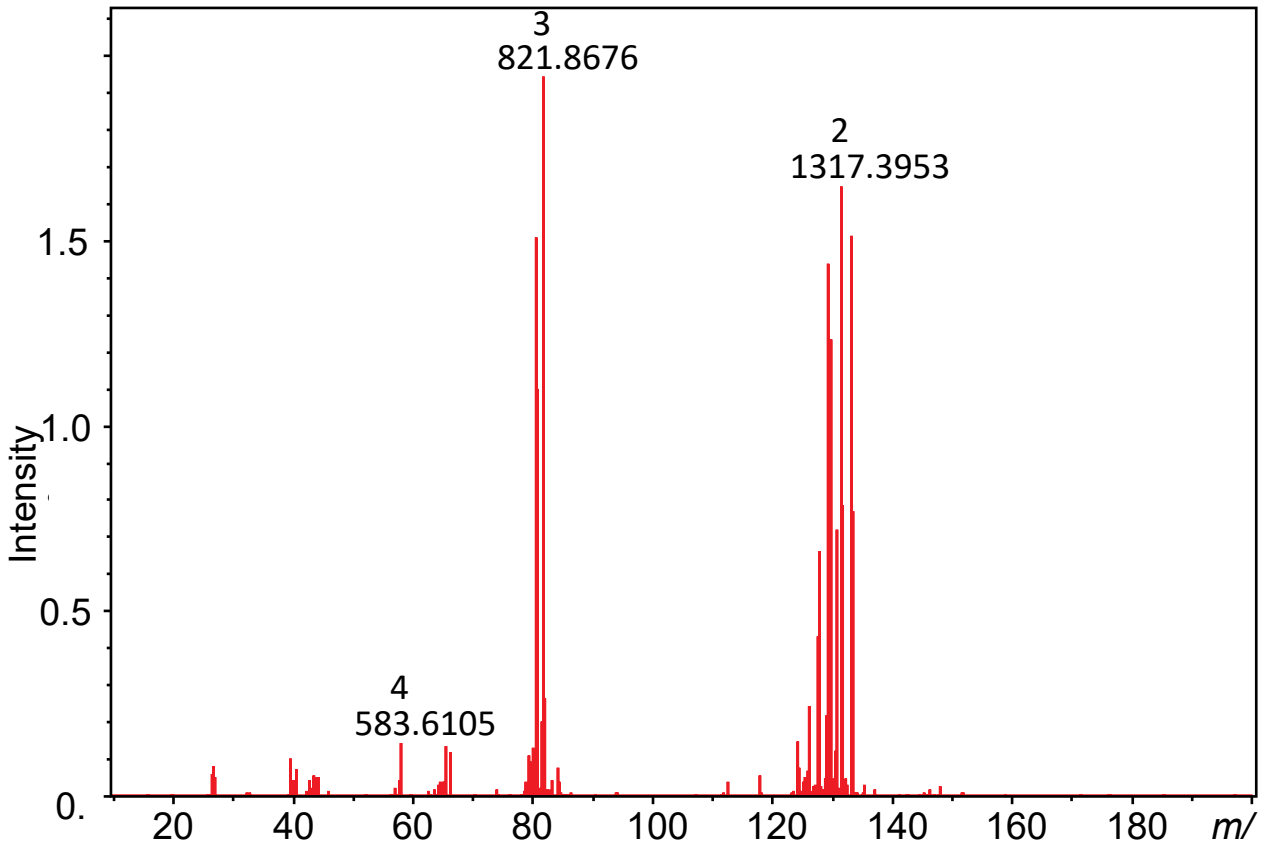

Figure S13. Full negative mode mass spectrum of the crystals soaked in aqueous CsBr solution followed by dissolution in DMF and dilution with MeCN.

Table S3. Selected negative ionisation mode mass spectrum data for crystals soaked in aqueous CsBr solution followed by dissolution in DMF and dilution with MeCN.

m/z (monoisotopic peak)	*m/z* (base peak)	Charge	Species	Mass Error (ppm)	%
583.35201	583.60465	-4	$[cage + (Et_4N)Cs]^{4-}$	-3.88	1.1
658.18834	658.68071	-4		-	1
666.72091	667.21334	-4		-	0.9
804.49608	805.16206	-3		-	1
809.81919	810.48446	-3	$[cage + (Et_4N)CsNa + DMF]^{3-}$	-0.62	11.4
820.27674	820.61027	-3	$[cage + (Et_4N)_3]^{3-}$	0.00	3.4
821.18882	821.85240	-3	$[cage + (Et_4N)_2Cs]^{3-}$	-3.92	14.8
822.10659	822.43943	-3	$[cage + (Et_4N)Cs_2]^{3-}$	-0.90	2.4
845.54184	845.87536	-3	$[cage + (Et_4N)_2Cs + DMF]^{3-}$	-1.32	0.6
1181.27721	1182.27765	-2		-	0.4
1244.32811	1245.30638	-2	$[cage + (Et_4N)Na_3 + 3DMF]^{2-}$	7.27	1.1
1254.79724	1255.77383	-2	$[cage + (HNEt_3)_3Cs]^{2-}$ *	-18.63	0.4
1262.75663	1263.27346	-2	$[cage + (Et_4N)CsNa_2 + 2DMF]^{2-}$	4.83	1.9
1278.47421	1279.44904	-2	$[cage + (Et_4N)_3Na + DMF]^{2-}$ *	29.80	3.3
1279.94562	1280.81415	-2	$[cage + (Et_4N)_2CsNa + DMF]^{2-}$ *	106.71	5
1291.31199	1292.30828	-2		-	1.7
1295.49463	1296.48253	-2	$[cage + (Et_4N)_4]^{2-}$	0.00	10.9
1299.27040	1300.27425	-2	$[cage + (Et_4N)CsNa_2 + 3DMF]^{2-}$	-5.01	9.4
1308.35264	1309.34288	-2	$[cage + (Et_4N)_2(HNEt_3)_2 + 2MeCN]^{2-}$ *	-104.88	5.5
1316.35977	1317.34789	-2	$[cage + (Et_4N)(HNEt_3)_2Na + 2DMF + MeCN + H_2O]^{2-}$ *	-68.35	12.5
1333.42580	1334.41156	-2	$[cage + (Et_4N)_3Cs + DMF]^{2-}$ *	23.89	11.5

* indicates assignment of species, where large mass error may be attributable to overlapping peaks in the mass spectrum.

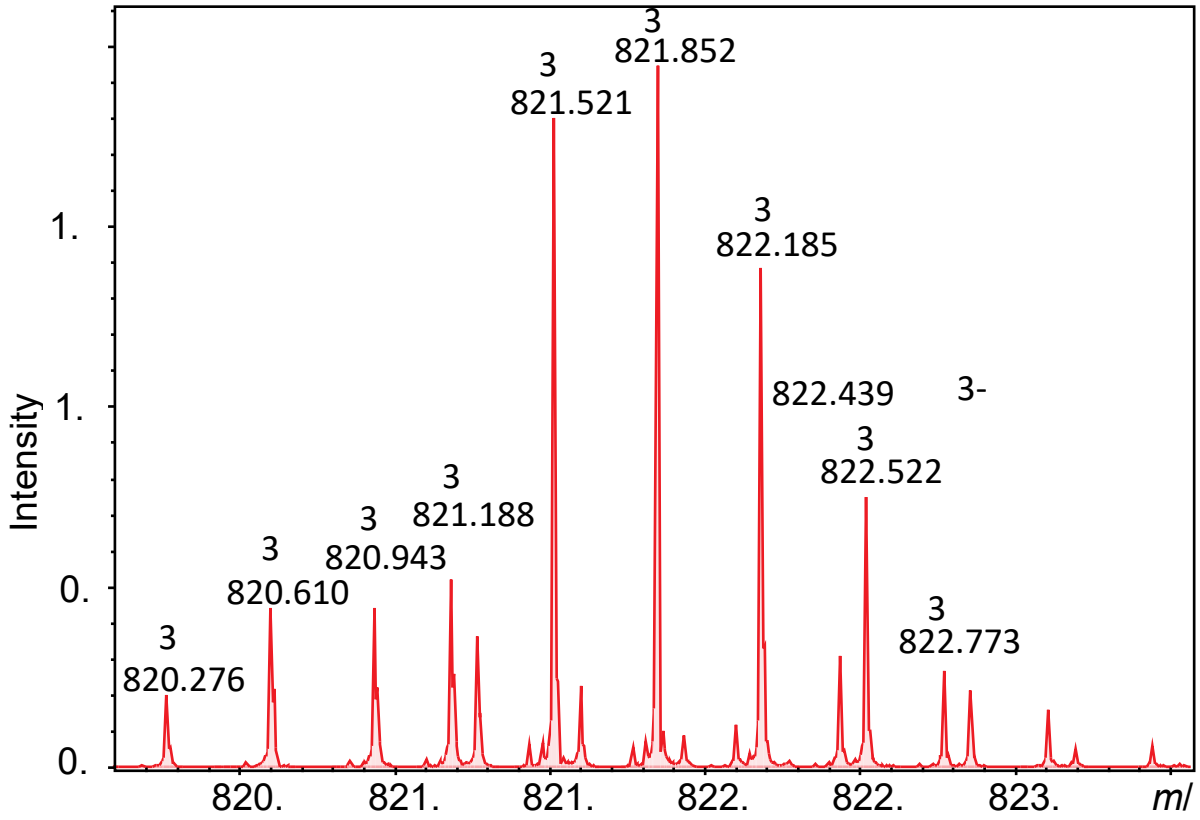

Figure S14. Shows three overlapping isotopic profiles of [cage + $(Et_4N)_3]^{3-}$ at *m/z* 820.61027, [cage + $(Et_4N)_2(Cs)]^{3-}$ (most abundant) at *m/z* 821.85240 and [cage + $(Et_4N)(Cs)_2]^{3-}$ at *m/z* 822.

5.3.9 S9. Infra-red spectroscopy

Infra-red spectrum $(NEt_4)_4(HNEt_3)_4[(PhSi)_6(ctc)_4]Br_2$·solvate (pressed KBr disc)

IR(KBr) cm^{-1}: 3431, 3065, 3025, 2984, 2918, 2854, 1619, 1498, 1384, 1277, 1254, 1171, 1119, 938, 890, 858, 738, 704, 672, 612, 521

The infra-red spectrum of $(NEt_4)_4(HNEt_3)_4[(PhSi)_6(ctc)_4]Br_2$·solvate (pressed KBr disc) is presented in Figure S15.

Infra-red spectrum of crystal after soaking in aqueous CsBr (pressed KBr disc)

IR(KBr) cm^{-1}: 3427, 3065, 3024, 2982, 2925, 2860, 1658, 1619, 1498, 1384, 1277, 1253, 1170, 1117, 1000, 937, 890, 858, 738, 704, 610, 521.

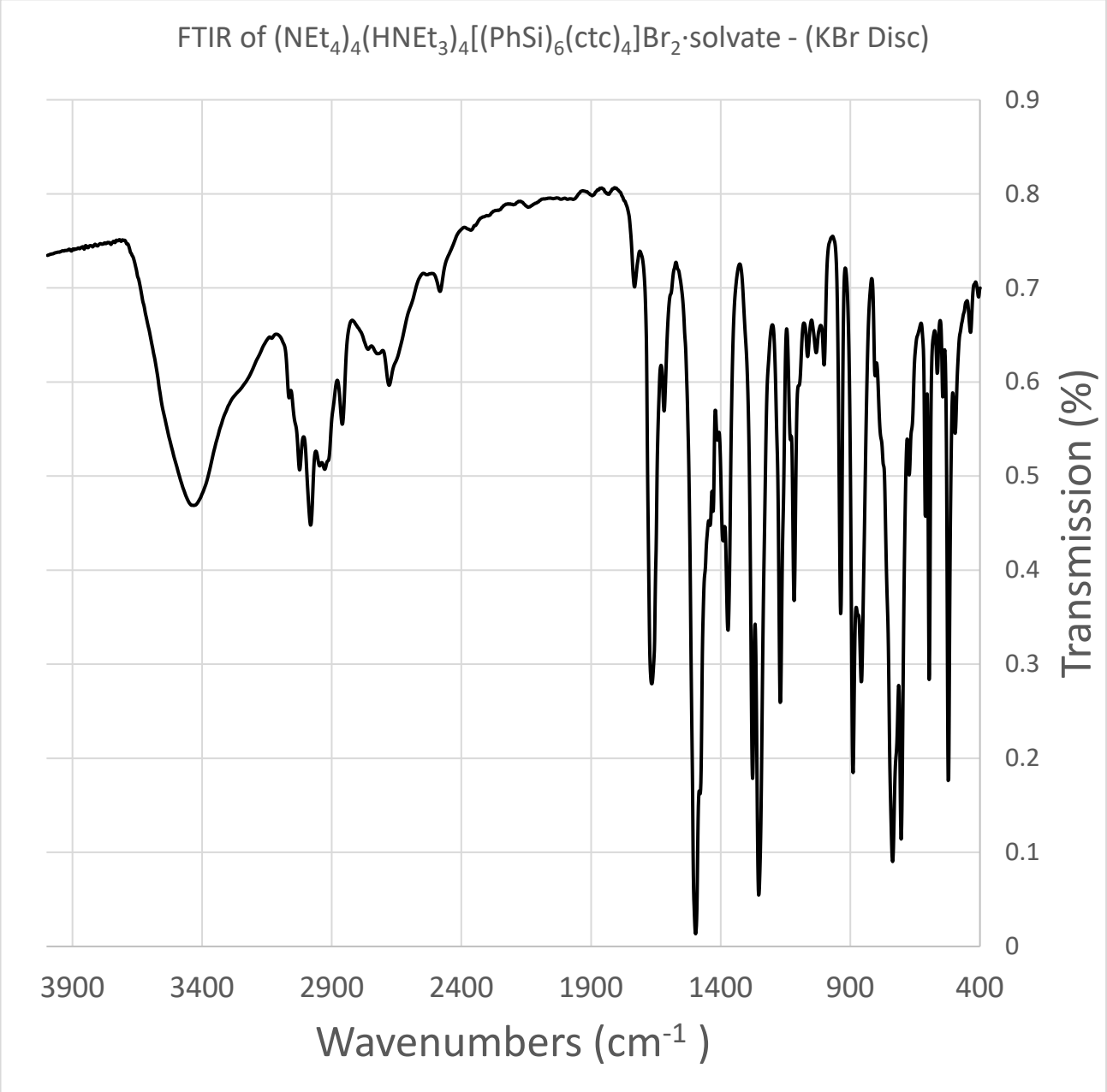

Figure S15. Infrared spectrum of $(NEt_4)_4(HNEt_3)_4[(PhSi)_6(ctc)_4]Br_2 \cdot$solvate (pressed KBr disc).

5.3.10 S10. References for Supporting information

1 A. Spek, *Acta Cryst. Sect. C*, 2015, **71**, 9-18

2 A. Spek, *Acta Cryst. Sect. D*, 2009, **65**, 148-155.

3 G. Sheldrick, *Acta Cryst Sect. A*, 2015, **71**, 3-8

4 G. Sheldrick, *Acta Cryst. Sect. C*, 2015, **71**, 3-8

5 L. Farrugia, *J. Appl. Cryst.*, 2012, **45**, 849-854.

6 O. V. Dolomanov, L. J. Bourhis, R.J. Gildea, J. A. K. Howard and H. Puschmann, *J. Appl. Cryst.* 2009, **42**, 339-341.

Chapter 6 Conclusion

The work conducted throughout the course of the candidate's PhD studies has demonstrated that an even wider variety of assemblies can be generated with cyclotricatechylene than had been anticipated prior to commencing the research. Within the group, previous research with ctc strongly tended towards investigations of cage-type assemblies with *d*- and *f*-block metal cations, and hydrogen bonded host-guest assemblies – both usually generated under basic conditions. The research presented in this thesis not only complements and extends these investigations, but also expands the scope of the work with ctc by combining it with elements from all blocks of the periodic table, from the lightest metal, lithium to the heaviest naturally occurring element, uranium.

Extensive structural diversity is present in systems arising from the combination of ctc with group 1 and 2 metal cations, and in particular the Cs^+ cation. Notably, $ctcH_6$ in its fully protonated state still forms crystalline supramolecular assemblies with cations from group 1. Counterions were shown to have an important role in the architecture of these assemblies by exerting a structure directing influence on the 3D packing arrangement of components in the crystals. Many of the highly symmetrical compounds reported with group 1 and 2 metal cations arise from complementary interactions between the symmetric cyclotricatechylene, and counterions, which were able to either coordinate through the oxygen atoms, hydrogen bond to hydroxyl groups or associate with the ctc bowl through metal cation–π interactions.

While most of the research described in chapters 2 to 5 primarily focused on the variation of cations, anions were also shown to be extremely important structure-directing components. A potentially rich vein of future research would be to further explore the way in which

substitution of anions can influence 1) the type(s) of assemblies that form (sheets, cages etc.) and 2) the 3D packing arrangement of the components. For example, it would be interesting to substitute oxyanions for either halides or other tetrahedral anions such as BF_4^- in the syntheses that yielded the metallocubes reported in chapter 3.

Large, anionic cage type assemblies have been shown to form from the combination of ctc with elements from the *p*-, *d*- and *f*-blocks of the periodic table. Whilst cages containing the vanadyl and uranyl cations are structurally fascinating, the cage reported in chapter 5 and in *Chemical Communications*[1], containing silicon centres is particularly impressive for its assembly from 24 equivalent covalent bonds. Once the correct formation conditions were determined, the $[(PhSi)_6(ctc)_4]^{6-}$ tetrahedral cage proved simple to synthesise and isolate. As noted in the publication, different groups may be interchanged for the phenyl group at the apical coordination site of the Si^{IV} centre to give a wide range of functionalized assemblies, and research in this vein was reported in 2019 by Kabe and co-workers.[2] Additionally, we found that the compound was an excellent candidate for host-guest studies, and while it was unable to be directly synthesised with Cs^+ counterions, they could be incorporated post-synthetically by immersion of crystals of the compound in a solution containing CsBr. Numerous opportunities exist to exploit the host properties and fifth coordination site on the Si^{IV} centres to generate an extensive family of related cage compounds.

This body of work achieved the research aims of exploring the structural diversity of supramolecular assemblies of ctc in combination with different chemical elements, investigating the host-guest and coordination chemistry of $ctcH_6$ in its protonated form, further characterising selected ctc-derived nanocages and generating novel, robust cage-assemblies with ctc.

References

[1] J. L. Holmes, B. F. Abrahams, A. Ahveninen, B. A. Boughton, T. A. Hudson, R. Robson, D. Thinagaran, *Chem. Commun.* **2018**, *54*, 11877–11880.
[2] Y. Kawakami, T. Ogishima, T. Kawara, S. Yamauchi, K. Okamoto, S. Nikaido, D. Souma, R. H. Jin, Y. Kabe, *Chem. Commun.* **2019**, *55*, 6066–6069.

Chapter 7 Instrumentation and experimental detail

7.1 Synthesis of cyclotricatechylene

The following procedure was used by the candidate to generate cyclotricatechylene and is based upon the synthetic procedure reported by Hyatt in 1978.[1]

Formaldehyde (14 mL, 0.18 mol) and veratrole (23 mL, 0.18 mol) were stirred with conc. HCl (200 mL, 37% v/v) for approximately 5 minutes until the mixture became a homogenous, dense, white paste. The mixture was periodically stirred over several hours after which the product was collected by vacuum filtration and washed with copious amounts of distilled water until the filtrate was determined to have a neutral pH. The solid was dried at low temperature (<50° C) then recrystallised from a minimum of hot ethyl acetate. Fine, white needles of the intermediate product, cyclotriveratrylene, were filtered and dried at the pump. The ctv was then dissolved in dichloromethane (ca. 150 mL) and stirred under a nitrogen atmosphere in a flask chilling in an ice-water bath. To this solution was added an excess of BBr_3 (ca. 7.5 mL). The solution was left to stir overnight, after which ice water (ca. 100 mL) was added to quench the reaction. The pink-grey solid was collected by vacuum filtration and washed with water then dried to give a fine powder. Yield: 6.8 g (31%). Elemental analysis calcd (%): C 68.9, H 5.0; found (%) C 68.9, H 5.1.

The crude product from each batch was analysed for purity using ^{1}H NMR. Where the product contained few impurities, it was used in its crude form. If the product was determined to contain impurities or was significantly discoloured it was recrystallised from hot dioxane as the dioxane solvate of ctc (ctc:dioxane approximately 1:1, but varies over time).

7.2 Instrumentation, analysis and software

Microwave reactor syntheses were performed using a Biotage Initiator Classic microwave reactor.

Powder X-ray diffraction experiments were performed at the Australian Synchrotron or on a Rigaku Synergy instrument. Unit cell parameters were extracted using Expo2014[2] and powder pattern diagrams were generated using Origin(Pro)[3].

Mass spectrometry was performed using an Agilent QTOF 6520. High resolution mass spectrometry was performed using a Bruker Daltonics (Bremen, Germany) SolariX 7 Tesla Hybrid MALDI/ESI-FT-ICR-MS.

^{1}H and ^{13}C NMR spectrometry was performed using a Varian 400 MHz NMR Spectrometer. MestRe Nova[4] was used to analyse NMR spectra.

Thermogravimetric analyses were performed using a Mettler TGA/SDTA851 apparatus under an N_2 atmosphere in 40 µL alumina crucibles. Analyses were for the temperature rage between room temperature and 450 °C.

Infrared spectroscopy was performed using a Bruker Tensor FTIR 27 using KBr discs.

Elemental microanalyses were performed at the Campbell Microanalytical Laboratory (University of Otago, Dunedin, New Zealand) and at the Microanalytical Unit at ANU Research School of Chemistry, Canberra, Australia.

7.3 X-ray crystallography

7.3.1 General crystallographic details

Single crystal X-ray diffraction experiments were performed using a SuperNova dual source diffractometer, Rigaku XtaLAB Synergy, Dualflex, HyPix diffractometer or an Xcalibur Sapphire3 diffractometer using CuKα radiation (λ = 1.5418 Å) or MoKα radiation (λ = 0 .7107 Å). Intensity data were collected using phi and omega scans.

Crystals suitable for X-ray diffraction were removed from their mother liquor and immersed in protective oil before being mounted on a loop. The loop was then mounted on a goniometer and the crystal exposed to a stream of N_2 from an Oxford Cryosystem Cooler (130 K).

Crystal structure solutions were obtained by direct methods using the following structure solution programs: SHELXS-2013 or SHELXT[5]. Structure refinements were performed within WinGX[6] or Olex2[7], using SHELXL-97 or SHELXL-2014[8], using a full-matrix least-squares refinement based on F^2. Absorption corrections were applied using the SADABS or Gaussian techniques within CrysAlisPro.[9] The PLATON suite of programs[10] was used to generate contour maps of residual electron density and perform higher symmetry cell checks and the for the SQUEEZE[11] routine.

For crystal structure representations: Pictures were generated using CrystalMaker,[12] Mercury[13] was used for generating representations of surfaces and voids in crystal structures and chemical schemes and diagrams were generated using ChemDraw.

Crystallographic details are available in CIF format for the compounds described in chapters 2, 3 and 4 at https://melbourne.figshare.com/s/40f11948cbeab8cf91a0.

7.3.2 Terminology

Crystallographic terms used throughout the thesis are defined by the following descriptions and equations:

The following equation gives the agreement value (*wR*2) between the observed and calculated structure factors (F_o and F_c) from the least squares refinement:

$$wR2 = \sqrt{\frac{\Sigma[w({F_o}^2 - {F_c}^2)^2]}{\Sigma[w({F_o}^2)^2]}}$$

The following equations describe the weighting scheme:

$$w = \frac{1}{[\sigma^2({F_o}^2)+(aP)^2+bP]} \quad \text{and} \quad P = \frac{\max(0, {F_o}^2)+2{F_c}^2}{3}$$

The following equation gives the agreement index for the merging of equivalent reflections based on F^2:

$$R_{int} = \frac{\Sigma|F_o - {F_o}^2(\text{mean})|}{\Sigma(F_o)^2}$$

where, for an equivalent set of reflections, F_o^2(mean) is the average observed structure factor.

The following equation gives the agreement index based on F between the calculated and observed structure factors:

$$R1 = \frac{\Sigma\big||F_o| - |F_c|\big|}{\Sigma|F_o|}$$

The following expression describes the goodness of fit (GooF) value based on F^2:

$$\text{GooF} = \text{S} = \sqrt{\frac{\Sigma[w({F_\text{o}}^2 - {F_\text{c}}^2)^2]}{(N_\text{R} - N_\text{P})}}$$

where N_R = number of independent reflections and N_P = the total number of parameters refined.

The following expression is used to obtain extinction parameters:

$$x = k\left[\frac{1 + 0.001{F_c}^2\lambda^3}{\sin 2\theta}\right]^{-\frac{1}{4}}$$

where k = overall scale factor.

The following equation gives the anisotropic temperature factor:

$$\text{T} = \exp[-2\pi^2(h^2\text{a}^{*2}\text{U}_{11} + k^2\text{b}^{*2}\text{U}_{22} + l2\text{c}^{*2}\text{U}_{33} + 2hk\text{a}^*\text{b}^*\text{U}_{12} + 2hl\text{a}^*\text{c}^*\text{U}_{13} + 2kl\text{b}^*\text{c}^*\text{U}_{23})]$$

The following equation gives the isotropic temperature factor:

$$\mathrm{T} = \exp\left[-8\pi^2 \mathrm{U}_{\mathrm{iso}} \left(\frac{\sin\theta}{\lambda}\right)^2\right]$$

7.3.4 Modelling disorder in crystal structures

Crystalline supramolecular assemblies containing oligomeric or polymeric frameworks often also contain regions filled with solvent or counterions. Using X-ray crystallography, regular frameworks can typically be modeled unambiguously, however disorder associated with solvent and counterions can be difficult to model. Consequently, $R1$ values can be significantly higher than ordinarily would be acceptable, yet detailed structural information is still provided about the main framework. In such cases where the $R1$ value is greater than 0.10, the value is often misleading with respect to the quality of the solution for the framework.

Many of the molecular cage assemblies in this thesis have very large solvent and cation filled voids in their crystal structures which cannot be modelled by assigning individual atoms. Where this is the case the general approach taken by the candidate has been to assign all counterions and solvent molecules possible when these are identifiable and can be modelled sensibly. Peaks of electron density at appropriate hydrogen bonding distances from each other and from framework oxygen atoms have generally been modelled as oxygen atoms (from water molecules) with isotropic displacement parameters and with full or partial occupancy. Typically, water molecules have not been modelled with their hydrogen atoms.

In all cases, significant effort has been expended to model the solvent and counterions as outlined above.

The above approach to modeling solvent still yields unsatisfactory $R1$ values in many cases. In some cases where mixed solvents are used in the preparation of a compound it is difficult to determine the identity and location of the disordered solvents, and thus modelling the solvent as water, as described above, is not appropriate. In both of the above situations, the SQUEEZE routine from the PLATON suite of programs was typically employed. SQUEEZE removes the contribution of the disordered solvent and counterions. It also provides an estimate of the solvent accessible void volume and the electron density removed by running the routine. A detailed description of the mechanism of the SQUEEZE routine is provided by Spek in the following reference.[11]

7.4 References

[1] J. A. Hyatt, *J. Org. Chem.* **1978**, *43*, 1808–1811.

[2] A. Altomare, C. Cuocci, C. Giacovazzo, A. Moliterni, R. Rizzi, N. Corriero, A. Falcicchio, *J. Appl. Crystallogr.* **2013**, *46*, 1231–1235.

[3] O. C. Northampton, MA, USA, **2019**.

[4] M. R. Willcott, *J. Am. Chem. Soc.* **2009**, *131*, 13180–13180.

[5] G. M. Sheldrick, *Acta Crystallogr. Sect. A Found. Adv.* **2015**, *71*, 3–8.

[6] L. J. Farrugia, *J. Appl. Crystallogr.* **2012**, *45*, 849–854.

[7] O. V. Dolomanov, L. J. Bourhis, R. J. Gildea, J. A. K. Howard, H. Puschmann, *J. Appl. Crystallogr.* **2009**, *42*, 339–341.

[8] G. M. Sheldrick, *Acta Crystallogr. Sect. C Struct. Chem.* **2015**, *71*, 3–8.

[9] *CrysAlisPro 1.171.40.36a, Rigaku Oxford Diffraction/Agilent Technol. UK Ltd* **2018**.

[10] A. L. Spek, *Acta Crystallogr. Sect. D Biol. Crystallogr.* **2009**, *65*, 148–155.

[11] A. L. Spek, *Acta Crystallogr. Sect. C Struct. Chem.* **2015**, *71*, 9–18.

[12] D. C. Palmer, *CrystalMaker 8.3, CrystalMaker Softw. Ltd, Begbroke, Oxfordshire, Engl.* **2014**.

[13] C. F. Macrae, P. R. Edgington, P. McCabe, E. Pidcock, G. P. Shields, R. Taylor, M. Towler, J. van de Streek, *J. Appl. Crystallogr.* **2006**, *39*, 453–457.

Chapter 8 Appendix

Contents

Additional compounds relevant to the work in this thesis

Many additional compounds, other than those reported in the main body of the thesis, were also synthesised during the candidate's PhD. These compounds were excluded from the main thesis on the basis of falling outside the scope of the work. Commonly, these compounds were not characterised beyond X-ray crystallography, and the crystallographic data obtained for some of these were poor. Three such compounds are included below to provide additional context in the discussion of the supramolecular assemblies of cyclotricatechylene described in this thesis.

$Li_xCl_y(Me_2DABCO)[Li_6(ctc)_2(H_2O)_{12}(Me_2DABCO)]\cdot$solvate

A system that shares similarities with the previously described clam-type compounds was also obtained during the candidate's PhD research. The compound, of formula $Li_xCl_y(Me_2DABCO)[Li_6(ctc)_2(H_2O)_{12}(Me_2DABCO)]\cdot$solvate, which is a fully open clam type compound, is presented here only for comparison with compound 2J. The compound was not investigated further, and while the crystallography has shortcomings, the ctc–Li^+ interactions are clear and provide an additional example of the small, 'hard' metal cation Li^+ interacting with catecholate oxygens, rather than the ctc bowl.

To determine whether a coordination cage could be formed with tin, $SnCl_4$, $ctcH_6$, and *N*,*N*'-dimethylDABCO diiodide were combined in aqueous ethanol and layered above a solution of LiOH with an ethanol:H_2O (3:1) buffer layer. Single crystal X-ray analysis on the obtained crystalline product revealed staggered and slightly offset pairs of ctc^{6-} enclosing a Me_2DABCO^{2+} guest (Figure 8.1). Each ctc^{6-} chelates three Li^+ cations. The lithium cations

are also bound to a pair of water molecules (some of which are crystallographically disordered) and have a distorted tetrahedral coordination geometry. Two water molecules associated with each ctc^{6-} hydrogen-bond to catecholate oxygens on the opposite ctc^{6-}. The clam-type interaction in this compound is considered that of a 'fully open' clam, as the ctc units are not directly hydrogen bonded to each other. Outside of the clam are crystallographically disordered chloride ions, water molecules and, potentially, additional Li^+ cations. The disorder could not be successfully modelled using the data available, and the SQUEEZE routine was employed.

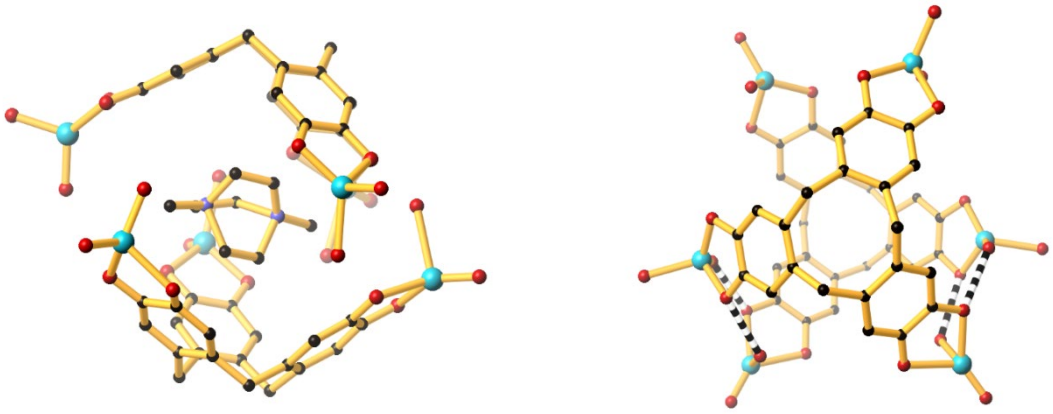

Figure 8.1 Ball-and-stick representations of the hydrogen-bonded fully open clam assemblies in $Li_xCl_y(Me_2DABCO)[Li_6(ctc)_2(H_2O)_{12}(Me_2DABCO)]\cdot$solvate. Hydrogen atoms have been omitted for clarity. Left: A side view of the $[Li_6(ctc)_2(H_2O)_{12}(Me_2DABCO)]^{4-}$ unit. The Me_2DABCO^{2+} is only shown in one of its two possible orientations. Aqua coloured spheres represent lithium cations. Right: A top view of the assembly showing complementary hydrogen bonding interactions. The Me_2DABCO^{2+} has been omitted for clarity.

Compound 2J and the fully open clam with chelated Li^+ ions show that ctc prefers to chelate small group 1 cations such as Li^+, rather than host them in its bowl, which is consistent with the results of the computational and nanoESI investigations reported in chapter 2. Notably, despite numerous attempts to generate a supramolecular assembly with only Li^+ cations, so

far, crystalline assemblies have only been observed in which a second cation is present in the ctc bowl.

Synthesis of $Li_xCl_y(Me_2DABCO)[Li_6(ctc)_2(H_2O)_{12}(Me_2DABCO)]\cdot$solvate: $ctcH_6$ (24 mg, 0.065 mmol) was dissolved in EtOH (4 mL). To this solution was added $SnCl_4\cdot 5H_2O$ (33.1 mg, 0.095 mmol) in H_2O (1 mL). Beneath this solution was layered a buffer layer of 3:1 EtOH:H_2O (1 mL). Below the buffer layer was injected a solution of $LiOH\cdot H_2O$ (65.4 mg, 1.56 mmol) and dimethylDABCO diiodide (25 mg, 0.065 mmol) in H_2O (1 mL). Yellow crystals suitable for X-ray crystallography were observed in the reaction mixture after several days. Space group: *P*4/*nmc* No further analysis was performed.

Crystallographic data table for compound $Li_xCl_y(Me_2DABCO)[Li_6(ctc)_2(H_2O)_{12}(Me_2DABCO)]\cdot$solvate

Empirical formula	$C_{29}H_{42}ClLi_3N_2O_{12}$	
Formula weight	666.91	
Temperature	130(1) K	
Wavelength	1.54184 Å	
Crystal system	Tetragonal	
Space group	*P*4/*mnc*	
Unit cell dimensions	*a* = 25.2462(2) Å	α= 90°.
	b = 25.2462(2) Å	β= 90°.
	c = 27.4191(2) Å	γ = 90°.
Volume	17476.1(3) $Å^3$	
Z	8	
Density (calculated)	0.507 Mg/m^3	
Absorption coefficient	0.590 mm^{-1}	
F(000)	2816	
Theta range for data collection	3.224 to 73.991°.	
Index ranges	$-31 \le h \le 27$, $-29 \le k \le 18$, $-33 \le l \le 20$	
Reflections collected	35005	
Independent reflections	8928 [*R*(int) = 0.0424]	
Completeness to theta = 67.684°	99.9 %	
Refinement method	Full-matrix least-squares on F^2	
Data / restraints / parameters	8928 / 1 / 393	
Goodness-of-fit on F^2	2.197	
Final *R* indices [*I*>2sigma(*I*)]	*R*1 = 0.1714, *wR*2 = 0.4661	
R indices (all data)	*R*1 = 0.1813, *wR*2 = 0.4836	
Largest diff. peak and hole	3.847 and -0.881 e.$Å^{-3}$	

$Cs_2(Bz_2DABCO)_{2.5}(BzDABCO)[Cu_6Cs_4(ctc)_4]\cdot 21H_2O$

With the intention of incorporating organic guest cations into the cavity of a tetrahedral cage containing Cu^{II} centres, a series of experiments was conducted in which $ctcH_6$ was combined with $CuCl_2$ and dibenzylDABCO dichloride in aqueous dioxane and treated with a solution of MOH ($M = Li^+$, Na^+, K^+, Cs^+, NEt_4^+). While the reactions containing Na^+ and K^+ yielded crystalline material, it was severely twinned and unsuitable for X-ray diffraction analysis.

X-ray diffraction studies performed on a suitable single crystal containing the Cs^+ cation revealed the presence of the expected $[Cu_6(ctc)_4]^{12-}$ molecular tetrahedron in a compound of formula $Cs_2(Bz_2DABCO)_{2.5}(BzDABCO)[Cu_6Cs_4(ctc)_4]\cdot 21H_2O$.

Within the asymmetric unit of the compound there is one tetrahedron present, comprising six crystallographically distinct Cu^{II} centres and four unique ctc^{6-} ligands. The Cu^{II} centres are not located at the corners of a perfect octahedron, with Cu^{II}–Cu^{II} separations (for adjacent centres) ranging from 8.88 Å to 9.40 Å. Within the bowl of each ctc is located a Cs^+ cation. Five partially occupied Cs^+ cations are also present in the crystal structure, between the cages and in some of the cage faces.

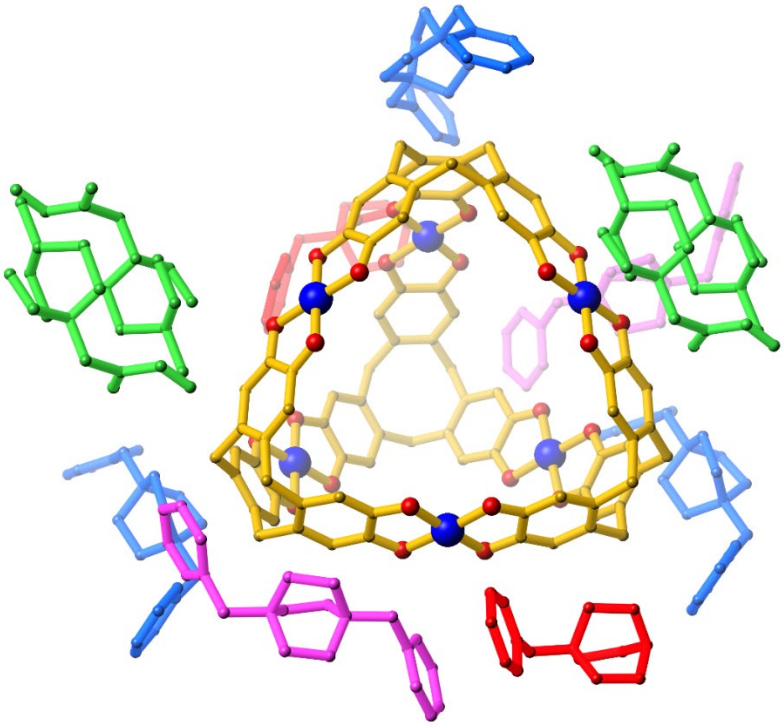

Figure 8.2 A ball and stick representation of one $[Cu_6(ctc)_4]^{12-}$ cage in $Cs_2(Bz_2DABCO)_{2.5}(BzDABCO)[Cu_6Cs_4(ctc)_4]\cdot 21H_2O$, showing the arrangement of the organic cations around it in the crystal structure. Each type of cation is represented by a different colour. Per cage there are one each of the pink and blue Bz_2DABCO^{2+} cations, one red $BzDABCO^{+}$ cation and half a (crystallographically disordered) green Bz_2DABCO^{2+} cation. The four full occupancy Cs^{+} cations within the cage and five additional partial occupancy Cs^{+} cations are not shown. Cu^{II} centres are shown as blue spheres. Hydrogen atoms have been omitted for clarity.

Given the presence of the Cs^{+} in the reaction mixture, it is unsurprising that this cation, rather than the organic cations are located within the cage. Four crystallographically distinct organic cations are, however, located outside of the cage, as shown in Figure 8.2. Two dibenzylDABCO^{2+} cations, shown in pink and blue in Figure 8.2, are crystallographically well defined and are present in the asymmetric unit with full occupancy, one per cage. Both of these cations participate in (similar, but distinct) interactions with methylene hydrogen atoms from ctc units in the cage; one such interaction is indicated in Figure 8.3, which shows the interaction of an aromatic ring of a Bz_2DABCO^{2+} cation with the methylene protons of the cage beneath it. Also present are interactions of methylene protons on the cation with the

aromatic faces of ctc units from the two cages shown above it. A severely disordered Bz_2DABCO^{2+}, shown in green, is also present in the crystal structure (half per cage). Interestingly a single monobenzylDABCO^{+} monocation is also present in the compound, which is attributable to impurities in the starting cation solid material used in the synthesis of the compound. The cations also participate in edge-to-face and face-to face interactions with each other.

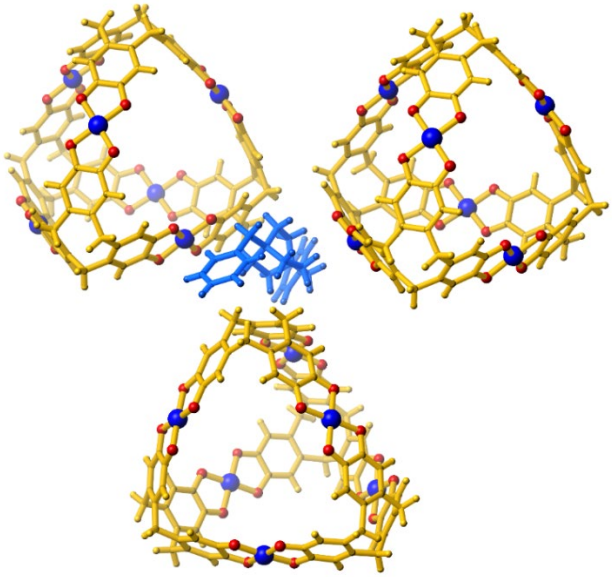

Figure 8.3 A ball and stick representation of three of the $[Cu_6(ctc)_4]^{12-}$ cages in $Cs_2(Bz_2DABCO)_{2.5}(BzDABCO)[Cu_6Cs_4(ctc)_4]\cdot 21H_2O$, showing their arrangement around one of the Bz_2DABCO^{2+} cations, shown in blue. Cu^{II} centres are shown as blue spheres. Hydrogen atoms have been omitted for clarity.

In the extended crystal structure, an inversion centre is located at the centre of each unit cell and four 2_1 screw axes run parallel to the crystallographic *b*-axis. The arrangement of the tetrahedra in the crystal structure (Figure 8.4) is lower in symmetry than cages containing only alkali metal cation countercations.

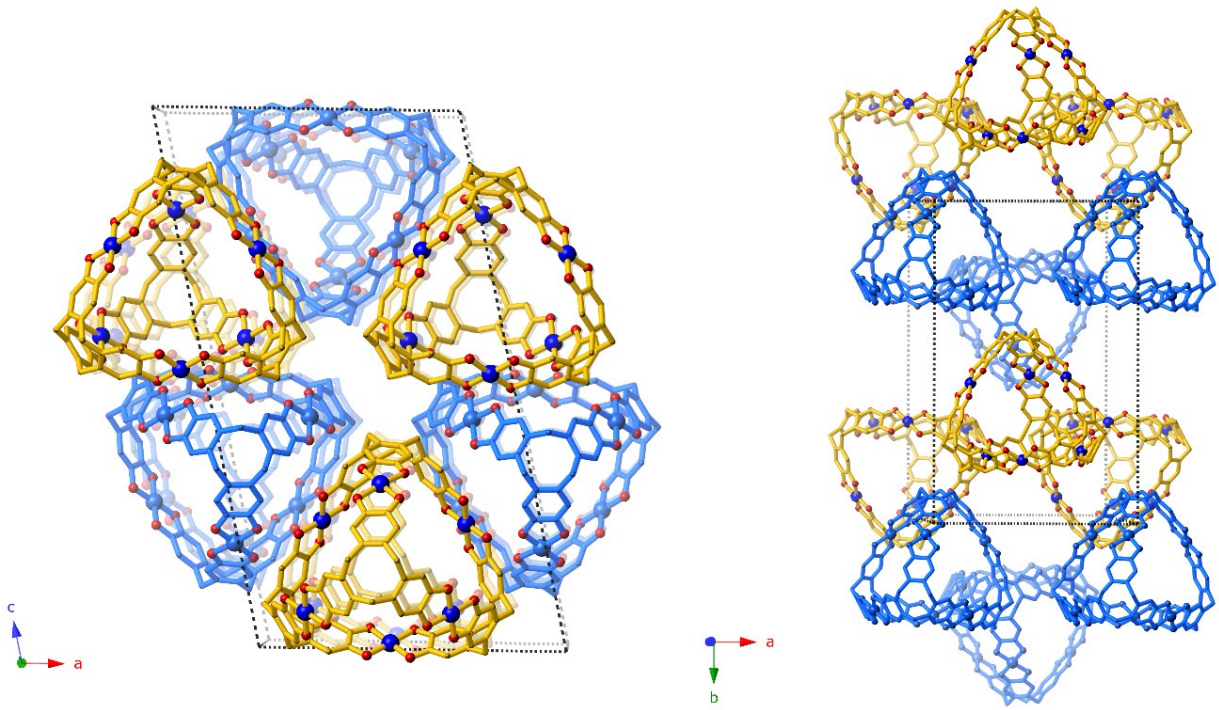

Figure 8.4 A ball and stick representation of the packing arrangement of the $[Cu_6(ctc)_4]^{12-}$ cages in $Cs_2(Bz_2DABCO)_{2.5}(BzDABCO)[Cu_6Cs_4(ctc)_4]\cdot 21H_2O$. Cages in different layers are represented by different coloured bonds. Left, a view along the crystallographic *b* axis. Right, a view along the crystallographic *c* axis.

Synthesis of $Cs_2(Bz_2DABCO)_{2.5}(BzDABCO)[Cu_6Cs_4(ctc)_4]\cdot 21H_2O$

$ctcH_6$ (24 mg, 0.065 mmol) was dissolved in dioxane (1 mL). To this solution was added $CuCl_2.2H_2O$ (16.6 mg, 0.097 mmol) dissolved in H_2O (1 mL) and $(Bz_2DABCO)Cl_2$ (140 mg, 0.39 mmol) in H_2O (1 mL). Finally, $CsOH\cdot H_2O$ (262 mg, 1.56 mmol) in H_2O (1 mL) was added. Deep yellow polyhedral crystals separated from solution within a week. A small amount of plate like crystals also separated from solution, which could not be identified crystallographically. Crystals of $Cs_2(Bz_2DABCO)_{2.5}(BzDABCO)[Cu_6Cs_4(ctc)_4]\cdot 21H_2O$ have monoclinic symmetry in space group $P2_1/n$. Yield (mixture): 4.2 mg. The second component present was unable to be manually separated and as a result, the bulk crystalline material was not sent for additional analysis.

Crystallographic details of $Cs_2(Bz_2DABCO)_{2.5}(BzDABCO)[Cu_6Cs_4(ctc)_4]\cdot 21H_2O$

Single crystal X-ray diffraction analysis was performed using CuKα radiation on a yellow rhomobohedral crystal that was mounted on a loop. The data indicated that the crystal possessed monoclinic symmetry. A satisfactory structure solution was obtained in the space group $P2_1/n$. All non-hydrogen framework atoms were clearly defined and refined with anisotropic displacement parameters. Crystallographically disordered Cs^+ cations, Cs5–Cs9 and atoms of the disordered partial dibenzylDABCO^{2+} were refined with isotropic displacement parameters. All hydrogen atoms were placed at geometrically estimated positions and refined with isotropic displacement parameters.

Crystallographic table for $Cs_2(Bz_2DABCO)_{2.5}(BzDABCO)[Cu_6Cs_4(ctc)_4]\cdot 21H_2O$

Empirical formula	$C_{14}\ H_{177}Cs_6Cu_6N_7O_{45}$	
Formula weight	3940.65	
Temperature	130(1) K	
Wavelength	1.54184 Å	
Crystal system	Monoclinic	
Space group	$P2_1/n$	
Unit cell dimensions	a = 19.4829(2) Å	α= 90°.
	b = 30.6512(3) Å	β= 102.068(1)°.
	c = 34.9625(3) Å	γ = 90°.
Volume	20417.3(3) $Å^3$	
Z	4	
Density (calculated)	1.282 Mg/m^3	
Absorption coefficient	9.424 mm^{-1}	
F(000)	7888	
Crystal size	0.49 x 0.34 x 0.29 mm^3	
Theta range for data collection	2.883 to 74.132°.	
Index ranges	$-23 \le h \le 24$, $-37 \le k \le 30$, $-43 \le l \le 42$	
Reflections collected	85001	
Independent reflections	40307 [R(int) = 0.0531]	
Completeness to theta = 67.684°	99.8 %	
Absorption correction	Semi-empirical from equivalents	
Max. and min. transmission	1.0 and 0.56	
Refinement method	Full-matrix least-squares on F^2	
Data / restraints / parameters	40307 / 0 / 1677	
Goodness-of-fit on F^2	1.111	
Final R indices [I>2sigma(I)]	$R1$ = 0.1004, $wR2$ = 0.2732	
R indices (all data)	$R1$ = 0.1174, $wR2$ = 0.2996	
Largest diff. peak and hole	3.947 and -4.286 e.$Å^{-3}$	

$Cs_8[Ni_6Cs_4(ctc)_4(4\text{-styryl pyridine})_6]\cdot$solvate

When $NiCl_2\cdot 6H_2O$, CsOH and the nitrogen donor ligand, 4-styryl pyridine, were combined in methanol, crystals of a compound containing a $[Ni_6(ctc)_4]^{12-}$ metallocage formed, which has been tentatively assigned the formula $Cs_8[Ni_6Cs_4(ctc)_4(4\text{-styryl pyridine})_6]\cdot$solvate. Crystals of this compound were highly susceptible to degradation on removal from their mother liquor, however, after numerous attempts, an X-ray crystal structure solution was obtained in which a tetrahedral cage possessing the same framework connectivity as the cage in compound 4A was clearly defined, as shown in Figure 8.5. The Ni^{II} centres in the $[Ni_6(ctc)_4]^{12-}$ metallocage each have a square pyramidal coordination geometry, with the axial coordination site on the metal cation occupied by a nitrogen donor atom from a 4-styryl pyridine ligand. Within the cage are four Cs^+ cations, occupying positions within the ctc bowls.

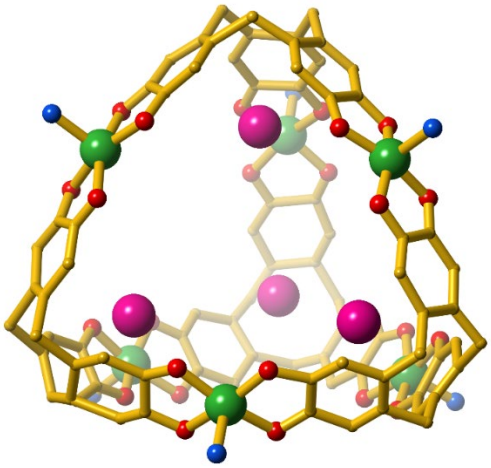

Figure 8.5 A ball and stick representation of the $[Ni_6Cs_4(ctc)_4]^{8-}$ cage in compound $Cs_8[Ni_6Cs_4(ctc)_4(4\text{-styryl pyridine})_6]\cdot$solvate, indicating the nitrogen atoms of the 4-styryl pyridine co-ligands, in blue, and the four Cs^+ cation guests in pink. Green spheres represent nickel centres. Hydrogen atoms and co-ligands have been omitted for clarity.

Interestingly, despite a very different arrangement of counterions and co-ligands than in $Cs_2(Bz_2DABCO)_{2.5}(BzDABCO)[Cu_6Cs_4(ctc)_4]\cdot 21H_2O$, the cages in $Cs_8[Ni_6Cs_4(ctc)_4$(4-styryl pyridine)$_6]$·solvate crystallised in the same space group. The crystal structure refinement of $Cs_8[Ni_6Cs_4(ctc)_4$(4-styryl pyridine)$_6]$·solvate was less than satisfactory, owing to the poor quality of the crystallographic data, however, at least one 4-styryl pyridine co-ligand could be crudely modelled, projecting outwards from the cage (Figure 8.6 at left). For other styryl pyridine ligands only some of the non-hydrogen atoms were revealed in Fourier difference maps. As in $Cs_2(Bz_2DABCO)_{2.5}(BzDABCO)[Cu_6Cs_4(ctc)_4]\cdot 21H_2O$, the packing arrangement appears to be dictated by interactions of aromatic units with methylene protons, as in Figure 8.6, at right.

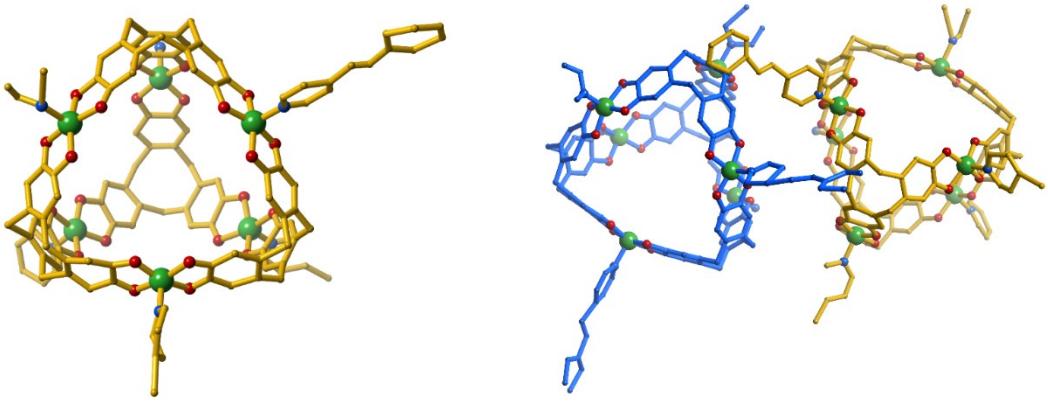

Figure 8.6 Ball and stick representations of the tetrahedra in $Cs_8[Ni_6Cs_4(ctc)_4$(4-styryl pyridine)$_6]$·solvate. Left: a representation of a tetrahedron showing the presence of 4-styryl pyridine co-ligands that are poorly crystallographically defined. For most of the styryl pyridine ligands, only some of the atomic positions could be identified; Right: a representation of the interaction of two molecular tetrahedra via interactions between methylene protons and aromatic units. Green spheres represent nickel centres. Hydrogen atoms and Cs^+ cations have been omitted for clarity.

Prior to the generation of $Cs_8[Ni_6Cs_4(ctc)_4$(4-styryl pyridine)$_6]$·solvate, all co-ligands present in compounds in this family had been incorporated serendipitously, rather than by design.

This example, though poorly characterised, has been included herein as proof of concept that co-ligands can be deliberately integrated into tetrahedral metallocage assemblies containing ctc. Future work in this vein of research could include the incorporation of preorganised metal-ligand building blocks into cages with ctc, in which the co-ligand is coordinated to the metal cation of interest prior to being combined with the ctc ligand.

Synthesis of $Cs_8[Ni_6Cs_4(ctc)_4(4\text{-styryl pyridine})_6]\cdot$solvate

$ctcH_6$ (24 mg, 0.065 mmol) was dissolved in MeOH (3 mL). To this solution was added $MePPh_3Br$ (116 mg, 0.325 mmol) in H_2O (1 mL) followed by 4-styryl pyridine (18 mg, 0.095 mmol). $NiCl_2\cdot 6H_2O$ (23.2 mg, 0.0975 mmol) was dissolved in H_2O (1 mL) and added to the solution, followed by $CsOH\cdot H_2O$ (131 mg, 0.78 mmol) in H_2O (0.5 mL) then an additional 1 mL of H_2O. Crystalline yellow rods formed after 1 – 2 days. Crystals suitable for X-ray diffraction were selected and immersed in cryo-protectant oil immediately upon being removed from the mother liquor of the reaction mixture. Despite this course of action, crystals of the compound began to discolour to a dark blue and completely lose structural integrity almost immediately on removal from the mother liquor. Consequently, no solid product could be collected for further analysis and the quality of the X-ray diffraction analysis was sub-par, despite being the best of numerous attempts.

$Na_{10}[Na_{14}(UO_2)_{24}(H_2O)_8(O_2)_{24}(OH)_{24}]\cdot 176H_2O$

The formation of a compound of formula $Na_{10}[Na_{14}(UO_2)_{24}(H_2O)_8(O_2)_{24}(OH)_{24}]\cdot 176H_2O$ containing a sphere with 24 uranyl centres was discussed in chapter 4. This compound was confirmed as a reaction product on two separate occasions, and a similar compound containing the $[(UO_2)_{24}(O_2)_{24}(OH)_{24}]^{24-}$ unit was also obtained during the candidate's MSc with Ca^{2+} counterions (space group: *I*4/*m*). The crystallographic details given below relate to a crystal obtained from the following synthesis.

Synthesis of $Na_{10}[Na_{14}(UO_2)_{24}(H_2O)_8(O_2)_{24}(OH)_{24}]\cdot 176H_2O$

UO_2SO_4 (42 mg, 0.0975 mmol), $ctcH_6$ (24 mg, 0.065 mmol) and alloxan (10 mg, 0.07 mmol) were combined in H_2O (4 mL). The mixture was treated with NaOH (62.8 mg, 1.56 mmol) in H_2O (1 mL), at which point any solids remaining in the mixture dissolved. The solution did not yield crystalline precipitate in the 4 weeks following preparation, however after approximately 2 years, yellow crystals were observed in the reaction vial. A single crystal suitable for X-ray diffraction was selected.

General data collection and refinement details of $Na_{10}[Na_{14}(UO_2)_{24}(H_2O)_8(O_2)_{24}(OH)_{24}]\cdot 176H_2O$

Single crystal X-ray diffraction analysis was performed using CuKα radiation on a large yellow block-like crystal that was mounted on a loop. The data indicated that the crystal possessed tetragonal symmetry. A structure solution and refinement was obtained in the space group *I*4/*m*. The highly absorbing nature of the crystals resulted in difficulties in the application of anisotropic displacement parameters. In the case of many atoms, refinement of anisotropic displacement parameters resulted in the atoms becoming 'non-positive definite'

indicating a physically unrealistic description of the thermal motion of the atom. In such cases the atom was refined with an isotropic displacement parameter.

Crystallographic table for $Na_{10}[Na_{14}(UO_2)_{24}(H_2O)_8(O_2)_{24}(OH)_{24}]\cdot 176H_2O$

Empirical formula	$H_{108}\ Na_{12}\ O_{108}\ U_{12}$	
Formula weight	4969.10	
Temperature	130(1) K	
Wavelength	1.54184 Å	
Crystal system	Tetragonal	
Space group	*I*4/*m*	
Unit cell dimensions	*a* = 19.3014(1) Å	α= 90°.
	b = 19.3014(1) Å	β= 90°.
	c = 25.3132(2) Å	γ = 90°.
Volume	9430.3(1) $Å^3$	
Z	4	
Density (calculated)	3.500 Mg/m^3	
Absorption coefficient	58.984 mm^{-1}	
F(000)	8832	
Theta range for data collection	4.582 to 71.162°.	
Index ranges	$-23 \le h \le 22, -21 \le k \le 23, -20 \le l \le 30$	
Reflections collected	33553	
Independent reflections	4660 [*R*(int) = 0.2045]	
Completeness to theta = 67.684°	99.9 %	
Refinement method	Full-matrix least-squares on F^2	
Data / restraints / parameters	4660 / 0 / 143	
Goodness-of-fit on F^2	1.910	
Final *R* indices [*I*>2sigma(*I*)]	*R*1 = 0.2350, wR2 = 0.4370	
R indices (all data)	*R*1 = 0.2360, wR2 = 0.4410	
Largest diff. peak and hole	15.416 and -37.861 $e.Å^{-3}$	

Analyses for compounds reported in chapter 2

Crystallographic information files for chapter 2 are available at:

https://melbourne.figshare.com/s/40f11948cbeab8cf91a0

Thermogravimetric analysis of compound 2A

Approximately 6.6 mg of compound 2A (described in chapter 2) was prepared by the synthetic procedure reported in chapter 2 and analysed by thermogravimetric means. The blue trace in Figure 8.7 indicates the mass of material vs. temperature, while the red trace is the scanning differential thermal analysis trace of the material.

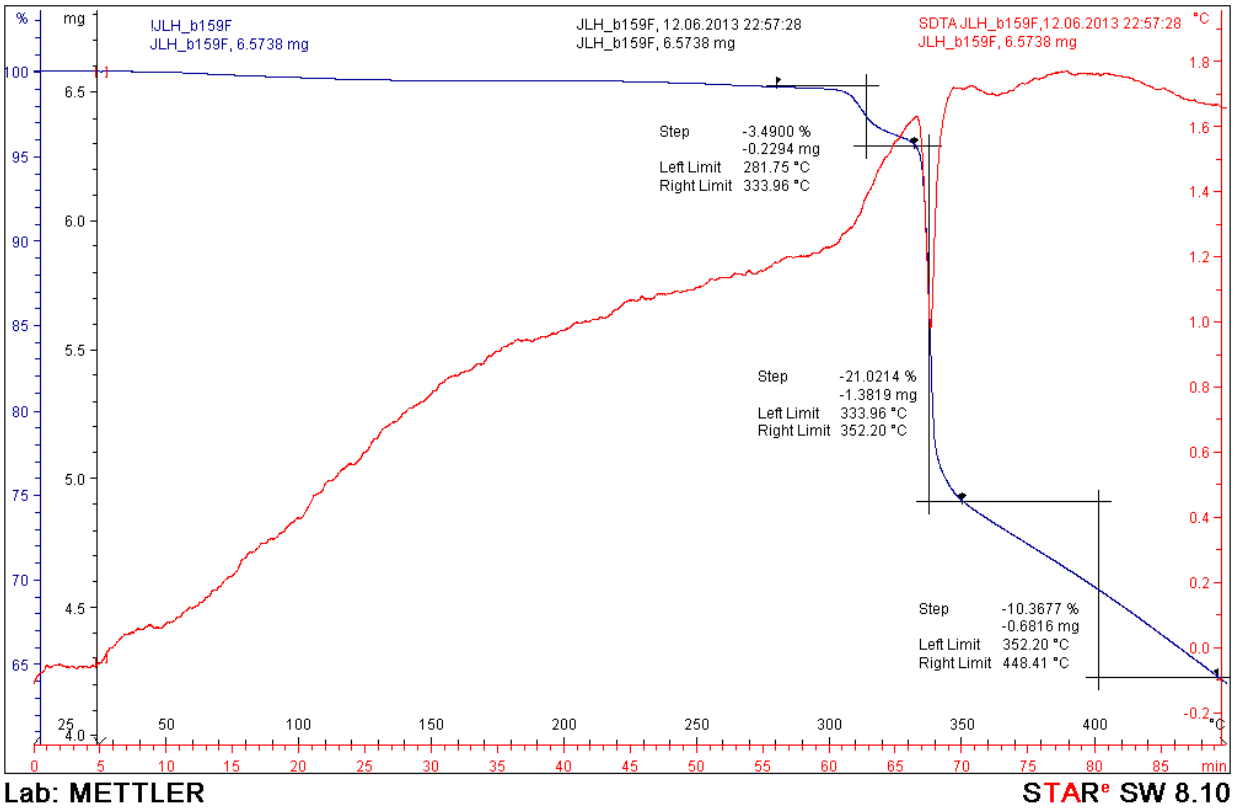

Figure 8.7 Thermogravimetric trace of compound 2A.

Solid state NMR of compound 2A

Solid state proton NMR investigations were undertaken by Dr Aditya Rawal at the University of New South Wales. Details of this investigation are described below. Solid state proton NMR was performed on a sample of compound 2A to determine the location of a hydrogen atom which was difficult to assign using X-ray crystallography. A sample of 2A was prepared as per the procedure in chapter 2, filtered on filter paper and dried at the pump. The results of the 1D- ^{1}H NMR displayed a change when samples were duplicated, indicated by the loss of a peak (circled in Figure 8.8, top), which may be attributable to surface solvent loss. While there are 11 crystallographically distinct hydrogen atoms in the asymmetric unit, there are a maximum of seven discernible peaks in the spectrum, in part as a consequence of some of these hydrogen atoms having near identical chemical environments and therefore substantial peak overlap. ^{1}H-^{1}H 2D correlation/exchange spectroscopy (Figure 8.8 bottom row) did not provide additional information, and ^{13}C-^{1}H (Figure 8.8 middle row) was not well resolved enough.

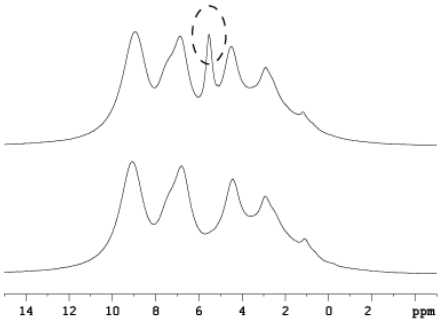

1H NMR

2D correlation/exchange spectroscopy

^{13}C-^{1}H

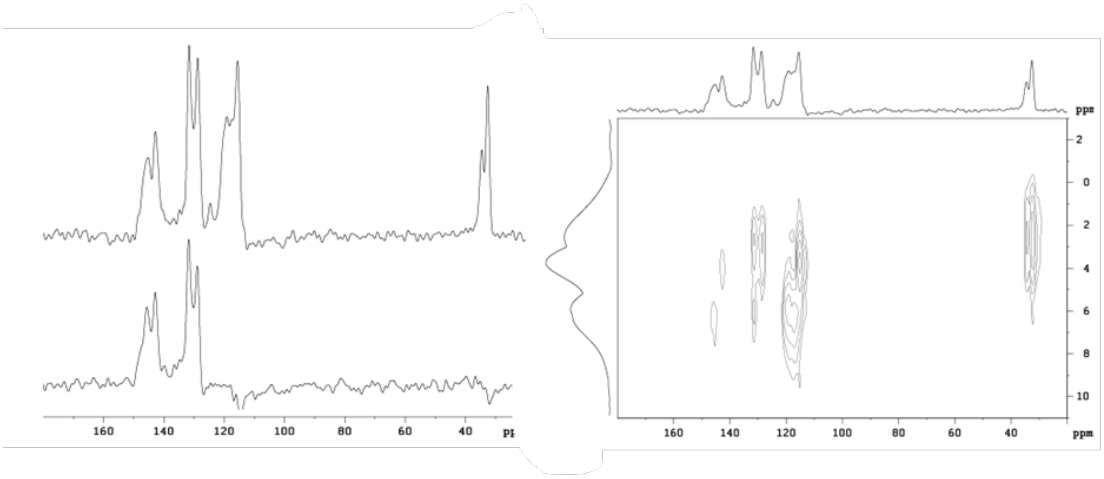

^{1}H-^{1}H

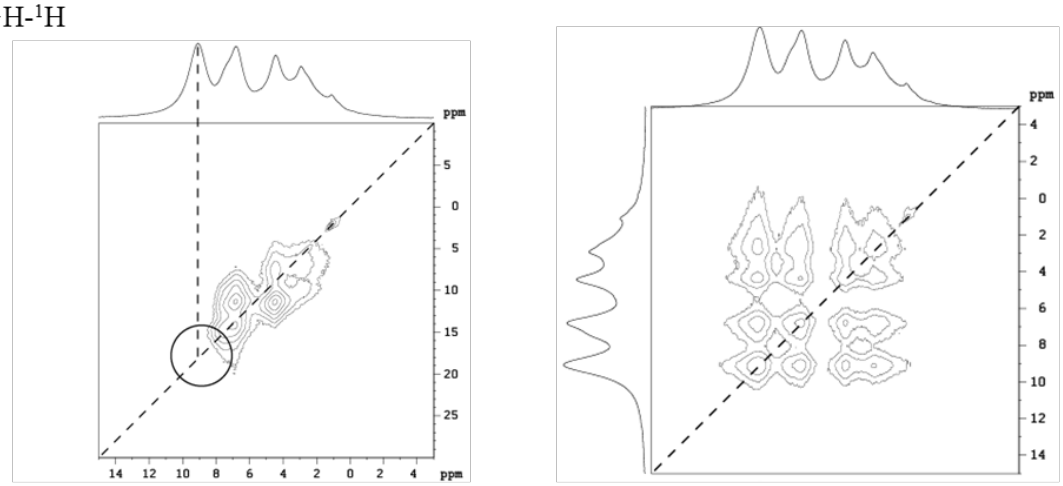

Figure 8.8 Solid state proton NMR spectra for compound 2A. Top: 1D ^{1}H NMR, Middle: 2D ^{13}C-^{1}H NMR, Bottom: ^{1}H-^{1}H NMR.

Analyses for compounds reported in chapter 3

Crystallographic information files for chapter 3 are available at:

https://melbourne.figshare.com/s/40f11948cbeab8cf91a0

Analyses for compounds reported in chapter 4

Crystallographic information files for chapter 4 are available at:

https://melbourne.figshare.com/s/40f11948cbeab8cf91a0

For the following experiments, crystals of $Na_{24}[(UO_2(H_2O))_{12}(ctc)_8]$·solvate were prepared by the synthetic procedure reported in chapter 4 for Dr. FitzGerald's cube, and the bulk material was collected for analysis, unless otherwise indicated.

Infrared spectrum of $Na_{24}[(UO_2(H_2O))_{12}(ctc)_8]\cdot$solvate

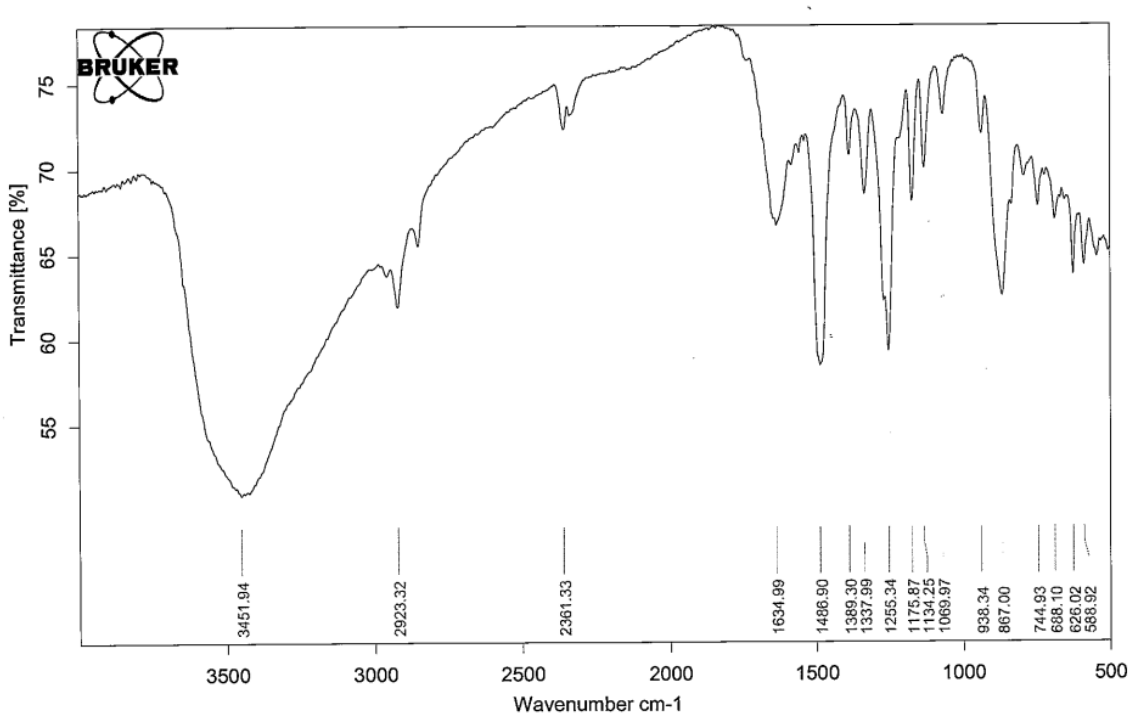

Figure 8.9 The infrared spectrum of a sample of $Na_{24}[(UO_2(H_2O))_{12}(ctc)_8]\cdot$solvate, sample form = KBr disc.

Powder X-ray diffraction of $Na_{24}[(UO_2(H_2O))_{12}(ctc)_8]\cdot$solvate

Powder X-ray diffraction data was collected for several samples of the bulk material from the reaction that yields $Na_{24}[(UO_2(H_2O))_{12}(ctc)_8]\cdot$solvate. Raw data of two powder X-ray diffraction patterns are shown (Figures 8.10 and 8.11) which are correspond to the best results obtained. It was concluded that X-ray diffraction data was not of sufficient quality to be used to identify the presence of a crystalline component containing a uranyl salt such as the U_{24} nanosphere. The data was therefore not analysed further and other avenues were pursued.

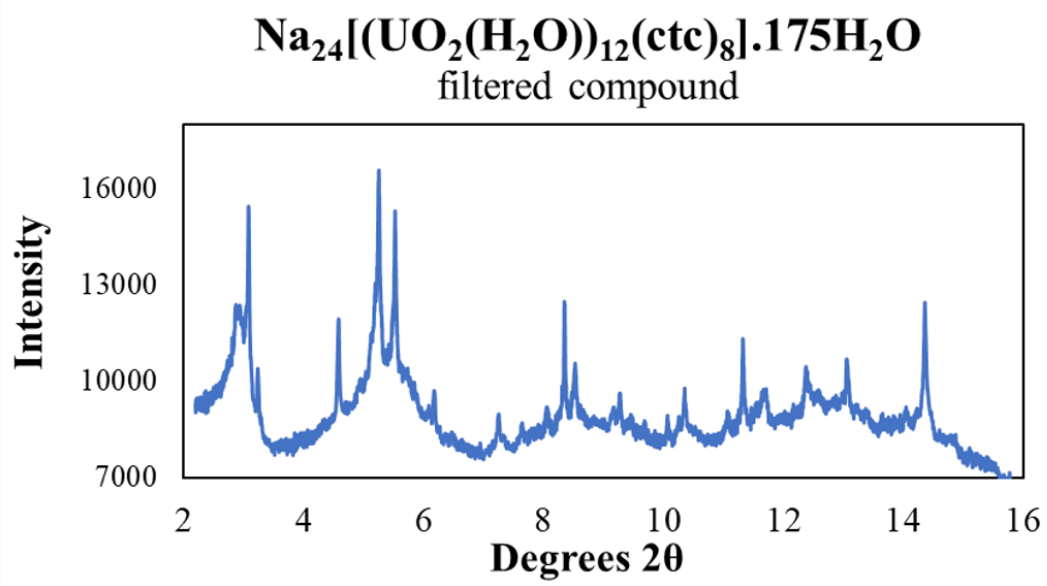

Figure 8.10 Synchrotron powder X-ray diffraction pattern of a filtered sample of the bulk material obtained from the synthetic procedure that produces $Na_{24}[(UO_2(H_2O))_{12}(ctc)_8]$·solvate. The material was mostly crystalline and was packed in a glass capillary tube.

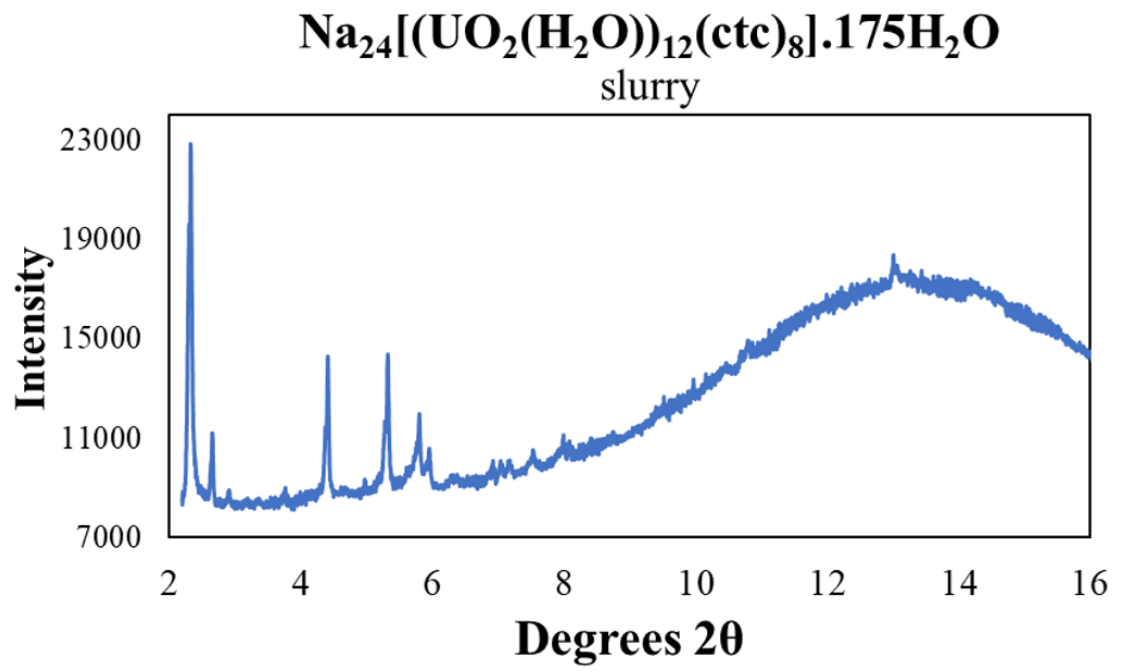

Figure 8.11 Synchrotron powder X-ray diffraction pattern of a slurry of the bulk material obtained from the synthetic procedure that produces $Na_{24}[(UO_2(H_2O))_{12}(ctc)_8]$·solvate. For PXRD analysis the slurry was sealed in a glass capillary tube.

Thermogravimetric analysis of $Na_{24}[(UO_2(H_2O))_{12}(ctc)_8]$·solvate

Three samples were prepared for thermogravimetric analysis using different treatments at the time of filtration. The purpose of the experiment was to determine if treating samples with an acetate buffer solution would result in samples which gave different TGA traces to the untreated sample. If the traces differed in character (shape) this might correspond to a sample for which side products had dissolved and been filtered off. Descriptions of sample preparation are given below.

Sample 1: The bulk material prepared from the reaction conditions that yielded $Na_{24}[(UO_2(H_2O))_{12}(ctc)_8]$·solvate was collected on a frit washed with acetone. The compound was only left on the frit unit no visible solvent remained in the funnel.

Sample 2: The bulk material prepared from the reaction conditions that yielded $Na_{24}[(UO_2(H_2O))_{12}(ctc)_8]$·solvate was collected on a frit washed with acetone and then a buffer solution (1:1 NaOAc:HOAc, 1:1 MeOH: H_2O). The compound was only left on the frit unit no visible solvent remained in the funnel.

Sample 3: The bulk material prepared from the reaction conditions that yielded $Na_{24}[(UO_2(H_2O))_{12}(ctc)_8]$·solvate was left in its vial with its mother liquor, which was treated with a buffer solution (1:1 NaOAc: HOAc, 1:1 MeOH: H_2O) for 2 hours. The material was then collected on a frit washed with acetone and was only left on the frit unit no visible solvent remained in the funnel.

The samples were analysed by thermogravimetric means. The black trace in Figure 8.12 indicates, for sample 1, which is the 'untreated sample', the mass of material vs. temperature,

while the red trace is the mass loss in milligrams per minute. The compound loses 17% of its mass before reaching 150 °C, which can be attributed to solvent.

Figure 8.13 shows the thermogravimetric trace of the three samples of $Na_{24}[(UO_2(H_2O))_{12}(ctc)_8]\cdot$solvate. The blue, red and black lines (top of figure) correspond to the TGA traces by mass for samples 1, 2 and 3 respectively. The orange green and purple lines indicate the percentage mass remaining of samples 1, 2 and 3, respectively, over the temperature range.

By comparison of the traces for each of the three samples in can be concluded that the solvation state of samples of the bulk material can vary substantially. The TGA traces for each sample were extremely similar in character, and bulk material for the treated and untreated samples appear to have the same properties with respect to solvent loss and stability to increasing temperatures, indicating that the treatments applied to samples 2 and 3 did not remove any substantial side product component.

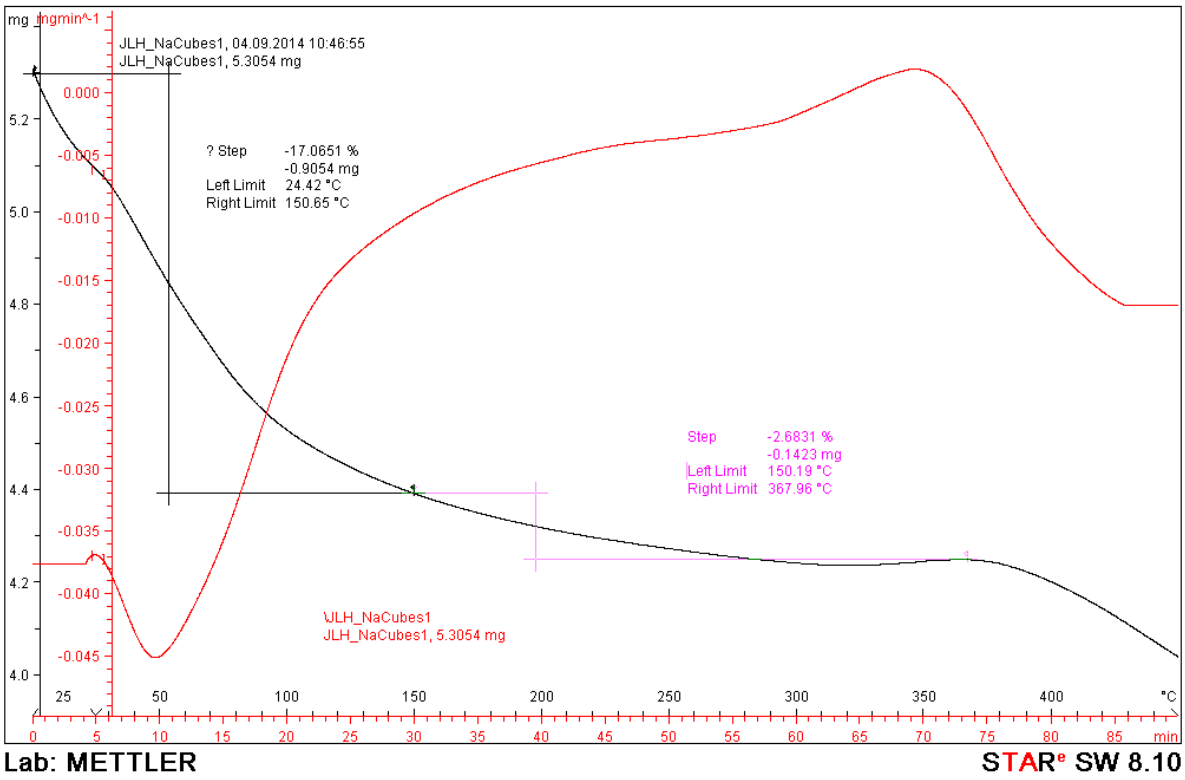

Figure 8.12 Thermogravimetric trace of $Na_{24}[(UO_2(H_2O))_{12}(ctc)_8]\cdot$solvate.

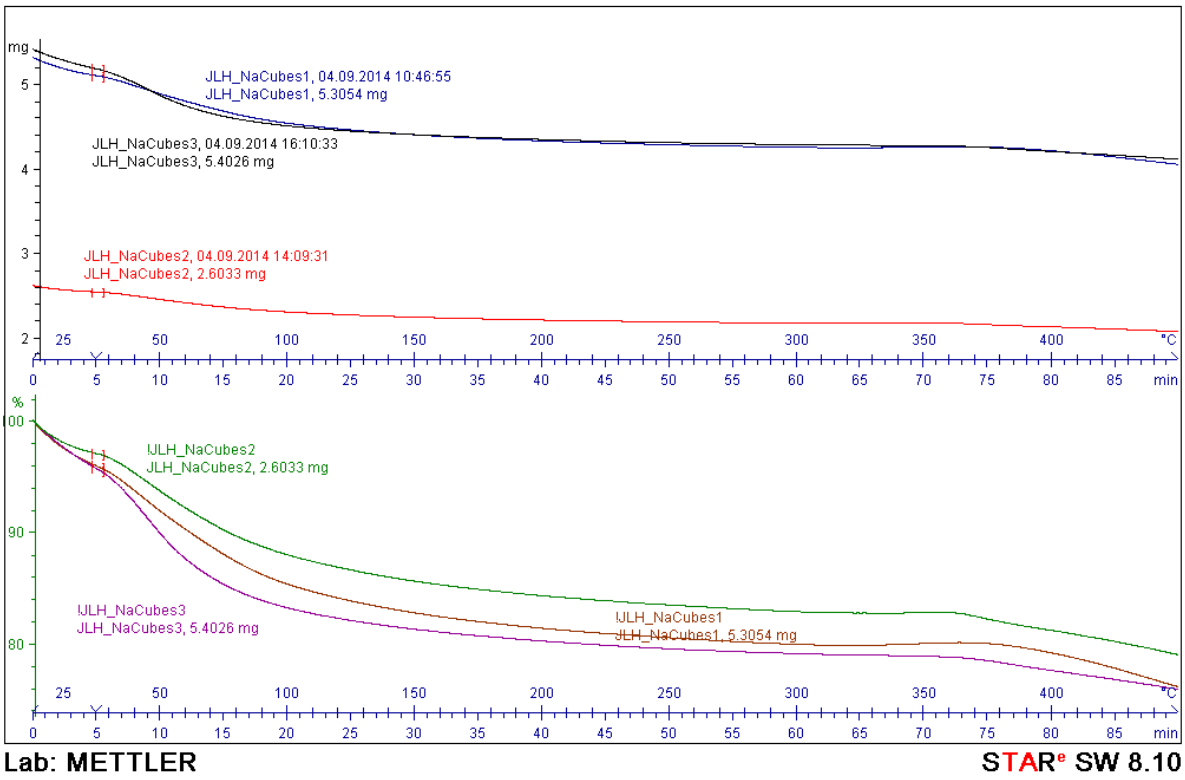

Figure 8.13 Thermogravimetric trace of three samples of $Na_{24}[(UO_2(H_2O))_{12}(ctc)_8]\cdot$solvate.

X-ray photoelectron spectroscopy of $Na_{24}[(UO_2(H_2O))_{12}(ctc)_8]\cdot$solvate

Crystals of $Na_{24}[(UO_2(H_2O))_{12}(ctc)_8]\cdot$solvate were synthesised as described in chapter 4. The crystals were collected on a glass frit and a suitable single crystal was attached to an adhesive carbon tape. The X-ray source was: X-Ray011 400um - FG ON (400 µm). The experiment was conducted to investigate the composition of a single crystal of the compound, thus eliminating the presence of side products contributing to the overall elemental analysis of the material.

The data provided by the experiment, as shown in Figure 8.14, with respect to both the ratios of the elements present and the chemical elements present are not consistent with those

expected for the compound. It is expected that unavoidable contamination on the surface of the crystal is, at least in part, responsible for this, despite selecting a section of crystal with no visible side products present. Similar XPS analysis of the side product itself, an image of which is shown in Figure 8.15, was unable to confirm whether the product shared the composition of the U24 nanosphere, in part due to the particles of side product being slightly too small for the X-ray beam.

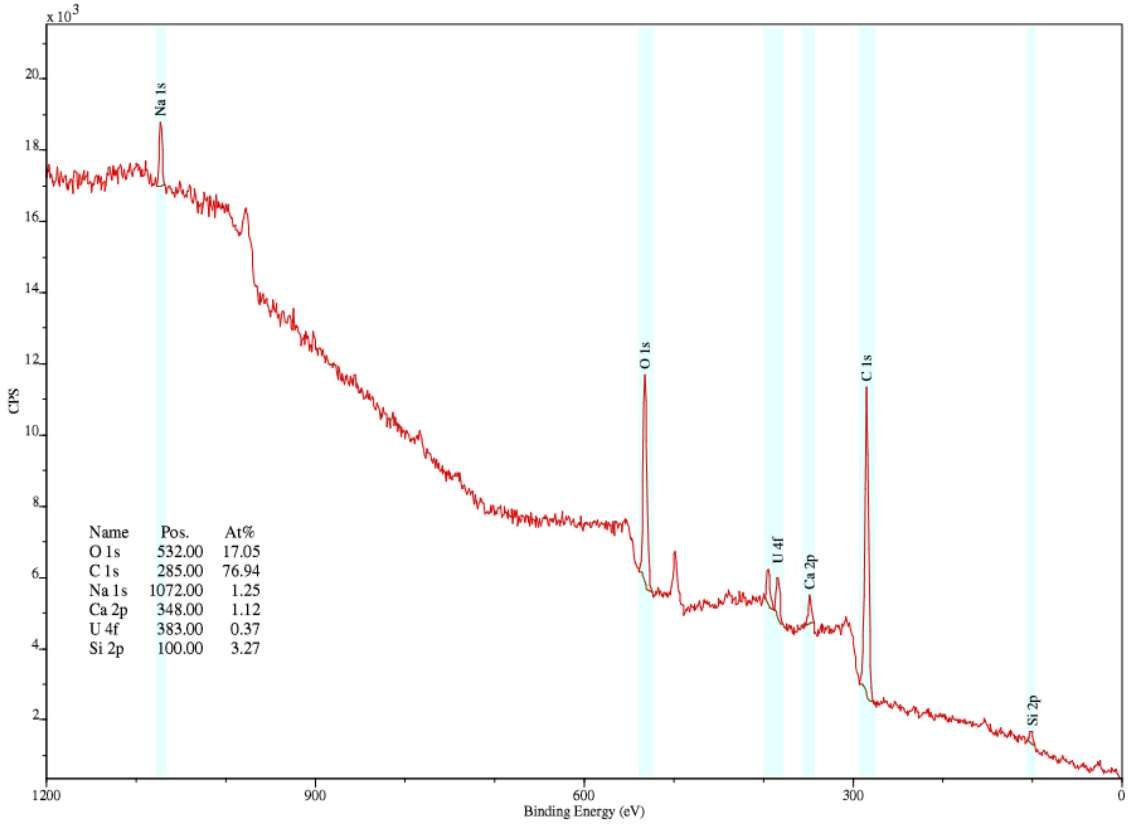

Figure 8.14 X-ray photoemission spectrum for crystals of a sample of Dr. Fitzgerald's cube of formula $Na_{24}[(UO_2(H_2O))_{12}(ctc)_8]$·solvate, containing the same metallocage as in compound 4C.

Microscope image of $Na_{24}[(UO_2(H_2O))_{12}(ctc)_8]$.solvate and a yellow side product

A single crystal of the compound of formula $Na_{24}[(UO_2(H_2O))_{12}(ctc)_8]$·solvate was adhered to carbon tape. A magnified photograph of the crystal was taken using a microscope. The crystal, which degraded over time as solvent was lost, is seen as a brown powdery substance. Yellow amorphous precipitate is stuck to the outer surface of the crystal. This type of precipitate was observed in a number of reactions containing ctc and the uranyl cation.

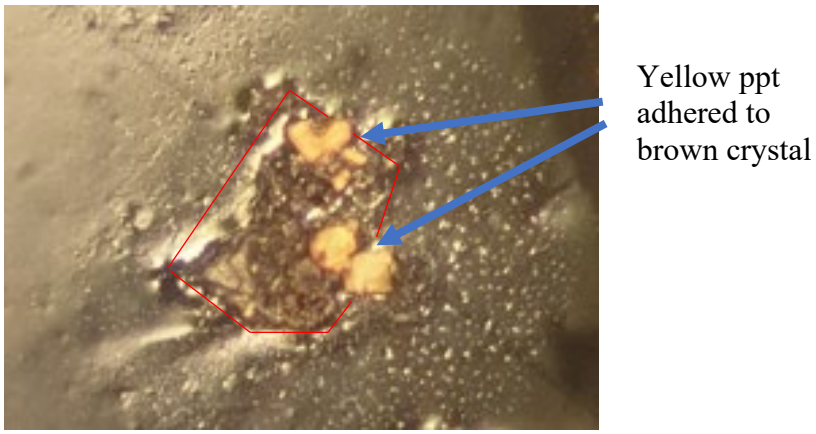

Figure 8.15 A single crystal of the compound of formula $Na_{24}[(UO_2(H_2O))_{12}(ctc)_8]$·solvate was adhered to carbon tape. The crystal, which degraded over time, can be seen as a brown powdery substance (outlined approximately, in red) with yellow amorphous precipitate adhered to the outside.

Analyses for compounds reported in chapter 5

Crystallographic information files for chapter 5 have been deposited with the CCDC (1860473). They can be accessed via the CCDC website using DOI: 10.1039/c8cc06405a and by reference codes ADUZOR and AFEPAF.